Optimising BWR spent fuel storage using the burnup credit method and exploring other solutions for the management of high-level waste

Thesis submitted in accordance with the requirements of the University of Liverpool for the degree of Doctor in Philosophy

by

Anna Detkina

June 2021

Abstract

The volumes of accumulated spent fuel from commercial power plants have significantly increased over the last decades and are projected to grow further. With a small part of the spent fuel being reprocessed and with the lack of delivered solutions for the long-term spent fuel management, the demand for interim spent fuel storage facilities is expected to grow in the foreseeable future. Currently, LWRs – PWRs and BWRs, are considered as the major contributor to the spent fuel accumulation. The given research is focused on analysing BWR spent fuel properties since it is less researched than PWR due to the more complex fuel assembly design.

The criticality safety analysis is a part of the safety assessment of the design of storage facilities. The criticality analysis can be performed by either the fresh fuel approach (unirradiated fuel) or by applying the burnup credit method (considers fuel burnup). The burnup credit method is widely applied to PWR storage systems and, in some countries, to BWR wet storage, but is still under development for BWR dry storage. The current study aims to develop a novel cutting-edge approach to the burnup credit analysis that can account for the realistic status of the BWR fuel assemblies through their lifetime in the reactor core. To achieve that, the approach incorporates the results of the reactor core nodal burnup simulations into the criticality safety assessment of the spent fuel storage cask. In addition, the study examines potential solutions for the long-term LWR spent fuel management.

Prior to development of the burnup credit model, supporting investigations have been performed to determine the quality of the computational tools for the nodal reactor core analysis. The research included evaluation of potential lattice physics codes for BWR burnup calculations and comparison of nodal and high-fidelity methods for the full-core analysis with heterogenous BWR fuel assembly design. According to the results, the lattice physics modules TRITON and Polaris of SCALE-6.2 package showed to be robust for BWR analysis, while the UK code WIMS-10A produced the least satisfactory results among analysed codes. As expected, the outcome of the reactor core analysis by nodal and high-fidelity approaches for BWR core differed from each other. The leading reasons for that were found in the difference in the estimation of the axial power profiles for 3D fuel assembly models performed under both approaches. The main advantage of the nodal approach was the significantly lower computational demand which allowed more comprehensive reactor core analysis which was to date not possible in full-depth using the high-fidelity approach.

The burnup credit study included the development of a 3D nodal fuel assembly model with coupled neutronics and thermal-hydraulics as well as steady-state reactor core analysis of four cycles of reactor operation with different initial parameters. The results of the reactor core analysis, such as fuel assembly's discharge burnup or its approximated operational conditions (no actual operational data from a plant has been used), were used to define the composition of the spent fuel for further criticality analysis of the BWR storage cask. The variation of the initial parameters was conducted to estimate their effect on the criticality of the storage cask. The varied initial parameters included refuelling scenarios, fuel assembly types, and target burnups. The study demonstrated that the utilisation of the more detailed 3D nodal model of the BWR fuel assembly can improve the accuracy of the 2D lattice approach while analysing the fuel assembly status, and lead to a reduction of the conservatism of existing approaches of criticality analysis such as the fresh fuel approach.

Although creating a detailed and realistic model of the fuel assembly for burnup credit analysis is more time-consuming and computationally expensive than just using a 2D lattice model or applying fresh fuel approach for the criticality analysis, it can potentially provide significant benefit in terms of reduction of the costs of spent fuel storage. The developed advanced modelling approach will mostly benefit the handling of complex and heterogeneous BWR fuel assemblies which are commonly used today in BWRs and are planned to be used in developing ABWRs.

At the final part of the study, it was shown that the molten salt reactors working directly on a spent fuel can be a cost-effective, safe, and feasible alternative to the generally accepted strategies of the long-term spent fuel management such as completely closed nuclear fuel cycle and direct disposal of spent fuel.

Acknowledgements

I would like to thank my two supervisors Prof. Bruno Merk and Dr Aiden Peakman for guiding me throughout the PhD. My knowledge and skills have grown significantly over the time we worked together. I am incredibly grateful for your support, advice and hours of discussion about the research project, and not only.

I would also like to thank the fantastic people I worked with at the University of Liverpool during my PhD. Dzianis, thank you for answering my million and one questions. Seddon, I really enjoyed doing a project together.

I would like to say a huge thank you to my dear husband Pavel who always encourages me to go further and never give up.

My wonderful mum deserves a special thank you for always believing in me and my abilities. I will be forever grateful for the sacrifices you made so I would have a chance to be where I am today.

My dear friends, I deeply appreciate your support and insightful advice. Elfriede, Marina and Alexandra, I am glad to have you in my life.

And last but not least, I would like to thank my cat Ace who comforted me during this journey without probably even realising it.

Anna

List of Publications

The thesis is based on the following articles published in peer-reviewed journals:

1) **Detkina, A.;** Peakman, A.; Litskevich, D.; Liang, J.-H.; Merk, B. Evaluation of BWR Burnup Calculations Using Deterministic Lattice Codes SCALE-6.2, WIMS-10A and CASMO5. Energies 2020, 13, 2573. *(Chapter 2)*

2) Atkinson, S.; **Detkina, A.;** Litskevich, D.; Merk, B. A Comparison of Advanced Boiling Water Reactor Simulations between Serpent/CTF and Polaris/DYN3D: Steady State Operational Characteristics and Burnup Evolution. Energies 2021, 14, 838. *(Chapter 3)*

3) **Detkina, A.;** Litskevitch, D.; Peakman, A.; Merk, B. Burnup Credit Evaluation for BWR Spent Fuel from Full Core Calculations. Appl. Sci. 2020, 10, 7549. *(Chapter 4)*

4) **Detkina, A.;** Litskevitch, D.; Peakman, A.; Merk, B. Criticality Analysis for BWR Spent Fuel Based on the Burnup Credit Evaluation from Full Core Simulations. Appl. Sci. 2021, 11, 1498. *(Chapter 5)*

Study 1), 3) and 4) were performed solely by the author except burnup calculations using CASMO5 code from work 1). These calculations were provided by Dr Aiden Peakman from National Nuclear Laboratory, UK.

Study 2) was conducted in collaboration with Dr Seddon Atkinson from the University of Liverpool. My contribution included lattice calculations with Polaris code, nodal calculations with Polaris/DYN3D sequence, evaluation and discussion of the results, delivering own SERPENT results for the cross comparison and quality assurance and writing and editing the manuscript.

The author also contributed to the publications which are not included in the thesis:

1) Merk, B.; **Detkina, A.;** Litskevich, D.; Atkinson, S.; Cartland-Glover, G. The Interplay between Breeding and Thermal Feedback in a Molten Chlorine Fast Reactor. Energies 2020, 13, 1609.

2) Merk, B.; **Detkina, A.;** Atkinson, S.; Litskevich, D.; Cartland-Glover, G. Evaluation of the Breeding Performance of a NaCl-UCl-Based Reactor System. Energies 2019, 12, 3853.

3) Merk, B.; Litskevich, D.; **Detkina, A.;** Cartland-Glover, G.; Atkinson, S.; Bankhead, M. A Zero-power Facility as a Multi-fold Opportunity to Support Quick Progress in Innovative Reactor Developments. Atw 2021, Vol. 66, Issue 3.

4) Davies, S.; Rohde, U.; Litskevich, D.; Merk, B.; Bryce, P.; Levers, A.; **Detkina, A.;** Atkinson, S.; Ravindra, V. CTF and FLOCAL Thermal Hydraulics Validations and Verifications within a Multiscale and Multiphysics Software Development. Energies 2021, 14, 1220.

My contribution to studies 1) and 2) consisted of: supporting the development of Polaris model (creating input files, data management structures, and data evaluation approaches); performing modelling and simulations in Monte Carlo code Serpent for the comparison with Polaris; supporting the data evaluation and interpretation; searching and interpreting the Russian literature for salt compositions and material data. My contribution to study 3) was in: discussing the opportunities of zero-power systems and reviewing the manuscript;

searching and interpreting the Russian literature on molten salt and zero power systems. For study 4) I provided theoretical and practical advice regarding different aspects of the research.

List of Figures

List of Tables

Abbreviations

2D	Two-dimensional
3D	Three-dimensional
ABWR	Advanced boiling water reactor
ADF	Assembly discontinuity factor
ADS	Accelerator driven systems
BEIS	Department for Business, Energy and Industrial Strategy
BoL	Beginning of life
BUC	Burnup credit
BWR	Boiling water reactor
CASL	Consortium for Advanced Simulation of Light Water Reactors
CFD	Computational fluid dynamics
CTF	Cobra-TF
DGR	Deep geological repository
EoL	End of life
ERU	Enriched reprocessed uranium
ESSM	Embedded self-shielding method
FA	Fuel assembly
FFS	Fusion-fission hybrid system
FP	Fission product
GDA	Generic design assessment
IAEA	International atomic energy agency
LWR	Light water reactor
MA	Minor actinide
MC	Monte Carlo
MOC	Method of Characteristics
MOX	Mixed oxide
MSR	Molten salt reactor
NEM	Nodal expansion method
NPP	Nuclear power plant
NURESIM	NUclear REactor SIMulation
P&T	Partitioning and transmutation
PRIS	Power reactor information system
PWR	Pressurised water reactor
RPV	Reactor pressure vessel
SF	Spent fuel
SFR	Sodium-cooled Fast Reactor
SI	Spectral indexes
SPH	Super-homogenisation factors
VVER	Water-water energetic reactor

1. Introduction

Spent fuel (SF) is often viewed as waste and its accumulation as a burden to society [1]. The lack of clear solution for the long-term spent fuel management is considered as one of the reasons for slowing down the nuclear industry growth [2]. Hence, addressing the challenges associated with spent fuel management is an important issue of nuclear power production.

When the nuclear fuel reaches the operational limits, it is removed from the reactor core and placed into the storage pool for cooling. Eventually, SF can be either:

- reprocessed – fissile and fertile materials such as uranium or plutonium are extracted from the irradiated fuel for further reuse in the reactor [3];

- disposed – the spent fuel is thoroughly packed and placed deep underground indefinitely [3];

- directly reused – the spent fuel is placed straight into the new type of reactor without reprocessing [4]; or

- remain in a long-term storage facility such as dry storage, until the final decision is made [1].

The nuclear fuel cycle that uses a final disposal strategy for the spent fuel management is often referred to as the open nuclear fuel cycle or once-through cycle [5]. If the strategy includes reprocessing of fissile materials, the nuclear fuel cycle is called partly closed fuel cycle or twice-through cycle [5]. Reprocessing was thought a preferable option for the spent fuel management at the beginning of the nuclear reactors' development due to the fear of possible shortages of the uranium supply [6]. However, the industry growth was not as rapid as expected and combining with the discovery of new uranium resources, the development of reprocessing technologies has slow downed [6]. Currently, only a few countries have the technology to reprocess the SF and, thus, made it a strategy for the spent fuel management. Other countries adopted an open cycle strategy or both. However, the majority of countries have not reached any decision and adopted a wait and see approach which means that their spent fuel is currently located at the storage facilities.

The strategies of the spent fuel management – final disposal and fissile materials recycling, are used for the reactors up to Generation III+. The Generation IV nuclear reactor design should fulfil the sustainability criteria which implies the effective use of nuclear fuel and minimisation of the produced nuclear waste volume [7]. It can be achieved for example by completely closing the nuclear fuel cycle where both fissile and fissionable materials are recycled in fast reactors. In recent years there has been growing interest in the concept of the Molten Salt Reactor (MSR) operating on non-reprocessed spent fuel [4] as a potential solution to the problem of the spent fuel accumulation from the previous and currently existing reactor generations. As spent fuel will be directly placed into the reactor core, an expensive reprocessing part of the nuclear fuel cycle can be removed. By reusing the spent fuel, the environmental impact from spent fuel accumulation can be reduced. The concept will be analysed in detail in Chapter 6.

According to the UxC estimate [8], in 2018 only 30% of the total 422 000 MT accumulated spent fuel from the commercial nuclear power plants (NPP) has been reprocessed, while the rest remains in storage facilities. The most widespread commercial

NPPs are Light Water Reactors (LWRs) such as Pressurised Water Reactors (PWRs) and Boiling Water Reactors (BWRs) [9]. According to the Power Reactor Information System (PRIS) of the International Atomic Energy Agency (IAEA) [10], BWRs are in the second place of the world nuclear power production with 64 operating NPPs and 65 GW(e) total net electrical capacity.

The LWR design utilises purified normal water as both coolant and neutron moderator. A PWR is a two-circuit system where, in the primary circuit, water in the liquid state at high pressure moves through the reactor core functioning as a coolant and moderator. In the secondary circuit, water at lower pressure boils and converts to steam which drives the turbine for electricity generation. A BWR is a one-circuit system where water at lower pressure boils directly in the reactor core playing a role of a coolant, moderator, and steam generator, simultaneously. The boiling of water in the BWR core leads to the production of a two-phase water/steam mixture at the core's upper part. The key difference between the PWR and BWR reactor types is that bulk boiling is allowed in the core of the latter. The water density is lower at top of the core in both PWR and BWR but far more pronounced in a BWR due to the phase change.

The reduction of the water density at the top of the BWR core results in a lower moderator-to-fuel ratio than in the bottom part. The moderator-to-fuel ratio in BWRs can be defined as the ratio of the water to fuel volumes [11]. The low moderator-to-fuel ratio in the top region of the BWR core can be increased by including several part-length rods in the BWR fuel assembly design [9]. The part-length rods are the regular fuel rods which end at a specific fuel element height [12]. The removal of the upper part of fuel rods leads to the water density increase in the considered region, improving the moderator-to-fuel ratio. Another way to enhance moderation within BWR fuel assembly is to include water rods or channels in the central part of the fuel assembly where the water flows in a liquid form. The water rods can have different shapes such as cylindrical or rectangular depending on the fuel supplier. An example of BWR fuel assembly design is presented in Figure 1.1.
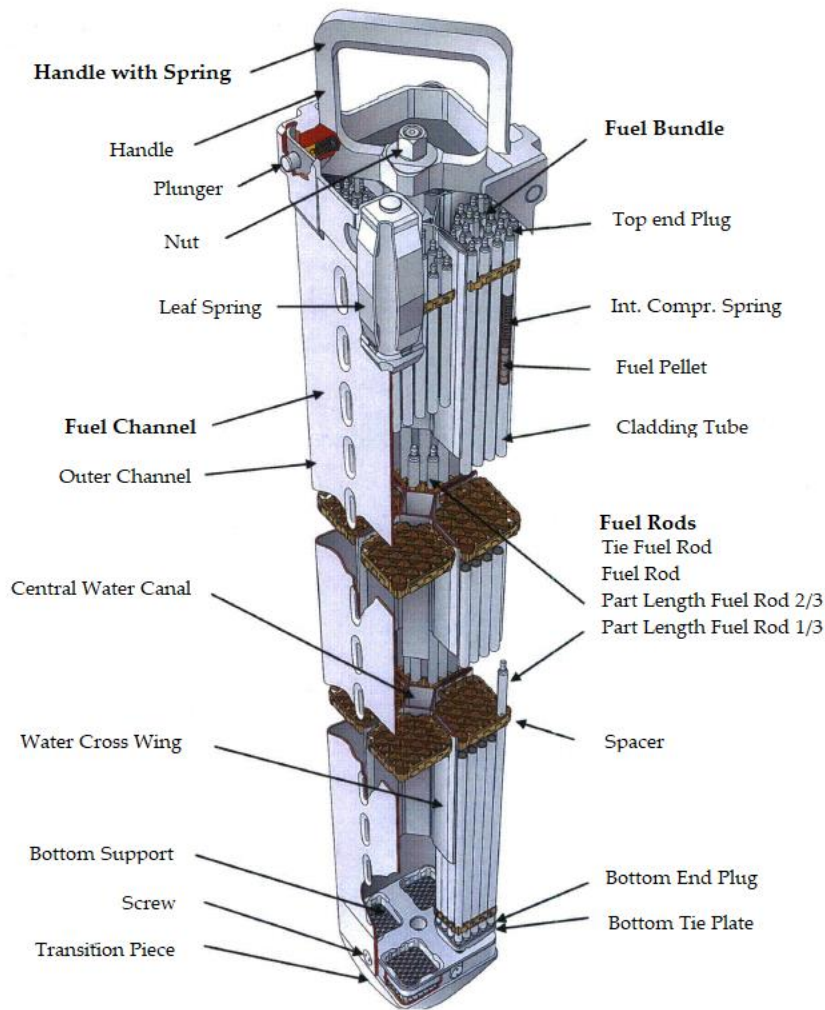
Figure 1.1. BWR SVEA-96 Optima 3 fuel assembly design (courtesy of Westinghouse Electric Company [13])

The reactivity control in BWRs can be carried out by control blades (rods) movements or modifying the coolant flow rate through the core [14]. The latter is achieved by controlling the speed of the recirculation pumps. Generally, control rods in BWRs are used for the reactor shutdown, SCRAM (emergency reactor shutdown) and control of the reactivity and power distribution in the core [15]. BWR has three control rod types [15]:

- safety rods used for the reactor startup or shutdown;

- regulating rods used for fine tuning of the reactor power's rate;

- shim rods used mainly used for larger power regulations and reactivity control.

Safety rods are fully withdrawn during the reactor operation. Shim rods can be inserted by various degrees (from partly to fully) in the reactor core during a considerable part of the operation cycle. The shim rods are used in conjunction with regulating rods which are typically less inserted in the reactor core. The excess core reactivity at the early stages of each operational cycle can also be managed by distributing the burnable absorber Gd_2O_3 in some fuel rods, reducing the initial fuel criticality. This measure helps to reduce the overall number of control blades movements [16]. Commercial BWR fuel assembly design often

includes variable axial and radial U-235 enrichment to flatten the FA power distribution so the fuel can be optimally utilised in the reactor [9]. To sum up, the BWR fuel assembly design is much more challenging than PWR, mainly due to the need to compensate for the non-uniform water density distribution in the reactor core. On the other side, the complexity of BWR fuel assembly design gives the vast opportunity for optimisation and flexibility, which any other existing reactor type cannot achieve. Combined with the upgradeability of the main circulation pumps, it can lead to a potential power uprate of about 10-30% in BWR plants.

As mentioned earlier, a significant proportion of all accumulated spent fuel currently is kept in storage facilities. It is estimated that the amount of spent fuel in storages will rise by approximately 55% in 2035 compared to 2018 levels [8]. Also, the lack of a clear strategy in some countries regarding the final SF management strategy and complications related to the final disposal, put additional pressure on the problem of the spent fuel accumulation. Combining with the rising costs of nuclear energy, it is crucial to minimise the price of SF storage without compromising safety. According to the International Atomic Energy Agency Fundamental Safety Principals [17], to ensure the safe operation of all nuclear facilities, the range of measures should be adopted:

(a) "To control the radiation exposure of people and the release of radioactive material to the environment;

(b) To restrict the likelihood of events that might lead to a loss of control over a nuclear reactor core, nuclear chain reaction, radioactive source or any other source of radiation;

(c) To mitigate the consequences of such events if they were to occur."

The design and operation of the spent fuel storage facilities, in particular, have to meet various safety requirements, such as ensuring confinement of the radioactive materials, maintaining subcriticality and decay heat removal under both normal and accidental conditions [18]. The subcriticality of the spent fuel storage system is assured by performing the criticality safety analysis. The main purpose of the criticality safety analysis is to evaluate the risk or opportunity of a self-sustaining nuclear chain reaction in the systems with fissile materials or to mitigate or control its consequences if the reaction takes place [19]. The criticality safety limits are often set by effective neutron multiplication factor (k_{eff}). The k_{eff} is estimated as the relation between the rates of neutron production and neutron loss occurring in a system [19]. Depending on the k_{eff} value, the system can be subcritical ($k_{eff} < 1$), critical ($k_{eff} = 1$) and supercritical ($k_{eff} > 1$). In other words, when the system with fissile materials is critical, the neutron generation is equal to its loss in the system. A critical system would stay in a continuous operation with a steady neutron population. When the system is subcritical, the neutron generation is less than the loss, and when supercritical, the neutron generation exceeds the loss. Generally, the systems with fissile materials should remain subcritical unless their design is critical on purpose, such as in a reactor core or critical assembly [19]. For example, the Specific Safety Guide SSG-26 [20] on the safe transport of radioactive materials recommends a safety margin of 0.05 for the transport packages, or k_{eff} no more than 0.95, which is used by most countries [21]. Overall, it is the decision of each country's regulator to approve appropriate safety margins for operations with spent fuel.

The criticality safety analysis of the spent fuel storage or transport is often performed under the fresh fuel approach. This approach assumes that the spent fuel has the same

reactivity and isotopic composition as unirradiated fuel without burnable absorber [22]. It makes the estimation of the k_{eff} value significantly conservative, and the required calculation effort is comparably low. The widespread use of the fresh fuel approach comes from historically limited computational power for modelling and simulations and small experimental evidence-base to validate other approaches. The growing volumes of the accumulated LWR spent fuel, and the limited capacity of the existing storage systems pushed the industry and regulators to develop new criticality analysis methods, which can reduce the excessive conservatism of the fresh fuel approach. Hence, the burnup credit (BUC) method, which takes credit for the reactivity reduction of the spent fuel during the irradiation or, in other words, as a result of the fuel burnup, has emerged [22]. The IAEA distinguishes four levels of the burnup credit [23]:

1) net fissile content level;

2) actinide only level;

3) actinide plus fission product level; and

4) integral burnable absorber level.

The burnup credit method at actinide only or actinide plus fission product levels is widely applied to the dry and wet storage and transport of PWR spent fuel in many countries [22]. The burnup credit for BWR spent fuel has been applied on the integral burnable absorber level and mostly for the wet storage up to now.

The application of the burnup credit method generally includes the following steps [24]:

1) the isotopic prediction in 2D lattice physics or other depletion codes;

2) the cask criticality calculations in 3D Monte Carlo codes; and

3) measurements of the spent fuel burnup on-site before specified operations.

The broader validation of the nuclear codes is required for the BUC analysis in comparison with the fresh fuel approach since it should be ensured that the computational tools are robust for burnup calculations as well. In terms of criticality analysis, additional sensitivity and uncertainty analysis should be implemented. Sensitivity analysis defines the change of the system response, for example, k_{eff} for criticality analysis, to a variation of the input parameters such as fuel temperature, enrichment, geometry and so on [25]. Uncertainty analysis identifies and describes the potential sources of the uncertainties arising during modelling and simulations, for example, uncertainties in the cross-section data [25]. The prediction of the spent fuel isotopic inventory is considered as a major possible source of uncertainty in BUC analysis [26]. To sum up, the outlined factors make the burnup credit method more complex than the fresh fuel approach in terms of application and regulation.

Although the potential benefit from the application of the burnup credit method is mostly economic – lowering the costs of spent fuel storage and transport, it can also reduce environmental impact from the spent fuel accumulation. If applied correctly, the BUC method can increase storage casks capacities or decrease the number of neutron absorbing components placed inside the storage casks [22]. Therefore, it can reduce the number of newly built wet or dry spent fuel storage facilities or avoid an extension of existing facilities [22]. Another ecological benefit is the possible reduction of the number of shipments of the

spent fuel casks outside of the nuclear facilities, which can lower the risk of accidents and harmful exposure of the personnel, public and environment to the ionising radiation [22].

As discussed before, a robust isotopic prediction of the spent fuel is an important first step in burnup credit analysis. As BWR fuel assembly design is more complex than PWR, some simplifications of the 2D lattice model may not accurately represent the FA behaviour, leading to the incorrect estimation of the final FA composition. The research [27] outlined that the axial fuel burnup profile and the coolant density distribution substantially impact the cask k_{eff} loaded with BWR spent fuel discharged beyond peak reactivity burnups. In contrast to PWRs, where the core reactivity is mainly controlled by changing the dissolved boron concentration in the water, BWRs rely on the control blades (CB) insertion and pump speed control. The prolonged control blades insertion, for example, results in the hardening of the neutron spectrum near the CB, leading to an increased Pu breeding and reduced consumption of burnable poison hence, increasing the final cask reactivity. The analysis of the control blades histories (both realistic and unrealistic) performed in [27] revealed that the storage cask reactivity is approximately 4.3 % higher for the most conservative control blades history scenario than the entirely removed control blades scenario. Hence, estimating the quality of different modelling approaches for the fuel assembly in the burnup credit analysis is vital to account for all operational and design challenges.

The current study aims to create a burnup credit method that can reflect on the realistic BWR fuel assembly behaviour in the reactor core and compare it to the existing BUC approaches used for BWR fuel and the fresh fuel approach. Considering the difficulties of the BWR modelling described above, the given research focuses on the following main objectives:

1) analysing the reliability of the existing lattice codes for BWR depletion analysis;

2) providing realistic characteristics of BWR spent fuel using data obtained from the nodal full-core analysis;

3) estimating the benefit from the application of burnup credit method with realistic spent fuel characteristics for different storage cask loadings; and

4) defining the limitations and ways to improve the nodal method which is widely used in the industry for the full-core analysis by comparing it with high-fidelity methods.

Besides the objectives outlined above, other options for nuclear waste management will be discussed. Although the thesis aims to apply realistic BWR spent fuel characteristics to the burnup credit method, the core design is rather an accumulation of the open-access data and not a real, operable core design. In addition, a series of simplifications have been made in the reactor core model. For example, it was assumed that control blades were fully removed from the BWR core during the operation. Thus, the so-called all-rods-out (ARO) approach had been implemented. As discussed earlier, this can lead to the underestimation of the effective multiplication factor of the storage cask. In addition, the uncertainties of the ARO approach are assumed to be lower than from the reloading scenarios, for example, which were analysed in the thesis. Moreover, the work presented in the thesis aims to demonstrate the opportunities of the application on the burnup credit method based on the realistic spent fuel characteristics. Hence, the ARO approach is deemed acceptable.

The thesis comprises the following sections:

- Chapter 1 introduces the topic of the research;

- Chapter 2 compares well-known deterministic lattice codes SCALE-6.2 (TRITON module) [25], WIMS-10A [28] and CASMO5 [29] for depletion analysis of BWRs;

- Chapter 3 discusses further validation work by the comparison of the high-fidelity methods for the full-core analysis with the traditional nodal methods;

- Chapter 4 presents the Advanced Boiling Water Reactor (ABWR) core model for steady-state analysis with the DYN3D [30] nodal code and 3D nodal model of BWR fuel assembly with realistic parameters. It also outlines the effect of different reloading patterns on the burnup distribution of discharged BWR fuel assemblies;

- Chapter 5 investigates the impact of the: reloading pattern; target discharged burnup; and change of the FA type on the burnup credit based on two distinct loadings of a storage cask;

- Chapter 6 examines the use of Molten Salt Reactors (MSRs) as a possible alternative way of dealing with LWR spent fuel;

- Chapter 7 presents the thesis conclusions;

- Chapter 8 discusses possible future work.

2. Lattice codes evaluation for BWR burnup analysis

The quality of the tools for isotopic prediction in depletion calculations plays an important role in the application of the burnup credit method. Incorrect estimation of the spent fuel composition can lead to under- or over-prediction of the criticality of the storage system with spent fuel. Both outcomes are undesirable since in the first case it can lead to a reduction in the safety margins which can potentially result in a criticality accident in the worst-case scenario. In the second case, it can lead to excessive and costly safety measures which would not be required otherwise. The isotopic composition can be estimated by performing burnup calculations for 2D slices of fuel assembly in lattice physics codes. The lattice codes are generally used for the cross-section data production for the reactor core analysis in nodal codes under steady-state or transient operational conditions [31]. Thus, a comprehensive evaluation of lattice codes is necessary as for the robust simulations of the reactor core as well as for the reliable estimation of the isotopic composition of spent fuel.

The validation of nuclear codes can be performed by comparing the computational results either to experimental results or to other well-validated codes, with the latter referred to as cross-verification. The cross-verification allows to compare computational results of the code of interest to the validated code without performing expensive experiments. The first part of the research compares three lattice codes: 1) TRITON module of SCALE-6.2 package (SCALE/TRITON), 2) WIMS-10A and 3) CASMO5, which can be potentially used for the isotopic prediction and preparation of the nodal cross-section data for further reactor core analysis. The comprehensive description of the utilised codes will be described later on. The CASMO5 code was considered a well-validated industry-standard tool for lattice calculations. Thus, an additional comparison with the Monte Carlo code which is normally performed in the validation of the lattice code was not included in this study to stay compatible with industrial standard. CASMO5 has been extensively benchmarked against critical experiments, continuous energy Monte Carlo calculations, etc [29, 32, 33] and has been used extensively for reactor operation sumlaition through a large number of consecutive cycles.

The LWR fuel assembly consists of series of fuel rods bundled together into a grid-like structure. Generally, the area around each fuel rod forms a so-called unit cell or pin-cell which includes fuel rod, fuel cladding and surrounding water. In the case of BWRs, the pin-cell has a square shape. Figure 2.1 represents a typical BWR pin-cell.
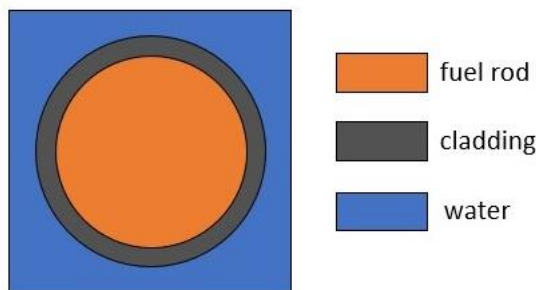
Figure 2.1. BWR pin-cell example

The comparison of the codes was performed using two simplified BWR models: 1) a UO_2 pin-cell and 2) 3 by 3 array of UO_2 fuel rods with gadolinia rod in the centre. The study included infinite multiplication factor estimation for all listed codes with further in-depth

analysis of SCALE/TRITON and WIMS-10A as SCALE/TRITON and CASMO5 produced close results and, thus, are already cross-verified against each other. The discrepancy between SCALE/TRITON and WIMS-10A reached 1600 pcm for the model with gadolinia poison rod. In-depth investigation of the large discrepancy between WIMS-10A and SCALE/Triton codes consisted of a comparison of spectral indexes, isotopic composition and neutron spectra produced by each code. The biggest differences were found in the U-235 and Pu-239 concentrations and for U-238, Pu-240 and Pu-242 fission cross-sections. The neutron spectrums obtained with both codes were in good agreement with each other.

Considering, that the SCALE/Triton results were close to CASMO5, the SCALE code system was chosen for cross-section data generation and isotopic prediction for further burnup credit analysis. It should be noted that shortly after the study has been finished, the developers of WIMS-10A code issued a warning for users regarding an error in a nuclear data library used in the given research. Since a rather high discrepancy has been already observed between WIMS-10A and SCALE/Triton and CASMO5 on a pin level, further investigation of the full-scale BWR fuel assembly model was considered unnecessary at this point. The study outcome has been published in Energies – a peer-reviewed open access journal, and is presented in subsection 2.2.

Article

Evaluation of BWR Burnup Calculations Using Deterministic Lattice Codes SCALE-6.2, WIMS-10A and CASMO5

Anna Detkina [1,*], Aiden Peakman [2], Dzianis Litskevich [1], Jenq-Horng Liang [3] and Bruno Merk [1]

[1] School of Engineering, University of Liverpool, Liverpool, L69 3GH, United Kingdom; d.litskevich@liverpool.ac.uk (D.L.); b.merk@liverpool.ac.uk (B.M.)
[2] National Nuclear Laboratory, Chadwick House, Warrington, WA3 6AE, United Kingdom; aiden.w.peakman@uknnl.com
[3] Institute of Nuclear Engineering and Science, National Tsing Hua University, Hsinchu 30013, Taiwan, Republic of China; jhliang@ess.nthu.edu.tw
* Correspondence: a.detkina@liverpool.ac.uk

Abstract: The UK nuclear innovation programme supported by the government includes preparation for future ABWR construction. The UK has significant expertise in building and operating gas-cooled nuclear reactors and some experience with PWRs, while there is limited knowledge in BWR technologies. Hence, an important aim of this work is to understand the discrepancies between codes to assess uncertainties in BWR lattice and depletion calculations, while identifying specific development demands to progress existing tools into extended applications. The objective of the study is to quantify the discrepancy between SCALE-6.2, CASMO5 and the UK WIMS-10A deterministic lattice code for BWR lattice and burnup modelling. Two models of BWR systems were considered for this new systematic comparison. They are a single BWR pin-cell with UO_2 fuel only, and a 3 by 3 array of BWR UO_2 fuel rods with gadolinia rod in the centre. Criticality over burnup was estimated for both models using these codes. Spectral indexes, number densities and neutron spectrum were compared for several burnup stages using SCALE-6.2 and WIMS-10A. The study showed that k_{inf} obtained with CASMO5 was in a good agreement with the SCALE-6.2. A clear discrepancy in behaviour was observed between WIMS-10A and SCALE-6.2 as well as CASMO5.

Keywords: nuclear fuel; burnup credit; BWR; SCALE-6.2; WIMS-10A; CASMO5; codes comparison; lattice computations

2.1. Introduction

The increasing levels of Light Water Reactor (LWR) spent fuel (SF) and the requirement of the dry storage of SF for long term interim storage have resulted in industry exploring the potential of application of the burnup credit method (BUC) to Pressurized Water Reactor (PWR) and Boiling Water Reactor (BWR) SF. BWRs are of particular interest since they are widely deployed internationally, but their fuel characteristics are studied less than PWRs due to complexity of the modelling associated with their highly heterogeneous fuel assemblies, as well as core arrangements known for BWR [1,2]. This has been recently confirmed for an advanced BWR in [3] with a published core design which had input (and was reviewed) by experts in reactor physics at HITACHI. The fuel assembly and core complexities not only reflect reactor operation but also into the following handling of the

spent fuel. Even if BWR fuel is less reactive and, thus, does not bring the same criticality safety concerns in relation to the BUC as PWR, the topic has gained significant traction in the last years [1,2].

Historically, the criticality safety analysis of SF dry storage facilities was performed with methods which treated SF in the system as fresh fuel without burnable poison—the so-called fresh fuel approach. This approach is considered to be highly conservative, and significantly overestimates the calculated reactivity of the cask filled with SF [2] as long as no burnable poison is apparent in the fuel. BUC tends to utilize realistic spent fuel characteristics and considers the depletion of fissile materials, as well as burnable poisons in the fuel assemblies during the reactor operation. For the fuel discharged at the targeted burnup, the application of BUC results in a reduction in the estimated reactivity of the system with SF when compared with an approach based on the assumption that the fuel is fresh. As was pointed out in [4], experimental measuring of the spent fuel reactivity is not convenient for BUC application; thus, it has to be demonstrated that the employed computational tools deliver robust results. To summarise, with the development of BUC, the capacity of the SF storage facilities can be expanded without affecting the safety margins by just relying on a more sophisticated modelling approach removing unnecessary conservative processes.

In the past few years, a number of studies were performed regarding the burnup credit method application to BWR spent fuel storage and transport. In [2], the computational benchmark was developed to explore the influence of fission products and minor actinides on reactivity in burnup credit calculations in comparison with those which use major actinides only. The study showed that reactivity in burnup calculations reduces by 70% due to major actinides, and by 30% due to additional nuclides. The application of the peak reactivity method to the transport and storage of BWR spent fuel was extensively investigated in [5]. Various parameters and modelling approaches were considered to determine their impact on peak reactivity. The study showed that void fraction and control blade insertion/position has the strongest influence, while other parameters such as fuel temperature or operation history have only a minor effect. The report [6] covers the effect of various axial moderator density distributions, control blade usage, and axial burnup distributions on BWR BUC beyond peak reactivity (for burnups 30–50 GWd/tU). The study showed that changes in axial moderator density and burnup profiles significantly affect the final storage cask reactivity, while the effect of control blade usage is not as large as was initially assumed.

As described above, the important part of developing BUC is a deep understanding of the fuel assembly behaviour in the reactor core over the burnup, as well as their robust modelling. The modern industrial modelling and simulation approach of steady state and transient modelling of the reactor core operations has two stages, which include the use of lattice and nodal codes. Nodal codes represent a reactor core as a set of homogenous coarse grid elements called nodes. Each node has homogenized, constant nuclear properties such as diffusion coefficient and material cross-sections. The nodal approach also does not reflect any geometric details of the fuel assembly such as fuel rods or control blades. This information has to be brought into the input constants based on higher-quality detailed modelling. In the applied sequence, lattice codes are used to prepare cross-section sets for each node providing multi-group transport informed constants as an input library. Fuel

assemblies consist of a lattice of fuel rods in the radial direction, which is represented in a two-dimensional unstructured mesh which is the currently used industrial standard, while the axial layers of an assembly with unique fuel characteristics, such as enrichment or design, are represented in the nodal core simulator. In the cross section matrix for the core simulator, the sets of condensed and homogenized constants are usually reduced to two groups for LWRs simulations from the multi-group flux distribution delivering the fast and thermal energy group [7]. After cross-section sets are generated in 2D lattice code, they are transferred to 3D nodal code where the reactor core is modelled as coupled neutronics and thermal-hydraulics system. This approach is widely used across the industry and is considered to be an optimum in terms of minimizing computational burden whilst maintaining sufficient accuracy. The quality of cross-section sets prepared in lattice codes directly affects the accuracy of the reactor core simulation results. Thus, for the future application of the UK code system WIMS to a future reactor system ABWR, it is essential to evaluate the quality of the lattice calculation as a first step for the robust BWR modelling and simulation.

The current study is used to investigate the quality and level of discrepancy between various deterministic lattice codes for burnup calculations, to evaluate the quality of the foreseen UK code system for the application to BWRs. The evaluation of different codes also supports the confidence into its quality for the cross-section preparation and, consequently, the following nodal analysis. The well-known lattice and burnup code system SCALE-6.2 [8] and the independent industrial standard code CASMO5 [9] are used to evaluate the quality of the WIMS-10A code [10] to answer the question 'Can WIMS be directly used for the modelling and simulation of future BWR reactors or is there some demand for upgrading of models to provide robust results?'. The answer to this question will provide guidance for further investment requests within the nuclear innovation programme of the Department for Business, Energy and Industrial Strategy [11].

Lattice code analysis is performed for two infinite BWR reactor systems, containing either a single UO_2 fuel rod (pin-cell) or a 3 by 3 array of 8 UO_2 fuel rods and a gadolinia-poisoned rod in the centre. The Gd-poisoned fuel rod is surrounded by uranium fuel rods to appropriately estimate its characteristics over the burnup.

Infinite multiplication factors calculated with SCALE-6.2 and WIMS-10A for burnups up to 57.5 GWd/tU were compared with each other and with the industrial standard code CASMO5. The limit of the burnup was chosen as the licensed maximum assembly average burnup of 55 GWd/tU [12] plus a safety gap. Deeper analysis, such as spectral indexes and number densities estimation, was performed using SCALE-6.2 to compare with WIMS-10A results, to deeper investigate the effect of the discrepancies on follow up nodal calculations and to evaluate the quality of the results and possible sources of discrepancies in detail.

2.2. Code Descriptions

Burnup calculations were performed using the deterministic lattice codes CASMO5, SCALE-6.2 and WIMS-10A. SCALE-6.2 is a modelling and simulation tool developed by the Oak Ridge Nuclear Laboratory (ORNL, USA) for criticality analysis, reactor and lattice physics calculations, and sensitivity and uncertainty analysis [8]. Multigroup (MG) neutron libraries based on ENDF/B-VII.0 and ENDF/B-VII.1 nuclear data libraries were used in the calculations. They have 238 and 252 energy group structure, respectively, and will be

referred to as v7_238 and v7_252. Burnup calculations were performed with the TRITON module of SCALE-6.2. TRITON uses 2D NEWT module for the transport calculations and ORIGEN, for depletion analysis. The NEWT transport solver is based on the discrete ordinates method (S_N) on unstructured mesh. The S_N order was set to 6 in the current calculations.

WIMS-10A is a long term existing code for cell and lattice calculations for a broad range of reactor types, which has been developed and is currently upgraded by Wood plc, and their predecessors in the UK [10]. The MG neutron library is based on ENDF/B-VII.0 nuclear data. The improved decay data from ENDF/B-VII.1 library version were used in the calculations. WIMS-10A utilizes 172 energy group scheme. WIMS-10A performs transport calculations in 2D using the CACTUS module which implements Method of Characteristics (MOC), while burnup analysis is made in a BURNUP module.

CASMO5 is a lattice physics code for PWR and BWR fuel modelling [9] developed by Studsvik Scandpower. The code is based on the proprietary E7R0LIB neutron library with 586 energy groups which is used for the calculations of the BWR pin-cell. While for the 3 by 3 array with gadolinia model, the same library was used with the number of groups condensed to 19 [13] in the second step of the calculation. The CASMO5 transport solver is based on Method of Characteristics. The commercial version of CASMO5 was used for this research.

2.3. Model Descriptions for BWR Burnup Calculations

As already described, two models were created for the burnup calculations in application to BWR systems. The first one is a modern BWR pin-cell with a 4% enriched uranium dioxide fuel rod. The second is a hypothetical 3 by 3 array containing 8 BWR UO_2 fuel rods and one central rod with UO_2 mixed with gadolinia. In both cases, the depletion calculations were performed under a constant power assumption.

2.3.1. BWR Pin-Cell Model

The pin-cell of a BWR GE14 assembly containing UO_2 fuel rod was chosen for the first level of code comparison. A comprehensive description of its characteristics is provided in [2]. Table 2.1 shows geometrical and operational parameters used in the simulations. Figure 2.2 displays the SCALE-6.2 model of the BWR pin-cell which consists of fuel, clad and moderator. Reflective boundary conditions were applied to the system.

Table 2.1. BWR pin-cell parameters.

Parameter	Data
Fuel radius, cm	0.447
Natural Zr clad radius, cm	0.513
Pitch step, cm	1.295
Fuel temperature, K	900
Natural Zr clad and moderator temperature, K	600
Fuel enrichment, wt %	4
Fuel density, g/cm^3	10.5216
Moderator density, g/cm^3	0.6
Average power density, W/g	40
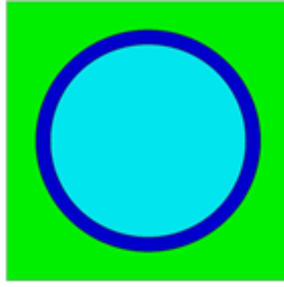
Figure 2.2. SCALE-6.2 model of BWR pin-cell.

2.3.2. BWR 3 by 3 Array Model with Gadolinia

The burnup calculations for a system containing burnable poison were evaluated based on an artificial BWR 3 by 3 array model with 8 UO_2 fuel rods and one gadolinia containing fuel rod in the centre as shown on Figure 2.3. The UO_2 fuel rods have the same specification as for BWR pin-cell case described in 3.1. The central poisoned rod consists of 4% UO_2 fuel with 5% of Gd_2O_3 burnable absorber. It has the same geometrical and temperature parameters as UO_2 fuel rod (Table 2.1). $(U,Gd)O_2$ fuel density is 10.24 g/cm^3. Figure 2.3 displays the BWR 3 by 3 array model created in SCALE-6.2 with the additional discretization introduced into the $(U,Gd)O_2$ fuel rod. Discretization was introduced to capture the so called "onion-skin" effect [7] in a Gd-poisoned fuel rod. This effect occurs since gadolinia isotopes have a large absorption cross-section which leads to the instant absorption of thermal neutrons entering the surface of the rod. It causes the Gd-poisoned rod to deplete by layers [7]. Hence, to model this effect, the $(U,Gd)O_2$ fuel rod was divided into 10 annular regions of equal area. Again, reflective boundary conditions were applied to the model.
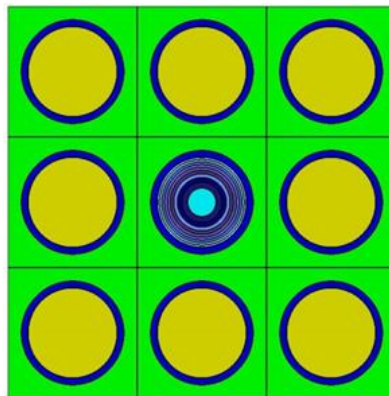
Figure 2.3. SCALE-6.2 model of BWR 3 by 3 array with Gd-poisoned rod in the centre.

2.3.3. Meshing

The spatial discretization of the cell in burnup calculations in deterministic codes is necessary to produce reliable results. The research in [14] outlines that the difference between k_{inf} in LWR-burnup calculations can vary from −400 to +400 pcm for the basic (3 regions) and reference (328 regions) discretization cases.

In the current research, the standard CASMO5 settings have been used for depletion calculations for both models. CASMO5 is well validated for BWR and PWR cases [9] and has

been used, in conjunction with the nodal code SIMULATE, for modelling ABWR nuclear reactor cores [3]. Sensitivity studies were performed in WIMS-10A to optimize the number of tracks used in the method of characteristics solution scheme and meshing. This resulted in 9 polar and 17 azimuthal angles used in the WIMS calculation with the XFINE and YFINE options also enabled in the WIMS-10A to subdivide each unit cell of the problem into 100 equi-volumes to increase fidelity. Sensitivity analysis in SCALE 6.2 showed that 16 by 16 grid (Figure 2.4) for the pin-cell is enough to produce accurate results. Furthermore, like in the SCALE-6.2 calculation, the UO_2 rods were modelled as a single material region in WIMS-10A, but the UO_2-Gd_2O_3 rods were subdivided into 10 equi-volume materials.
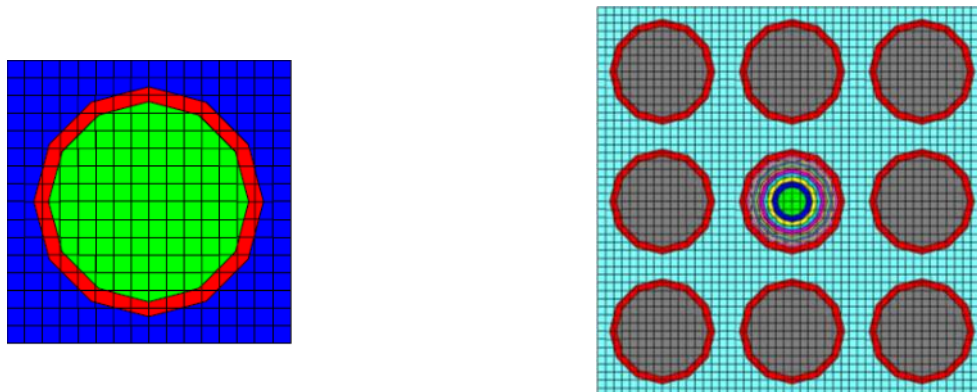
Figure 2.4. Mesh grid used in SCALE-6.2 for BWR pin-cell (**left**) and BWR 3 by 3 array with gadolinia rod (**right**) models.

2.4. Results and discussion

2.4.1. Infinite Multiplication Factor

The infinite multiplication factor (k_{inf}) for both models was calculated from 0 to 57.5 GWd/tU range of burnup. CASMO5 and WIMS-10A results were compared against SCALE-6.2 with ENDF-VII.1 library. The discrepancy in k_{inf} between codes was defined as:

$$d = \frac{\left(k_i - k_{SCALEv7_{252}}\right)}{k_i k_{SCALEv7_{252}}} \times 10^5 \qquad (1)$$

where d is the discrepancy between code i and SCALE-6.2 code in pcm; $k_{SCALEv7\_252}$ is the k_{inf} calculated with SCALE-6.2 (v7_252); k_i is the k_{inf} calculated with code i; i is one of the considered codes CASMO5, WIMS-10A or SCALE-6.2 (v7-238).

Figure 2.5 (left) shows the discrepancy in k_{inf} for BWR pin-cell model obtained using the SCALE-6.2 (v7-238), WIMS-10A and CASMO5 codes in relation to SCALE-6.2 (v7-252). It can be seen that results obtained using CASMO5 are in good agreement with SCALE-6.2 and v7_252 library, which gives an independent evaluation of the quality of the used reference code. The discrepancy between SCALE-6.2 (v7_252 library) and CASMO5 codes lies in the interval from −30 to +140 pcm. The infinite multiplication factor calculated by SCALE-6.2 with v7_238 library has a negative bias of around 300 pcm from SCALE-6.2 (v7_252 library), with discrepancy lying in the interval from -170 to -330 pcm. This bias is obviously caused by the usage of the somewhat older nuclear data libraries which have also slightly different energy structure, since the used solver is identical for these two cases. WIMS-10A and SCALE-6.2 (v7_252 library) comparison showed that the discrepancy between codes

systematically increases with burnup and lies in the interval from −850 to 270 pcm, with a clear negative gradient over the whole burnup period.

Figure 2.5 (right) gives information about the discrepancy in k_{inf} between the considered codes for BWR 3 by 3 array with one gadolinia rod. In this much more challenging case, larger differences are observed. According to the results, there is an initial bias between SCALE-6.2 (v7_238), CASMO5 and SCALE-6.2 (v7_252) k_{inf}, which is equal to -110 and 230 pcm, respectively. The discrepancy between given codes over burnup lies in the intervals from -325 to -110 pcm (v7_238 library) and from 160 to 280 pcm (CASMO5). Thus, it can be considered that SCALE-6.2 and CASMO5 codes are also in good agreement with each other for the much more challenging systems with burnable absorbers. As for the BWR pin-cell model, a large discrepancy has been observed between WIMS-10A and SCALE-6.2 results. It varies from −1600 to 200 pcm for v7_252 library of SCALE-6.2 and increases with burnup and requires some further, in depth investigation. In this second case, the discrepancy for the WIMS-10A code once more grows with a strong negative gradient. Figure 2.5 also shows that the discrepancy in k_{inf} between WIMS-10A and SCALE-6.2 significantly increases for the case with the burnable absorber which is more challenging for the solver. Consequently, these large discrepancies will propagate through the cross section set into the core simulator and can lead to shifts in the moderator density and burnup profiles in the full core analysis, which will affect the spread of the burnup distribution over the reactor core.

The university available, SCALE-6.2 and CASMO5 standard codes indicated a very good agreement in k_{inf}, so an investigation between WIMS-10A and SCALE-6.2 was performed for the following sections.

Moderator density in the BWR reactor core varies significantly in terms of distance from the bottom of the core as it can be seen in Figure 2.6. Thus, it is necessary to identify the impact of the moderator density on the level of discrepancy between codes. Burnup calculations for the BWR pin-cell model with several typical moderator densities such as 0.2, 0.3, 0.4 and 0.6 g/cm^3 were performed in the follow up analysis. Figure 2.7 shows that the level of discrepancy between SCALE-6.2 and WIMS-10A increases slightly when the moderator density decreases. This means that for higher density configurations, closer to PWR operation conditions, WIMS-10A performs better than for lower density BWRs. However, all considered cases show the same tendency of a clear negative gradient which is much stronger than the effect of the water density changes. Thus, the water density variation does not have a significant effect on the systematic character of the discrepancy occurring over burnup. In this case, the typically considered challenge of BWRs, the wide spread of the water density and the resulting massive change in the criticality of the fuel assemblies are captured by both codes very well.
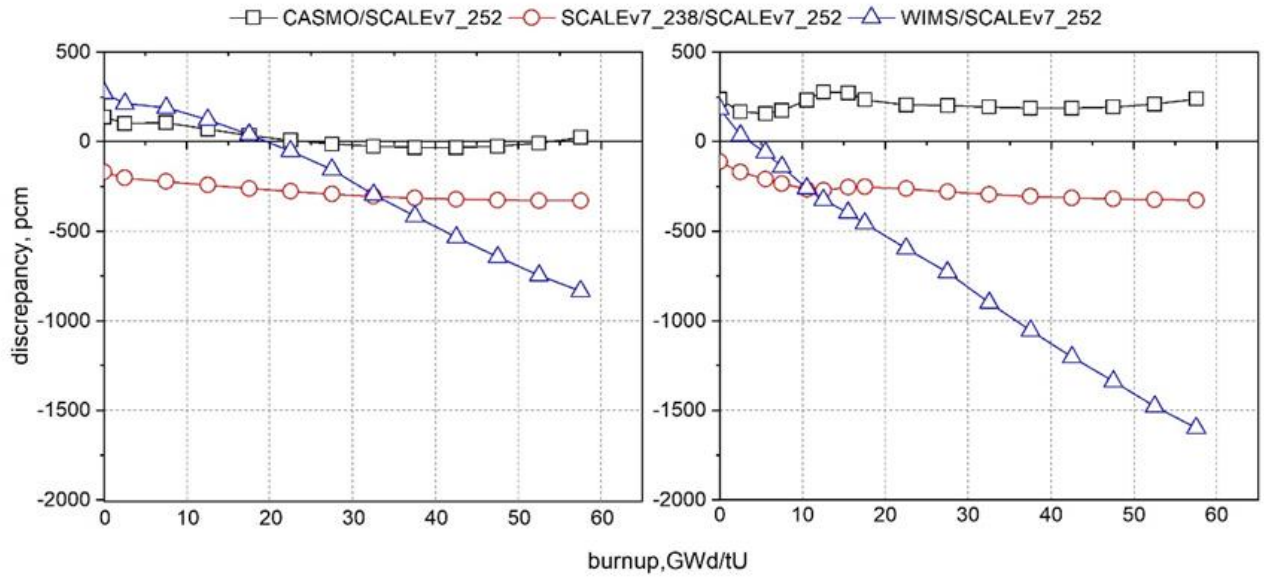
Figure 2.5. Difference in k_{inf} between SCALE-6.2, WIMS-10A and CASMO5 as a function of burnup for BWR pin-cell (**left**) and BWR 3 by 3 array with gadolinia rod (**right**) models.
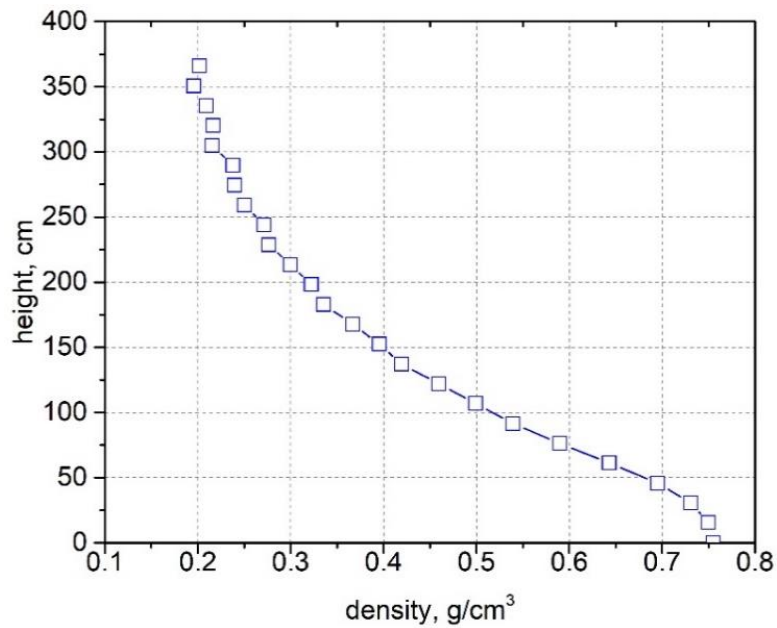
Figure 2.6. Moderator density profile in BWR reactor core.
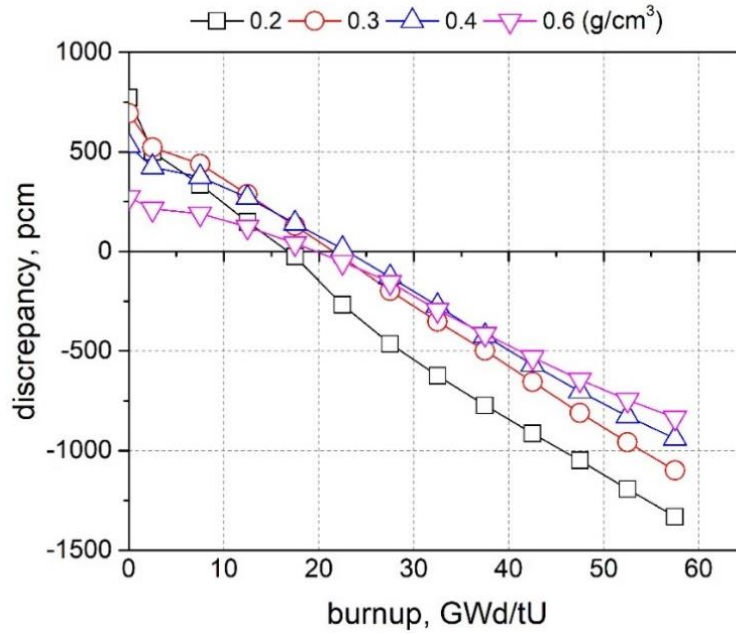
Figure 2.7. Difference in k_{inf} between SCALE-6.2 and WIMS-10A codes as a function of burnup for various moderator densities for BWR pin-cell model.

We consider SCALE-6.2 as a reference solution for the further steps of our analysis since it is the currently used university standard tool. It is obvious that there is a good agreement between the industry standard code CASMO-5 and SCALE-6.2. In addition, the code is very well validated for different types of light water reactors and for burnup calculations against Monte-Carlo solutions as given in the user manual [8] and in an extensive report [15] as well as against experimental data published in Nuclear Engineering and Design [16].

2.4.2. Spectral Indexes Method

Spectral indexes (SI) are a method often used in the dosimetry and experimental analysis to get a deeper insight into the differences between model and experiment [17] without taking too much weight into the absolute value of specific reaction rates. SI is described as a ratio between averaged over the same spectrum cross-sections of the isotope of interest and reference one [18]. The method helps to reduce the effect of systematic biases, e.g., in the cross section set, and is often used for code quality and nuclear data library assessment. We will follow the idea of the SI method to identify the specific differences of the reaction rates produced by the different lattice codes to judge the consequence on the full core simulations. In [17], spectral index was defined as the ratio of two microscopic fission cross-sections averaged over the same neutron distribution:

$$SI = \frac{\bar{\sigma}^i}{\bar{\sigma}^r} = \frac{\int_E \sigma^i(E)\varphi(E)dE}{\int_E \sigma^r(E)\varphi(E)dE} \tag{2}$$

where i and r are the isotopes of interest and the reference one respectively; $\acute{\sigma}^i$ and $\acute{\sigma}^r$ are averaged microscopic cross-sections of the isotope i and r, respectively; σ^i and σ^r are microscopic cross-sections of the isotope i and r respectively; φ is the neutron flux; E is an energy.

Since the depletion calculations were performed under a constant power approach, the neutron flux estimated by each code is not necessarily identical. Hence, the averaged

microscopic cross-sections cannot be used for the SI evaluation since they contain integrated neutron flux in the denominator which will not necessarily cancel out in (2). For the current study, we will define SI through the ratio of reaction rates between the reference isotope and the isotope of interest as:

$$SI = \frac{\int_E \Sigma^i(E)\varphi(E)dE}{\int_E \Sigma^r(E)\varphi(E)dE} \qquad (3)$$

where Σ^i and Σ^r are macroscopic cross-sections of the isotope i and r, respectively.

The analysis was performed for SCALE-6.2 and WIMS-10A codes. SI were estimated for the both models over total neutron spectrum for fission cross-sections of:

U-238 to U-235 or F28/F25;

Pu-239 to U-235 (F39/F25);

Pu-240 to Pu-239 (F40/F39);

Pu-241 to Pu-239 (F41/F39);

Pu-242 to Pu-239 (F42/F39).

The difference between spectral indexes was calculated as:

$$d_{SI} = \left(\frac{SI_{WIMS}}{SI_{SCALE}} - 1\right) \times 100\%, \qquad (4)$$

where SI$_{WIMS}$(SI$_{SCALE}$) is the spectral index obtained with WIMS-10A and SCALE-6.2, respectively.

Figure 2.8 depicts the difference between the spectral indexes obtained using WIMS-10A and SCALE-6.2 codes and calculated for both considered models. It should be noted that for both models, U-238 and Pu-240 fission cross-sections are overestimated by WIMS-10A in comparison with SCALE-6.2, while for Pu-242 the cross-sections are underestimated. For the BWR pin-cell model the difference in the F40/F39 spectral index varies from 1.8% to 3.7%, for the F28/F25, from 0.4% to 1.5% and for the F42/F39, from −1.9% to 0.2%. For the BWR 3 by 3 array model, the difference in the F40/F39, F28/F25 and the F42/F39 spectral indexes gradually rises as burnup and varies from 2.3% to 3.3%, 0.5% to 2% and −1.5% to 0.4% respectively.

The difference in the F39/F25 spectral index rises with burnup in both models and varies roughly from −0.7% to 0.4%, while for the F41/F39 spectral index it has an opposite trend, and lies in the interval from approximately −0.4% to 0.4% for both models.

It should be noted that adding burnable poison to the system does not affect the main trends in spectral index difference as a function of burnup when compared to the UO$_2$ fuel-containing system. Besides, the effect of the burnable poison is limited to the initial phase up to ~20 GWd/tU until the major part of the burnable poison is diminished. At this phase, Gd is competing in absorbing neutrons which affects Pu-239 accumulation and in addition the destruction of Pu-239 through the neutron absorption, leading to a reduced buildup of all higher plutonium isotopes. In the short term, it suppressed the deep in F39/F25 SI at the burnup 5 GWd/tU and, in the long term, decreased the difference between codes for this SI. Furthermore, in contrast with other SIs, F41/F39 sees almost no change for the model with burnable absorber in comparison with UO$_2$ only.

The effect of spectral index discrepancy depends on the amount of isotopes appearing in the system. For example, inaccurate prediction of the Pu-240 fission cross section will lead to the incorrect estimation of its content, which will influence the capture reactions and thus the accumulation of isotopes along the breeding chain will not be preserved. It can significantly impact the final isotopic concentrations and the criticality of the spent fuel, especially in the case of modern high burnup fuel.
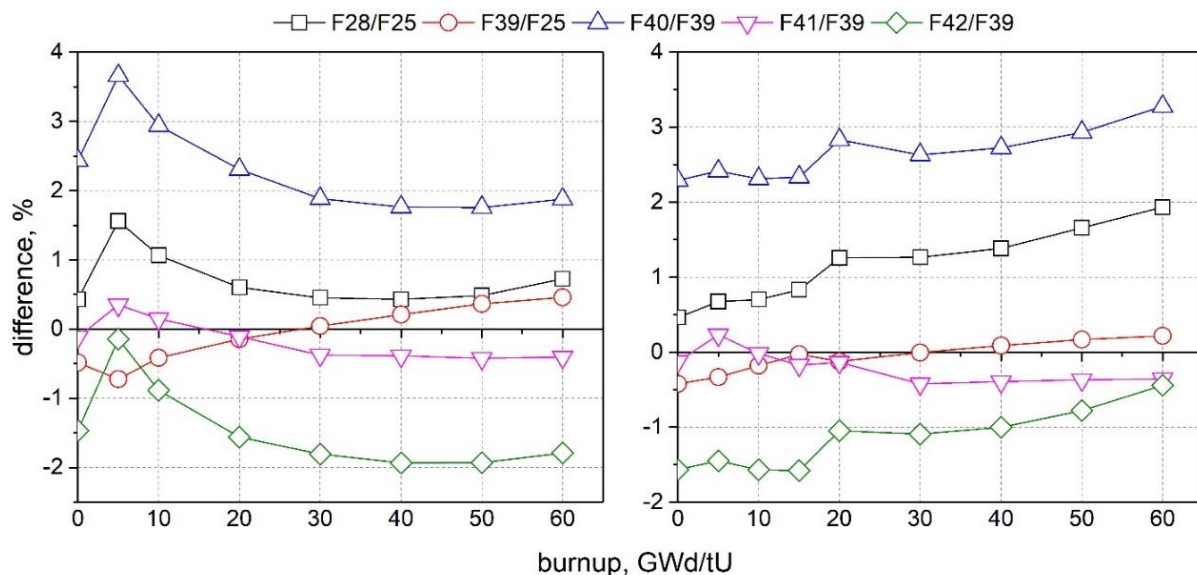
Figure 2.8. Difference in % between spectral indexes obtained with the WIMS-10A and SCALE-6.2 codes for the BWR pin-cell (**right**) and BWR 3 by 3 array (**left**) models.

2.4.3. Isotopic Composition

The number densities of several main actinides for both models were calculated at the same set of burnup points using the SCALE-6.2 and WIMS-10A codes with Gd-155 for the BWR 3 by 3 array model. The difference between the number densities as a function of burnup for both models is shown in Figure 2.9. It was estimated as a subtraction of SCALE-6.2 number densities from WIMS-10A ones at every burnup point of interest.

Already at first glance, it is clear that in both cases the two leading fissile isotopes U-235 and Pu-239 show different trends, with the Pu-239 content lower through the whole burnup period and the U-235 content lower after a short initial peak. This can partly explain the observed differences in the infinite multiplication factor. The trend to the increasing negative discrepancy correlates to a slightly lower amount of the main fissile isotopes. However, it would be unwise to claim here that the burnup model has deficiencies, since the formation and destruction of the leading Pu isotope 239 is a complex balance between power, isotopic composition, capture cross sections, neutron flux and neutron spectrum. All these parameters can be easily influenced by other parameters, e.g., discretization and/or self-shielding [14].

The difference in number densities between WIMS-10A and SCALE-6.2 behaves similarly for U-235, Pu-240 and Pu-241 nuclides in both models. The behaviour changes for Pu-239 nuclide when instead of decreasing, the difference after 30 GWd/tU as in case of BWR pin-cell, it starts to gradually decrease slightly for the BWR 3 by 3 array model.

From initial time and up to 15 (10) GWd/tU in the case of the BWR pin-cell (3 by 3 array), U-235 is consumed more slowly in WIMS-10A than in SCALE-6.2; however, at around 30 GWd/tU the trend changes to the opposite effect and U-235 is being consumed faster.

As for the Pu-239 and Pu-241 isotopes, they accumulate constantly slower in WIMS-10A (underestimation) for both the pin-cell and 3 by 3 array models, while Pu-240 starts to build up faster from roughly 30 GWd/tU burnup.

Overall, the difference in U-235 number densities in WIMS-10A and SCALE-6.2 is almost twice as small for the model with the burnable absorber for burnups up to 20 GWd/tU. It can be related to the high absorption of neutrons by Gd at the beginning of the assembly life, which leads to a reduction in the thermal neutron flux and to the lower depletion of U-235 and, hence, a difference in the number densities.

As was mentioned in [2], 70% of the reactivity reduction in the storage cask system with BWR spent fuel comes from major actinides. Hence, it is important to have a reliable, robust estimate of their number densities for the high target burnups. The given results show that for fuel assemblies with typically discharged burnups (40–50 GWd/tU), the difference in number densities between SCALE-6.2 and WIMS-10A for major actinides becomes significant in both cases. For example, number densities for Pu-239 differ by around 1.5% at the EoL in the case of BWR pin-cells. This would account to a 180 pcm difference in k_{inf}, while the change in number densities of the other observed isotopes would account for the additional 150 pcm.
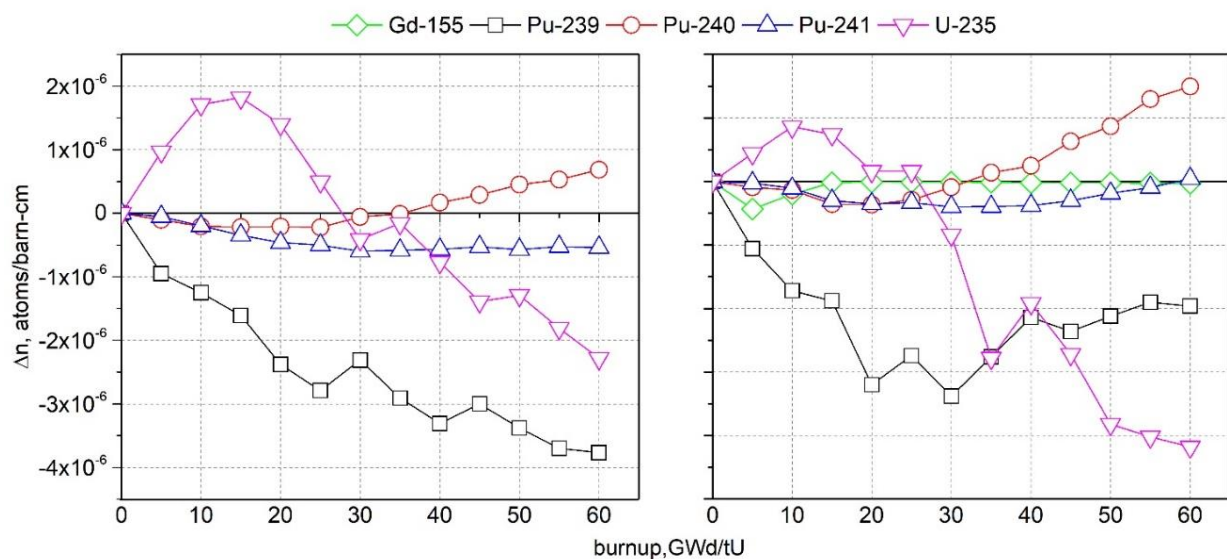
Figure 2.9. Difference in number densities for several nuclides obtained with the WIMS-10A and SCALE-6.2 codes for the BWR pin-cell (**left**) and BWR 3 by 3 array (**right**) models.

2.4.4. Neutron Spectrum

The neutron spectrum in the form of neutron flux per unit lethargy was investigated in the SCALE-6.2 and WIMS-10A codes for both the BWR pin-cell and BWR 3 by 3 array models. Figures 2.10 and 2.11 present the flux over energy distribution obtained in both codes for two burnup points—0 and 57.5 GWd/tU (beginning and end of life). The results

show that neutron flux in the thermal energy region is in good agreement in SCALE-6.2 and WIMS-10A for all considered models and burnups. This is due to the comparable, almost identical, energy group number and structure in the thermal region used in both codes. The epithermal and fast energy regions have slight depressions in the neutron flux caused by absorption resonances which are much more pronounced in SCALE due to the higher number of energy groups and due to the different energy bin structure in these regions. SCALE-6.2 has approximately 1.5 times more energy groups in those regions in comparison to WIMS-10A leading to more detailed visibility of resonance structures. For the case with the burnable absorber, neutron flux in the thermal region at the BoL is lower than for the pin-cell configuration.
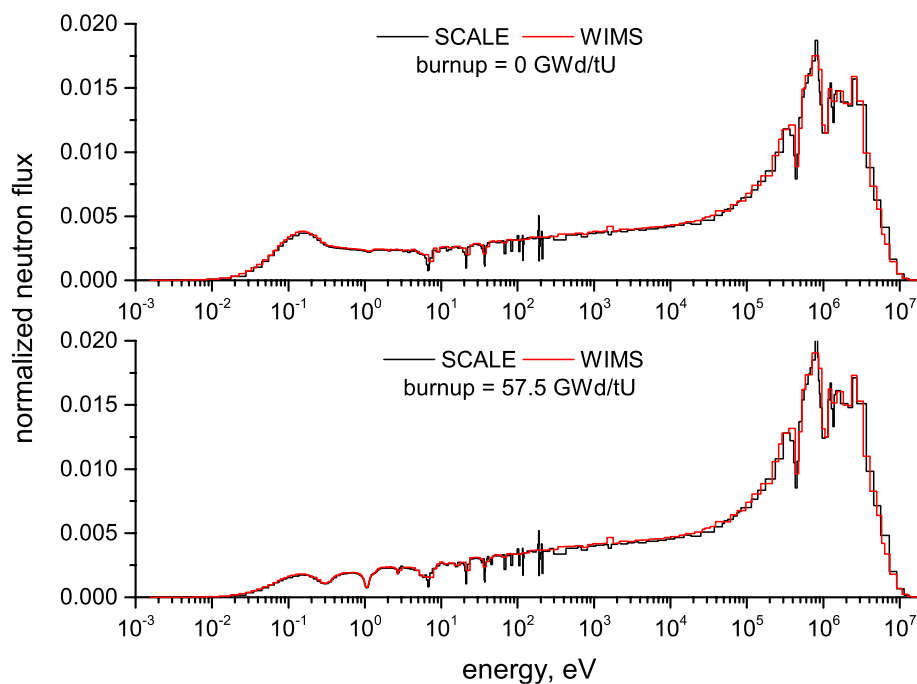
Figure 2.10. Flux distribution over neutron energy for the BWR pin-cell model in SCALE-6.2 (252 energy groups) and WIMS-10A (172 energy groups) for the BoL and EoL.
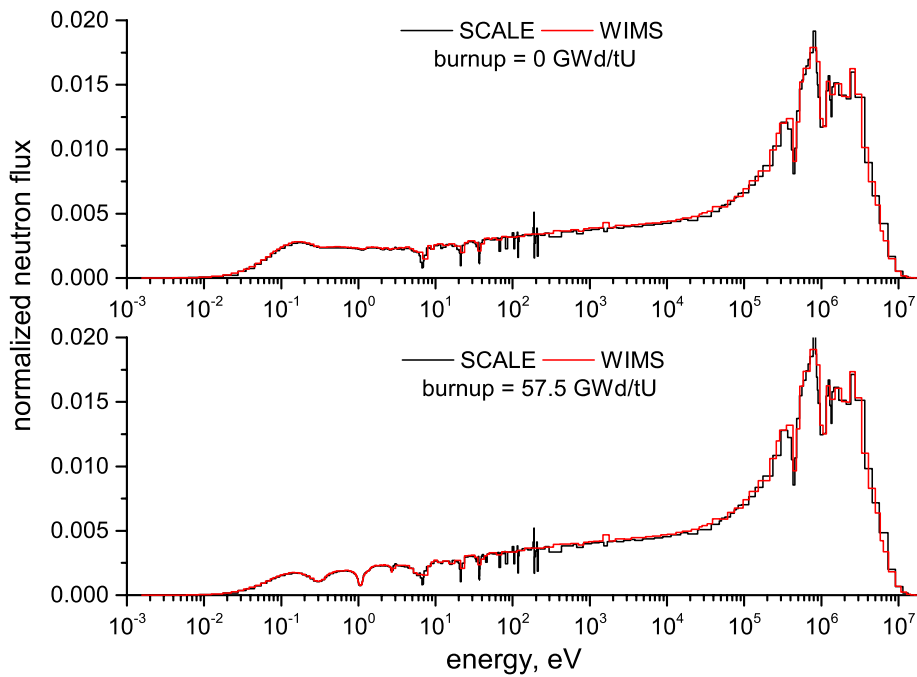
Figure 2.11. Flux distribution over neutron energy for the BWR 3 by 3 array model in the SCALE-6.2 (252 energy groups) and WIMS-10A (172 energy groups) for the BoL and EoL.

2.5. Conclusions

Development and application of burnup credit methods for Boiling Water Reactors require a deep understanding of the fuel assembly behaviour in the reactor core. Lattice physics computations are an essential part of this analysis and thus reliable and robust code results are an essential part of building trust in the future application of the method. Therefore, it is important to estimate the quality of the lattice codes and identify the level of discrepancy between them. For this purpose, the UK code system WIMS-10A is compared with the US code system SCALE-6.2, and the leading independent industrial code CASMO5 for BWR burnup calculations. Two different models were investigated in the present study for boiling water reactor systems: a pin-cell and a 3 by 3 array, with gadolinia poison rod in the centre. For both models, the SCALE-6.2 and CASMO5 results of burnup calculations demonstrated very good agreement. However, bias is observed for the infinite multiplication factor estimated with the ENDF/B-VII.0-based neutron library of SCALE-6.2 for both models, and with ENDF/B-VII.1, for 3 by 3 array model only.

A large discrepancy for higher burnups is detected between WIMS-10A and SCALE-6.2 along with CASMO5 k_{inf} values. The difference between WIMS-10A and SCALE-6.2 (v7_252 library) increases with burnup and reaches a maximum of −850 and -1600 pcm for the BWR pin-cell and 3 by 3 array model, respectively. Thus, WIMS-10A generally underestimates the infinite multiplication factor in comparison with the SCALE-6.2 and CASMO5 codes. Furthermore, it was demonstrated that the discrepancy between the infinite multiplication factors calculated by WIMS-10A and SCALE-6.2 rises as the moderator density decreases, but these differences are almost negligible compared to the discrepancies over burnup. Since the SCALE-6.2 and CASMO5 results were in a good agreement with each other for k_{inf},

further evaluation of WIMS-10A was based on the SCALE-6.2 code system to provide a deeper understanding of possible sources of the discrepancies.

The spectral indexes analysis showed that for both models, the U-238 and Pu-240 fission cross-sections are overestimated by WIMS-10A in comparison with SCALE-6.2, while the fission cross-section for Pu-242 is underestimated. The number density analysis detected that U-235 burns faster in the WIMS-10A model for burnups higher than 30 GWd/tU, while Pu-239 builds up slower on the whole range of considered burnups. In both cases, the trend in isotopic composition variance is similar, which may result from the difference in the burnup chains included in the solvers.

The neutron spectrum analysis revealed that the WIMS-10A and SCALE-6.2 neutron flux distribution over energy for both models have similar behaviour, with small depressions in the epithermal and fast energy regions due to the different energy group number and structure of those regions.

Based on the above, SCALE-6.2 provides more conservative results for k_{inf} estimation in comparison with WIMS-10A. For burnups above 30 GWd/tU, WIMS-10A in both cases underestimates number densities of important fissile materials. Since CASMO5 and SCALE-6.2 codes produce close results, it makes SCALE-6.2 a more reliable tool for burnup computations for LWRs as required for burnup credit analysis. Hence, SCALE-6.2 will be used as a basic lattice code for further burnup credit development, and the deviations have been fed back to the code developer of WIMS.

The considered models and results were not compared against experiments, hence it is difficult to judge in the differences between WIMS-10A and SCALE-6.2 and CASMO5 in a form to decide which code would be closest to a real experiment. However, due to a very good validation base and the wide industrial use, there is high confidence in the CASMO5 results, and the code-to-code comparison offers access to very detailed results for comparison which would hardly be possible on the basis of experimental data. The possible reasons for the discrepancies can vary from the nuclear data inconsistencies—for instance, in the code specific cross-section or decay data libraries—to the differences in computational methods utilized by the considered codes. Even if the master libraries are based on the same nuclear data library—such as ENDF/B-VII.0 in a case of WIMS-10A and SCALE-6.2—the way they were processed to the code master library can vary, which may lead to the difference in the depletion results. The difference between the master libraries could be estimated by a comparison of specific nuclide reactions from those libraries.

With the BEIS nuclear innovation programme in mind, we recommend a deeper investigation into the discrepancies, working with the code developer to improve the trust in the UK lattice code system WIMS-10A for the Boiling Water Reactor application if this code system is foreseen for future applications.

Author Contributions: Conceptualization, A.D., A.P. and B.M.; Data curation, A.D. and D.L.; Formal analysis, A.D.; Investigation, A.D.; Software, A.D. and A.P.; Supervision, J.-H.L. and B.M.; Validation, A.D. and A.P.; Visualization, A.D.; Writing—original draft, A.D.; Writing—review & editing, A.P., D.L., J.-H.L. and B.M. All authors have read and agreed to the published version of the manuscript.

Conflicts of Interest: The authors declare no conflict of interest.

References

1. Mueller, D.E.; Bowman, S.M.; Marshall, W.J.; Scaglione, J.M. *Review and Prioritization of Technical Issues Related to Burnup Credit for BWR Fuel*; NUREG/CR-7158, ORNL/TM-2012/261; Oak Ridge National Laboratory: Oak Ridge, TN, USA, 2012.
2. Mueller, D.E.; Scaglione, J.M.; Wagner, J.C.; Bowman, S.M. *Computational Benchmark for Estimation of Reactivity Margin from Fission Products and Minor Actinides in BWR Burnup Credit*; NUREG/CR-7157, ORNL/TM-2012/96; U.S. Nuclear Regulatory Commission, Oak Ridge National Laboratory: Oak Ridge, TN, USA, 2013.
3. Peakman, A.; Grove, C.; Fitzgerald, K.; Gregg, R. Development of an equilibrium loading pattern and whole-core fuel performance assessment in the Advanced Boiling Water Reactor (ABWR) with UO_2 and U_3Si_2 fuels. *Progress Nuclear Energy* **2019**, *117*, 103053.
4. Okuno, H.; Naito, Y.; Suyamu, K. OECD/NEA Burnup Credit Criticality Benchmarks Phase IIIB: Burnup Calculations of BWR Fuel Assemblies for Storage and Transport; Japan Atomic Energy Research Institute: Tokai, Japan, 2002.
5. Marshall, W.J.; Ade, B.J.; Bowman, S.M.; Gauld, I.C. *Technical Basis for Peak Reactivity Burnup Credit for BWR Spent Nuclear Fuel in Storage and Transportation Systems*; NUREG/CR-7194, ORNL/TM-2014/240; U.S. Nuclear Regulatory Commission, Oak Ridge National Laboratory: Oak Ridge, TN, USA, 2015.
6. Marshall, W.J.; Ade, B.J.; Bowman, S.M.; Martinez-Gonzalez, J.S. *Axial Moderator Density Distributions, Control Blade Usage, and Axial Burnup Distributions for Extended BWR Burnup Credit*; NUREG/CR-7224, ORNL/TM-2015/544; U.S. Nuclear Regulatory Commission, Oak Ridge National Laboratory: Oak Ridge, TN, USA, 2016.
7. Cacuci, D.G. (Ed.) *Handbook of Nuclear Engineering*; Springer: Boston, MA, USA, 2010; 3574p.
8. SCALE Code System. *ORNL/TM-2005/39*, Version 6.2.2; Oak Ridge National Laboratory: Oak Ridge, TN, USA, 2017.
9. Rhodes, J.; Smith, K.; Lee, D. CASMO5 Development and Applications. In Proceedings of the PHYSOR-2006, ANS Topical Meeting on Reactor Physics, Vancouver, BC, Canada, 10–14 September 2006.
10. *WIMS A Modular Scheme for Neutronics Calculations*; User Guide for Version 10, ANSWERS/WIMS/REPORT/014; Publisher: Dorchester, UK, 2014.
11. Funding for Nuclear Innovation. Available online: https://www.gov.uk/guidance/funding-for-nuclear-innovation (accessed on 28 April 2020).
12. Nuclear Fuel Safety Criteria Technical Review; OECD: Paris, France, 2012.
13. Rhodes, J.; Gheorghiu, N.; Ferrer, R. CASMO5 JENDL-4.0 and ENDF/B-VII.1beta4 libraries. In Proceedings of the PHYSOR 2012—Advances in Reactor Physics—Linking Research, Industry, and Education Knoxville, TN, USA, 15–20 April 2012.
14. Merk, B. On the influence of spatial discretization in LWR-burnup calculations with HELIOS 1.9—Part II: Mixed oxide (MOX) fuel. *Ann. Nuclear Energy* **2009**, *36*, 168–182.
15. Mertyurek, U.; Betzler, B.R.; Jessee, M.A.; Bowman, S.M. SCALE 6.2 Reactor Physics Code Accuracy Assesment for Light Water Reactor Fuel. United States. Available online: https://www.osti.gov/servlets/purl/1559746 (accessed on 20 February 2020).

16. Gauld, I.C.; Mertyurek, U. Validation of BWR spent nuclear fuel isotopic predictions with applications to burnup credit, *Nuclear Engineering and Design*, Volume 345, **2019**, Pages 110-124, https://doi.org/10.1016/j.nucengdes.2019.01.026.

17. Borms, L.; Domergue, C.; Lyoussi, A.; Mellier, F.; Wagemans, J. Spectral Indices Measurements Using Miniature Fission Chambers at the MINERVE Zero-Power Reactor at CEA Using Calibration Data Obtained at the BR1 Reactor at SCK·CEN. In Proceedings of the 2nd International Conference on Advancements in Nuclear Instrumentation, Measurement Methods and their Applications, Ghent, Belgium, 6–9 June 2011.

18. Griffin, P.J. Covariance Propagation in Spectral Indices. *Nuclear Data Sheets* **2015**, *123*, 104–108.

3. High-fidelity and nodal methods comparison

Nodal methods are currently the main tool for reactor core analysis in commercial light water reactors [34]. Nodal codes estimate neutron flux on a fuel assembly level with averaged properties, rather than on a fuel pin level. This limitation can be overcome by using pin power reconstruction methods in nodal codes which can estimate the power distribution within the fuel assembly, or in other words, the power rating for a specific pin, using superposition of the nodal flux distribution and the power map from the lattice calculations. However, at the current stage of the development of pin power reconstruction methods, they give less accurate results than the direct pin by pin transport calculations [35]. Also, incorporation of the thermal-hydraulic feedback on a pin level is not foreseen in the current industrial implementations of the methodology. Therefore, pin power reconstruction is currently performed without thermal-hydraulics feedbacks on the pin level which result in significant safety margins for the pin-power values. Among other things, in some countries, the regulator sets the limit on the maximum pin burnup which is permitted in the reactor. If the estimation of the maximum pin burnup is inaccurate for a specific fuel assembly design and, in countries where the regulator sets limits on maximum burnup, it may result in either exceeding the regulatory limits during the reactor operation or, on contrary, if the estimation is over conservative, in the inefficient fuel utilisation [36]. Thus, the development of high-fidelity methods for the application in nuclear modelling has been widely discussed in the last few years. New computational approaches can potentially help to:

- overcome the limitations of the traditional modelling approaches to the reactor core analysis;

- reduce safety margins; and

- maximise the fuel usage and the output of nuclear power plants.

This chapter examines the difference between the traditional nodal approach and the high-fidelity method based on the coupling of a Monte Carlo and subchannel codes applied to full-core modelling of BWR systems. The comparison was performed for a highly heterogeneous BWR fuel assembly design and the core configuration of GE-Hitachi's advanced boiling water reactor (ABWR) system. The nodal sequence included cross-section data preparation in the recently developed lattice physics module of SCALE Polaris [37] and the nodal analysis in DYN3D code. The high-fidelity sequence consisted of neutronics analysis in Monte Carlo (MC) code Serpent [38] which was then coupled with the CTF subchannel code [39] providing thermal-hydraulics feedback. It should be noted that the fully coupled DYN3D solution mentioned several times throughout the paper means DYN3D nodal analysis with included thermal-hydraulics feedback and thermodynamics of the fuel rod. The overall aim of the research presented in this chapter is to understand how well the nodal approach can simulate complex BWR systems in comparison to high-fidelity calculations. In addition, the Polaris deterministic code has been validated against Serpent MC code for 2D depletion cases using the same nuclear data library. The study utilised a bottom-up approach through which the complexity of the analysed model is gradually increasing.

Chapter 2 showed that results of the burnup calculations in the TRITON module of SCALE-6.2 code agreed well with the industry standard CASMO5 code. During the time of

the research described in Chapter 2, Polaris module has just been released by the SCALE developers, so TRITON was used for the BWR depletion analysis at that time. Since Polaris has: a simpler input; is optimised for the LWR analysis; and produces close results to the transport calculations in TRITON [40], it was chosen as a tool for cross-section data generation and depletion analysis throughout the rest of the research.

The results demonstrated that Polaris produce very close results to Serpent for all considered 2D models of the selected BWR fuel assembly configurations. Comparison of the 3D BWR fuel assembly models under hot full power conditions demonstrated a good agreement between nodal and high-fidelity approach. The depletion analysis of the 3D BWR fuel assembly models, without thermal-hydraulics feedback (i.e. neutronics only), revealed significant discrepancies in k_{eff} between two approaches at some parts of the burnup curve. The discrepancies were found to be a result of the difference in the axial power profiles produced by each code. The thermal-hydraulics feedback was not included in the depletion analysis of the 3D fuel assembly model since significant computational resources would have been required for coupling Monte Carlo code with the subchannel code over the burnup, which were at that time unavailable within the project. For example, in the CASL project [41], the coupling of MPACT/CTF for a quarter of the PWR reactor core over one cycle took around 36000 core hours [42]. Since MPACT is a deterministic code, the computational time is expected to be even larger for a Monte Carlo code such as SERPENT. However, despite considerable discrepancies in fuel assemblies' k_{eff} at some burnup stages, an acceptable difference between the two methods was demonstrated for the neutronic analysis of the reactor core. The fully-coupled solution for the full core did not converge in Serpent/CTF sequence, so the outcome of the coupled neutronics and thermal-hydraulic analysis could not be compared between nodal and high-fidelity approaches. To summarise, the Polaris/DYN3D sequence can be considered a robust tool for the further BWR reactor core calculations which will be performed further in this research.

This study was conducted in collaboration with post-doctoral research assistant of the University of Liverpool Dr Seddon Atkinson. The author's contribution to the research outlined in the List of Publications section.

Article

A Comparison of Advanced Boiling Water Reactor Simulations between Serpent/CTF and Polaris/DYN3D: Steady State

Operational Characteristics and Burnup Evolution

Seddon Atkinson *, Anna Detkina, Dzianis Litskevich and Bruno Merk

School of Engineering, The University of Liverpool, Brownlow Hill, Liverpool, L69 3BX, UK; a.detkina@liverpool.ac.uk (A.D.); dzianis@liverpool.ac.uk (D.L.); merk@liverpool.ac.uk (B.M.)
* Correspondence: seddon.atkinson@liverpool.ac.uk

Abstract: High fidelity modelling for nuclear power plant analysis is becoming more common due to advances in modelling software and the availability of high-performance computers. However, to design, develop and regulate new light water nuclear reactors there are, up until now, limited requirements for high fidelity methods due to the already well-established computational methods already being widely accepted. This article explores the additional detail which can be obtained when using high fidelity methods through Monte Carlo/Sub-channel analysis compared to industrial methods of cross-section/nodal analysis using the Advanced Boiling Water Reactor as a case study. This case study was chosen due to the challenges in modelling two phase flow and the high levels of heterogeneity within the fuel assembly design. The article investigates how to implement such an approach, from a bottom-up procedure, by analysing each stage of the modelling process.

3.1. Introduction

Modelling and simulation in the topic of nuclear reactor cores has made very strong progress over the last few decades, mainly sponsored through large international programmes like NURESIM [1] or through national efforts like Consortium for Advanced Simulation of Light Water Reactors (CASL) [2]. However, not all of the new efforts seem to be suitable for near term industrial application; thus, the UK has recently delivered their own industrial nuclear reactor core simulation [3] approach. In addition, all the new approaches have been targeted towards pressurized water reactor (PWR) development as these are the current leading reactor technology worldwide. We intend in this publication to have a deeper look into the application of high-fidelity methods for boiling water reactor (BWR) core modelling to determine the requirements which will be used to help improve future industrial BWR simulation technology.

The relevant key safety parameters and their evaluation in industrial application in nuclear reactors have not significantly changed over the past thirty years, despite significant advancements in computation power within this time frame. The main reason for this is that new high-fidelity methods, such as Monte Carlo analysis are yet to efficiently show greater depths of understanding when compared to the traditional methods which are significantly less computationally expensive [4]. Presently, there is no motivation to change the current

methodology from an industrial perspective as regulatory bodies are satisfied with the detail being provided because the designs being commissioned are often well understood.

Today's industrial methods determine few-group neutronics cross section sets for the core simulator via 2D, multi-group transport solvers in the lattice codes [5–7] for each fuel assembly, or several levels for axially varying fuel assemblies. These cross sections are then provided to a core simulator software package such as a 2D-1D nodal diffusion solver [8–10] which is coupled with an internal heat transfer module consisting of thermal fluid dynamics and a fuel rod model. These well-established solvers have the advantage of being extremely time efficient and have low computational requirements, which allows for full core burnup analysis, fuel re-shuffling and transient analyses to be performed with reasonable accuracy in acceptable time. The current industrial standards of different countries are listed in Table 3.1 for light water reactors (LWRs); however, the methodology within these simulation packages very similar.

Table 3.1. A description of potential cross-section generation and system tool codes used for several countries.

Country	Cross-Section Generation	Core Simulator
UK	WIMS [11]	Panther [12]
France	APOLLO-2 [13]	MANTA/SMART [14] CRONOS-2 [15]
Sweden/USA	CASMO	SIMULATE [16]
USA	Scale-Polaris [17]	PARCS/RELAP [18]

By obtaining the power and temperature distributions, these results can be later coupled to external system codes and fuel performance codes to provide sufficient regulatory information for the licensing process. The benefit of these methods is that they are widely accepted as they have been developed alongside years of experimental data. One of the main drawbacks of the current safety evaluation methodology is that nuclear regulators place a high emphasis on the most challenged pin under steady state and transient conditions. Individual pins are not specifically modelled within the current industrial standard methodology as these methods use a representative pin per node model. Pin power reconstruction is implemented offline which requires large safety margins due to the estimations of pin powers without appropriate thermal hydraulics feedback [3]. This conservative offline approach is widely used to ensure the safety of the nuclear installations.

In recent years, the USA has created the largest nuclear modelling and simulation project, CASL, which was provided with $242M by the US government over ten years to advance the country's nuclear reactors modelling capability [19,20]. In addition to this, the USA has access to the most powerful super computers in the world [21] which have been utilised to produce high-fidelity models of their current reactor designs [22]. One of the drawbacks of these methods is the massive computational power and time required, although the consortium has made a significant effort to reduce these requirements by simplifying the process through the use of MPACT/CTF coupling, where MPACT is a 2D-1D method of characteristics neutron transport solver and CTF is the Nuclear Regulatory Commission's subchannel code [23]. The high computational requirements and lack of access to the CASL software rules out most of these procedures for current industrial

application, as well as for smaller nations. The complexity of the modelling procedure within CASL places only very few people in the world to be able to use these toolkits.

High fidelity modelling and its application is becoming increasingly popular within the research community [1], with Monte Carlo and Computational Fluid Dynamics (CFD) or subchannel models recently gaining momentum. It is often argued that these methods are required for non-conventional nuclear systems, due to the complexity of some designs and the absence of specially designed tools, which has also contributed to this area of research [24]. As computational power becomes more easily accessible, the modelling industry is likely to incorporate these methods more. Recent developments have seen a short transient being performed in 3D by coupling Serpent [25], a Monte Carlo neutron transport solver and SUBCHANFLOW [26], a subchannel code this project produced a pin by pin power profile of a small core during a reactivity control insertion [27]. The computational power required was 1000 cores, which is currently seen as inaccessible to most industrial institutions; however, two decades ago, this achievement would have been thought to be impossible.

The UK governments Department for Business, Energy and Industrial Strategy (BEIS) has supported the development of the UK nuclear industry under the £180M multidisciplinary Nuclear Innovation Program. This program aims to support the UK's civil nuclear industry and reduce the overall cost of nuclear power plants by 30% which will support the decarbonisation of the country [28]. A part of this work aims to increase the UK's skillset and ability to provide high fidelity modelling techniques and it is, therefore, important to understand the additional benefits that using high fidelity modelling provides over the conventional industrial standard methods.

The main focal point for high fidelity modelling has been on PWRs, which are the most common deployed reactor technology globally. There are several benefits with these designs as their geometry is relatively simple, with symmetrical fuel assemblies, an almost uniform water density and the fuel assemblies have uniform material properties. This has meant that the validation of the modelling procedure has been relatively straightforward. The second most deployed reactor type is the BWR, which are significantly more challenging to model, due to their two-phase flow and the complex fuel assembly design to promote a varying power profile. As most modelling and simulation toolkits have focused on the development of PWRs (for commercial application), the inclusion of BWRs has not received as much attention and simplified thermal-hydraulic models have been adapted to support two phase flow regimes. This poses the question: Would there be any benefit for the BWR community to embark on a high-fidelity modelling and simulation programme as we have seen for PWRs? Such a program could further the understanding of the transition of the power profile which is vital to understand when determining the most challenging pins for safety cases.

The overarching aim is to be able to understand where the current methods fall short of the high-fidelity methods, which will allow for an insight into where the industrial methods can be improved, without becoming too computationally expensive. This leads to the research question: Can we judge and observe the effect of increased complexity of BWR cores by using cutting edge coupled methods? This would allow us to identify the requirement for model improvements for standard coupled core simulators for BWR application. This work focuses on the Advanced Boiling Water Reactor (ABWR) as this is one of the most complex advanced reactor design types due to the presence of two-phase

flow and axial heterogeneity. The ABWR has passed the UK's Generic Design Assessment (GDA) [29]; however, GE-Hitachi have recently pulled out of committing to building the ABWRs due to concerns over the costs and financing of the project [30].

To model the ABWR, a standard industrial method is used, which takes a four-level approach to cross-section generation using Scale-Polaris (SP) [31] which are then applied to the core simulator package DYN3D [10]. The high-fidelity method couples the Monte Carlo transport solver Serpent [25] to the subchannel code Cobra-TF (CTF) [32]. The benefit of this method is that Serpent can provide an accurate pin power representation and CTF is then able to perform a thermal-hydraulic analysis on the fuel assemblies.

3.2. Model Description

As the ABWR is a commercial product the exact arrangements of their fuel assemblies as well as the loading pattern is not available within open literature so this work uses a patent filed by Global Nuclear Fuel-Americas in 2014 [33] which contains several fuel assembly types. Global Nuclear Fuel America is a GE-led joint venture with Hitachi limited [34] and, therefore, the patent does not provide proprietary information; however, the 10 × 10 assembly design provides a reasonable starting point. The patent provides seven assembly types; however, this study considers only two, thus reducing the modelling complexity and effort. Minor adjustments to the design filed within the patent have been made to provide a more realistic fuel assembly and the pin layout and pin compositions are shown in Figures 3.1 and 3.2, respectively.
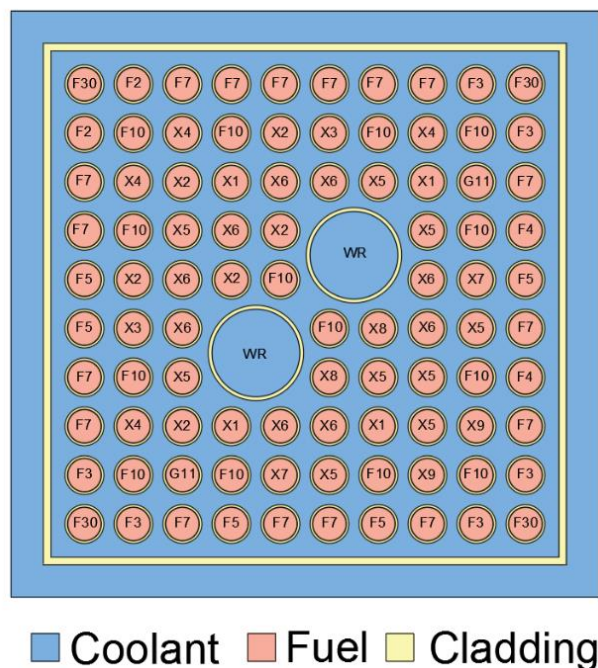
Figure 3.1. Horizontal 2D 10x10 fuel assembly map of each pin type based on an edited version of a patent filed by Global Nuclear Fuel-Americas [33]
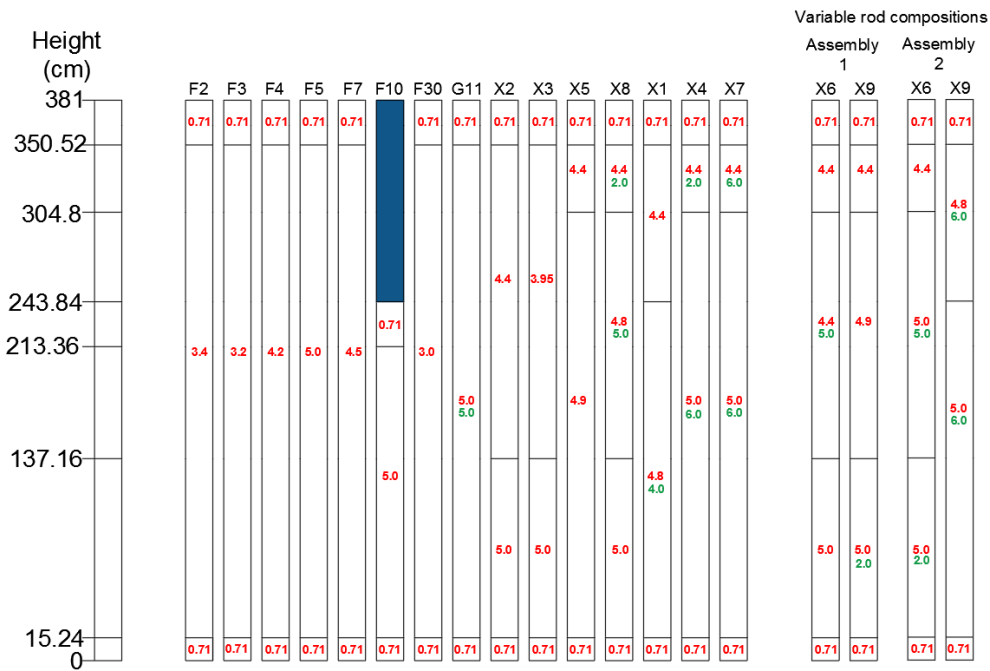
Figure 3.2. Axial pin description of the pins of both assembly one and two. Red representing the 235U enrichment and green the weight percent of gadolinium oxide. Only pins X6 and X9 have their compositions vary between the two assemblies as highlighted. F10 represent a reduced height fuel pins, where the blue section represents water as a material.

The initial water density within the assemblies is provided using benchmark data for boiling water reactor [35] and further data used can be found within Table 3.A1-3.A3 within the Appendix A.

The full core model is achieved by arranging the assemblies with four different burnup stages (0, 5, 10 and 30 GWd/TU) which are slightly adopted from the ABWRs equilibrium core arrangement to provide a critical core configuration. The full core arrangement and the cycle number is depicted in Figure 3.3, which is taken from the ABWRs GDA [36]. Similarly, to the ABWR design, this analysis uses an assembly supercell arrangement, where the bottom right-hand corner of Figure 3.1 is always at the center of each four-assembly group.
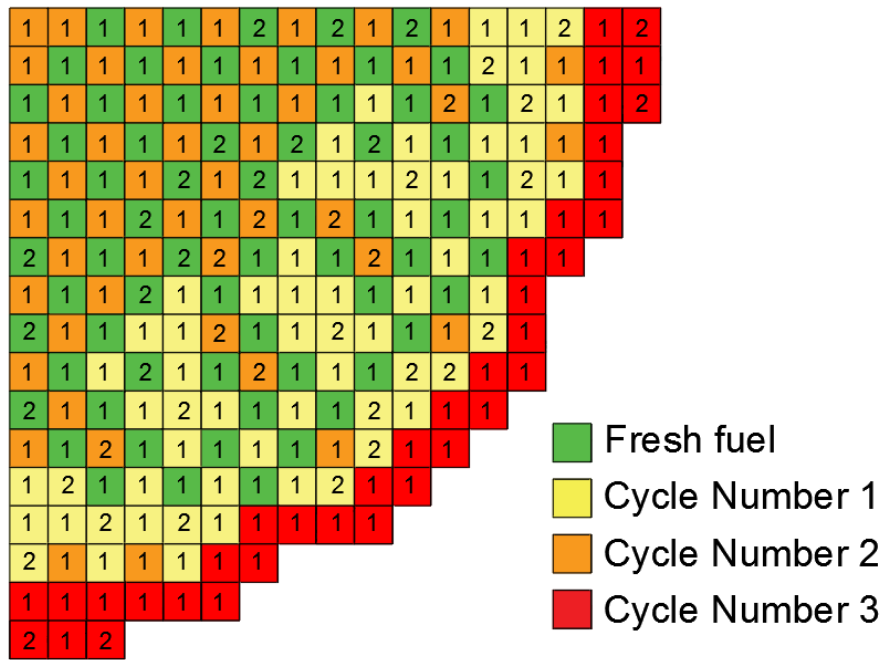
Figure 3.3. Full core equilibrium layout, with assembly numbers 1 or 2 and their burnup cycle inferred by the colour.

3.3. Codes and Toolkits Used

3.3.1. Scale Polaris

SCALE 6.2 is a modelling and simulation tool developed by Oak Ridge Nuclear Laboratory (ORNL, USA) for criticality analysis, reactor and lattice physics calculations, sensitivity, and uncertainty analysis. Polaris has recently introduced the SCALE 6.2 module into the code for lattice physics calculations. Polaris performs transport calculations using Method of Characteristics (MOC). Self-shielding cross-sections are obtained with Embedded Self-Shielding Method (ESSM) which uses Bondarenko interpolation approach [31]. Polaris can perform lattice calculations using ENDF/B-VII.1 [37] nuclear data library with 252- or 56-energy groups.

3.3.2. DYN3D

DYN3D is three-dimensional code designed for performing coupled neutronic/thermal hydraulic steady state and transient analysis of LWRs. Helmholtz-Zentrum Dresden-Rossendorf (HZDR) have developed the code for more than 20 years [10]. DYN3D was verified and validated against various benchmarks, mostly for Russian VVER-type reactors and is a NURESIM reference code. BWR analysis was performed for the BWR Turbine Trip Benchmark developed by OECD/NEA [38]. DYN3D is widely used in academia for research purposes and also provides 16 licenses to industrial stakeholders in 7 countries [10].

The nodal expansion method, implemented within DYN3D for neutron kinetics, solves the neutron diffusion equations for Cartesian and hexagonal geometry in two- or multi-group approximation. Balanced equations for mass, energy and momentum are being solved using code's internal thermal-hydraulics model for one- and two-phase flow in the reactor core linked with a fuel rod model for heat transfer.

3.3.3. Serpent

Serpent is a continuous energy Monte Carlo neutron transport code developed at the VTT Technical Research Centre of Finland. Serpent provides a pin-by-pin power profile across the core. To provide an accurate comparison with SP, a beta version of the ENDF/VII.1 data library was provided by the Serpent development team as Polaris is unable to use the ENDF/VII.0 data library which has been validated with Serpent. The Serpent version used within this article was version 2.1.30 and all burnup calculations were implemented using the Transmutation Trajectory Analysis (TTA) burnup method.

3.3.4. CTF

CTF is a sub-channel code produced by North Carolina State University (and now ORNL) within the framework of the CASL project [39]. The CTF project aims to advance the 1980's Cobra-TF to a higher standard by providing significantly more thermal-hydraulic data required for regulation than its predecessor. The CTF version used within this work is version 3.7.0.

3.3.5. Serpent and CTF Coupling Procedure

Serpent provides an axial pin power profile across the geometry based upon twenty-five axial dependent positions along the length of the assembly and one for each pin in radial direction. This allows for a full 3D power profile to be provided along the fuel pins to CTF, which uses a total amount of nodal heights of 250, to allow for an accurate representation of the flow regime which must capture the development of the two-phase flow across the geometry. CTF does not directly output the coolant temperature yet provides the nodal enthalpy and pressure which are then input into a Python module [40, 41] produced by The International Association for the Properties of Water and Steam (IAPWS) to provide the coolant temperature. CTF's 250 nodes are then averaged across 30 axial heights to return the temperatures and densities back to Serpent. Within the full core analysis, the crossflow between assemblies is ignored, which is acceptable within ABWRs due to their wrapped assembly structure. A brief description of the coupling procedure is highlighted within Figure 3.4 to demonstrate in interplay between both codes and the developed script.
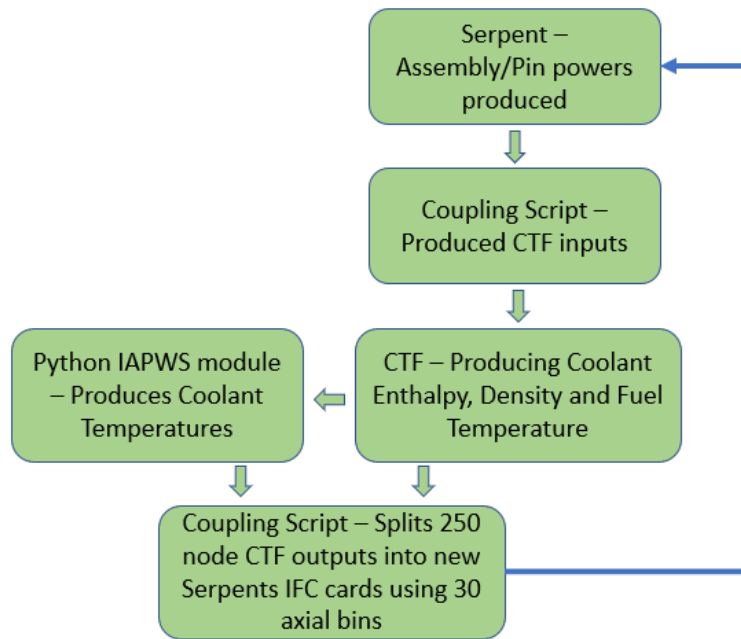
Figure 3.4. The code coupling procedure between Serpent and Cobra-TF (CTF).

3.4. Methodology

The first investigation explores the preparation of cross sections and, thus, the neutron transport solver and burnup modules of Serpent and Scale/POLARIS (SP). To achieve this, four 2D cut outs of the assemblies are taken at intervals which would be used to define the axial variations within the nodal method as highlighted in pink in Figure 3.5.
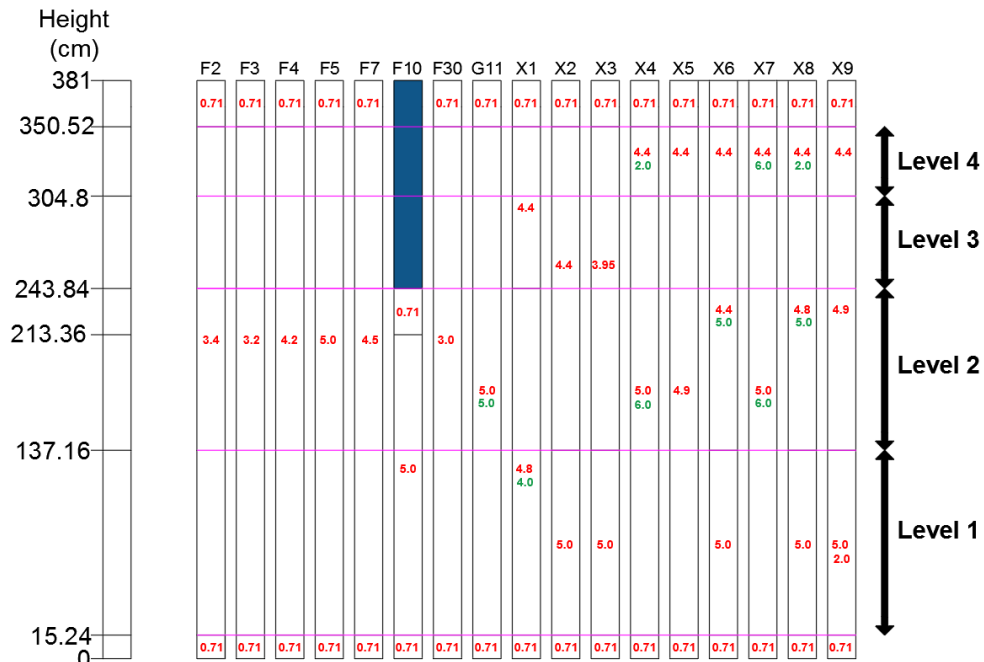
Figure 3.5. Highlighting the levels of the axial variation of the fuel assemblies used for the cross-section preparation. The axial variations in BWRs are used to control the axial power profile.

Figure 3.5 highlights that the fuel assembly levels are placed at standard positions where the materials compositions change within the assemblies. One small discrepancy between SP and Serpent is the natural uranium cap on F10, which is modelled as purely fuel within SP whereas Serpent explicitly models the natural uranium.

The cross-sections from SP are then exported to DYN3D and the cross-section preparation as well as the correct transfer are verified via a comparison of DYN3D and SP. The next stage aims to understand the differences between Serpent and SP by investigating the 2D cross-section preparation under reflective boundary conditions for each of the fuel levels which are depleted in stages up until 60 GWd/TU to represent the maximum burnup experienced during operational conditions. This will highlight any differences in the burnup procedures within Serpent and SP and determine if any errors are being introduced by using Serpent's beta ENDF/VII.1 data library and any discrepancies when the cross-section set is used within DYN3D.

The second investigation evaluates a fuel assembly, and this takes part in two stages, firstly purely neutronic and secondly a coupled neutronic and thermal hydraulic procedure. Within this study reflective boundary conditions are used on the sides of the assembly with vacuum boundaries at the top and bottom to provide the correct power profile. The purely neutronic study explores how high-fidelity methods vary from the industrial standard in the areas shown in Table 3.2.

Table 3.2. Single assembly progressive test comparisons performed.

Model Description	Water Density Distribution	Aims
Uniform fuel	Uniform	To understand any differences in a standard model, like Pressurised Water Reactors (PWR)s, first validation of the modelling in both systems
Uniform fuel	Non-uniform	To understand how the water density averaging in levels in the industrial method affects the modelling approach
Four-level fuel	Uniform	To understand how the high flux gradients of the fuel behaves between the models
Four-level fuel	Non-uniform	To understand how the high flux gradients of the fuel is represented between the models and the water density combined

The coupling procedure between neutronics and thermal hydraulics is automatic in the nodal diffusion solver; however, this will take several iterations between Serpent and CTF to determine the final power profile and the related feedbacks which will be measured by the effective multiplication factors (k_{eff}) variation between iterations. By using either method, the correct operational water density distribution in axial direction will be obtained, which is important to provide vital safety parameters within the design.

The third investigation aims to model the full ABWR core under steady state operating conditions under normal operation. Within this case all boundary conditions are vacuum at the outer surfaces and Polaris's assembly discontinuity factors (ADFs) [42] feature was used to provide ADFs at the boundary between fuel assemblies and between the exterior fuel assemblies and the reflectors. ADFs aim to provide a more realistic representation of the

heterogeneous flux distribution at the boundary between nodes, as this is unaccounted for within the homogenized nodal diffusion approximation and can lead to errors at high flux gradient boundaries, in the thermal neutron flux, especially. One of the challenges within this study arises from obtaining the materials at each cycle for Serpent; this requires a highly detailed fuel assembly model which accounts for spatial self-shielding and each material to be modelled separately. An evaluation of the burnup curves over the fuel cycle is performed to provide an understanding of the effect of the different levels of detail the water density in combination with the material levels has on the burnup curve. Following this, the full core is modelled using both solutions and the cores power distribution is compared on a 25-node level to determine the power variations.

3.5. Results and Discussion

3.5.1. Single Assembly 2D Levels Results

This investigation aimed to understand the differences within the softwares solvers, and the master cross-section used by taking 2D cross-sections for each level of each fuel assembly, these were then burnt up to 60 GWd/TU using a constant fuel temperature of 900 K. This will provide an understanding of the way that each code handles burnup sequences and comparing them to one another. The results are presented for infinite multiplication factor (k_{inf}) in Figures 3.6 and 3.7 with results for DYN3D added to test the few group cross section preparation and transfer procedure for SP to DYN3D as well as the burnup module.
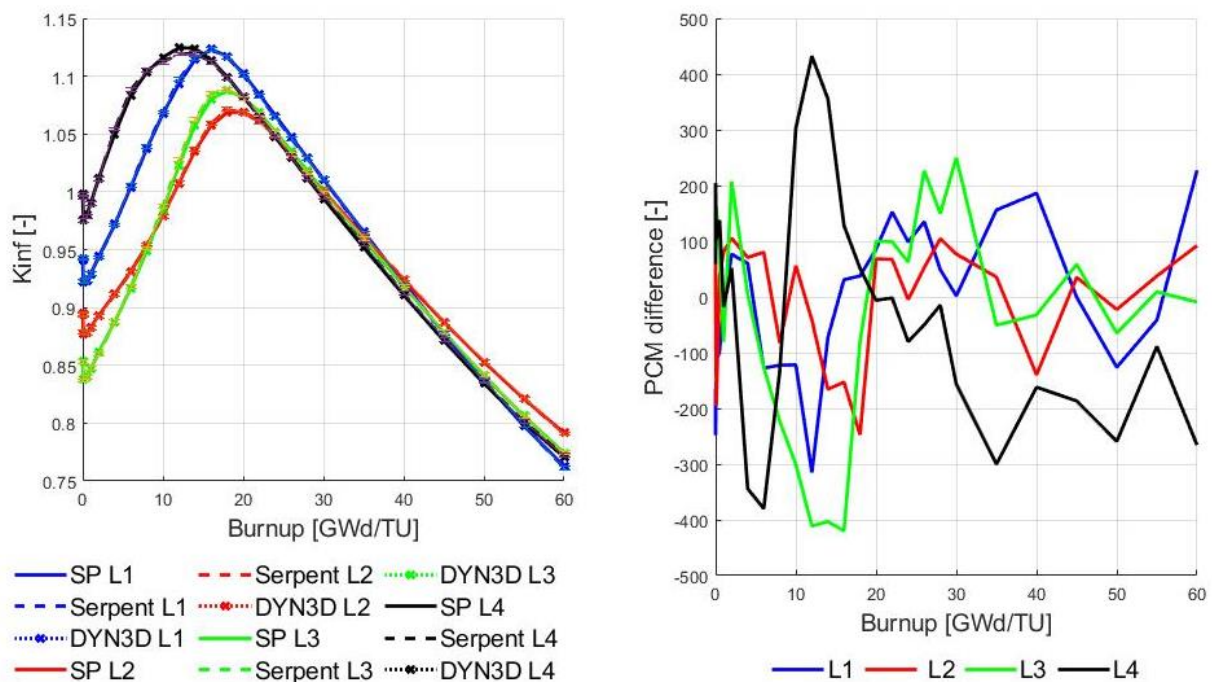
Figure 3.6. Left: kinf over burnup of assembly one in full power operation up until 60 GWd/TU comparing Scale-Polaris (SP), DYN3D and Serpent. Right: The PCM variation at each burnup stage (SP-Serpent).
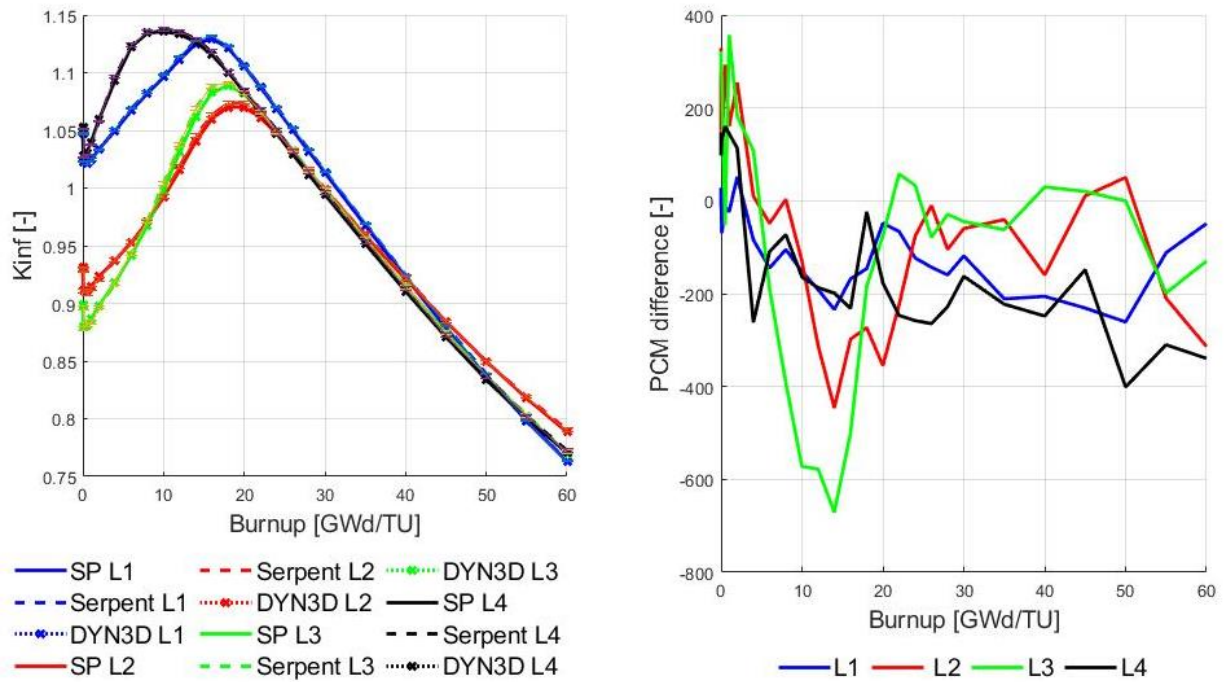
Figure 3.7. kinf over Burnup of assembly two up until 60 GWd/TU comparing SP, DYN3D and Serpent. The PCM variation at each burnup stage (SP-Serpent).

The two assemblies were very similar, with only two fuel pin types (X6 and X9) materials being changed; however, it impacts on k_{inf} on all levels leading to different results. Each pin within the assembly plays a role in controlling the power distribution over time and the bottom level is heavily poisoned using Gd_2O_3 to reduce the initial reactivity which is caused by the higher water density present. In general, the results coincide very well for all 8 shown levels keeping in mind the different master libraries used for the calculations. The initial test is to determine if the cross-sections within DYN3D matched those which were produced in SP and this was confirmed within the figures as these values were identical between the codes. The maximum discrepancies between SP and Serpent occurs at the peak reactivity positions when the Gd_2O_3 is depleted and the speed at which this happens is dependent on the method used. There is a trend that Serpent reaches a peak reactivity at an earlier time to SP, with the maximum discrepancy being 671 pcm, in level three of assembly two which is caused by the large amount of Gd_2O_3 within this level. The bottom level of the model plays the highest role in the behaviour of the fuel assembly and will determine how quickly the power profile moves axially. Within this case the maximum variation is 315 pcm in assembly one, which occurs after at 12 GWD/TU, which is prior to the peak reactivity. The peak reactivity at 18 GWD/TU is in a very good agreement between the codes with a variation of 38 pcm. From Figures 3.6 and 3.7 it is clear that Serpent and SP are in good agreement with one another and that the beta data library in Serpent seems to be compatible with SP's validated library.

3.5.2. Single Assembly 3D Neutronic Evaluation

The 3D single assembly evaluation aims to progressively increase the complexity of the design to determine at which points the assumptions within the software methods start to affect the results. The initial study assumes a uniform fuel composition based on level one of

fuel assembly two for the whole height of the fuel, with a uniform water density but real boundary conditions; this represents the simplest case study with the axial power profile depicted in Figure 3.8. The power profiles are in very good agreement with one another with this simple test.
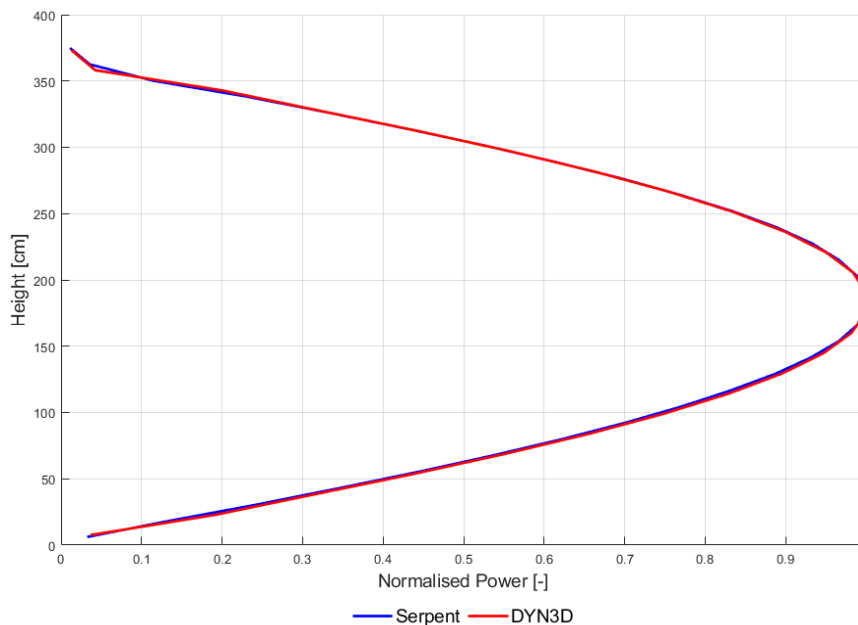
Figure 3.8. Assembly two's uniform material composition and uniform water density power profile with leakage boundary condition.

The next stage introduces the water density variation across the axial height while the material is kept constant through the whole axial assembly; thus, the first case is created with real influence of a thermal hydraulics parameter but still without the coupling of neutronics and thermal hydraulics. Within the industrial method, the water density must be averaged across the heights represented by that cross-section, which deviates from the high-fidelity method which can incorporate each stage of the water density. It must be mentioned here that the water density in the core simulator is based on the water density of the four levels of the cross-section preparation while in later simulations the real water density is finally determined through the thermal hydraulics module of the core simulator.

Within Figure 3.9, it becomes obvious that the averaging process (based on four levels) plays a significant role within the peak power location as DYN3D's power peak is at a different location to Serpent's. DYN3D also shows that following a new water density input, there is a change in gradient of the power profile; this is due to the averaging process creating a virtual boundary between these levels, and the diffusion equation must determine the flux distribution between these levels and, hence, the power change. The results in the analysis are concerning as the assumptions for the purely neutronic model does seem to break down once the water distribution is added. It should be noted that as DYN3D is meant to be used as a coupled solver and a further evaluation of these results is required once DYN3D produces its own water density profile across the geometry as the boundaries seen within Figure 3.9 will be reduced in this case as the water density variation between nodes becomes smaller.
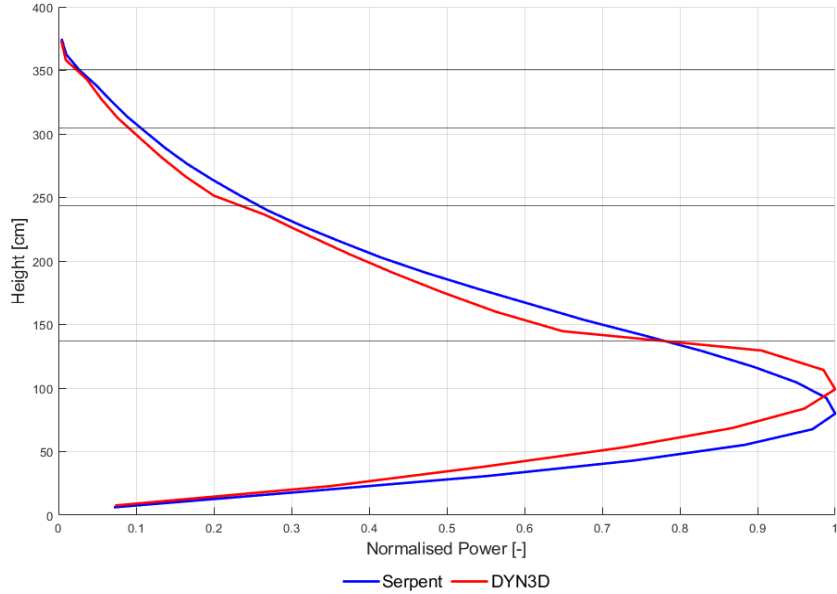
Figure 3.9. Assembly two's uniform material composition and non-uniform water density power profile. For clarity, the water density's average regions are shown using the black lines on the Y-axis.

The criticality of the system (k_{eff}) provides an insight into the behaviour of the neutronic solver and is often used as a method of validation. Within this case two tests were performed using Serpent, one with and one without the thermal scattering libraries linked to the coolant material, these libraries increase the accuracy when bound atoms such as water [43] are used. In the case of the industrial method, the thermal scattering libraries are already applied within SP when the cross-sections are produced. Table 3.3 highlights the very prominent role of the thermal scattering libraries within the Monte Carlo simulations accuracy, as the discrepancy reduces from 590 pcm to 74 pcm. Due to the differences in the power profile, it is difficult to determine if this is an error reduction as the systems behave in very different ways; however, the inclusion of the scattering libraries does play a significant role within the systems' behaviour. This highlights one drawback when using the high-fidelity method, as the current version of Serpent does not support the inclusion of thermal scattering libraries when using the interface cards feature which is required for the coupling procedure to assign the water density and temperature axially. Thus, this study has highlighted that the high-fidelity method will include an error when modelling BWR's due to the modelling methodology not currently being capable of accurately predicting the criticality effect of the thermal scattering in water.

Table 3.3. Comparison of the reactivity coefficients of the single assembly with a uniform fuel material.

Model	DYN3D keff	Serpent keff	Serpent Error (±) 95% Confidence [pcm]	Variation [pcm]
Uniform water density no thermal scattering library	1.04872	1.04227	12	-590
Uniform water density thermal scattering library	1.04872	1.04953	11	74

Model	DYN3D keff	Serpent keff	Serpent Error (±) 95% Confidence [pcm]	Variation [pcm]
Non-uniform water density	1.03798	1.02540	11	-1182

The next stage represents the real fuel assembly, with four axial material compositions (see Figure 3.5) with each using a new cross section set to account for the change in materials while the water density is kept uniform. Nodal diffusion methods have been shown to work accurately when passing through a uniform material although this method breaks down at high flux gradient boundaries which could occur between the fuel levels due to the inclusion of fixed burnable poison or between high/low moderated regions. Figure 3.10 investigates the severity of the flux gradients between the fuel levels. In this case, the codes are within very good agreement of one another, which implies that these flux gradients caused by the material compositions are on a magnitude that can be treated to an acceptable accuracy through diffusion approximation; thus, no major differences can be noticed between the solvers.
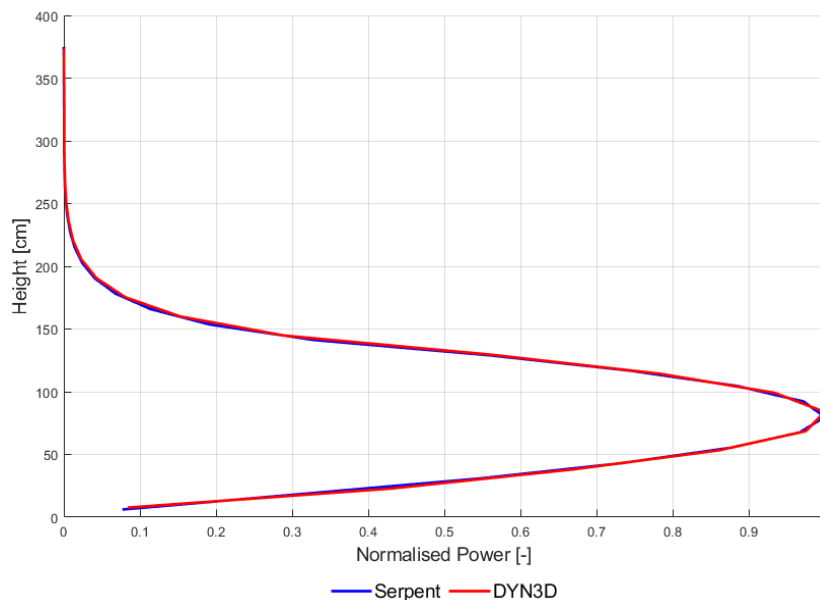
Figure 3.10. Assembly two's four-level design with a uniform water density across the axial height of the assembly.

The final study aims to determine the combined effect of all the previous cases, with four levels and a non-uniform water distribution based on the levels, without direct neutronic/thermal hydraulic coupling.

Applying the full set (four levels with different materials and different water densities) leads to a similar power peak shift within Figure 3.11, as with the earlier study and this was determined to be caused by the non-uniform water density (Figure 3.9). An emphasis on the importance of the thermal scattering libraries is evident from Table 3.4. However, the total discrepancies for the four leveled approach are slightly lower than with the uniform fuel case with different water densities. Overall, up until now, this study has already highlighted several key aspects. Initially the high-fidelity method is unable to use the thermal scattering libraries when a non-uniform water density is used which has been shown to create quite large deviations under a uniform water density. Secondly, due to the averaging process

used for the cross-section preparation for DYN3D, the power profile is unable to match that of Serpent's for a purely neutronic analysis with the peak power shifting using the current industrial standard method.
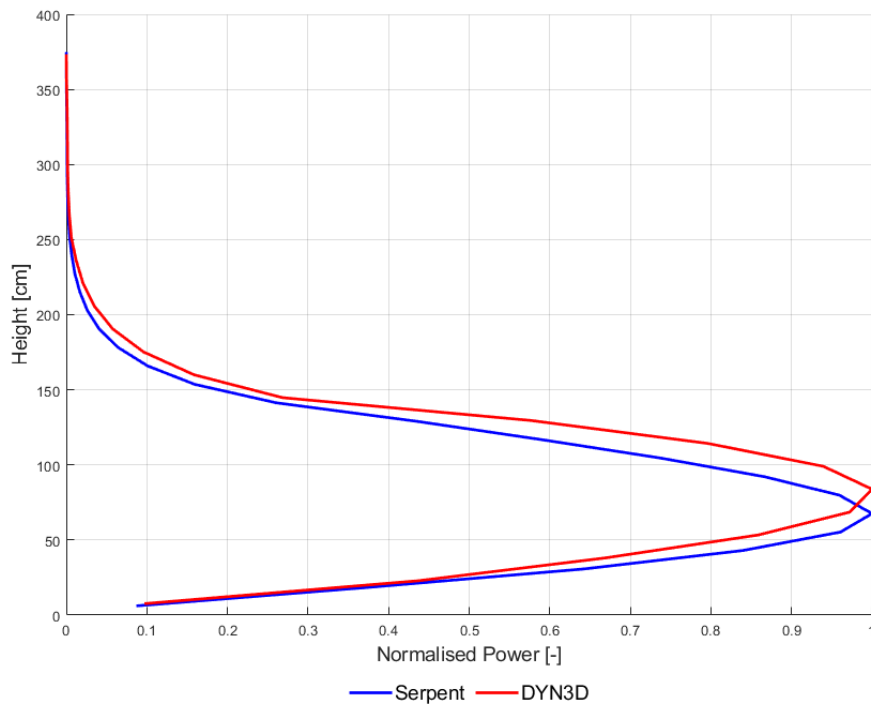
Figure 3.11. Pure neutronic axial power profile of DYN3D and Serpent. Serpent's power profile is averaged across each pin within the axial node.

Table 3.4. Four leveled fuel assembly reactivity coefficients comparison.

Model	DYN3D k_{eff}	Serpent k_{eff}	Serpent Pcm Error (±) 95% Confidence	Pcm Variation
Four-level assembly uniform water density no thermal scattering library	1.03108	1.04924	11	1679
Four-level assembly uniform water density thermal scattering library	1.03108	1.03172	11	60
Four-level assembly non-uniform water density	1.02430	1.01703	17	−698

To reduce this shift in the peak, a serial analysis was performed to see if a refined averaging process will provide a closer match in the power profile. To achieve this, level one's cross sections were split into section by using the two different water density averaging schemes shown in Figure 3.12 to reduce the strong step change in water density between level one and two.
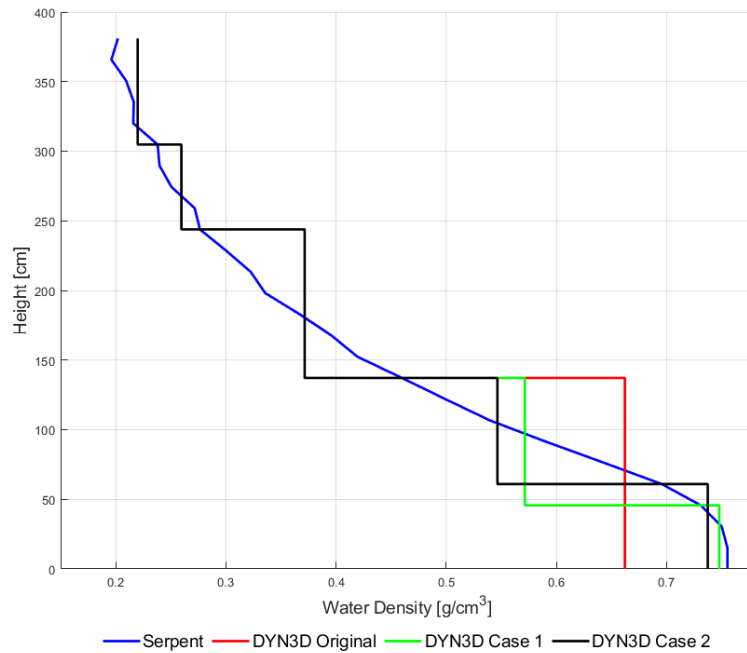
Figure 3.12. The input water densities across each for both DYN3D and Serpent, with the inclusion of the additional two.

The new power distributions in Figure 3.13 highlights that case 1 and 2 both provide a power profile which more accurately represents that of Serpent with a broadening of the power peak in DYN3D. It is, therefore, confirmed that the power profiles do experience a shift due to the averaging process used within the nodal analysis, which especially within the lower region of the core which could produce inaccuracy in identifying the peak power location. This has highlighted that a refinement study could be considered within nodal methods to achieve the correct location of the power peaks in the case the problem still appears in the fully coupled solution. This would be less important in PWRs due to the less severe axial variations in the water density.
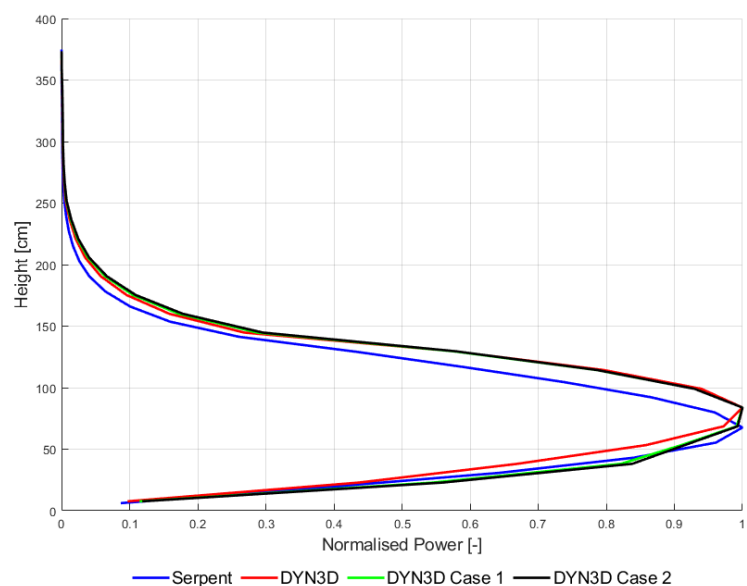
Figure 3.13. New power density profiles with the additional levels added to DYN3D.

The effective multiplication factor is also improved by splitting the bottom as depicted in Table 3.5. Further evaluations within this article use the original DYN3D model, to best represent the industrial method applied. This has also implied that the use of the thermal scattering libraries is likely to have minimal affect and that the main driver for the errors comes from the nodalisation process of the water density during the cross-section preparation process.

Table 3.5. Keff of the three different assembly models.

	Serpent	DYN3D Original	DYN3D Case 1	DYN3D Case 2
k_{eff}	1.0170	1.0243	1.0205	1.0189
pcm variation from Serpent	-	698	332	184

3.5.3. Single Assembly Coupled Neutronic and Thermal-Hydraulic Evaluation

The core simulator DYN3D comes with a complete coupled neutronics and thermal-hydraulics package which provides steady state and transient opportunities by using a coupling scheme which is determined to have converged once the users defined k_{eff} variation between iterations is achieved [44]. Similarly, the coupling process between Serpent and CTF focused on the variation in k_{eff} between iterations due to thermal feedback effects, where these results are presented in Table 3.6.

Table 3.6. Serpent/CTF variations between iteration numbers.

Iteration Number	k_{eff}	Serpent pcm Error (±) 95% Confidence	pcm Variation from Previous Stage
1	1.01703	17	NA
2	0.989339	18.1	2752
3	0.987905	18.5	147
4	0.989163	17.7	−129
5	0.988656	17.4	52
6	0.988832	16.8	−18
7	0.988786	16.4	5

After seven iterations the variations of k_{eff} the model has converged within the statistical error of the Monte Carlo calculation. A further analysis of the pcm variation per step is provided within Figure 3.14, where the largest deviation occurs after the first stage as the water density and temperature deviated from the initial assumption. After stage four, the variations between stages becomes minimal, thus hinting that the system has converged. Earlier efforts highlighted that, despite a low variation in k_{eff}, the power profile can still vary significantly; to determine if this was the case, Figure 3.15 shows that, similarly to k_{eff}, the power variations are minimal after iteration 5, which represents step 4 in Figure 3.14. Following the convergence being met, the full radial power distribution is presented within Figure 3.16 where the pin powers remain within their original position and just small deviations in the power are visible as the model converges.
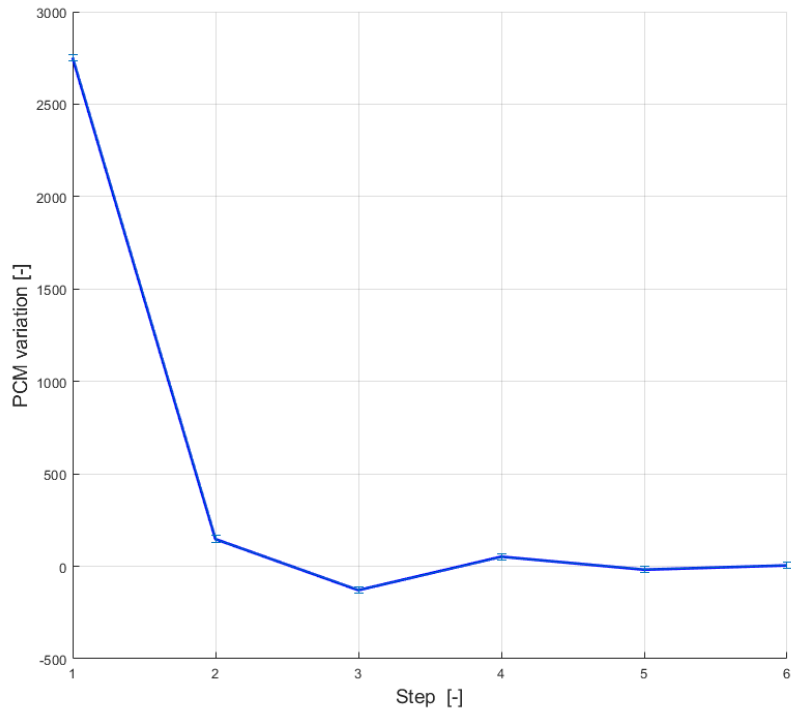
Figure 3.14. PCM variation per stage of iteration between Serpent/CTF stage.
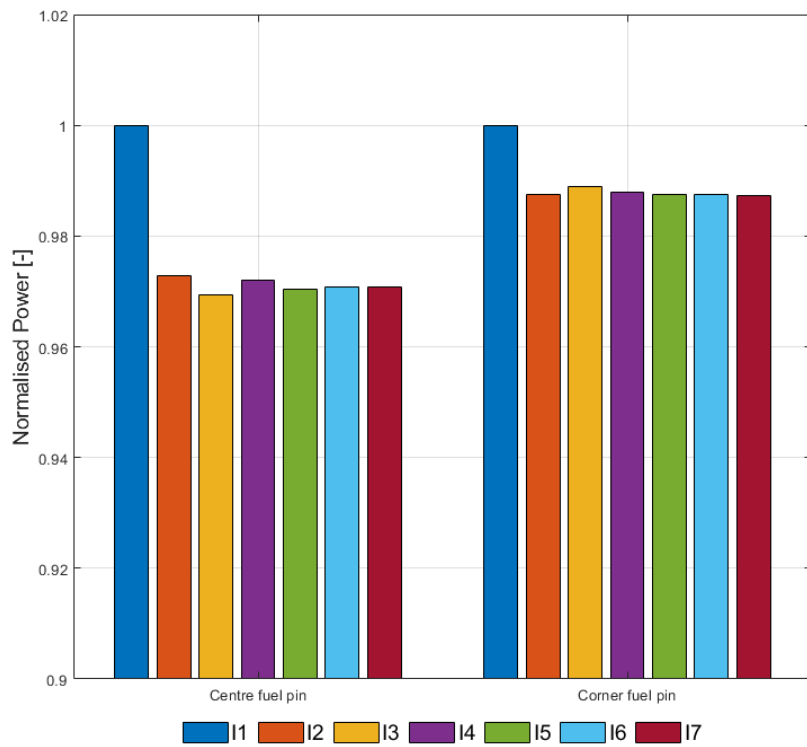
Figure 3.15. Pin powers for each iteration (I) for the centre and corner fuel pins of the assembly. Pin power is normalised by the maximum power of the pin.
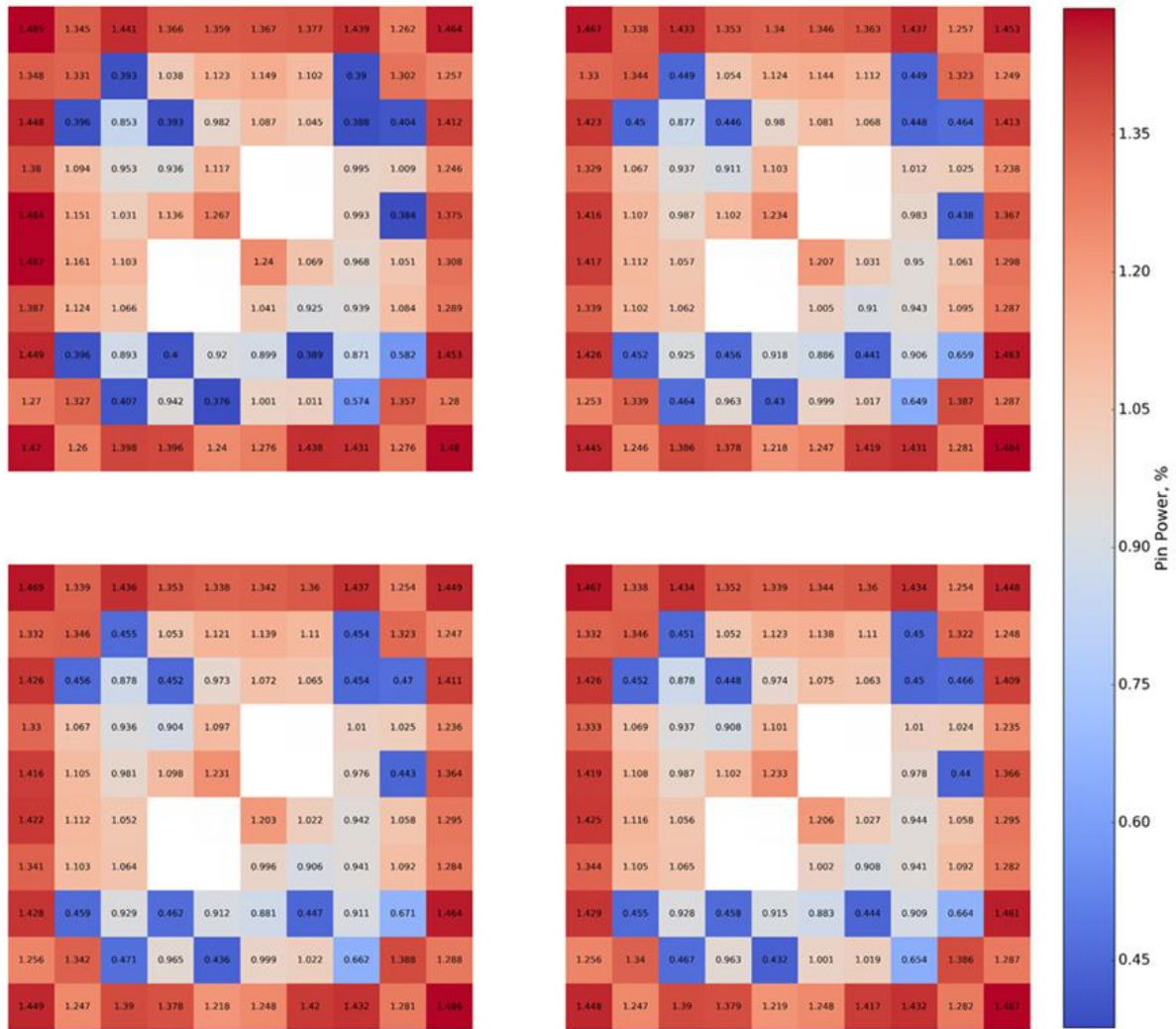
Figure 3.16. Single assembly pin power profile between iterations normalised to the total assembly power (100%). **Top left**, iteration zero, **Top right**, iteration one, **Bottom left**, iteration two and **bottom right**, iteration three.

Figure 3.17 shows the axial power profile delivered by the coupled high-fidelity calculation is within good agreement with the DYN3D results once the simulations have converged. A similar pattern where Serpent's power profile is slightly lower than DYN3D's has been observed in the previous chapter; however, this deviation is reduced in the coupled results. This result provides confidence that the 2D-1D approach in DYN3D is able to accurately predict the axial power profile to a high degree of accuracy for this fuel assembly.
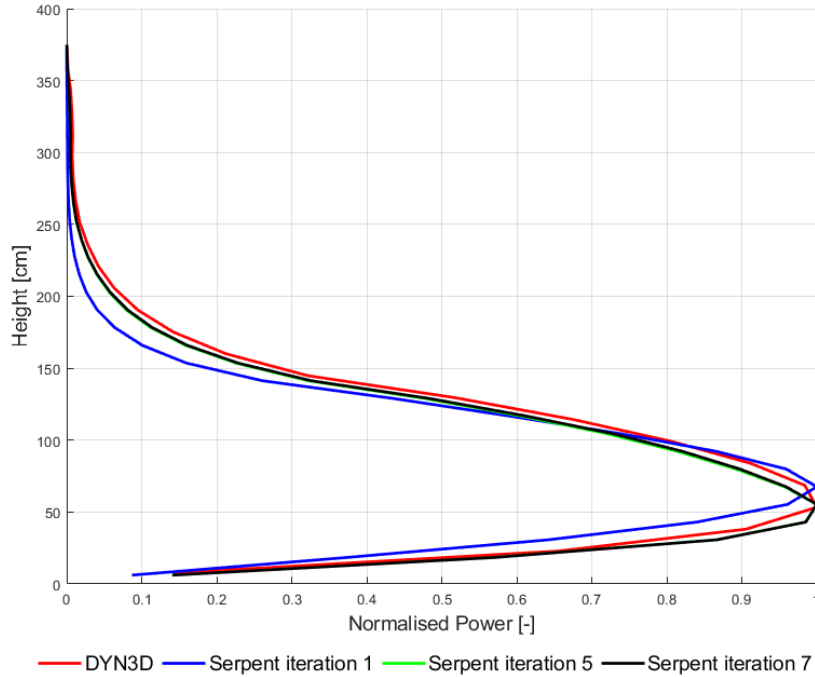
Figure 3.17. Normalised power profile of DYN3D and Serpent following the inclusion of thermal hydraulics.

From a safety perspective, the fuel temperature is one of the key parameters for the design process together with the related cladding temperature, as these values provide the safety margin for the design of the fuel itself, but also for the core design. CTF provides a new in-built fuel performance module which provides the fuel surface temperature and centreline temperature which can be obtained for each pin via the pin powers provided by Serpent. DYN3D does not obtain any details within the node, since the approach is based on one representative fuel rod per node, so the fuel centreline temperature is approximated by assuming an even power distribution across all pins which provides the average fuel centreline temperature. To obtain the maximum fuel temperature of the assembly, DYN3D would use an offline pin power reconstruction procedure based on the pin-power map of the lattice calculation. The results can be refined by coupling to a fuel performance code, such as ENIGMA [45] or TRANSURANUS [46,47]; however, this is beyond the scope of this project, so only the average temperatures are considered here.

The slightly shifted power peak in Serpent leads to a similarly shifted fuel temperature peak as highlighted in Figure 3.18. The average fuel temperatures between the codes are in very good agreement with one another, showing that the industrial method can provide a good representation of these average results. DYN3D's slightly elevated temperature would also provide a small safety margin within this case—thus, the result of the industrial code is conservative.
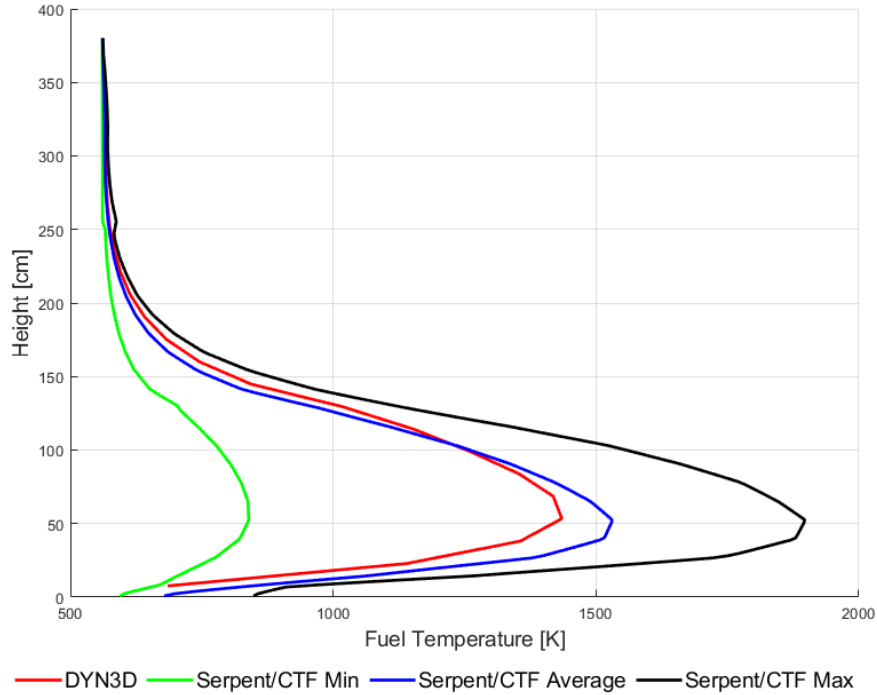
Figure 3.18. Maximum centreline temperature (K) of the fuel pins in DYN3D and CTF.

The density of the coolant is one of the key parameters, since within a BWR steam is formed inside the fuel assembly and later is used within the turbine. However, the heat transfer ability of steam is lower than water and the steam bubbles reduce the moderation of neutrons; thus, the coolant density curve is of high importance for any BWR simulation. The average density can be seen in Figure 3.19 where the horizontal lines in water density are the positions of the grid spacers. The grid spacers accumulate water due to the restricted flow and induce a slight pressure change; this effect is ignored in DYN3D, which cannot incorporate grid spacers. The grid spacers also create a pressure drop across the axial height, which would slightly reduce the mass flow rate which could account for the slightly higher coolant temperature. The average water density profiles are nearly identical between the two codes, which shows that the high-fidelity method does provide addition detail, while the average value does not differ significantly. This is an impressive outcome keeping in mind the fully modelling each channel and the inclusion of crossflow within the assembly and the inclusion of grid spacers in the high-fidelity solution.
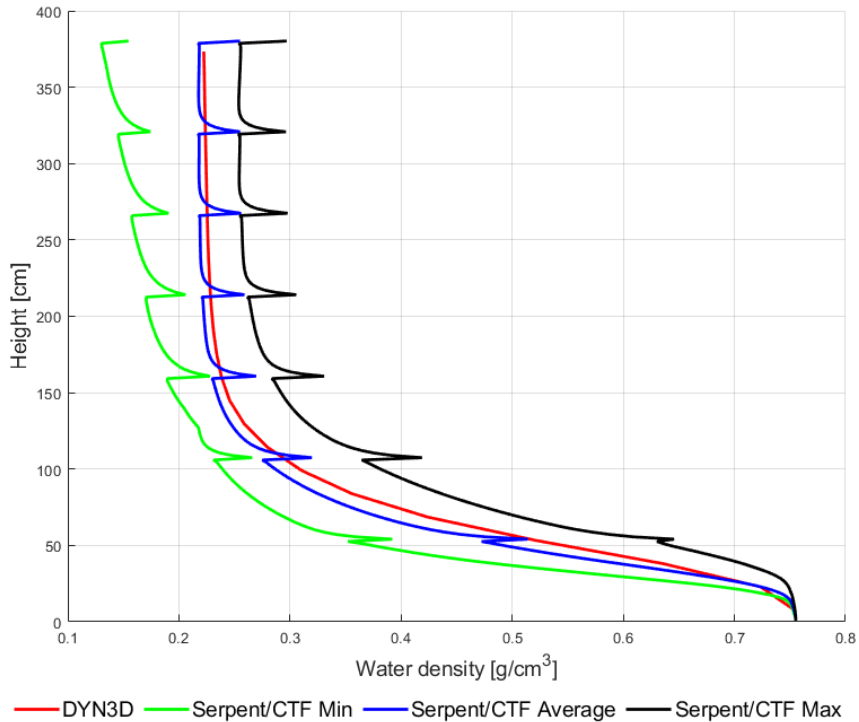
Figure 3.19. Water density (g/cm^3) comparison between DYN3D and CTF.

The coolant temperature is also important to understand the phase change location of the water, which significantly reduces the heat transfer properties of the coolant. Within Figure 3.20, CTF shows an accelerated heating up of the water compared to DYN3D. This is caused by the slightly shifted power profile; however, this effect should not be as significant as the figure suggests which is partly based on the very much stretched *x*-axis spanning only over 25 K. It should be noted that DYN3D has a directional change in the water temperature at ~144 cm; this is the location of the transition between fuel level one and two. It seems as if DYN3D is unable to accurately determine the temperature across this nodal boundary; this is likely to be caused by the large reduction in power across these boundary levels which causes this instability. To try and reduce this effect, both DYN3D's internal two-phase flow method and the ASME IFC-67 thermodynamic steam tables (IFC-67 were replaced by IAPWS-IF97 in 1997 [48]) were compared and showed very little difference with the results.

Overall, the codes are in good agreement with one another, with their only being a 4 K temperature difference in the coolant temperature, which has negligible effect on the coolant density compared to the void content.
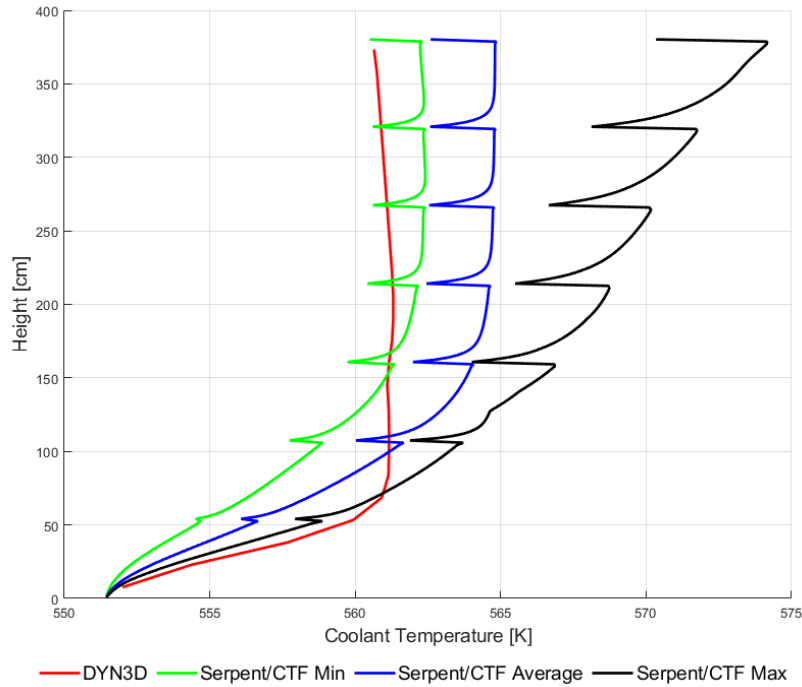
Figure 3.20. Subchannel temperature (K) comparison between DYN3D and CTF.

The coupled neutronic and thermal-hydraulic performance of DYN3D on fuel assembly basis has shown to provide a high level of agreement within the critical safety parameters which have been evaluated here. Despite the purely neutronic version showing a deviation in the peak power, this has been resolved once both code suites have provided their converged fluid flow regimes. The largest deviation came from DYN3D's coolant temperature, which showed quite a variation compared to CTF; however, the total deviation was only 4 K, which is unlikely to be significant for safety procedures. Thus, based on these results, we can claim a substantial basis of good agreement on fuel assembly level between both approaches.

3.5.4. Full Core Pure Neutronic Evaluation

The first part of this investigation was to obtain a detailed set of assembly materials required for the full core analysis; this procedure took place by depleting both fuel assemblies to the required burnup cycle stages using a uniform fuel temperature of 900K and the benchmarked water density. This task was a non-trivial one in Serpent as each fuel pin containing gadolinium had to be subdivided into ten radial regions and all pins were axially divided into thirty regions to account for changes in radial and axial depletion. The fuel assembly multiplication factor variation with the burn-up are presented in Figures 3.21 and 3.22. The fuel assembly burnup curve of the modelled BWR fuel assembly is significantly different to the curves regularly seen for PWR assemblies with burnable poisons. Both codes deliver comparable trends showing a first peak about 5 GWd/TU, a dip between 12 and 27 GWd/TU and a second peak around 32 GWd/TU, but with clear differences in the height of the peaks and especially in the form of the dip. To deepen the understanding of the effect of the level structure and the constant fuel temperature in neutronics a fully coupled DYN3D burnup calculation is added in green. First, there is the initial bias which is just confirming the differences seen in Table 3.6. Second, there is the

strong dip in the DYN3D result around 12 to 13 GWd/TU, where the results significantly differ from the Serpent results. This seems to be an artefact of the level structure. Thirdly, there is the stretching of the whole burnup curve over time which could be an effect of the real fuel temperature and water density distribution which has typically an influence on the burnup behaviour. Finally, the proposal for a next, future step to apply a history correction [49] in the DYN3D calculation to eliminate or reduce the effects created by the assumptions of water density and fuel temperature in the lattice calculation.
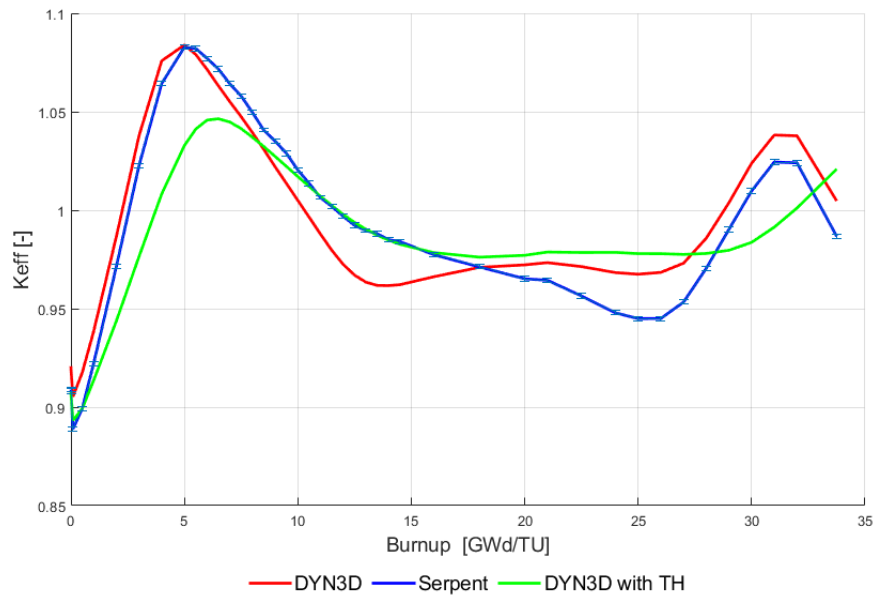
Figure 3.21. Fuel assembly one fuel burnup comparison between DYN3D and Serpent.
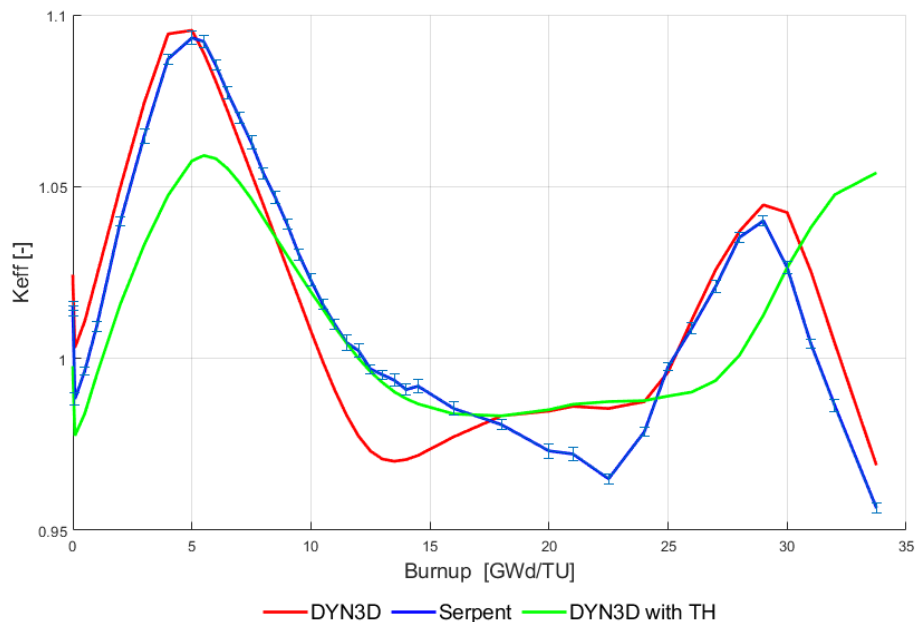
Figure 3.22. Fuel assembly two fuel burnup comparison between DYN3D and Serpent.

Table 3.7. Pcm variation at each burnup stage for both fuel assemblies.

Assembly Number	A1				A2			
Burnup (GWd/TU)	0	5	10	30	0	5	10	30
Serpent	0.9089	1.0827	1.0204	1.0098	1.0154	1.0933	1.0228	1.0265
DYN3D	0.9208	1.0839	1.0050	1.0238	1.0243	1.0955	1.0079	1.0425
Pcm variation	−1414	−97	1505	−1353	−860	−183	1441	−1496

From Figures 3.21 and 3.22 and Table 3.7, the fuel assemblies k_{eff} across the fuel lifecycle show large discrepancies between Serpent and DYN3D; however, the trends in the curves are similar. The initial pcm deviation at day zero was earlier demonstrated to be strongly influenced by the thermal scattering library in Serpent, which is currently not available in the required setup, another cause can be in the water density averaging across the axial levels of DYN3D. This could be further reduced by adding an additional level of cross-sections to reduce the errors incorporated by the averaging process as shown before. From a modelling perspective, the additional natural uranium region on the F10 fuel pins in Serpent could account for the slight initial reduction in k_{eff} due to the parasitic absorption within these regions and, over time, this could see ^{239}Pu being bred, which could account for the higher k_{eff} later in the cycle, but the total effect of this is unlikely to be significant. To account for this, ^{239}Pu in the industrial methods would require more cross-section productions between levels 2 and 3, and this level would only have a minor effect on the systems' behaviour. Similarity to the second investigation, the original water density model was used within DYN3D, which has caused an overestimation in the bottom of level two, thus depleting the uranium faster over the full burnup curve; this is likely to be the driving factor for the differences between the two softwares. Overall, the accumulated differences within the model all contribute towards the significantly different results shown by DYN3D and Serpent, which could lead to an overestimation or underestimation of the reactivity coefficient of the equilibrium core.

Due to the lack of symmetry within the assembly, which is created by the water holes and the assembly map, a nonsymmetrical power distribution is created which Serpent can account for, while this not possible in the nodal approach of DYN3D due to the homogenisation process. To determine the severity of this effect, the pin power profile for assembly one is determined across the burnup cycle as shown in Figure 3.23. It should be noted that the supercells within the ABWR often contain cross shaped control rods between the assemblies, leading to asymmetric water gaps around each fuel assembly. If the control rods are inserted, this would cause additional power distribution imbalances, which would also be missed by nodal methods; these are likely to be more severe, yet more localised than the pin power distributions.
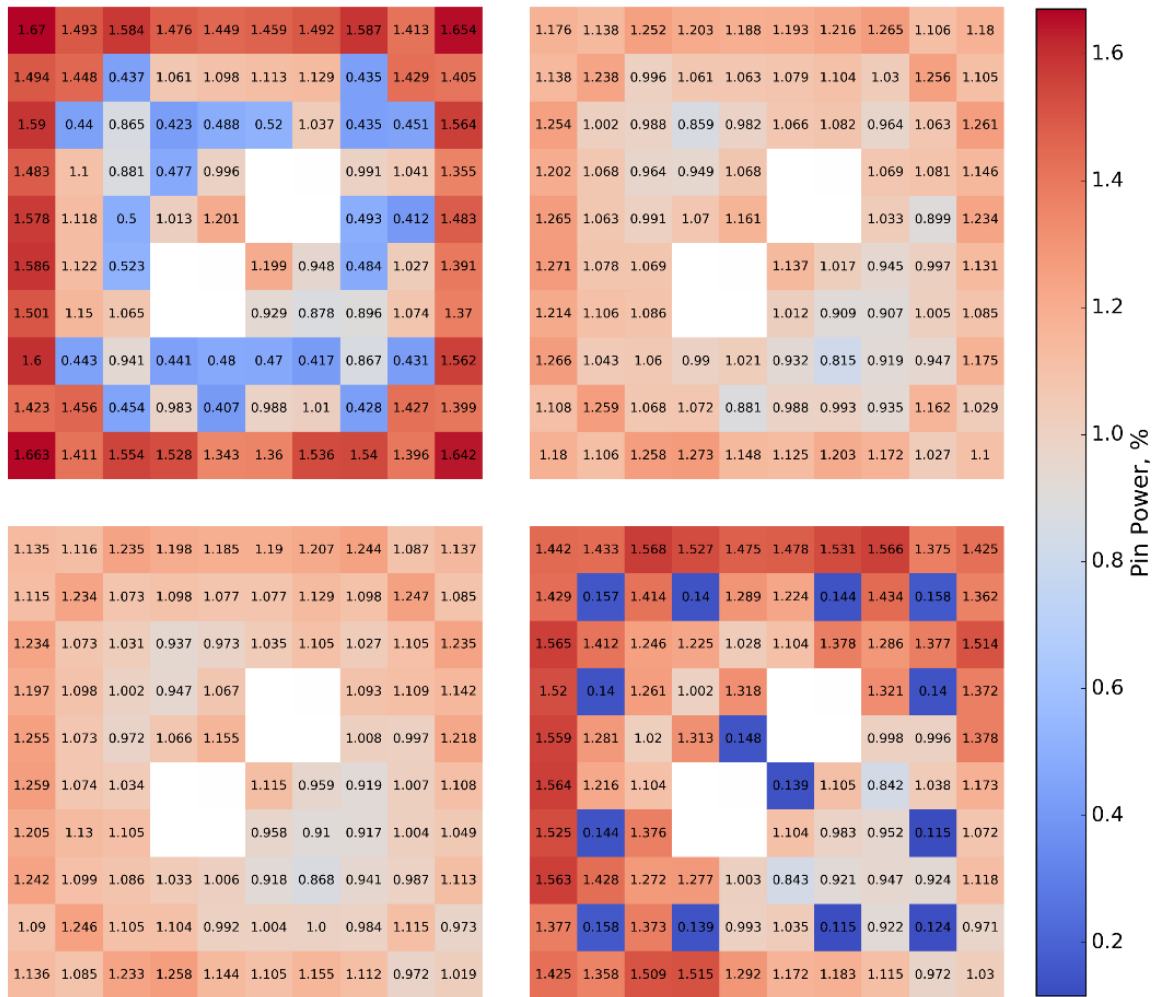
Figure 3.23. Pin power reconstruction from Serpent, where the pin power % is proportional to the total assembly power (100%). Top left, fresh fuel, Top right, 5 GWd/TU, Bottom left, 10 GWd/TU and Bottom Right 30 GWd/TU.

From Figure 3.23, the fresh fuel power profile is non-symmetrical from the design of the fuel assemblies and due to the water holes, there is only corner to corner symmetry whereas with a PWR there is usually full quarter symmetry. Through the burnup procedure, the power profile becomes highly non-symmetrical; this effect becomes quite severe at 30 GWd/TU with the power in the top left and bottom right showing 40% discrepancies. To account for the non-symmetrical power distribution, SP provides the option to create ADFs for each burnup and branching steps as well as for each assembly side separately. From Figure 3.23, it becomes obvious that a side ADF will produce an average boundary flux, where the true unbalance within the assembly is more corner based. Some studies have been performed to provide corner ADF's for hexagonal assembly LWR's [50]; however, this study has identified that a similar treatment is likely to be beneficial for modelling BWR's due to the highly non-symmetrical nature of the fuel assemblies. ADF's within SP is a simplification for assemblies as SP assumes that the neighbouring assembly is of the same type as that assembly being modelled; however, this is currently the only available approach to account for the non-symmetry of the problem inside the homogenization area of a full fuel assembly. ADFs are also used for assemblies adjacent to the reflector within the full core model, for

which SP has its own method of producing ADFs. It can be expected that calculation of the ADFs using, for example, two-dimensional models (i.e., super cells) can potentially lead to further improvements. However, this approach would require much higher efforts for generation of the cross-section libraries due to the larger sizes of the super cells in comparison with a single fuel assembly.

Following on from Figure 3.11, Figure 3.24 shows the axial power profiles for the assembly one at different burnup stages. Within the second study the axial power profile of Serpent was slightly lower than that of DYN3D and this was deemed to be due to the assumptions of the water density in the lattice calculation which is forwarded into the nodal calculation. This work has been further investigated in Figure 3.24, as the depletion of the ^{235}U will vary across each material zone axially, with this model using 30 axial depletion regions in Serpent and 26 in DYN3D. As Serpent's power profile starts at a lower point, the materials within the lower section are depleted faster than in DYN3D and this explains the transitional discrepancies of the power profile between the burnup stages two and three within Figure 3.21. The different speeds at which the power profile moves between the stages is critical for a safety analysis as these determine where the hottest pin or pin section is at any point in time. This study has identified that the pure neutronic assumptions within DYN3D and Serpent cause large variances of the speeds at which the power profiles move in BWR's due to the high levels of axial heterogeneity within the design which are not considered within current high-fidelity methods for PWRs. To fully investigate this, a coupled high-fidelity model is required for each assembly at each burnup step to determine if these match the coupled DYN3D burnup curve which is already included within Figure 3.21. This fully coupled calculation result with DYN3D is achieved using the water density as calculated through the thermal hydraulic module and the fuel temperature as calculated through the fuel rod model. These results help to deepen the understanding of the effect of the approximations which are introduced through the level structure of the lattice calculations. Overall, while the peak powers between the pure neutronic models do not differ significantly, their exact locations vary between the codes, while in all three cases the coupled solution shows reduced peaks which indicates that all results seem to be conservative. However, the identified differences between the codes does pose the question as to whether the used methods can accurately determine the time and location of the hottest pin to the required degree of accuracy through the life of a fuel assembly. This would be very helpful to justify to the quality of the safety analysis and to reduce over conservative safety margins. Nevertheless, the history of reactor operation with only very limited number of fuel failures confirms the approach used up to now as sufficiently accurate for reactor operation so long as the boundaries are not pushed to a too large extent.
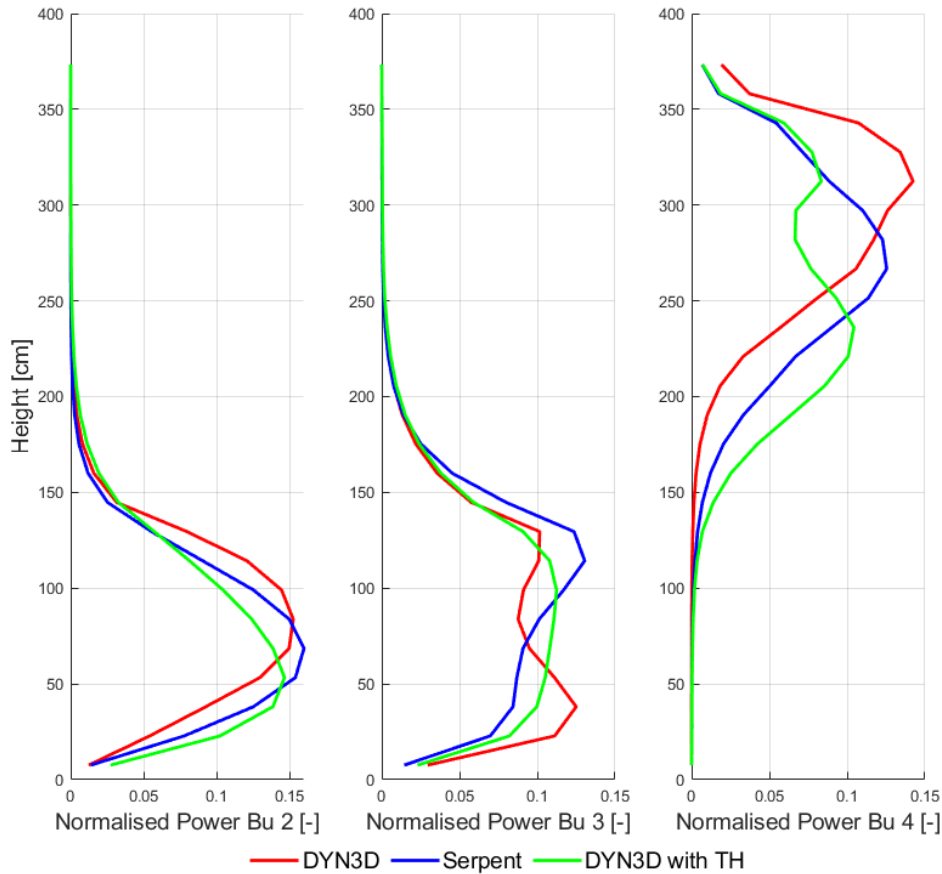
Figure 3.24. The normalised axial power profile for each burnup stage from left to right, 5, 10 and 30 GWd/TU for assembly one.

The full core simulations of the ABWR were performed using Serpent's MPI feature on the University of Liverpool's High-Performance Computer cluster, Barkla. Due to the memory requirements the simulation used 80 Intel Xeon Gold Skylake processors. The simulation used 8M neutron populations for 1000 active cycles and 300 inactive cycles, after the fission source convergence was shown to be achieved with this configuration. The limitation of this simulation is like in other research institutes, where the queue times become significant due to other users and runtime limits for simulations are set to a maximum of three days.

The k_{eff} of the full core neutronic model in Serpent was 1.02394 (±8 pcm) which provides only a 48 pcm variation from DYN3D, despite the differences in the material compositions which shows that, in large systems, the differences can be easily overlooked due to error cancellation if only comparing a single variable. The previous steps have shown significant differences between the two softwares outputs, which would have been missed if only the k_{eff} of the full core was evaluated.

From Figure 3.25 it is obvious that the power profile is not completely symmetrical with Serpent, with the top right of the figure having a slightly higher power than the opposing corner. This is due to the non-symmetrical power distribution in each fuel assembly as highlighted in Figure 3.23.
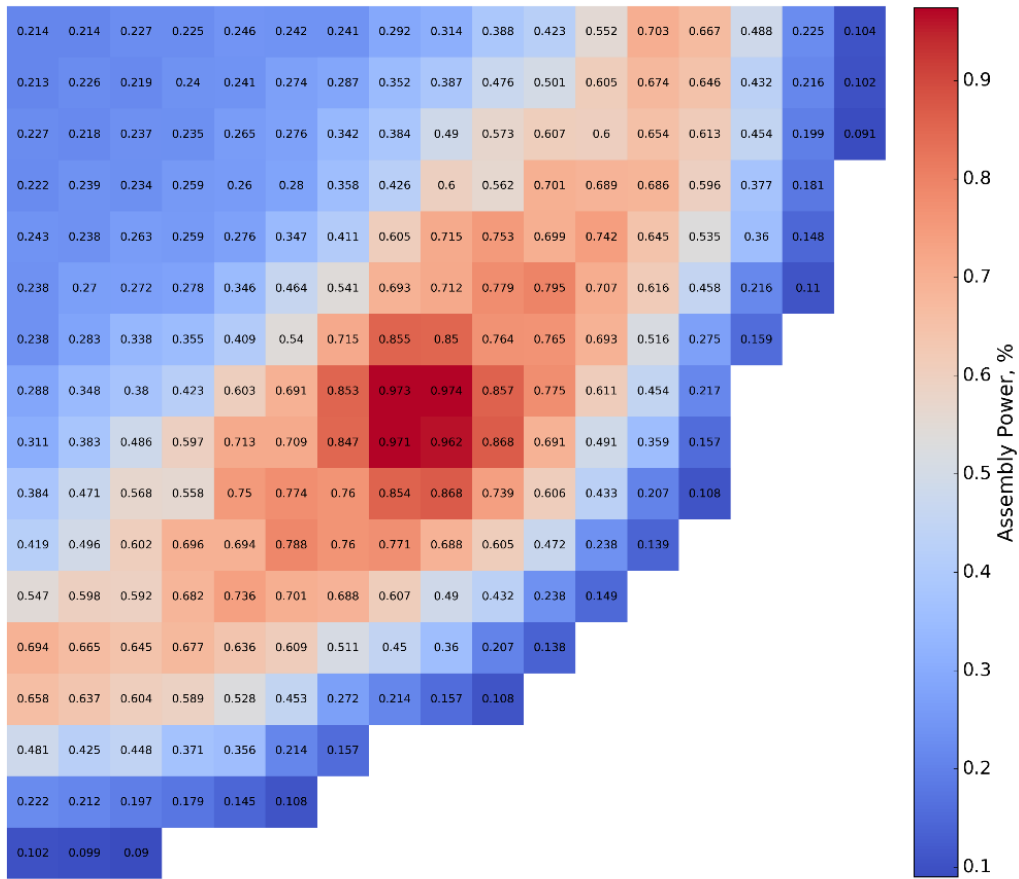
Figure 3.25. Serpent's full core assembly power profile.

Figure 3.26 shows the difference in each assembly power as the % of the total full core power, where the negative values represent a higher value in DYN3D compared to Serpent. Within this analysis DYN3D overestimates the highest power assemblies, which is a more conservative approach as these are the assemblies with the hottest pins. This can be explained due to DYN3D showing a larger value of k_{eff} for the central assemblies within the burnup stage, which implies the loading pattern provided this conservativeness and not the modelling procedure. The largest discrepancies occur near the exterior boundaries; this is within the vicinity of the assemblies where assembly burnup of 30 GWd/TU are positioned, and these have the second largest deviation in error from the assembly burnup models, and, since the evaluation is based on percentages of power, the error in low power areas is higher. It should be noted that the use of the reflector ADFs in DYN3D significantly reduced the discrepancies within the assemblies adjacent to reflector. Errors also occur within the centre of the core; this can be explained due to the largest variation burnup assembly on 10 GWd/TU being mainly positioned within this vicinity.

The radial power differences in the models can all be directly related to the input assembly compositions, a cascading effect of the modelling variances. Figure 3.26 emphasises the maximum deviation in the top right to 0.05% whereas the opposing assembly is only 0.043. Overall, the purely neutronic assembly power distribution is within reasonable agreement between the two codes and both codes identified the same fuel assembly as the limiting one with the highest power.
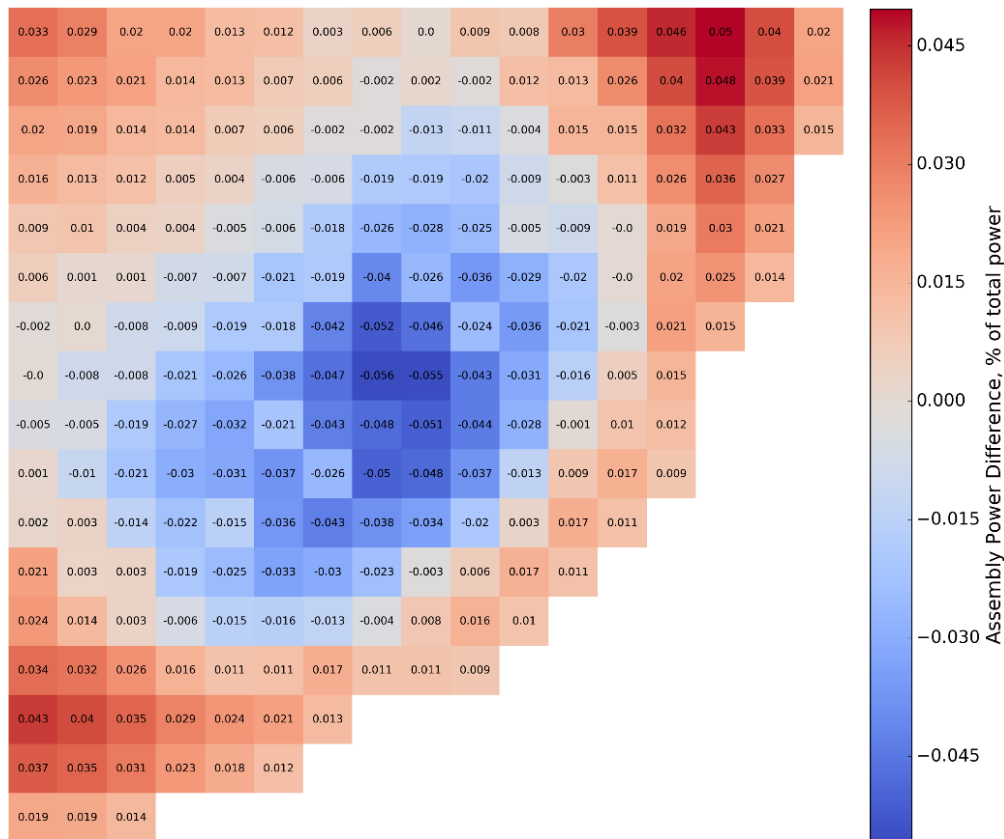
Figure 3.26. Purely neutronic assembly power difference (Serpent—DYN3D) between Serpent and CTF with relation to the % of the total power.

The purely neutronic normalised axial power profile is displayed within Figure 3.27 and the axial shift in power is like the single assembly analysis. There are now more factors within the production of the full core axial power profile compared to Figure 3.24 which has highlighted that the overall shift in power during burnup with each assembly with its burnup stage contributing towards the axial power profile. These effects of each fuel assembly are weighted to with the total power distribution per assembly shown in Figure 3.25 which has determined that the highest power assemblies are in burnup stages one and two. In this stage the fuel assembly simulations show that the lowest variations in their power profiles between the software. This allows Figure 3.27 to obtain the familiar shape and a good agreement between the codes; however, this could change if the core behaviour would be followed over the full cycle. Beyond the axial height of 150 cm, the power peaking shown within DYN3D is provided by the assemblies within burnup stage four, which within DYN3D will provide a higher flux at high axial points within the design. Despite this area not being critical from a safety perspective, the flux distribution is, therefore, slightly distorted due to the burnup discrepancies identified in Figure 3.24.
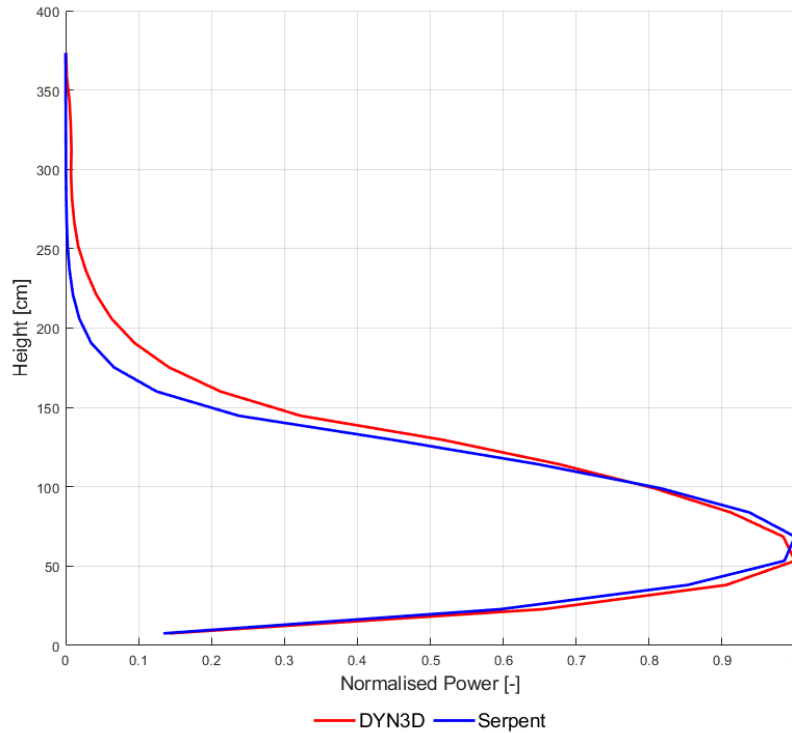
Figure 3.27. Axial full core power profile for DYN3D and Serpent, purely neutronic calculation.

Overall, the purely neutronic code comparison for the full core is within good agreement between the two codes within the critical areas of interest within a snapshot in time at the core start up. In this instance the hottest power pins are within assemblies in burnup stages one and two, which have almost similar power profiles. This is very much dependent on the exact burnup stage as this investigation has highlighted that DYN3D's axial power profile lags slightly behind Serpent's over burnup and this gives evidence to the thought that the hottest power pins further into the burnup cycle are likely to shift, which would occur at different rates between the codes. The analysis has highlighted that the detailed behaviour of both modelling methods is significantly different between the models following the initial burnup stages, which has caused an overall cascading error through the results.

3.5.5. Full Core Neutronic and Thermal-Hydraulic Evaluation

The coupling procedures for the iteration steps for Serpent/CTF are shown in Table 3.8 which shows that the coupling procedure does not converge in the same manner as the single assembly with a visual representation in Figure 3.28.

Table 3.8. Full core Keff iterations between Serpent and CTF.

Stage	k_{eff}	Pcm Error 95% Confidence	Pcm Variation from Previous Stage
0	1.02394	8	NA
1	0.99218	8	−3126
2	0.99412	8	196
3	0.99587	8	177

Stage	k_{eff}	Pcm Error 95% Confidence	Pcm Variation from Previous Stage
4	0.99939	8	354
5	1.00765	8	820
6	1.00938	9	170
7	1.01227	8	283
8	1.01110	8	−114
9	1.01241	8	128
10	1.01125	9	−113
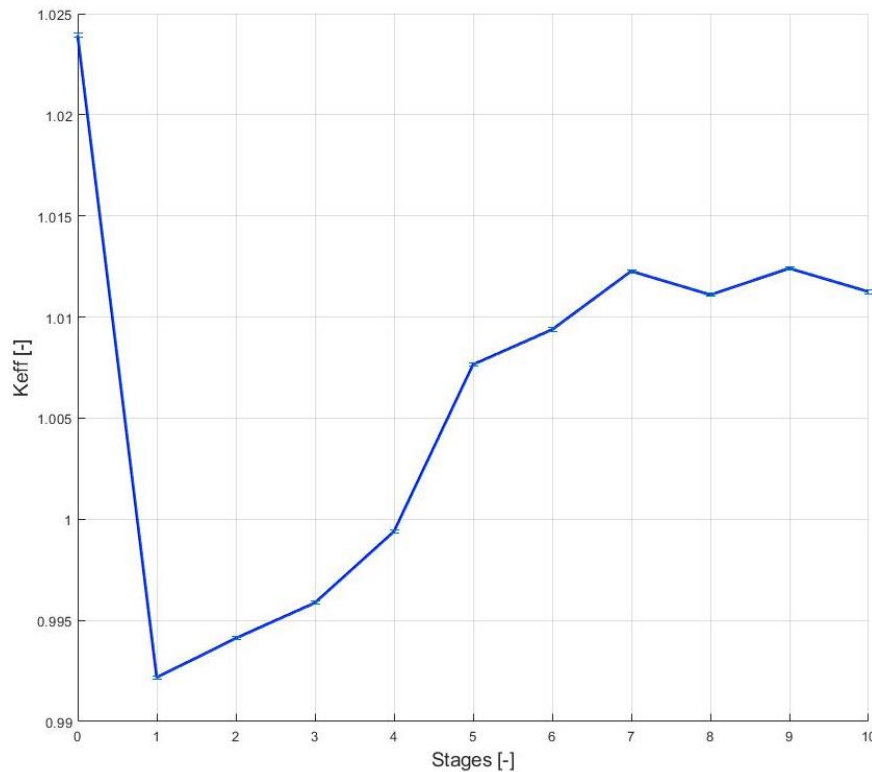
Figure 3.28. Full core convergence between iterations on Serpent/CTF.

Up until stage four, the effective multiplication factor seems to be converging and then the results suddenly start to become unstable. The first area to determine why the system has not converged by investigating the radial power profile in Serpent, as shown in Figure 3.29 which shows that following the first iteration the build-up of unsymmetrical power profiles which shifts the power to the top right of the core layout after the second iteration. The effect of this is that the highest power assemblies become less favourable to fission within stage three because of the increase Doppler broadening and the lower water density. This affect then has the exactly opposite effect on the proceeding iteration, which identifies that this is the cause of the instability of the coupling procedure. This affect is thought to be more severe than the single assembly because the water and fuel temperatures variation is much wider in the full core system compared to the single assembly. One of the drawbacks of this, is that the hottest power assembly is also obtaining higher power values per each iteration which implies that the results will be inaccurate.
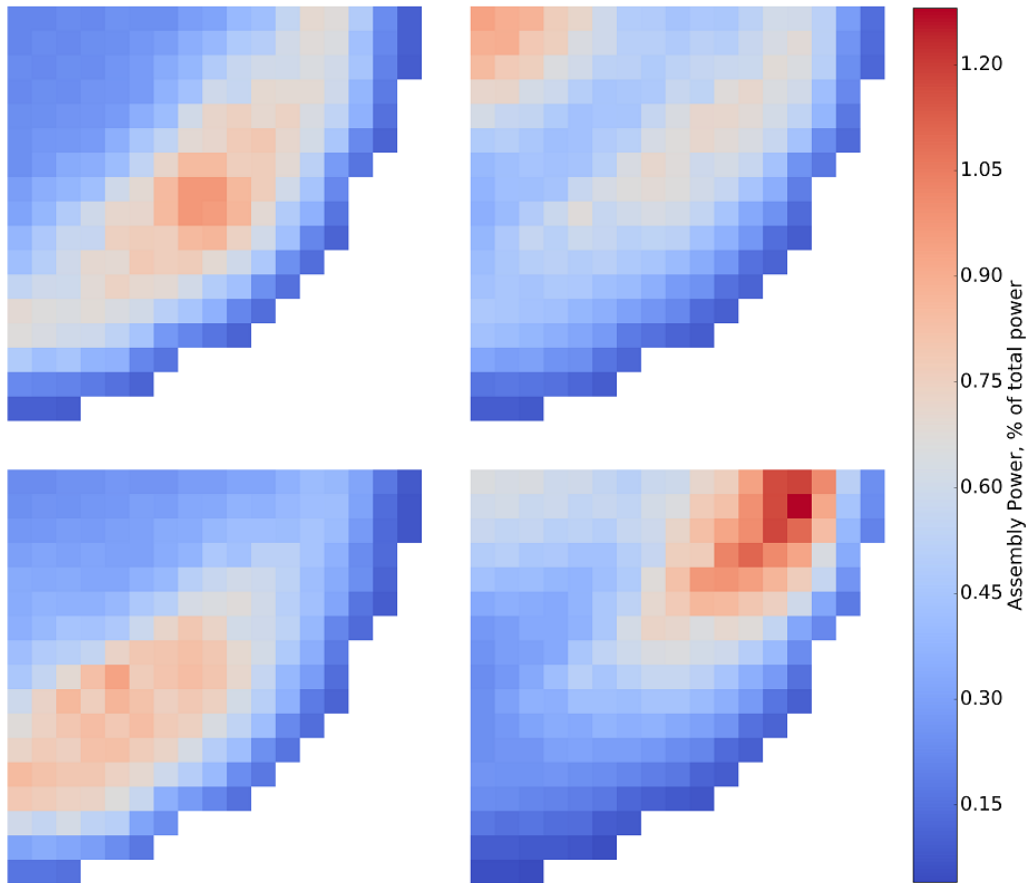
Figure 3.29. Power profiles from Serpent per iteration between Serpent and CTF where the assembly power % is proportional to the total reactor power (100%). Top left, stage zero (purely neutronic), top right, stage 1 coupled, bottom left, stage 2 coupled and bottom right, stage three coupled.

Stage ten of the coupling process had the same power distribution arrangement but not as high peak values as stage four within Figure 3.29. Due to convergence not being achieved, it would not be promising to go into a deeper comparison of any radial results; thus, only a short investigation will be performed on the integral values to see what has been achieved through convergence of k_{eff} as an integral value and to demonstrate what kind of additional information can be delivered using the fully resolved fluid dynamics with CTF.

The fully coupled axial power profile comparison in Figure 3.30 shows that Serpent's higher axial profile trend continues, with Serpent having a slightly broader peak power than DYN3D, which can be explained by the 10 GWd/TU assembly power profiles power contribution.
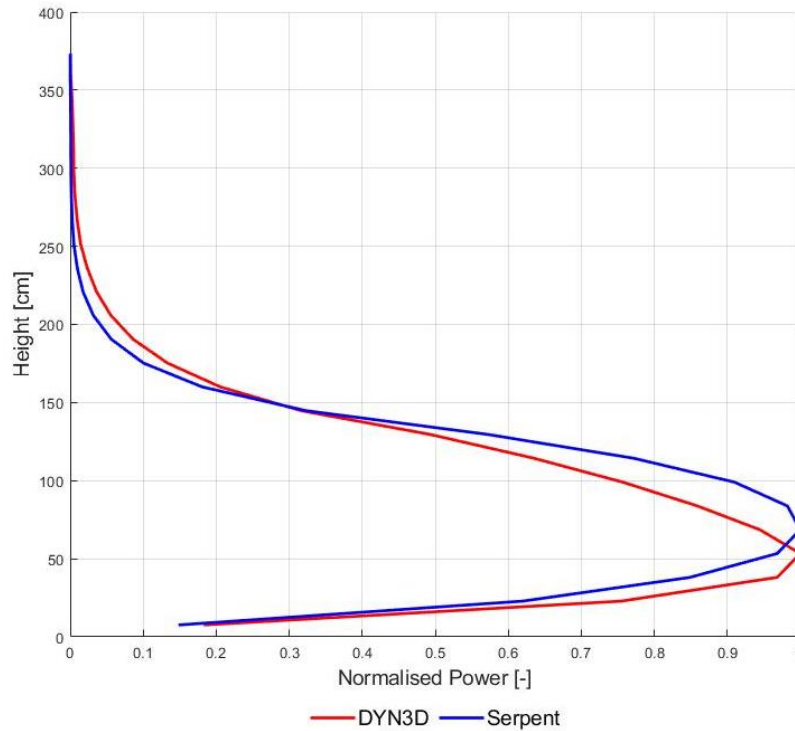
Figure 3.30. The axial power profile of Serpent/CTF and DYN3D.

The coupled results of the full core could not be used as a direct comparison due to the not achieved convergence on the coupled high-fidelity solver. However, this section has shown that the input material compositions of the equilibrium core varied significantly between the two codes which implies that even at the start of life there is a difference between DYN3D and Serpent to be expected. This could be investigated further by reducing the number of variables between the models to determine the main cause; however, this study has highlighted that the most likely cause is due to the different water density representation used within the different codes. Further analysis is required with regard to how to best apply high-fidelity methods with BWRs, where the lack of symmetry and high levels of heterogeneity have shown on a full core level that these could have significant implications for the long-term operation of the design and its fuel assemblies and following the potential for further optimisation of BWR fuel assembly design and the related operation.

3.5.6. Discussion of Possible Ways to Improve the Results

As it was demonstrated in the previous sections, the results of the currently applied industrial techniques can have significant discrepancies in comparison with the high-fidelity coupled neutronics-thermal hydraulics simulations. Undoubtedly, the results of the industrial codes used in present study can be further improved by applying more advanced techniques for ADF generation or, for example, application of the SPH factors (which were not used in the current study) or the combination of both mentioned techniques. However, all these techniques would require additional significant investments into the developing of the appropriate computational models, verification and validation and will not overcome the limit of nodal codes delivering only coarse mesh results instead of fuel pin related data.

Therefore, this way can become computationally expensive and not so attractive for application by industry since it will still require the offline pin power reconstruction.

To overcome mentioned above limitations, another approach can be proposed. As it has been demonstrated in the present study, high fidelity coupled pin-by-pin neutronics and thermal hydraulic simulations can be very interesting, but unfortunately costly and difficult to implement and use in day-to-day industrial work. Therefore, another method was proposed [51,52] to overcome these challenges while keeping the computational time on the level acceptable for industrial application. In this technique, high fidelity methods would be applied only to the assemblies where high errors are expected (for example, assemblies adjusting to the reflector or control rods) or the highest loads will be needed to determine safety parameters. These assemblies could be resolved down to the pin level (using the boundary conditions from the full core nodal solution), while the fuel assemblies in the less challenging surrounding (i.e., central assemblies) would be still simulated on the nodal level. The idea of this approach is schematically shown in Figure 3.31.
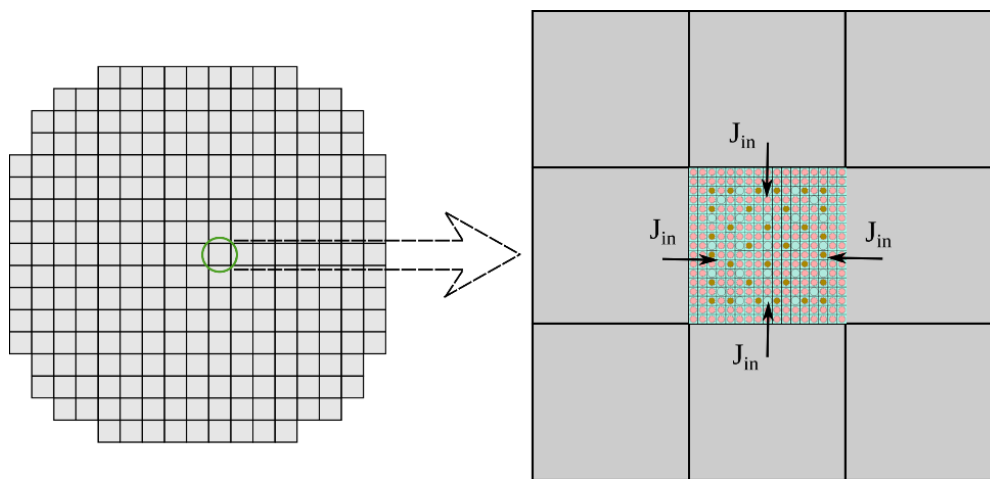
Figure 3.31. The multi scaling scheme for the smart high-fidelity coupling [28].

Considering the multi physics nature of the reactor simulations, the application of the Monte Carlo codes as a neutronics solver is expected to still be time consuming even when applied on the level of a single assembly. Therefore, less general but faster neutron transport solvers should be used for this task (see, for example, [53,54]) and coupled to thermal hydraulics solvers. This approach, in our view, has strong potential to resolve the problems outlined in the present study without involvement of the ADF and SPH factors and other approximations aiming to reduce the naturally inherent error in diffusion approximation.

3.6. Conclusions

This article aimed to determine the variations between the industrial toolkit SCALE-POLARIS/DYN3D and a high-fidelity method of a coupled Serpent/CTF approach for the application in BWRs to determine where the industrial code struggles to find the details which were highlighted in the high-fidelity methods. This approach used a bottom-up procedure, where code to code comparisons were made from the 2D fuel assembly to, finally, a full core comparison. The depletion methods within both codes for 2D arrangement were in near perfect agreement between SCALE-POLARIS and Serpent,

despite the different methods used within the software and the use of Serpent's beta version of the ENDF/VII.1 data library.

Stage two investigated the performance of a single assembly with reflective boundary conditions by using the cross-sections from four axial levels from SP in DYN3D. From a purely neutronic perspective, the SCALE-POLARIS/DYN3D was not able to capture the axial power distribution in as much detail as required for the highly heterogeneous problem and this was identified to be due to the assumptions when splitting the axial geometry into the traditionally used four levels. Further improvements with the axial power profile shape and a reduction in K_{eff} variation were achieved by dividing the bottom level into more sections. A hot full power analysis was performed, and SCALE-POLARIS/DYN3D's average fuel temperature and water density were in a good agreement with the high-fidelity methods and the axial power profile shape became closer to the high-fidelity methods. It was noted that SCALE-POLARIS/DYN3D did not produce the same water temperatures, yet matched the water density, which implies that the code used different water property data. Using the SCALE-POLARIS/DYN3D, a new fully coupled approach for the burnup case has been delivered for the investigated fuel assembly which significantly differs from both pure neutronic results.

Stage three investigated a full core supercell arrangement based upon the ABWR design. This stage highlighted that the burnup procedures of the individual assemblies provided large discrepancies between the two software tools and the axial power profile transition within Serpent varied significantly compared to DYN3D. These discrepancies are attributed to the long-term implications of the different power shapes between the methods, which will have an accelerated affect due to depletion. SCALE-POLARIS/DYN3D overestimated the power within the hottest fuel assemblies, which provided a slightly more conservative approach towards the modelling high fidelity approach; however, this was determined to be due to the fortunate arrangement of the core layout and this trend would not hold. Unfortunately, the third study could not provide a converged fully coupled Serpent/CTF model. Due to the large variations within the burnup procedure, this work has identified that the assemblies used within the equilibrium core layout could be significantly different when using industrial methods compared to high fidelity methods. At the time of writing, there is no solution to resolve the coupling errors of the full core analysis; however, it is assumed that these discrepancies of the full core model will be magnified and will have an impact on the safety parameter assumptions we make within BWR safety analysis.

Finally, a possible way to overcome the mentioned problems with the help of the novel multiscale and multi physics approach is proposed to support the future development of a more accurate industrial approach with acceptable computational demand.

3.7. Further Work

This work has identified that the materials used within an equilibrium core can be significantly different to those predicted by industrial methods. Due to limitations in the convergence of the high-fidelity method, the severity of these impacts could not be investigated in all detail; however, the power level profile is likely to be broadened from early indications. This could have a positive effect, due to the reduced peaking of the fuel axial power profile, but this must be established with further work. Thus, it would be ideal to apply the newly developed tools of the CASL project (even if this will require massive

computational resources) to this kind of analysis to create reference solutions for the upgrading of industrial tools for BWR analysis.

Conflicts of Interest: The authors declare no conflict of interest.

Appendix A

This section provides the relevant simulation data for the software inputs.

Table 3.A1. Thermal hydraulic data used within the model.

Thermal Hydraulic Data	Value	Unit
Pressure at the outlet	7.171	MPa
Power per assembly	4502	KW
Mass flow rate per assembly	16	$kg \cdot s^{-1}$
Inlet temperature	278.3	°C
Gas gap conductance	2942	$W \cdot m^{-2} \cdot K^{-1}$

Table 3.A2. Serpent's initial coolant channel data.

Hight (cm)	Assembly Model Density (g·cm^{-3})	Initial Temperature (K)
0	0.7552	600
15.24	0.7552	600
30.48	0.7500	600
45.72	0.7309	600
60.96	0.6956	600
76.2	0.6433	600
91.44	0.5903	600
106.68	0.5395	600
121.92	0.4993	600
137.16	0.4598	600
152.4	0.4194	600
167.64	0.3958	600
182.88	0.3670	600
198.12	0.3357	600
213.36	0.3225	600
228.6	0.3002	600
243.84	0.2764	600

Hight (cm)	Assembly Model Density (g·cm⁻³)	Initial Temperature (K)
259.08	0.2717	600
274.32	0.2506	600
289.56	0.2398	600
304.8	0.2380	600
320.04	0.2159	600
335.28	0.2164	600
350.52	0.2095	600
365.76	0.1961	600
381	0.2020	600

Table A3 provides an overview of the materials that are within the core.

Table 3.A3. Material information used.

Part	Description	Value (cm)
Fuel pin	Fuel pin diameter	0.876
	Gas gap outside diameter	0.894
	Fuel Cladding outside diameter	1.026
	Fuel pin pitch	1.295
Water rod	Water rod water diameter	2.322
	Water rod cladding outside diameter	2.522
Assembly cladding	Inside cuboidal dimensions	13.42
	Outside cuboidal dimensions	13.82
Water surrounding the assembly	Cuboidal dimensions	15.539
Steel/water mixture below the assembly	Height	50
Outside of the reflector	Diameter	710

Table 3.A3. *Cont.*

Part	Density (g·cm⁻³)	Temperature (K) if not fixed, starting temperature provided	Fixed Density	Fixed temperature
Water rod	0.7552	600	Yes	Yes
Water rod cladding	6.57	600	Yes	Yes
Outside cladding	6.57	600	Yes	Yes
Outside water	6.57	600	Yes	Yes
Natural uranium ends	10.424	900	Yes	Yes
Fuel Pellets	10.424	900	Yes	No
Fuel cladding	6.57	600	Yes	No
Subchannel coolant	Varies axially	Varies axially	No	No

References

1. Chauliac, C.; Aragonés, J.M.; Bestion, D.; Cacuci, D.G.; Crouzet, N.; Weiss, F.P.; Zimmermann, M.A. NURESIM—A European simulation platform for nuclear reactor safety: Multi-scale and multi-physics calculations, sensitivity and uncertainty analysis. *Nucl. Eng. Des.* **2011**, *241*, 3416–3426, doi:10.1016/j.nucengdes.2010.09.040.
2. Szilard, R.; Kothe, D.; Turinsky, P. *The Consortium for Advanced Simulation of Light Water Reactors (No. INL/CON-11-22917)*; Idaho National Laboratory (INL): 2011.
3. Lindley, B.; Allen, D.; Lillington, J.; Smethurst, A.; Smith, P.; Bowman, D.; Dwyer, L.; Lai, K.; Levers, A.; Vikhorev, K.; et al. Modelling and simulation activities in support of the UK nuclear r&d programme on digital reactor design. *Int. Conf. Nucl. Eng. Proc. ICONE* **2018**, *3*, doi:10.1115/ICONE26-81090.
4. Kochunas, B.; Collins, B.; Scott Palmtag, F.F. Validation and Application of the 3D Neutron Transport Code Mpact within Casl VERA-CS. Available online: https://www.osti.gov/servlets/purl/1214019 (accessed on 22 October 2020).
5. Jessee, M.A.; Wieselquist, W.A.; Evans, T.M.; Hamilton, S.P.; Jarrell, J.J.; Kim, K.S.; Lefebvre, J.P.; Lefebvre, R.A.; Mertyurek, U.; Thompson, A.B.; et al. Polaris : A New Two-Dimensional Lattice Physics Analysis Capability for the Scale Code System. *Physor* **2014** .
6. Martinolli, E.; Carter, T.C.; Clément, F.; Demy, P.M.; Leclère, M.; Magat, P.; Marquis, A.; Marotte, V.; Marten, J.; Misu, S.; et al. APOLLO2-A—AREVA's new generation lattice physics code: Methodology and validation. *Int. Conf. Phys. React. 2010 PHYSOR 2010* **2010**, *2*, 1075–1087.
7. Rhodes, J.; Smith, K.; Lee, D. CASMO-5 development and applications. *PHYSOR-2006— Am. Nucl. Soc. Top. Meet. React. Phys.* **2006**, *2006*, 1–11.
8. Graphiques, S.; Flux, D.U.; Cellule, P.A.R. *Cronos 2 : Un Logiciel de Simulation Neutronique des Cœurs de Réacteurs*; Technical Report: Saclay, France, 2000.
9. Tomasz, C.L.; Deokjung, K.; Yunlin, L.; Jun, X. *PARCS : Purdue Advanced Reactor Core Simulator*; *Purdue*, 2002.
10. Rohde, U.; Kliem, S.; Grundmann, U.; Baier, S.; Bilodid, Y.; Duerigen, S.; Fridman, E.; Gommlich, A.; Grahn, A.; Holt, L.; et al. The reactor dynamics code DYN3D—Models, validation and applications. *Prog. Nucl. Energy* **2016**, *89*, 170–190, doi:10.1016/j.pnucene.2016.02.013.
11. ANSWERS. WIMS—A General Purpose Code For Reactor Core Analysis. Available online: https://www.answerssoftwareservice.com/resource/pdfs/wimscore.pdf (accessed on 22 February 2019).
12. ANSWERS. PANTHER—An Advanced 3D Nodal Code for Reactor Core Analysis. Available online: https://www.answerssoftwareservice.com/panther/ (accessed on 22 February 2019).
13. Santamarina, A.; Commission, A.E.; Bernard, D.; Commission, A.E.; Blaise, P.; Commission, A.E.; Leconte, P.; Commission, A.E. *APOLLO2 8: A Validated Code Package for PWR Neutronics Calculations*; PHYSOR, Pennsylvania 20010
14. E. & AREVA. *PCSR—Appendix 14a—Computer Codes used in Chapter 14*;ONR, UK 2012.
15. IAEA. *Advanced Calculational Methods for Power Reactors and LWR Core Design Parameters*; IAEA, Cadarache, 1992; p. 389.
16. Studsvik. SIMULATE5. Available online: https://www.studsvik.com/our-solutions/products/simulate5/ (accessed on 21 October 2020).
17. Rearden, B.T.; Jessee, M.A. SCALE Code System. Available online: https://www.ornl.gov/sites/default/files/SCALE_6.2.3.pdf (accessed on 22 February 2019).

18. NRC. U.S Nuclear Regulatory Commission Computer Codes. Available online: https://www.nrc.gov/about-nrc/regulatory/research/safetycodes.html (accessed on 22 February 2019).

19. DOE. Energy Department Announces Five Year Renewal of Funding for First Energy Innovation Hub—Department of Energy. Available online: https://www.energy.gov/articles/energy-department-announces-five-year-renewal-funding-first-energy-innovation-hub (accessed on 20 February 2018).

20. DOE. Technology Transition Case Study Consortium for the Advanced Simulation of Light Water Reactors (CASL). Available online: https://www.energy.gov/sites/prod/files/2015/09/f26/CASL Tech Transition Case Study v7 06-18-15 FINAL CR.pdf (accessed on 20 February 2018).

21. TOP500. November 2018_TOP500 Supercomputer Sites. Available online: https://www.top500.org/lists/2018/11/ (accessed on 21 February 2019).

22. Ray, S.; Kucukboyaci, V.; Sung, Y.; Kersting, P.; Brewster, R.; Clarno, K.; Godfrey, A. *Industry Use of Casl Tools*. Westinghouse, 2018

23. Franceschini, F.; Godfrey, A.T.; Stimpson, S.; Evans, T.; Collins, B.; Gehin, J.C.; Turner, J.; Graham, A.; Downar, T. AP1000® PWR startup core modeling and simulation with VERA-CS. In *5th Top. Meet. Adv. Nucl. Fuel Manag. ANFM 2015 Adv. Nucl. Fuel Manag. V*; South Carolina, 2015; pp. 241–252.

24. Aufiero, M.; Rubiolo, P.; Fratoni, M. Monte Carlo/CFD coupling for accurate modeling of the delayed neutron precursors and compressibility effects in molten salt reactors. *Trans. Am. Nucl. Soc.* **2017**, *116*, 1183–1186.

25. Leppänen, J.; Pusa, M.; Viitanen, T.; Valtavirta, V.; Kaltiaisenaho, T. The Serpent Monte Carlo code: Status, development and applications in 2013. *Ann. Nucl. Energy* **2015**, *82*, 142–150, doi:10.1016/j.anucene.2014.08.024.

26. Imke, U.; Sanchez, V.H. Validation of the subchannel code SUBCHANFLOW using the NUPEC PWR tests (PSBT). *Sci. Technol. Nucl. Install.* **2012**, *2012*, doi:10.1155/2012/465059.

27. Ferraro, D.; García, M.; Valtavirta, V.; Imke, U.; Tuominen, R.; Leppänen, J.; Sanchez-Espinoza, V. Serpent/SUBCHANFLOW pin-by-pin coupled transient calculations for the SPERT-IIIE hot full power tests. *Ann. Nucl. Energy* **2020**, *142*, 107387, doi:10.1016/j.anucene.2020.107387.

28. Merk, B.; Bankhead, M.; Litskevich, D.; Gregg, R.; Peakman, A.; Shearer, C. On a Roadmap for Future Industrial Nuclear Reactor Nuclear Renaissance. *Energies* **2018**, *11*, 3509, doi:10.3390/en11123509.

29. ONR. *New Nuclear Reactors : Generic Design Assessment Guidance to Requesting Parties*; UK, 2014.

30. BBC News. Nuclear Hitachi "withdraws" from £20bn Wylfa Project. Available online: https://www.bbc.co.uk/news/uk-wales-54158091 (accessed on 22 September 2020).

31. Rearden, B.T. *SCALE Code System*;ORNL, Tennassey; 2016; ISBN 1800553684.

32. Salko, R.K.; Lange, T.; Palmtag, S.; Gehin, J.; Avramova, M. *Development of COBRA-TF for Modeling Full-Core, Reactor Operating Cycles. Advances in Nuclear Fuel Management V; ANFM, South Carolina*; 2015.

33. William Earl Russell, I. U.S. Patent US 8,842,802 B2. Available online: https://patents.google.com/patent/US8842802B2/en (accessed on 11 January 2019).

34. General Atomics. Global Nuclear Fuel Extends Joint Venture Agreement with ENUSA. Available online: https://www.genewsroom.com/press-releases/global-nuclear-fuel-extends-joint-venture-agreement-enusa (accessed on 13 February 2020).

35. Office of Nuclear Regulatory Research. Axial Moderator Density Distributions, Control Blade Usage, and Axial Burnup Distributions for Extended BWR Burnup Credit.

Available online: https://www.nrc.gov/docs/ML1623/ML16237A100.pdf (accessed on 30 January 2018).

36. Hitachi-GE. UK ABWR Generic Design Assessment Generic Chapter 11 : Reactor Core. Available online: http://www.hitachi-hgne-uk-abwr.co.uk/downloads/2017-12-14/UKABWR-GA91-9101-0101-11000-RevC-PB.pdf (accessed on 10 June 2019).

37. Chadwick, M.B.; Herman, M.; Oblo, P.; Pritychenko, B.; Arbanas, G.; Arcilla, R.; Brewer, R.; Brown, D.A.; Capote, R.; Carlson, A.D.; et al. ENDF/B-VII. 1 Nuclear Data for Science and Technology : Cross Sections, Covariances, Fission Product Yields and Decay Data. *Nucl. Data Sheets* **2011**, *112*, 2887–2996, doi:10.1016/j.nds.2011.11.002.

38. Dynd, A.; Grundmann, U.; Kliem, S.; Rohde, U.; Grundmann, U.; Kliem, S.; Rohde, U. Analysis of the boiling water reactor turbine trip benchmark with the codes DYN3D and ATHLET/DYN3D. *Nucl. Sci. Eng.* **2004**, *148*, 226–234, doi:10.13182/NSE04-A2453.

39. Salko, R.K.; Avramova, M.N. *COBRA-TF Subchannel Consortium for Advanced Simulation of LWRs Code (CTF) Theory Manual*; Pennsylvania State University; Pennsylvania; 2015.

40. IAPWS. The International Association for the Properties of Water and Steam. Available online: http://www.iapws.org/ (accessed on 17 May 2019).

41. Romera, J.J.G. IAPWS Github. Available online: https://iapws.readthedocs.io/en/latest/index.html (accessed on 17 May 2019).

42. Smith, K.S. Assembly homogenization techniques for light water reactor analysis. *Prog. Nucl. Energy* **1986**, *17*, 303–335, doi:10.1016/0149-1970(86)90035-1.

43. Scotta, J.P.; Noguere, G.; Bernard, D.; Damian, J.I.M.; Santamarina, A. Impact of the thermal scattering law of H in H 2 O on the isothermal temperature reactivity coefficients for UOX and MOX fuel lattices in cold operating conditions. *EPJ Nucl. Sci. Technol.* **2016**, *2*, 28, doi:10.1051/epjn/2016020.

44. Grundmann, U.; Rohde, U.; Mittag, S.; Kliem, S. *DYN3D Version 3.2 Description of Models and Methods 2005*; Forschungszentrum Rossendorf: Dresden, Germany, 2005.

45. Rossiter, G. Development of the ENIGMA fuel performance code for whole core analysis and dry storage assessments. *Nucl. Eng. Technol.* **2011**, *43*, 489–498, doi:10.5516/NET.2011.43.6.489.

46. Lassmann, K. TRANSURANUS: A fuel rod analysis code ready for use. *Nucl. Mater. Fission React.* **1992**, 295–302, doi:10.1016/b978-0-444-89571-4.50046-3.

47. Holt, L.; Rohde, U.; Seidl, M.; Schubert, A.; Van Uffelen, P.; Macián-Juan, R. Development of a general coupling interface for the fuel performance code TRANSURANUS—Tested with the reactor dynamics code DYN3D. *Ann. Nucl. Energy* **2015**, *84*, 73–85, doi:10.1016/j.anucene.2014.10.040.

48. Wagner, W.; Cooper, J.R.; Dittmann, A.; Kijima, J.; Kretzschmar, H.J.; Kruse, A.; Mareš, R.; Oguchi, K.; Sato, H.; Stöcker, I.; et al. The IAPWS industrial formulation 1997 for the thermodynamic properties of water and steam. *J. Eng. Gas Turbines Power* **2000**, *122*, 150–180, doi:10.1115/1.483186.

49. Bilodid, Y. Spectral History Modeling in the Reactor Dynamics Code DYN3D. Available online: https://inis.iaea.org/collection/NCLCollectionStore/_Public/46/021/46021401.pdf (accessed on 20 November 2020).

50. Bilodid, Y.; Grundmann, U.; Kliem, S. The HEXNEM3 nodal flux expansion method for the hexagonal geometry in the code DYN3D. *Ann. Nucl. Energy* **2018**, *116*, 187–194, doi:10.1016/j.anucene.2018.02.037.

51. Fensin, M.L. Optimum Boiling Water Reactor Fuel Design Strategies to Enhance Reactor Shutdown by the Standby Liquid Control System. Available online: http://etd.fcla.edu/UF/UFE0005364/fensin_m.pdf (accessed on 11 January 2019).

52. Litskevich, D. Development of an Advanced Neutron Transport Solver for Zooming in DYN3D. Available online: https://publications.rwth-aachen.de/record/707654/files/707654.pdf (accessed on 15 October 2019).

53. Litskevich, D.; Atkinson, S.; Davies, S. Verification of the current coupling collision probability method with orthogonal flux expansion for the assembly calculations. *Prog. Nucl. Energy* **2020**, *130*, 103562, doi:10.1016/j.pnucene.2020.103562.

54. Boyd, W.; Shaner, S.; Li, L.; Forget, B.; Smith, K. The OpenMOC method of characteristics neutral particle transport code. *Ann. Nucl. Energy* **2014**, *68*, 43–52, doi:10.1016/j.anucene.2013.12.012.

4. BWR full core model for burnup credit analysis

Understanding the fuel assembly behaviour in the reactor core during irradiation is an important part of the burnup credit analysis as it affects the spent fuel composition. The behaviour is often analysed using 2D lattice codes which model different fuel assembly slices in axially infinite geometry and reflective radial boundary conditions. BWR fuel assemblies design has become significantly more complex in recent decades. A typical BWR fuel assembly design today is highly heterogeneous both in axial and radial direction and have complex design features such as part-length rods or variable axial and radial enrichment which were not present in earlier versions of the design. The results of the research described in Chapter 3 showed that the reactivity curve (infinite or effective multiplication factor as a function of burnup) for modern BWR fuel assembly design, in realistic 3D approximations, can differ from the expected one form of criticality curve of the 2D lattice approach. Under 2D approximation for BWR fuel assemblies with burnable poison, the reactivity curve would have a single reactivity peak. However, the depletion analysis of the 3D assembly model with realistic properties showed that the reactivity curve under both nodal and Monte Carlo approaches have a second peak resulting from the depletion of the upper fuel assembly layers later in the burnup process. Recent research [43] showed substantial differences between criticality curves near the peak reactivity in 2D and 3D fuel assembly models with non-uniform axial properties. Thus, the capabilities of a 2D lattice approach were shown to be limited in simulating realistic BWR fuel assemblies' behaviour over the burnup, so the development of advanced 3D models which can capture complexities of the FA design and operating conditions is required.

Chapter 3 analysed ABWR core using nodal and high-fidelity approaches at the steady-state conditions at the beginning of life (no depletion). This chapter extends the performed in Chapter 3 nodal analysis by including burnup calculations in order to track the fuel assembly behaviour during its lifetime in the reactor core. The simulations were performed for different fuel assembly type than those considered in Chapter 3. Four shuffling procedures have been developed to model the reloading schemes after each operational cycle to represent the potential range of FAs' discharge burnups. The 3D realistic BWR fuel assembly nodal model was also described in detail.

As expected, a substantial difference between criticality curves of 2D lattice and 3D nodal approaches was observed for the analysed BWR GE14 fuel assembly. It should be noted that for 2D lattice models, the estimated neutron multiplication factor is an infinite multiplication factor (k_{inf}). For 3D nodal models, it is an effective multiplication factor (k_{eff}) since leakage boundary conditions were set at the top and bottom of the FA. It was shown that the parameters of the burnup distribution of the discharged FAs depend on the reloading pattern. The shuffling procedures producing optimal and least optimal distributions have been determined. The shuffling procedure was considered optimal if the distribution corresponding to this shuffling procedure had the lowest difference between the maximum and minimum fuel assemblies' burnups, and, vice versa, for the least optimal shuffling procedure. The potential benefit from the burnup credit method application has been investigated for optimal and least optimal shuffling procedures. Although the average reactivity gain was approximately the same for both shuffling procedures, more fuel assemblies from the optimal distribution have benefited from the BUC method than from

the least optimal distribution. The results of the research have been summarised in the paper published in a peer-reviewed journal Applied Sciences and are presented below.

Article

Burnup Credit Evaluation for BWR Spent Fuel from Full Core Calculations

Anna Detkina [1,*], Dzianis Litskevitch [1], Aiden Peakman [2] and Bruno Merk [1]

[1] School of Engineering, University of Liverpool, Liverpool L69 3GH, UK; d.litskevich@liverpool.ac.uk (D.L.); b.merk@liverpool.ac.uk (B.M.)

[2] National Nuclear Laboratory, Chadwick House, Warrington WA3 6AE, UK; aiden.w.peakman@uknnl.com

* Correspondence: a.detkina@liverpool.ac.uk

Abstract: Due to the challenges of spent fuel accumulation, the nuclear industry is exploring more cost-effective solutions for spent fuel management. The burnup credit method, in application for storage and transport of the spent fuel, gained traction over recent decades since it can remove the over-conservatism of the "fresh-fuel" approach. The presented research is focused on creating an innovative, best estimate approach of the burnup-credit method for boiling water reactor (BWR) spent fuel based on the results of neutronic/thermal-hydraulic coupled full core simulations. The analysis is performed using a Polaris/DYN3D sequence. Four different shuffling procedures were used to estimate the possible range of the BWR fuel discharged burnup variation. The results showed a strong influence of the shuffling procedure on the final burnup distribution. Moreover, a comparison of the 2D lattice and 3D coupled nodal approaches was conducted for the criticality estimation of single fuel assemblies. The analysis revealed substantial improvement in criticality curves obtained with the full-core model. Finally, it was shown that the benefit from the burnup-credit method is larger in the case of more optimal fuel utilisation-based shuffling procedures. The new approach developed here delivers a promising basis for future industrial optimisation procedures and thus cost optimisation.

Keywords: burnup credit; BWR; Polaris; DYN3D; full-core simulations

4.1. Introduction

The amount of discharged spent nuclear fuel (SF) has been steadily growing over recent decades [1]. In 2019, the International Atomic Energy Agency (IAEA) estimated that around 10,000 MtHM/year of spent fuel (SF) is being discharged from nuclear power plants (NPPs), from which approximately 4000 MtHM/year goes to reprocessing and the rest remains in the storage facilities [2]. The data from [3] shows that light water reactors (LWRs) contributed to 89.2% of energy production from the NPPs worldwide at the end of 2018, with boiling water reactors (BWRs) producing approximately 20% of energy obtained with LWRs. The IAEA estimates that in the high case, nuclear power capacity may increase up to 25% by the year 2030 from current levels and up to 80% by 2050 [4]. According to the low estimate, the capacity may drop by 7% in 2050. Under both scenarios, the need for the spent fuel storage will remain for several decades.

In the case with LWRs, spent fuel is removed from the reactor core to wet storage at the plant, such as spent fuel storage pools, for cooling for approximately 5–10 years [1]. After that, the fuel is moved, in most cases, to dry storage for interim storage. The demand for dry storage emerged at the beginning of the 1980s when it became clear that the existing storage

pools capacities were insufficient to keep all fuel assemblies for long-term storage while the development, construction and commissioning of the final disposal capacities had not been accomplished. Since then, many spent fuel storage systems have been developed, such as concrete containers lined by steel or metal casks. The current spent fuel management strategies suggest that at the end, the SF can be disposed as a high-level waste or can be reprocessed with the separated fission product stream disposed as radioactive waste [2]. The Generation IV reactor design targets mostly a closed fuel cycle conception when the spent fuel can be reused in the reactor core [5]. One of the potential candidates is the sodium-cooled fast reactor (SFR) due to efficient utilisation of plutonium and minor actinides [6]. Recent works [7,8] showed that another opportunity for the SF management could be spent fuel utilisation in molten salt reactors, which significantly reduces fuel cycle facility demands. Considering that final SF disposal is a complex problem which remains unsolved for most countries, the need for a cost-effective solution for SF storage will grow in the foreseeable future.

LWRs' average fuel discharged burnups have been steadily increasing since the beginning of their industrial operation, as the data from Germany show [9]. According to the data published by the U.S. Energy Information Administration in 2015 [10], the average burnup of BWR fuel assemblies (FAs) has reached 45 GWd/tU. In general, there is a clear economic driver for targeting higher burnup since an increased fuel utilisation results in a decrease in the fuel cycle cost as well as spent fuel volume [11]. Furthermore, the higher burnt fuel contains less fissile material which may help to either reduce expenses on SF storage or expand the storage facilities' capacity [1].

For most spent fuel types, the criticality safety analysis is performed under the so-called "fresh fuel" approach. It implies that the SF system contains unirradiated (fresh) fuel without burnable poison. The approach results in a substantial overestimation of the calculated system's criticality, especially for the fuel with increased enrichment and high discharged burnup [1]. The reduction in the system's reactivity associated with the fuel burnup can be taken into account using the burnup credit (BUC) method [1]. During fuel irradiation, the total amount of fissile material present significantly decreases, which leads to a noticeable reduction in reactor core criticality. At the same time, transuranic elements are accumulating and fission products content is rising. If the fuel contains burnable absorber, such as gadolinium in case of BWRs [12], its concentration is declining, leading to an increase in criticality until all burnable poison has been depleted. The IAEA defines four frequently used levels of the burnup credit [13]:

- "Credit for the net decrease of the fuel fissile content, taking into account both burnup and build-up of the different fissile nuclides (net fissile content level).

- Credit for the net fissile content and for the absorption effect of actinides (actinide only level).

- Credit for the actinides and the neutron absorption in fission products (actinide plus fission product level).

- Credit for the presence of integral burnable absorbers in the fuel design (integral burnable absorber level). This credit uses the maximum reactivity of the fuel, which is often not the initial reactivity."

According to the data published in [14], the BUC on the actinide-only and actinide plus fission product level is widely applied to pressurised water reactors (PWR) fuel at the various stages of SF management. For BWR spent fuel, the BUC on the integral burnable absorber level is mainly applied to wet storage. However, the method is still under development or consideration in some countries for the dry storage and transport of BWR spent fuel [14].

Oak Ridge National Laboratory has recently finished their five-year program regarding the burnup credit development for the transport and storage of BWR spent fuel [15]. The project aimed to analyse the specific points of BWR operation and estimate their impact on BUC. The research was focused on the influence of various operating parameters, such as axial moderator density distribution, control blades movements and operating conditions, on the validation of the isotopic predictions and effective neutron multiplication factor (k_{eff}) calculations. The series of newly published studies [16,17] was focused on the development and benchmarking of an advanced BWR lattice model with further application to the criticality analysis of the BWR storage cask, along with burnup credit, sensitivity and uncertainty studies. The research was conducted for BWR spent fuel discharged at the peak reactivity burnup where the burnable absorber gadolinia does not affect fuel assembly criticality anymore [17]. The current study aimed to create the best estimate for BUC in application to BWR spent fuel discharged at realistic final burnups. For this purpose, the FA behaviour in the reactor core was evaluated by performing full core nodal simulations with different fuel reloading patterns, which provided the comprehensive data for each assembly in the core. The project is divided into two parts. The first part, which is presented in this paper, is focused on the simulation of the BWR reactor operation and optimisation of the burnup distribution of the discharged FAs. In addition, the paper evaluates the benefit of burnup credit application for the realistic BWR assembly model at the estimated discharged burnups. Overall, the study aims to answer the following two research questions: "How strong is the influence of different core loading strategies on the discharge burnup distribution?" and "How much credit can we gain for the best estimate analysis of the BWR spent fuel at the discharged burnups in comparison to the fresh fuel standard and the peak reactivity approach?". In the second part of the project, the criticality analysis of the different SF storage cask loadings will be conducted using the realistic BWR spent fuel composition obtained in the full core simulations. The result will be compared against the traditional fresh fuel approach to define the possible gain from the BUC.

4.2. Codes Description

In the current study, a BWR full core analysis was performed using the Polaris/DYN3D sequence. Polaris is a newly introduced module of SCALE 6.2 code system for the 2D lattice physics computations, adjusted for LWR design [18]. The SCALE package was developed by Oak Ridge Nuclear Laboratory (ORNL, Oak Ridge, TN, USA). It is designed to solve various problems of nuclear safety analysis and design, such as criticality safety analysis or reactor physics computations. Before incorporating Polaris into the SCALE package, lattice physics analysis was performed using the TRITON module within the SCALE package. Polaris has significant advantages in comparison with TRITON, such as an easy input file structure and improved running time without affecting the quality of the results [19]. For these reasons, the Polaris module was chosen for the lattice calculations and the cross-section preparations for the BWR fuel assembly design. Polaris utilises an Embedded Self-Shielding Method

(ESSM) based on the Bondarenko interpolation approach for calculating multi-group self-shielded cross-sections [18]. The transport calculations are being performed using the Method of Characteristics (MoC). Polaris is supplied either with 252 or 56 energy groups' nuclear data libraries generated from the ENDF/B-VII.1 library. The study [20] showed that TRITON module of SCALE 6.2 with 252 energy groups' data library has a discrepancy with well-validated commercial code CASMO5 in the range of less than ±100 pcm for the BWR pin-cell. Thus, lattice physics computational tools of SCALE 6.2 code used in the current study can be considered as a robust means for cross-section preparation for industrial standard light water reactor problems.

The simulation of BWR reactor operation was performed in the DYN3D nodal core simulator. DYN3D is a multi-physics, three-dimensional nodal code for steady-state and transient analysis of LWRs developed by Helmholtz-Zentrum Dresden-Rossendorf (HZDR, Dresden, Germany) [21]. The neutron physics model uses the nodal expansion method (NEM) for solving the three-dimensional two-group or multi-group neutron diffusion equations. The code can simulate square and hexagonal fuel assemblies' designs, such as those of BWR and water-water energetic reactor (VVER) fuel assemblies, respectively. This study used the multi-group version of the DYN3D code. The calculated reactor thermal-hydraulics parameters, such as fuel temperature, coolant density and temperature, are fed back to the neutronics solver within DYN3D to estimate the thermal-hydraulics feedback. DYN3D can also simulate the reactor fuel cycle by incorporating burnup and fuel shuffling options into the analysis. DYN3D was initially developed for VVER reactor type, where it is the NURESIM (European Reference Simulation Platform for Nuclear Reactors) reference code [22]. However, DYN3D is currently extensively verified and validated for different types of LWRs [21]. For BWRs, the code was compared against the Nuclear Energy Agency of the Organisation for Economic Co-operation and Development (OECD/NEA) BWR Turbine Trip Benchmark [23].

4.3. Models Description

4.3.1. Fuel Assembly Design

BWR fuel assembly design has evolved noticeably from the first reactor generations. For example, the lattice size has been increased from 7 × 7 to 10 × 10, with a gradual decrease in the rod diameter [24]. The goal of BWR fuel assembly optimisation is to use fuel as efficiently as possible during reactor operation. Over the last few decades, BWR fuel vendors have iteratively enhanced FA design to improve fuel performance. Despite some differences between FA constructions, the main features, such as non-uniform axial and radial fuel enrichment, rods containing burnable poison, water rods and part-length rods, have always been present in the various designs. For this study, GE14 10 × 10 fuel assembly described in [25] was chosen for the BUC analysis. The fuel is uniformly enriched by 4.5 wt% of U-235 and the FA contains 15 gadolinia-poisoned rods with 7 wt.% of Gd_2O_3. The study [16] showed that the impact of averaging radial enrichment in comparison to the non-uniform one, which is typical for the modern BWR fuel, only has a minor effect on the k_{eff} and final isotopic composition in the BWR fuel assembly. Thus, the usage of the uniformly enriched fuel rods in this study will not significantly affect the results of the BUC analysis. The FA design includes 14 part-length rods which divide the FA into two axial regions. At the bottom region, all fuel rod positions are filled with fuel, forming the so-called "dominant"

lattice (DOM) [25]. The upper part has empty rod spaces, providing additional moderation. This region is called a "vanished" lattice (VAN) [25]. The fuel assembly was modelled with naturally enriched (NE) uranium blankets (0.71 wt% of U-235) on top and bottom. The FA design is presented in Figure 4.1. Table 4.1 represents the main parameters of the BWR GE14 assembly.

The described fuel assembly design is preferable for the study because it is based on a real, currently operated fuel assembly configuration and contains all main features of the modern BWR GE14 assembly [25] but has a lower degree of complexity in the modelling and simulations.
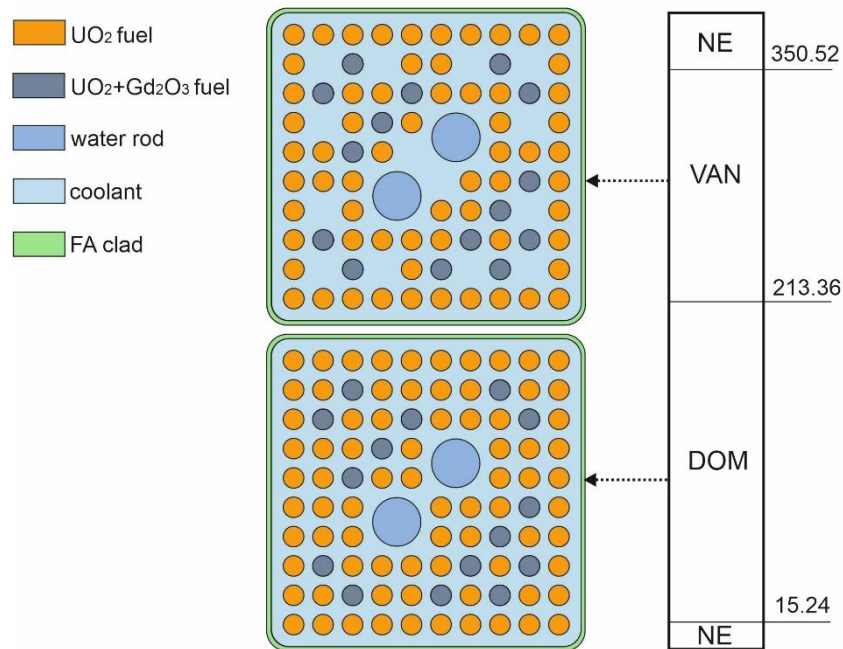
Figure 4.1. Boiling water reactor (BWR) GE-14 10 × 10 fuel assembly design as used for the study.

Table 4.1. BWR 10 × 10 assembly parameters [26].

Parameter	Value
Fuel pellet radius, cm	0.447
Zr clad radius, cm	0.513
Fuel rod pitch, cm	1.295
Assembly pitch, cm	15.24
Water rod inside radius, cm	1.1605
Water rod outside radius, cm	1.2605
Assembly height, cm	381

4.3.2. Full Core Design

The openly available information about the BWR full core design and operational data is limited to either an outdated reactor configuration, as in [27], or is not presented in all required detail [28]. The recently published study [29] provided insight on an advanced BWR design based on openly available data, including the loading pattern, the operational

parameters and the modern BWR GE-14 10 × 10 fuel assembly design. The reactor data from [29] were taken as a basis for the full core analysis.

The reactor core described in [29] contains 872 fuel assemblies from four different cycles, each having a cycle length of 11.25 GWd/tU, with the layout of a quarter of the core shown in Figure 4.2. The number of FAs in each cycle is summarised in Table 4.2, with an identical number of 224 assemblies in the first three cycles and four assemblies less in the last cycle. The main reactor core parameters are represented in Table 4.3. Thermal-hydraulics data at rated conditions are described in Table 4.4. Peaking factor estimated for the BWR core without control rods usage has a value around 1.8 [30]. This limitation factor, along with the parameters from Table 4.4, was used to verify that the developed model is close to the realistic full-core design.

Analysis conducted in [31] for the realistic control blades histories showed that control blade insertion affects the criticality of the storage cask with BWR spent fuel by approximately 0.6–1.2% of the final value. Meanwhile, for the unrealistic histories with massive control rod insertion (92% of irradiation time), the difference was found to be up to 4.3%. Hence, the effect of control rods' movements does not contribute significantly to the criticality of the storage cask as long as the insertion time is limited, as it is assumed in normal, industrial reactor operation, and thus, control rods were omitted in the current study.

The current full-core simulations do not aim to develop a complete and precise model of the BWR reactor operation but rather a model sufficient to determine the fuel assembly burn-up behaviour in the reactor core. Hence, the evaluation of some safety parameters, such as linear power level in fuel rods [30] or expected transient behaviour, were omitted in the current study.
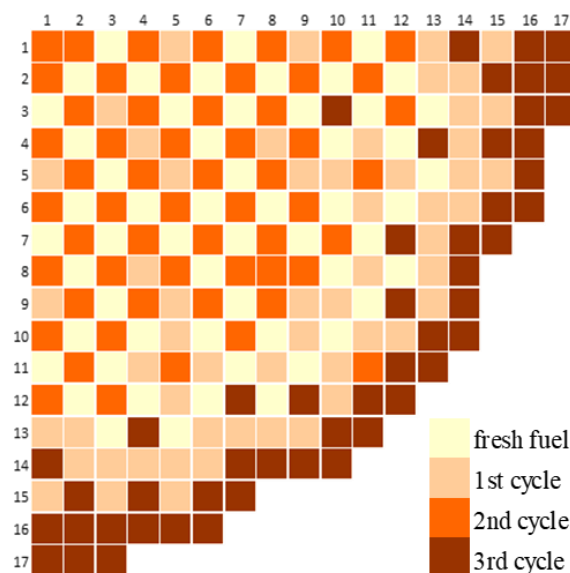
Figure 4.2. Advanced boiling water reactor (ABWR) full-core configuration of one quarter of the core.

Table 4.2. Fuel assemblies (FAs) number at each cycle.

Cycle Number	FAs Number
0	224

Cycle Number	FAs Number
1	224
2	224
3	200

Table 4.3. Design parameters for ABWR reactor core [32].

Parameter	Value
Outlet reactor pressure, MPa	7.171
Inlet coolant temperature, °C	278.3
Core mass flow rate, kg/s	14,502
Thermal output, MWth	3926
Number of fuel assemblies	872

Table 4.4. Thermal hydraulic parameters at rated conditions [33].

Parameter	Value
Average heat flux	430 kW/m²
Maximum heat flux	1365 kW/m²
Peak fuel pellet temperature throughout the cycle	1760 °C
Core average void fraction	0.43

4.4. Full-Core Modelling

4.4.1. Cross-Section Preparation

Nodal core simulators require homogenised cross-sections and diffusion data for each unique layer of the FA and the radial and axial reflectors at the different state points of the reactor operation. The diffusion data include homogenised multi-group or two-group cross-section sets, assembly discontinuity factors (ADFs), scattering tables, etc. [34]. For this purpose, a case matrix containing state points that comprehensively describe the FA and reflector design for the envisaged operational envelope was created [5]. It covers the possible range of depletion steps and changes in the operational parameters, such as moderator density, fuel temperature or the control rods' movements. Lattice codes produce the diffusion data by performing burnup and branch calculations in the form of a matrix. The nodal code then interpolates the unknown operational conditions lying between two branches or burnup steps or extrapolates them based on the available data if they are outside the set. The latter procedure can lead to incorrect results; thus, it is vital to cover the whole expected range of operating conditions while creating the case matrix [34].

Cross-section sets for the FA and reflector were prepared using the Polaris module of SCALE 6.2 [18]. The ENDF/B-VII.1 data library with 56 energy groups' structures was used in the calculations since it is optimised for LWR analysis [35] and significantly reduces the computational time in comparison with 252-energy group library. Cross-sections were homogenised for two energy groups as in a standard approach for nodal LWR modelling [5]. Post-processing was performed on Polaris lattice physics archive for use with DYN3D code.

Figure 4.3 shows the computational models of dominant and vanished lattices in Polaris. The meshing is standard for the BWR fuel type provided by the code [18].
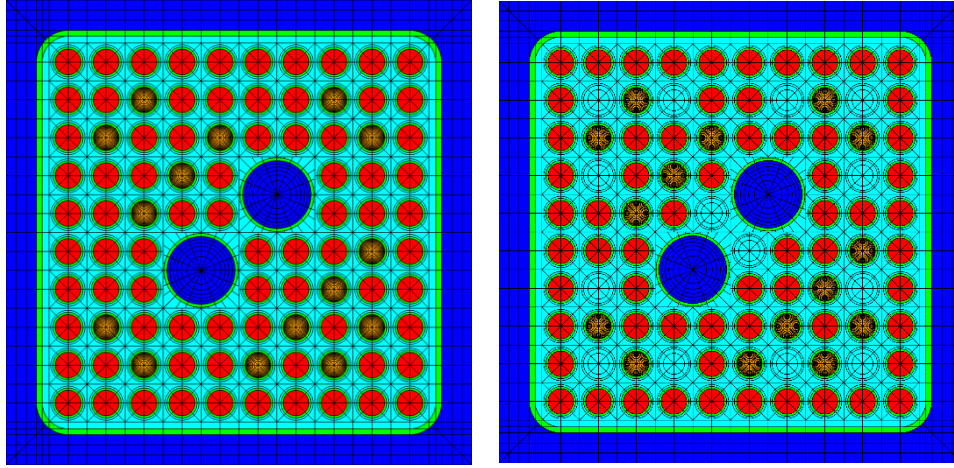
Figure 4.3. Polaris models of dominant (**left**) and vanished (**right**) FA layers for the cross-section preparation.

The fuel assemblies in the BWR reactor core are surrounded by the reflector, which can be water, a steam–water mixture or a mixture of water and structural material. The reflector model in the lattice code is typically developed by adding a reflector region to the east boundary of the typical FA configuration. This study considered three reflector types located at the bottom, side and top of the reactor core. The minimum size of the reflector is typically the width of the one FA [34]. For the current study, the bottom and top reflectors were modelled as two fuel assemblies in width, while the radial (side) reflector size was estimated by the equation from [34]:

$$H = \frac{W^3}{6R^2 \left(2arcsin\left[\frac{W}{2R}\right] - sin\left[2arcsin\left[\frac{W}{2R}\right]\right]\right)}$$

(1)

where

H is the average distance from the FA bundle to the reactor pressure vessel (RPV);

W is the width of the flat part of the FA bundle closed to the RPV;

R is the RPV radius.

The schematic reflector model is shown in Figure 4.4. The bottom reflector material is a mixture of stainless steel and water and the radial reflector consists of water, while the top, from the low-density water imitating the steam–water mixture.
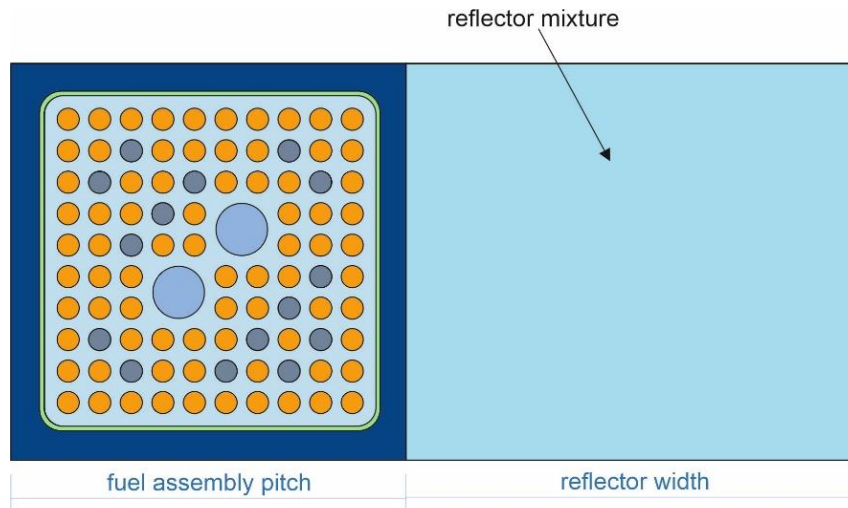
Figure 4.4. Reflector model for the cross-section preparation.

4.4.2. Refuelling Simulations

The BWR FA average discharge burnup varies for different reactor generations, FA lattice sizes and fuel enrichments. For the modern BWR fuel, it lies in a range of 45–50 GWd/tU [36,37]. For this study, burnup limitations described in the generic design assessment of UK ABWR [38] were used. The data is summarised in Table 4.5.

Table 4.5. Summarised data about burnups for BWR fuel as used in this study [38].

Parameter	Burnup, GWd/tU
Average discharge burnup	50
Maximum assembly average burnup	60
Maximum pin burnup	65

In LWRs, a fraction of the core (usually the assemblies from the final cycle) is discharged after each cycle to the storage pond. The other FAs change their positions in the reactor core according to the specific shuffling procedure, and the new fresh fuel assemblies are loaded to the empty spaces. This process is called refuelling. The cycle length for modern BWRs is 12–18 months, while a single FA stays in the reactor core for approximately four years [39] over 3 to 4 cycles. The open data about refuelling patterns are limited, so four shuffling procedures (SP) have been developed in this study to cover the possible scope of the discharged fuel burnups of the individual fuel assemblies. Considered SPs are shown in Figure 4.5.
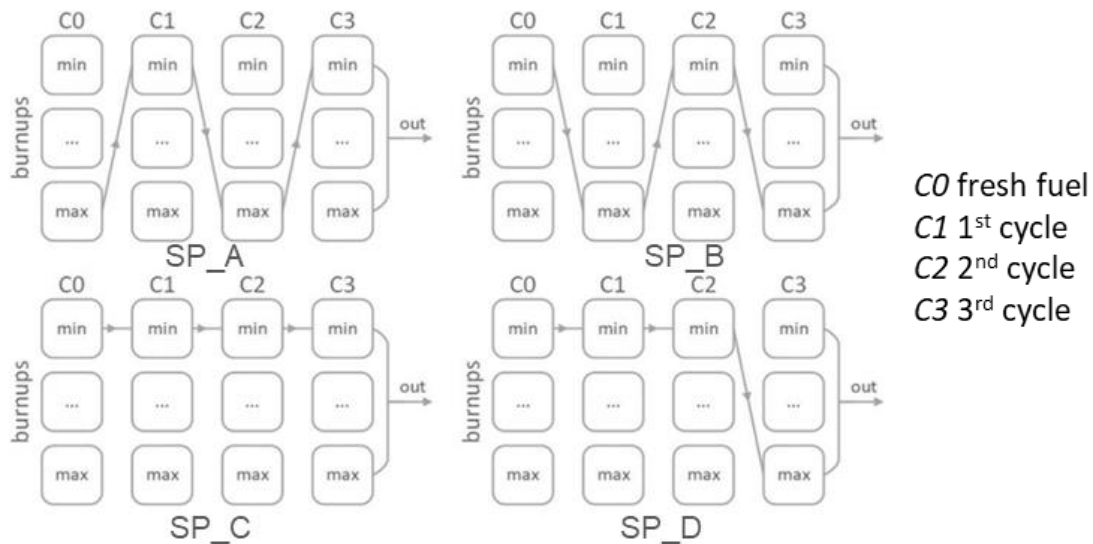
Figure 4.5. Shuffling procedures developed and tested to determine the discharge burnup of the individual fuel assemblies.

The refuelling process/shuffling procedure was programmed using Python script, which determined the new position for FAs after each cycle according to the SP algorithm from Figure 4.5 and then passed these data to the DYN3D code for further calculations. The script updates all DYN3D input files and launches the code, so the user only needs to create the initial DYN3D input and choose the appropriate shuffling procedure and cycle length, while further burnup and shuffling calculations will be performed automatically for an unlimited number of cycles.

In all considered SPs, fuel burnups of the FAs were sorted from minimum to maximum at each cycle and then moved according to the pattern showed in Figure 4.5. In the SP_A procedure, the FA coming from a maximum burnt position of the cycle C0 moves to the position of the least burnt FA of cycle C1, then it goes to the most burnt position of cycle C2, and finally, it is located to the least burnt position of the C3 cycle, while assemblies from the cycle C3 are removed from the core and the fresh FAs are loaded to the empty C0 cycle positions. In other words, maximally burnt fuel assemblies from one cycle move to the positions where the fuel assemblies of the next cycle accumulated the lowest increase in burnup. The SP_B procedure has a reversed-to-SP_A order of FAs movements, so the least burnt fuel assemblies from the cycle C0 go to the highly burnt FA positions of the cycle C1 and so on. The SP_C shuffling procedure implies that the FAs remain on the same burnup positions at each cycle, or in other words, the least burnt fuel assemblies from C0 go to similar positions of C1, and the process repeats until cycle C3. The shuffling procedure SP_D follow the SP_C shuffling procedure up to the cycle C2. Then, the FAs from C2 with the smallest burnups are moved to the maximally burnt FAs positions of the C3, and C3 FAs are discharged from the reactor core.

4.4.3. Reactor Cycle Simulation

The fuel assemblies from a single cycle accumulate a different average burnup depending on their positions in the reactor core. Four fuel burnup and shuffle sequences were performed to obtain the loading map and the realistic, individual burnup distribution

for the fuel assemblies. The number of sequences corresponded to the four fuel cycles, or in other words, to the full length of an assembly lifetime in the reactor, which seems to be sufficient for this study, even if the achieved burnup distribution will not be in complete equilibrium. For a future, more realistic evaluation, a real burnup distribution of real operational cycles could be investigated. In the beginning, the loading map consisted of FAs from four cycles with burnup distributions estimated by burning a single FA in infinite XY geometry (reflective boundary conditions at the sides of the FA as traditionally used in lattice calculations and leakage, from top and bottom). After producing a starting map, the four cycles of the reactor operation were simulated. At the end of each cycle, FAs from the third cycles were discharged and then the fuel was reshuffled. The shuffling procedure was kept equal for creating the starting loading map as well as for the reactor operation simulations.

The reactor core was burnt in 5-day steps. The model consisted of 27 axial layers, 25 for the assembly and 2 for top and bottom reflectors. The fuel contained an excess reactivity of 1500–2500 pcm at the beginning of each cycle. The core critical state was achieved by diving the multiplication cross-sections by k_{eff} since other reactivity control features, such as control rods' movements, were not simulated and boron in the coolant is traditionally not used in BWRs.

4.5. Results and Discussion

4.5.1. BWR Full-Core Analysis

4.5.1.1. Defining the Cycle Length

For the core map developed in [29] and used in this study, the cycle length for the average discharge burnup of 50 GWd/tU is 12.6 GWd/tU per cycle. However, the full core model described in [29] did not consider the effects of the fuel reloading process. A series of calculations were performed for different shuffling procedures to define an optimal cycle length and possible adjustments of the core configuration to achieve the target burnup of 50 GWd/tU while not exceeding limits set in [38] (Table 4.5). On the one hand, the analysis showed that the limit on maximum assembly average burnup of 60 GWd/tU was exceeded for the SP_C procedure (Figure 4.6), indicated by the appearance of several fuel assemblies with higher burnup (last bar on the right end of the right figure). The average discharged burnup over the core in this case (49.7 GWd/tU) is close to the set target of 50 GWd/tU. On the other hand, the SP_A procedure produces the narrowest discharged burnup distribution, indicating a very efficient fuel use for most fuel assemblies. The average discharged burnup is 50.8 GWd/tU, thus higher than in SP_C for the same cycle length, which makes it the preferred one in terms of fuel utilisation. However, as seen in Figure 4.6, there are still fuel assemblies detached from the main distribution (56 and 58 GWd/tU) which could be further optimised to improve the average discharge burnup. In this study, we refer to these assemblies as assembly-burnup outliers.
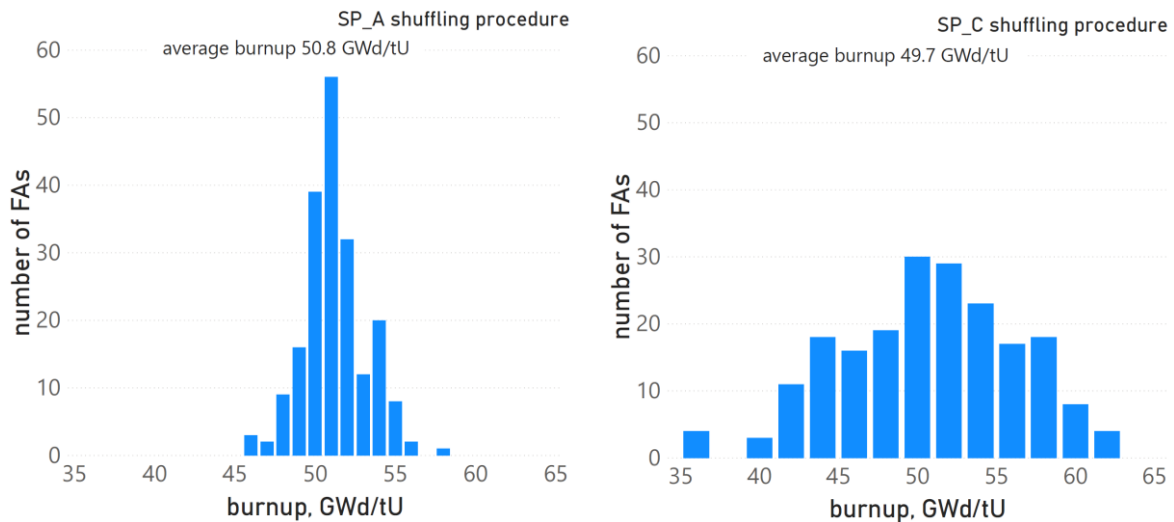
Figure 4.6. Discharged burnup distributions of two different shuffling procedures based on the reference core map.

Further analysis showed that the assembly located at the position (3, 10) caused the outlier effects described above. To resolve this problem, the full core map was slightly modified/optimised compared to the reference, as shown in Figure 4.6. The FA from the (3, 10) position was moved to (3, 14), while (3, 14) was placed to (3, 12) and (3, 12) back to (3, 10). For the improved full core layout, the optimal cycle length was estimated as 11.75 GWd/tU. The impact of the modification on discharged FA burnup distribution will be discussed more extensively in the next section.

4.5.1.2. Optimisation of the Discharged Fuel Burnup Distribution

As was discussed earlier, due to the limited open information about reloading patterns used in modern BWRs, the authors applied four different models of the shuffling procedures (Figure 4.5) to deliver a full core analysis in order to evaluate the possible range of burnups of the discharged fuel assemblies. Seven different cases of fuel reloading were generated based on four shuffling procedures and two core layouts, described above. SP_A_new (SP_C_new) and SP_A_old (SP_C_old) cases use SP_A (SP_C) shuffling procedure and adjusted (Figure 4.7) and reference (Figure 4.2) full core layouts, respectively.

The SP_B, SP_D and SP_E cases are based on the more promising, adjusted core layout. SP_B and SP_D utilise the shuffling procedures with the same name, given above in Figure 4.5, while SP_E is an additional case where the shuffling procedures SP_A and SP_B were altered with each other for each new fuel cycle, starting with SP_A in the first cycle followed by SP_B in the second cycle and so on.

Figure 4.8 depicts the burnup distributions of the fuel assemblies discharged from the reactor core during four cycles of operation for the seven different cases with identical cycle lengths. The reactor core has a 90-degree reflective symmetry; hence, results are presented for a quarter of the core which contains 218 FAs in total (Figure 4.7). Fifty FAs of the third cycle were removed from the core after each operational cycle which, after four cycles, resulted in a total number of 200 discharged fuel assemblies.
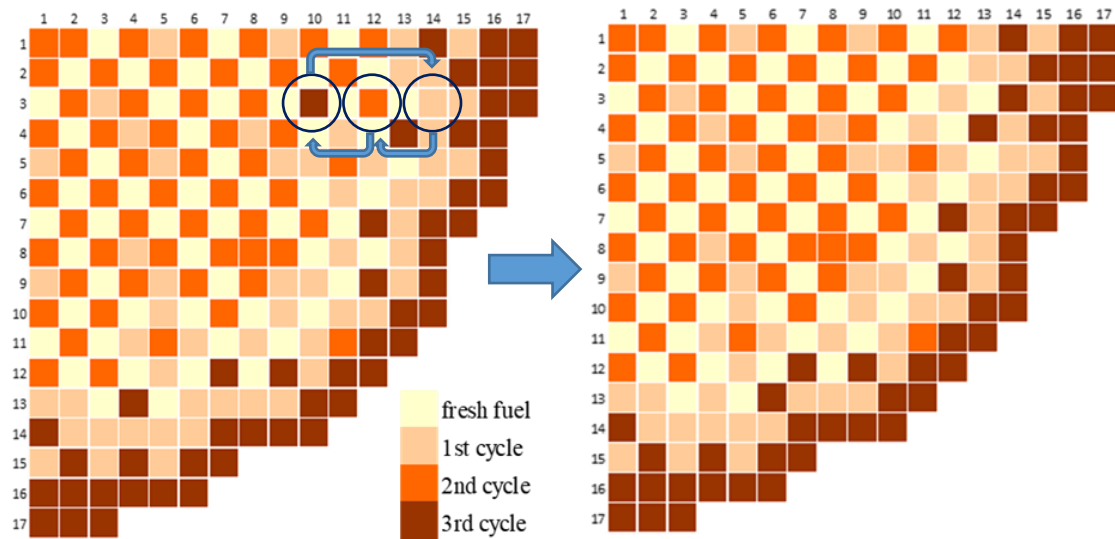
Figure 4.7. BWR full core layout adjustment.

The quality of the burnup distributions was analysed using the following parameters:

- Average burnup of the discharged fuel assemblies (B_{avrg}).

- Average burnup of the 5% least burnt fuel assemblies ($B_{5\%L}$).

- Average burnup of the 5% highest burnt fuel assemblies ($B_{5\%H}$).

- Average burnup of the 68 fuel assemblies from the centre of the distribution (B_{68}). The number of FAs is equal to the capacity of the BWR storage cask.

- Burnup range (BR)—the difference between the minimum and maximum fuel assemblies' burnups.

Table 4.6 summarises the change in the developed above parameters for the produced burnup distributions in comparison with SP_A_new which represents the most optimal distribution due to its smallest burnup range. The analysis shows that the shuffling procedure and core layout adjustment do not significantly affect B_{AVRG} and B_{68} burnups. However, it has to be kept in mind here that SP_C_old would not be permitted due to exceeding the suggested burnup limit in some fuel assemblies. At the same time, the $B_{5\%L}$, $B_{5\%H}$ and BR parameters are more sensitive to the choice of the shuffling procedure, with SP_C_new/SP_C_old cases being significantly away from the SP_A_new. The modification of the core layout significantly improved burnup range of the distributions (by 3 GWd/tU) which was produced with the optimal SP_A shuffling procedure, while BR did not change noticeably for the SP_C case. This indicates that the adjustment has taken away the assembly-burnup outliers into lower flux positions and thereby limited the burnup accumulation. It opens new optimisation potential since the whole core could now be burnt in a slightly longer cycle, thus achieving an even higher averaged burnup. The analysis of the deltas from Table 4.6 shows that SP_B and SP_E scenarios are closed to the optimal SP_A_new. However, they have a wider burnup range in comparison with SP_A_new because of the assemblies-outliers, thus there is less potential for extending the cycle time. This issue could be fixed by identifying the outlying assemblies and performing loading map optimisation as described in 5.1.1. The wide BR and high **Δ5%L** and **Δ5%H** parameters of

the SP_C_new and SP_C_old distributions compared to the others indicate that the shuffling procedure SP_C is far from optimal.

Table 4.6. Analysis of the differences in the burnup distribution parameters in comparison with the SP_A_new case as a reference (Δ_j *, GWd/tU).

Case	Δ_{AVRG}	$\Delta_{5\%L}$	$\Delta_{5\%H}$	Δ_{68}	Δ_{BR}
SP_A_new	0	0	0	0	0
SP_A_old	0.07	−0.2	0.9	0.08	3
SP_C_new	−1	−8.9	4.1	−0.3	15.3
SP_C_old	−1	−8.6	5	−0.5	16.4
SP_B	−0.4	0.1	0.9	−0.6	3.1
SP_D	−0.7	−1.2	2.4	−0.8	5.5
SP_E	−0.3	0.4	0.5	−0.4	3.1

* $\Delta_j = B_{ij} - B_{SP\_A\_new,j}$.

where

j is the index of the burnup distribution parameter (B_{avrg}, $B_{5\%L}$, $B_{5\%H}$, B_{68} or BR);

i is one of the considered cases;

$BR_{P\_A\_new,j}$ is the value of the burnup distribution parameter with index j for the SP_A_new case;

B_{ij} is the value of the burnup distribution parameter with index j for the case i.
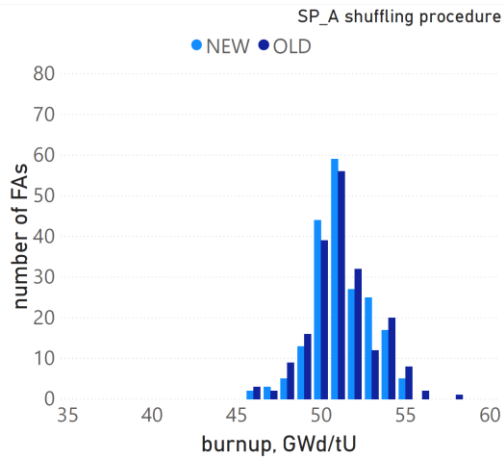
(a) Case SP_A_new/SP_A_old
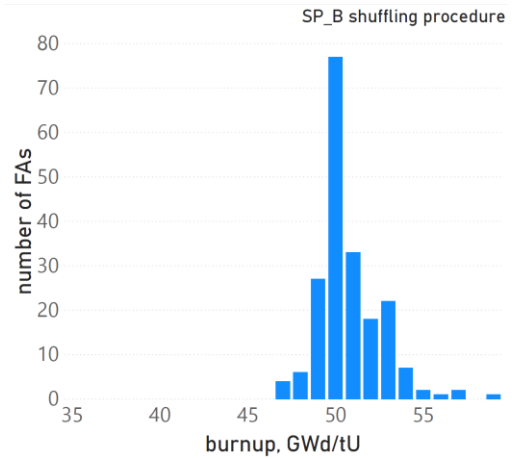
(b) Case SP_B
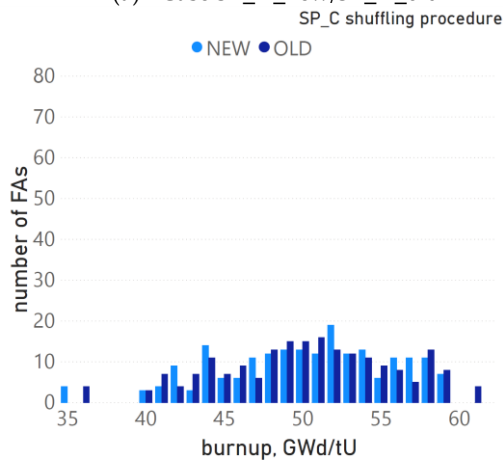
(c) Case SP_C_new/SP_C_old
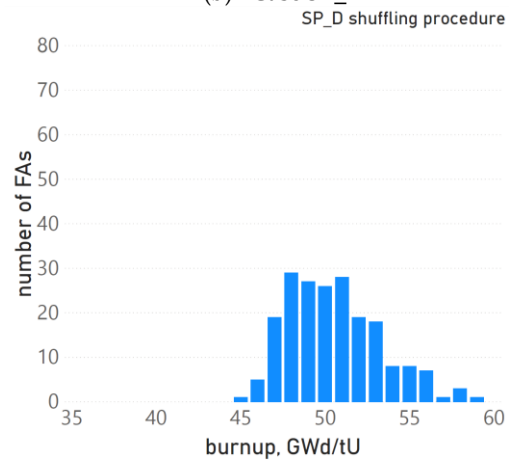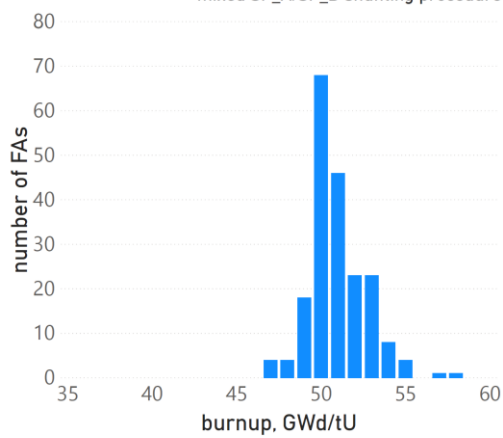
(d) Case SP_D

(e) Case SP_E

Figure 4.8. Burnup distribution of the discharged fuel assemblies after four cycles from one quarter of the core for the cases with different shuffling procedures and core layouts described above: (a) SP_A_new/SP_A_old, (b) SP_B, (c) SP_C_new/SP_C_old, (d) SP_D and (e) SP_E (NEW—adjusted layout; OLD—reference layout).

4.5.2. Burnup Credit Analysis for the Realistic BWR FA Model

4.5.2.1. Criticality Estimation for Single BWR FA

Lattice codes simulate fuel assembly in an infinite 2D geometry, typically with one reference water density, an estimation of the average fuel temperature and the use of a constant power approximation over burnup. However, in a real reactor core, the assembly has a limited size, surrounded by fuel assemblies from other cycles and by a reflector at the top and bottom of the fuel assembly. At the same time, the FA power varies due to burnup processes as only the reactor power is kept constant. Thus, the peak assembly power changes axially during the burnup, which is opposite to the constant power approach of the lattice calculations. At the same time, the fuel assembly power is balanced with the other FAs through the core power. In the current section, the authors aim to determine how the transition from the lattice computations (radial infinite medium approach) to a more realistic assembly model in a core simulator—a 3D approach with realistic water density distribution and fuel temperatures, but still employing reflective boundary conditions in the radial direction—affects the function of k_{eff} over burnup and to estimate the impact of the given 3D approach on the burnup credit. For this purpose, the following models based on the BWR GE14 assembly design (Figure 4.1) were analysed:

- A 2D lattice model of the dominant layer (DOM) without burnable poison or in terms of the burnup credit, the so-called "fresh fuel" approach, which is referred to as Model 1 (M1).

- A 2D lattice model of the DOM layer with burnable poison, or the "peak reactivity" approach (M2).

- A 3D nodal model of the realistic FA with DOM and vanished layers (VAN), natural uranium blankets, non-uniform axial coolant density distribution and the reflectors on the fuel assembly ends (M3). The boundary conditions are set to reflective in the radial direction and vacuum in the axial. In addition, two separate 3D nodal models of the FA, containing DOM and VAN layers only, were created to estimate the contribution of each layer to the total criticality of the FA.

The "fresh fuel" approach is considered as the most traditional method of criticality safety analysis with respect to analysing spent fuel storage systems, which implies that the system is loaded with unirradiated fuel without burnable poison. Due to today's widespread use of fuel assemblies containing burnable poisons, the "peak reactivity" approach has been adopted by the nuclear community [12]. As burnable absorber depletes faster than uranium during fuel irradiation, this leads to a reduction in the initial excess reactivity at the beginning of assembly life, with further rise of the fuel assembly criticality up to a maximum level referred to as the peak reactivity, followed by a further decline. The given method assumes that the fuel in the considered system is at its peak reactivity burnup when loaded. This approach is less conservative than the fresh fuel approach which is the most conservative for criticality safety analysis [26].

As will be shown later, the dominant layer mainly contributes to the criticality of the current BWR assembly and, thus, it was chosen as the reference layer for the M1 and M2 models. The coolant density in lattice calculations was set as an average for the DOM layer (0.6 g/cm^3). The estimation is based on the averaged coolant density profile for various BWR

fuel assemblies described in [31]. For the 3D nodal model M3, DYN3D calculates coolant density distribution based on the channel model as well as other thermal-hydraulics and thermo-dynamics parameters of the fuel assembly at each burnup step.

Figure 4.9 depicts the comparison of the depletion analysis for the three different models described above. The results show that the peak reactivity occurs earlier in the M3 case, when the fuel assembly is modelled under representative operational conditions, in comparison with the lattice approach M2. Furthermore, the assembly criticality at the peak is approximately 5% lower in the M3 case. A similar effect was observed in the study [16], where authors performed depletion analysis for 2D and 3D models of the BWR fuel assembly with uniform and non-uniform axial coolant density distributions. However, the investigation was limited to the peak reactivity area, while the current analysis covers the criticality evolution over the whole targeted burnups of the fuel assembly. The analysis of the M3 burnup curve beyond peak reactivity reveals a second increase in criticality near 30 GWd/tU burnup. Furthermore, after approximately 45 GWd/tU, the M3 curve has a steady negative bias with M1 and M2 cases. It occurs due to the leakage boundary conditions applied to the top and bottom.
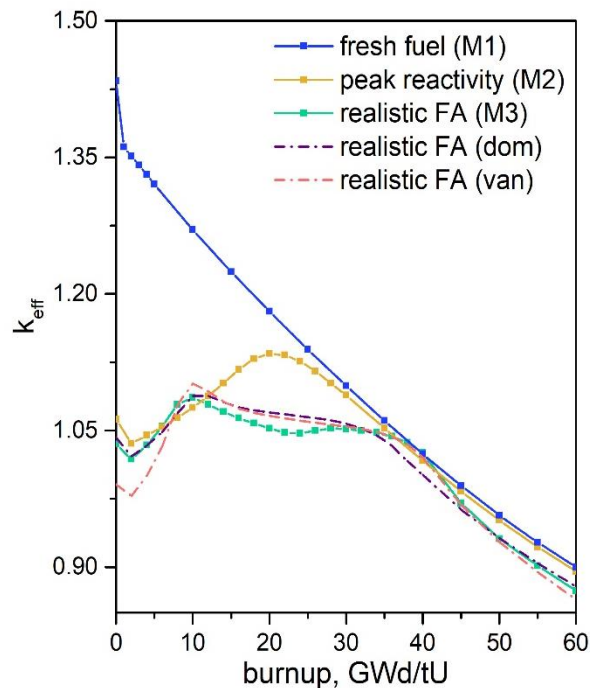
Figure 4.9. k_{eff} as a function of burnup for the discussed 2D lattice models and 3D nodal code model of BWR assembly.

The power profile evaluation for the realistic FA model M3 at four different burnup stages is represented in Figure 4.10. The power distribution was normalised at the maximum power value observed at the 30 GWd/tU burnup step. It is seen that at the initial burnups steps, for example, 0 and 10 GWd/tU, the peak power is located at the bottom (dominant) FA layer. As the fissile material depletes and gadolinium burns in this layer, the power shifts towards the top (vanished) layer where the fuel is fresher and still has a higher fissile content, as seen from Figure 4.10 (30 GWd/tU burnup stage). This results in the formation of the second reactivity peak on the M3 burnup curve (Figure 4.9) since the fissile depletion and the gadolinium burning are now accelerated in the top part of the fuel assembly due to

the increased power. Finally, when the burnable poison is completely depleted and the fissile content in the central parts of the fuel assembly is significantly reduced, the power distribution peaks at the least burnt parts of the fuel assembly, the very top and bottom (50 GWd/tU burnup stage). Overall, the dominant layer plays a significant role in power production, defining the reactivity of the whole FA. This is also seen from the comparison of the M3 and the dominant layer criticality curves (Figure 4.9). The curves mostly coincide on the whole range of the considered burnups, except in the interval between 35 to 45 GWd/tU where the vanished layer is prevalent; see the power curve in Figure 4.10.

Since the M3 approach showed a substantial decrease in criticality at the peak reactivity in comparison with M2, it can be considered as an alternative approach to evaluate the burnup credit. In this case, the credit comes not only from the fuel burnup and residual gadolinium, as in the case of the peak reactivity method, but also from the increase in FA model complexity, which allows us to follow the changes in the axial power distribution while relying on calculated coolant properties and fuel temperatures. For further analysis, we will call this approach "peak reactivity of the realistic FA model".

The development of the burnup credit methods intends to reduce the cost of spent fuel management. Hence, the gain from the BUC should be recognisable when either boral plates, which are used in the storage and transport casks as neutron absorbers, can be removed or their number can be substantially reduced, or the spent fuel storage system's capacity can be increased.
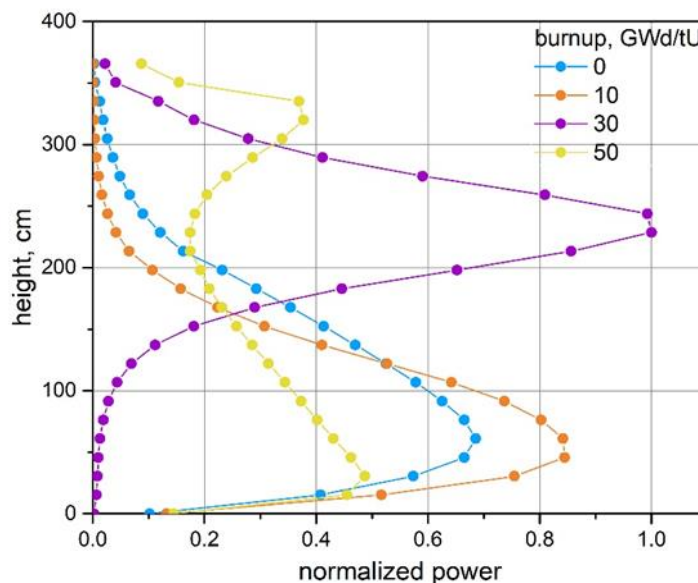
Figure 4.10. Power profile distribution for different burnups of the BWR assembly (M3 case).

4.5.2.2. The Burnup Credit of the Core

In this section, the authors aim to estimate the possible credit from the reactivity reduction of the irradiated BWR fuel assembly based on the realistic FA model M3 combined with the number of fuel assemblies discharged at the burnups of the least and most optimal burnup distributions SP_C_new and SP_A_new, respectively. This approach will be called "burnup credit of the core". It should be noted that the criticality estimation of

the FA based on M3 model does not reflect on its position in the reactor core (see description given above) since M3 simulates a single FA in the reflective radial boundary conditions. The here suggested approach for BUC analysis is based on full core modelling and, hence, is significantly more time-consuming and requires more computational power than the lattice approach or the M3 approach. However, it is crucial to create an understating about the gain which could be harvested in the case of a higher investment into the modelling or maybe just the use of fuel management data which would be available for most of the operating nuclear power plants nowadays. For this purpose, the authors developed the concept of the normalised reactivity gain from applying the BUC approach, based on the discharged burnup distributions SP_C_new and SP_A_new, to the M3 FA model in comparison with the existing BUC approaches. The normalised reactivity gain was estimated as:

$$\rho_i^j = \frac{(k_j - k_i)}{k_j k_i} \cdot \frac{n_i}{N} \cdot 10^5 \qquad (2)$$

where

i is the burnup bin number from the discharged burnup distribution;

j is one of the approaches, fresh fuel, peak reactivity or peak reactivity, of the realistic FA model;

ρ_i^j is the normalised reactivity gain between the FA criticality at the bin i and the FA criticality at the approach j;

k_j is the FA k_{eff} at the approach j;

k_i is the FA k_{eff} at the bin i of the considered discharged fuel burnup distribution;

n_i is the number of FAs in the bin i;

N is full number of FAs in the distribution.

The normalised reactivity gain shows how much reactivity (in the form of the delta to the more approximate method) is gained by the fuel assemblies from a specific burnup bin of the considered burnup distribution. Thus, the introduced parameter correlates the gain from the optimisation of the loading pattern (achieving higher FA burnup) with the optimisation of the modelling and simulation (return on the investment in the modelling).

The results of the analysis are summarised in Figure 4.11. At the SP_C_new distribution, the 35 GWd/tU and 40 GWd/tU bins have the same number of the FAs as at 60 GWd/tU. However, the normalised reactivity gain from the last bin is higher. Thus, the high burnup bin at 60 GWd/tU contributes over proportionally. In the case of the SP_A_new distribution, the gain from the first two bins is close to the gain from the last bin (the number of the FAs are equal for both sets of bins). For both cases, the reactivity gain is almost negligible for 5% of the least burnt fuel assemblies in comparison to the FAs with burnups close to average and 5% of the highest burnt FAs. Here, the value could even change the sign in the case the fuel assemblies have not achieved the estimated peak value. Furthermore, the normalised reactivity gain for the optimal shuffling procedure (SP_A_new) is approximately three times higher than for the least optimal (SP_C_new) near the averaged discharged burnups. Table 4.7 represents the reactivity gain over the whole reactor core for the BUC of the core approach in comparison with the fresh fuel, the peak reactivity and the peak reactivity of the

realistic FA model approaches. It is seen that the reactivity gain is approximately 1120 pcm higher for the SP_A_new burnup distribution than for the SP_C_new one.

To sum up, shuffling procedure optimisation can substantially increase the number of FAs benefiting from the application of the BUC method applied to the FAs at their discharged burnups.

(**a**) SP_C_new   (**b**) SP_A_new
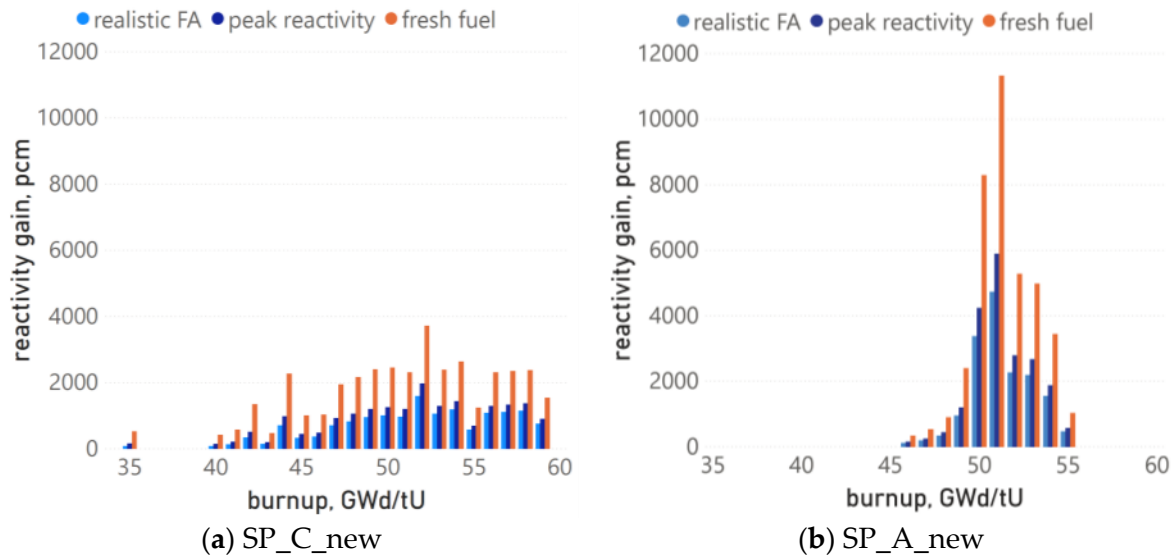
Figure 4.11. The normalised reactivity gain of the burnup credit (BUC) of the core approach in comparison with the fresh fuel, peak reactivity, and the peak reactivity of the realistic FA model approaches for BWR fuel for least optimal (a) SP_C_new and most optimal (b) SP_A_new burnup distributions.

Table 4.7. The full core reactivity gain for the suggested BUC of the core approach in comparison with approximate ones.

BUC Approach	Reactivity Gain, pcm	
	SP_A_New	**SP_C_New**
Fresh fuel	38,503	37,384
Peak reactivity	20,097	18,977
Realistic FA at the peak reactivity	16,179	15,060

4.6. Conclusions

In the given study, the authors created a BWR full core reactor model based on the information available in open source. Since the fuel reloading procedure is commercially sensitive information, especially for modern reactors, the authors developed and applied a few different shuffling procedures to estimate the possible spread/variation of the fuel-discharged burnups. The analysis showed that the loading pattern from [18], used as a basis for this study, required minor adjustments to eliminate the assemblies-outliers. Overall, seven reloading patterns were analysed, two for the initial loading map and five for the adjusted one. The FA-discharged burnup distribution for the adjusted map was optimal (in terms of fuel utilisation) under the SP_A shuffling procedure with the burnup range 47.5 to 54.5 GWd/tU and least optimal under the SP_C procedure, with the burnup range 34.5 to 59 GWd/tU. The SP_B and mixed SP_A/SP_B shuffling procedures are defined as potentially

optimal drafts. To achieve an industrially applicable optimum, the loading map requires further adjustments.

A single BWR FA model was analysed in the 2D lattice and 3D nodal approaches. The aim was to identify the impact of the increased level of FA model complexity on the criticality curve and the BUC. The results showed that the peak reactivity appears, by 10 GWd/tU, earlier on the criticality curve for the 3D BWR FA model with burnable poison in comparison with 2D lattice model and the criticality at the peak is substantially reduced. The given result coincides with the conclusions from [16]. Thus, the introduction of more detailed features in the BWR FA model using a nodal code can decrease the conservatism of the peak reactivity method when calculations are performed using the 2D lattice approach. Further investigation of the 3D model's criticality curve revealed the presence of a second spike in criticality which, according to the power profile analysis, occurs due to the fuel depletion from the vanished layer (upper core).

Finally, the authors estimated the potential benefit from applying the burnup credit method to the modern BWR SF using the criticality curve for the 3D BWR FA model (M3) and the discharged burnup distributions obtained from the full core nodal simulations with two shuffling procedures, SP_A and SP_C. The results showed that the average reactivity gain in comparison with the fresh fuel and peak reactivity approaches is close for both SP_A_new and SP_C_new burnup distributions, even if the loading patterns are very different. The minimum reactivity decrease was 15,000 pcm or 14% in the SP_C_new case in comparison with the peak reactivity approach with the realistic FA model, while the maximum was 38,500 pcm or 35.5% for the SP_A_new case in comparison with the fresh fuel approach. On the other hand, more fuel assemblies from the distribution with the optimal shuffling scheme SP_A achieve the same level of burnup and thus show the larger reduction in reactivity in comparison with the standard BUC approaches for the BWR, and thus, future cask loading is estimated to be less sensitive.

References

1. Crossland, I. *Nuclear Fuel Cycle Science and Engineering*; Elsevier: Amsterdam, The Netherlands, 2012.
2. Wolff, D.; Bevilacqua, A.; Carlsen, B.; Chiguer, M.; González-Espartero, A.; Grahn, P.; Saegusa, T.; Sampson, M.; Seelev, I.; Wasinger, K.; et al. *Storing Spent Fuel until Transport to Reprocessing or Disposal*; International Atomic Energy Agency: Vienna, Austria, 2019.
3. International Atomic Energy Agency. *Nuclear Power Reactors in the World*, 2019 ed.; International Atomic Energy Agency: Vienna, Austria, 2019.

4. International Atomic Energy Agency. *Energy, Electricity and Nuclear Power Estimates for the Period up to 2050*; International Atomic Energy Agency: Vienna, Austria, 2018.

5. Cacuci, D.G. *Handbook of Nuclear Engineering*; Vol. 1: Nuclear Engineering Fundamentals; Vol. 2: Reactor Design; Vol. 3: Reactor Analysis; Vol. 4: Reactors of Generations III and IV; Vol. 5: Fuel Cycles, Decommissioning, Waste Disposal and Safeguards; Springer Science & Business Media: Berlin, Germany, 2010.

6. Merk, B.; Stanculescu, A.; Chellapandi, P.; Hill, R. Progress in reliability of fast reactor operation and new trends to increased inherent safety. *Appl. Energy* 2015, *147*, 104–116.

7. Merk, B.; Litskevich, D.; Whittle, K.R.; Bankhead, M.; Taylor, R.J.; Mathers, D. On a Long Term Strategy for the Success of Nuclear Power. *Energies* 2017, *10*, 867.

8. Merk, B.; Litskevich, D.; Peakman, A.; Bankhead, M. IMAGINE—A disruptive change to nuclear or how can we make more out of the existing spent nuclear fuel and what has to be done to make it possible in the UK?. *ATW Int. J. Nucl. Power* 2019, *64*, 353–359.

9. Merk, B.; Broeders, C.H.M. Auswirkungen von verschiedenen Brennstoffzyklusoptionen auf die anfallenden Aktinidenmengen im deutschen Reaktorpark. *Atw. Internationale Zeitschrift für Kernenergie* 2008, *53*, 404–412.

10. Annual Commercial Spent Fuel Discharges and Burnup, 1968–30 June 2013. Available online: https://www.eia.gov/nuclear/spent_fuel/ussnftab3.php (accessed on 8 May 2020).

11. International Atomic Energy Agency. *High Burnup Fuel: Implications and Operational Experience, IAEA-TECDOC-1798*; IAEA: Vienna, Austria, 2016.

12. Marshall, W.B.; Ade, B.J.; Bowman, S.M.; Gauld, I.C.; Ilas, G.; Mertyurek, U.; Radulescu, G. *Technical Basis for Peak Reactivity Burnup Credit for BWR Spent Nuclear Fuel in Storage and Transportation Systems*; Oak Ridge National Lab (ORNL): Oak Ridge, TN, USA, 2015.

13. Implementation of Burnup Credit in Spent Fuel Management Systems, IAEA-TECDOC-1013. In Proceedings of an Advisory Group Meeting Held in Vienna, Austria, 20–24 October 1997.

14. Advances in Applications of Burnup Credit to Enhance Spent Fuel Transportation, Storage, Reprocessing and Disposition. IAEA-TECDOC-CD-1547. In Proceedings of a Technical Meeting Held in London, UK, 29 August–2 September 2005.

15. Marshall, W.J.; Ade, B.J.; Gauld, I.C.; Ilas, G.; Mertyurek, U.; Clarity, J.B.; Radulescu, G.; Betzler, B.R.; Bowman, S.M.; Gonzalez, M. *Overview of the Recent BWR Burnup Credit Project at Oak Ridge National Laboratory*; Oak Ridge National Lab: Oak Ridge, TN, USA, 2019.

16. Radaideh, M.I.; Price, D.; O'grady, D.; Kozlowski, T. Advanced BWR criticality safety part I: Model development, model benchmarking, and depletion with uncertainty analysis. *Prog. Nucl. Energy* 2019, *113*, 230–246.

17. Price, D.; Radaideh, M.I.; O'Grady, D.; Kozlowski, T. Advanced BWR criticality safety part II: Cask criticality, burnup credit, sensitivity, and uncertainty analyses. *Prog. Nucl. Energy* 2019, *115*, 126–139.

18. SCALE Code System. *ORNL/TM-2005/39*, Version 6.2.2; Oak Ridge National Laboratory: Oak Ridge, TN, USA, 2017.

19. Jessee, M.A.; Wieselquist, W.A.; Evans, T.M.; Hamilton, S.P.; Jarrell, J.J.; Kim, K.S.; Lefebvre, J.P.; Lefebvre, R.A.; Mertyurek, U.; Thompson, A.B. *Polaris: A New Two-Dimensional Lattice Physics Analysis Capability for the SCALE Code System*; PHYSOR 2014; Oak Ridge National Lab.(ORNL), Oak Ridge, TN, USA, 2014.

20. Detkina, A.; Peakman, A.; Litskevich, D.; Liang, J.-H.; Merk, B. Evaluation of BWR Burnup Calculations Using Deterministic Lattice Codes SCALE-6.2, WIMS-10A and CASMO5. *Energies* 2020, *13*, 2573.

21. Rohde, U.; Kliem, S.; Grundmann, U.; Baier, S.; Bilodid, Y.; Duerigen, S.; Fridman, E.; Gommlich, A.; Grahn, A.; Holt, L.; et al. The reactor dynamics code DYN3D—Models, validation and applications. *Prog. Nucl. Energy* 2016, *89*, 170–190.

22. Gomez, T.A.M.; Sanchez, E.V.H.; Kliem, S.; Gommlich, A.; Rohde, U. Integration of DYN3D inside the NURESIM platform. In Proceedings of the 17th Pacific Basin Nuclear Conference, Cancun, Mexico, 24–30 October 2010.

23. Grundmann, U.; Kliem, S.; Rohde, U. Analysis of the Boiling Water Reactor Turbine Trip Benchmark with the Codes DYN3D and ATHLET/DYN3D. *Nucl. Sci. Eng.* 2004, *148*, 226–234.

24. Fennern, L. Design evolution of BWRs: Dresden to generation III †. *Prog. Nucl. Energy* 2018, *102*, 38–57.

25. Ade, B.J.; Marshall, W.B.J.; Ilas, G.; Betzler, B.R.; Bowman, S.M. *Impact of Operating Parameters on Extended BWR Burnup Credit, NUREG/CR-7240, ORNL/TM-2017/46*; Oak Ridge National Laboratory: Oak Ridge, TN, USA, 2018.

26. Mueller, D.E.; Scaglione, J.M.; Wagner, J.C.; Bowman, S.M. *Computational Benchmark for Estimated Reactivity Margin from Fission Products and Minor Actinides in BWR Burnup Credit*; ORNL Report to the NRC.; Oak Ridge National Laboratory: Oak Ridge, TN, USA, 2013.

27. Solis, J.; Ivanov, K.N.; Sarikaya, B.; Olson, A.M.; Hunt, K.W. *Boiling Water Reactor Turbine Trip (TT) Benchmark*; Volume I: Final Specifications (No. NEA-NSC-DOC--2001-1); Organisation for Economic Co-operation and Development: Paris, France, 2001.

28. International Atomic Energy Agency. *Boiling Water Reactor Simulator Workshop Material*, 2nd ed.; International Atomic Energy Agency: Vienna, Austria, 2005.

29. Peakman, A.; Grove, C.; Fitzgerald, K.; Gregg, R. Development of an equilibrium loading pattern and whole-core fuel performance assessment in the Advanced Boiling Water Reactor (ABWR) with UO2 and U3Si2 fuels. *Prog. Nucl. Energy* 2019, *117*, 103053.

30. Kurihara, K.; Takeda, R.; Uchikawa, S.; Yokomi, M. Power-Flattening Method for Boiling Water Reactor. *Nucl. Sci. Technol.* 1981, *18*, 116–124.

31. Marshall, W.J.; Ade, B.J.; Bowman, S.M.; Martinez-Gonzalez, J.S. *Axial Moderator Density Distributions, Control Blade Usage, and Axial Burnup Distributions for Extended BWR Burnup Credit. NUREG/CR-7224, ORNL/TM-2015/544*; US Nuclear Regulatory Commission: Rockville, MD, USA; Oak Ridge National Laboratory: Oak Ridge, TN, USA, 2016.

32. Yamada, K.; Tajima, S.; Tsubaki, M.; Soneda, H. ABWR design and its evolution-primary system design of ABWR and ABWR-II. GENES4/ANP2003. *Kyoto* 2003, 15–19.

33. Hitachi-GE Nuclear Energy. *UK ABWR Generic Design Assessment Generic PCSR Chapter 11: Reactor Core*; Hitachi-GE Nuclear Energy, Ltd.: Ibaraki-ken, Japan, 2017.

34. Ade, B. *SCALE/TRITON Primer: A Primer for Light Water Reactor Lattice Physics Calculations*; ORNL/TM-2011/21; Oak Ridge National Laboratory: Oak Ridge, TN, USA, 2012.

35. Rearden, B.T.; Marshall, W.B.; Williams, M.L.; Jessee, M.A.; Mertyurek, U.; Betzler, B.R. *Accuracy and Runtime Improvements with SCALE 6.2*; Oak Ridge National Lab (ORNL): Oak Ridge, TN, USA, 2017.

36. Nakano, Y.; Okubo, T. Plutonium isotopic composition of high burnup spent fuel discharged from light water reactors. *Ann. Nucl. Energy* 2011, *38*, 2689–2697.

37. Brown, C.; Hartley, K.; Hulsman, J. Extended Power Uprates and 2-yr Cycles for BWRs—Where Do We Go from Here? *Nucl. Technol.* 2005, *151*, 120–125.

38. Hitachi-GE Nuclear Energy. *Generic Design Assessment: Disposability Assessment for Wastes and Spent Fuel arising from Operation of the UK ABWR Part 1: Main Report*; Hitachi-GE Nuclear Energy, Ltd.: Ibaraki-ken, Japan, 2016.

39. Tsoulfanidis, N. *The Nuclear Fuel Cycle*; American Nuclear Society: La Grange Park, IL, USA, 2013.

5. Burnup credit analysis based on the realistic BWR spent fuel characteristics

As shown earlier, the modern BWR fuel assembly design is very complex and cannot be adequately modelled under the classical 2D lattice approach. In this chapter, the ABWR reactor core model developed in Chapter 4 was used to estimate BWR spent fuel characteristics for further criticality analysis of the spent fuel storage cask. The study [44] showed that the axial burnup profile has the biggest impact on the criticality of the storage cask loaded with BWR spent fuel discharged at burnups beyond peak reactivity. The next significant parameter was the axial coolant density profile, followed by the control blade movements, fuel temperature, specific power etc. The first two major factors affecting the cask criticality – axial coolant density distributions which each FA sees over its lifetime in the reactor core and the axial burnup distribution of the FA discharged from the reactor, were tracked in the full-core simulations and then used to estimate spent fuel isotopic composition. Including the lower-impact parameters in the analysis can be a part of the follow up research.

At the first step, the criticality analysis of the storage cask was performed for spent fuel assemblies from discharged burnup distributions corresponding to the refuelling scenarios developed in Chapter 4 for the adjusted full-core configuration. Two types of cask loading were analysed: 1) 5% of FAs with the lowest burnup from the considered distribution and 2) 68 FAs from the centre of the distribution or, in other words, 68 FAs with burnups closed the average discharge burnup. In addition, the impact on the cask criticality was estimated for the following parameters:

- two target burnups for GE14 fuel assembly – the first one is planned for the GE14 FA type examined here (50 GWd/tU) and the second is based on the German regulations for BWR fuel assemblies (44.5 GWd/tU);

- two types of BWR fuel assembly design – GE14 and SVEA100 which represent modern and previous generation design respectively.

The SVEA design concept was first presented in work [45] in 1981. At that time, the concept was seen as a substantial achievement for the BWR fuel development [46]. The first full SVEA-100 reload was performed in 1990 into Oskarshamn 3 [13]. The GE14 fuel design has been initially introduced in the 1990s. So far, GE14 has the most extensive operating experience out of all BWR fuel (more than 3 million fuel rods) [47]. The GE14 fuel design has been approved and used in 8 countries such as Germany, Sweden, the USA etc., and operated in 43 reactors in those countries. As of 2016, the GE14 fuel has been almost replaced with a more advanced GNF2 fuel design leaving only three nuclear power plants operating on GE14 fuel [48].

The results of the criticality analysis of the cask filled with FAs from different burnup distributions were compared against each other to determine the level of impact of the shuffling procedure on the cask criticality. The impact of FA type and target burnup were analysed for the least and most optimal shuffling procedures as defined in Chapter 4. The k_{eff} for each case was compared against fresh fuel and peak reactivity approaches to determine the reactivity gain from using realistic spent fuel properties in the criticality analysis. The estimations used the isotopic set recommended for the burnup credit analysis of LWRs [49].

The criticality estimation of the storage cask loaded with spent fuel from different refuelling scenarios revealed that k_{eff} of the load with 68 typically burnt FAs changes insignificantly with the change of scenario. While criticality of the cask loaded with 5% of the lowest burnt FAs varies substantially with the refuelling scenario. This change can be explained by a bigger range in the burnup values of the considered sets of FAs as well as in the different axial coolant density profiles these FAs have seen during operation. In terms of target burnup variation, the most surprising effect was observed for the 5% of the least burnt FAs for the least optimal shuffling procedure with target burnup set by German regulatory standards. The criticality of the FAs from the described set was significantly lower than expected due to the presence of the Gd_2O_3 burnable poison in its upper part which demonstrated again the significance of 3D modelling of the BWR fuel assembly. The most significant outcome of the BWR fuel assembly type variation is that the benefit of the burnup credit method was bigger for the modern GE14 FA type than for the previous generation SVEA100 in comparison to the fresh fuel approach and lower, in comparison to the peak reactivity. The latter effect arises due to the lower k_{eff} value near the peak reactivity for GE14 fuel assembly.

The results of the research have been published in the peer-reviewed journal Applied Sciences, with the paper provided below.

Article

Criticality Analysis for BWR Spent Fuel Based on the Burnup Credit Evaluation from Full Core Simulations

Anna Detkina [1,*], Dzianis Litskevitch [1], Aiden Peakman [1,2] and Bruno Merk [1]

[1] School of Engineering, University of Liverpool, Liverpool L69 3GH, UK; d.litskevich@liverpool.ac.uk (D.L.); a.peakman@liverpool.ac.uk (A.P.); b.merk@liverpool.ac.uk (B.M.)

[2] National Nuclear Laboratory, Chadwick House, Warrington WA3 6AE, UK

* Correspondence: a.detkina@liverpool.ac.uk

Abstract: This study performed criticality analysis for the GBC-68 storage cask loaded with boiling water reactor (BWR) spent fuel at the discharged burnups obtained from the full-core simulations. The analysis was conducted for: (1) different reloading scenarios; (2) target burnups; and (3) two fuel assembly types—GE14 and SVEA100—to estimate the impact each of the three factors has on the cask reactivity. The BWR spent fuel composition was estimated using the results of the nodal analysis for the advanced boiling water reactor (ABWR) core model developed in this study. The nodal calculations provided realistic operating data and axial burnup and coolant density profiles, for each fuel assembly in the reactor core. The estimated cask's k_{eff} were compared with the fresh fuel and peak reactivity standards to identify the benefit of the burnup credit method applied to the BWR spent fuel at their potential discharge burnups. The analysis identified the significant cask criticality reduction from employing the burnup credit approach compared to the conventional fresh fuel approach. However, the criticality reduction was small compared to the peak reactivity approach, and could even disappear for low burnt fuel assemblies from non-optimal reloading patterns. In terms of cask manufacturing, the potential financial benefit from using the burnup credit approach was estimated to be USD 3.3 million per reactor cycle.

5.1. Introduction

Criticality safety analysis is a mandatory procedure for all facilities and activities dealing with fissile material [1]. It determines if the system of interest is subcritical, critical, or supercritical for both normal and accident conditions. Most often, the safety limits for the analysed system are defined by the value of the effective multiplication factor (k_{eff}). In the current project, the authors will focus on the criticality analysis of the storage cask loaded with boiling water reactor (BWR) spent fuel (SF).

In general, criticality analysis is based on different approximations which take into account the uncertainties in the initial data [2]. The most traditional and conservative approach regarding criticality analysis for operations involving spent fuel is the so-called "fresh fuel approach", where the fuel in the system is modelled as unirradiated and without burnable absorber present. The limitations of the fresh fuel approach become obvious when the fuel enrichment is high [3], as with a higher initial fissile material content, the assembly criticality also increases, and thus additional safety measures are required for the spent fuel

handling. The advantage of the fresh fuel approach is that it does not require sophisticated calculations or extensive nuclear codes' verification and validation. As computational tools have been improved and more experimental information has been accumulated about spent fuel properties [4], it has become possible to perform reliable estimations of spent fuel properties or, in other words, to take credit for the reactivity reduction in the nuclear fuel during irradiation. This approach of the criticality analysis is called burnup credit (BUC) method. Application of the burnup credit method can reduce costs of spent fuel management, for example, by increasing storage or transport casks capacity or by removing absorbing panels and thereby reducing the costs associated with cask manufacturing [4].

The burnup credit method can be applied on different levels such as actinides only, actinides and fission products or integral burnable absorber [5]. On the first two levels, credit is taken for the set of specific nuclides (major actinides on the first level, and additional minor actinides and fission products on the second level) defined in [6] as suitable for burnup credit as they play a major role in the system's reactivity reduction and have a comprehensive experimental data. On the last, integral burnable absorber level, the credit is taken for the reactivity reduction at the maximum reactivity value of the fuel assembly (FA) with burnable absorber (poison) in comparison with the fresh fuel approach. For poisoned FAs (gadolinia in the case of BWRs), the initially low reactivity increases up to certain value (peak reactivity) and then declines after the absorber is burnt. The given BUC approach is often referred to as peak reactivity. The safety criteria for burnup credit are based on the loading curve of the analysed system. The loading curve determines the minimal fuel assembly burnup as a function of its initial enrichment under which the assembly can be placed into the storage or transport system [7]. The loading curve should be estimated for each licensing condition, such as different assembly cooling times. Another important part of the BUC analysis is the validation of the codes used for depletion and criticality analysis along with their nuclear data libraries. The study [8] performed as the part of this project showed that even well-known lattice codes can produce noticeably different results. Hence, the burnup credit method is more complicated in comparison with fresh fuel approach in terms of regulatory requirements, computational methods, as well as software verification and validation, but can potentially gain a significant benefit for spent fuel management.

BWRs are of particular interest for the burnup credit analysis due to their complex assembly design (e.g., multiple rod geometries and compositions per fuel assembly) in comparison with pressurised water reactors (PWRs) and being less researched, despite the global deployment of BWR technology [9]. Moreover, some future Generation III+ reactor designs such as advanced boiling water reactor (ABWR) or economic simplified boiling water reactor (ESBWR) [10] are based on BWR technology. The most recent extensive research regarding burnup credit application to transport and storage of BWR spent fuel was performed by Oak Ridge National Laboratory (ORNL) as a part of their five-year program with the US Nuclear Regulatory Commission (NRC) [11]. The project had two phases: (1) burnup credit analysis for BWR spent fuel near the peak reactivity; and (2) for the burnups beyond peak reactivity or so-called extended BUC. The authors investigated the effect of design and operating parameters of BWR systems on the final storage and transport cask criticality, along with verification and validation of the utilised tools [11]. Although the effect of axial burnup and moderator densities profiles were studied during the project, the limitation of the tools did not allow to track changes of these profiles over the cycle, so

analysis was performed using the cycle-averaged data [12]. The different modules and versions of SCALE [13] nuclear code were used for the project. Another recent study [14], investigated the compound effect: the effect of the variation of the several operating parameters on burnup credit for various assembly burnups. The authors showed the correlation between effective multiplication factor (keff) of the storage cask and fuel burnup for single and compound effects of the operating parameters variation. However, the study included a range of assumptions and simplifications regarding fuel assembly design and operating parameters.

Other research on the BWR BUC is presented in a series of works [15,16]. In the first part of the study [15], the authors created an advanced 3D model of the BWR fuel assembly with complex design and compounding operating parameters for depletion analysis and compared it to the simplified 2D lattice models. The results showed substantial changes in the criticality curve and U-235 and Gd-155 depletion when using the advanced model. The second part of this research [16] was focused on the criticality analysis and uncertainty quantification (UQ) for the cask loaded with BWR spent fuel discharged at the peak reactivity using depletion models developed in the first part of the research [15]. Authors concluded that the advanced 3D model of the BWR fuel assembly is highly beneficial for the burnup credit since it can incorporate parameters which significantly affect the cask criticality such as axial burnup or coolant density profiles.

Uncertainty analysis is an essential part of the burnup credit method. Fuel depletion in criticality analysis leads to many additional uncertainties in comparison with the fresh fuel approach. The isotopic prediction is viewed as a possible primary source of uncertainties related to the fuel burnup [17]. There have been several studies on uncertainty analysis associated with BWRs in recent years [18–21]. The work [18] related to the isotopic uncertainty, comparing two approaches for the uncertainty analysis: (1) computational (uncertainty in the input parameters), and (2) data-driven (usage of the experimental data and previous expertise in the criticality assessment). The authors identified that the data-driven approach provides a larger contribution to the uncertainty value than the computational approach.

The present study is an extension of the work [22] which was focused on creating the BWR reactor core model for the nodal analysis using the Advanced BWR design [23] to get the spent fuel (SF) data for further criticality analysis of the BWR transport and storage cask. The nodal calculations were performed for various core loading strategies to estimate the possible range of the assemblies' discharge burnups. In this part of the study, the authors will focus on applying the results of the full-core simulations to the extended burnup credit for BWR spent fuel. The study will also investigate the impact of the loading strategy (refuelling process in particular), target burnup and assembly type on the results of the BUC. In summary, the authors pose the following research question: "Will further investigation into the application of new modelling and simulation techniques benefit existing burnup credit strategies?".

The paper is structured as follows: Section 2 gives an overview of the utilised computational tools. Section 3 describes the FAs models, reactor core design and storage cask design. Section 4 outlines the methods for the nodal reactor core analysis and criticality analysis sequence of the storage cask. Section 5 describes and discusses the criticality

analysis results for different FAs designs, refuelling scenarios, and target burnups. Section 6 summarises conclusions of the study.

5.2. Computational Tools

The current study utilises the SCALE 6.2 code system as the main tool for the reactor physics and criticality calculations. The SCALE 6.2 package is developed and supported by Oak Ridge National Laboratory (ORNL), USA, and distributed by the OECD/NEA databank [13]. The 2D lattice physics calculations were performed using the Polaris module of SCALE, which employs the method of characteristics as the transport solver [24,25]. The self-shielding effect is calculated using embedded self-shielding method (ESSM). Polaris is optimised for light water reactor analysis and can be used with 252 and 56 multigroup ENDF/B-VII.1 based cross-section libraries. In this research, Polaris was utilised for the homogenised two-group cross-section preparation for use in nodal analysis with DYN3D code [26] and estimation of the spent fuel composition of BWR fuel assemblies for further criticality analysis.

Polaris is internally combined with the ORIGEN module to conduct depletion and decay calculations on fuel assembly level [13]. This calculation sequence is referred to as the Polaris/ORIGEN sequence in this study when referring to fuel isotopic predictions due to depletion/decay processes. The OPUS module, which parses results from the ORIGEN binary concentration files, is utilised here for spent fuel composition extraction after lattice physics calculations in Polaris. KENO V.a, another module within the SCALE package, is used to perform criticality estimations for the storage cask filled with BWR spent fuel assemblies. KENO is a 3D Monte Carlo module within the SCALE package which can estimate effective multiplication factor (k_{eff}), flux densities and other parameters of interest in 3D systems [13]. It can perform criticality analysis based on multigroup or continuous nuclear data libraries. KENO V.a is an earlier version of KENO VI module and has less flexible geometry capabilities but has a significantly lower computation burden and was therefore employed in this study.

The reactor core analysis was performed using DYN3D nodal core simulator [26] developed by Helmholtz-Zentrum Dresden-Rossendorf (HZDR), Germany. Two-group macroscopic cross-section library was used to provide fully coupled neutronic/thermalhydraulic analysis based on the nodal approach. DYN3D produced axial burnup profiles of the discharged FAs and axial coolant density distributions for FAs during the reactor operation used in further depletion calculations.

5.3. Models Description

5.3.1. Fuel Assembly Design

5.3.1.1. BWR GE14 10 × 10

The work presented here considered two different fuel assembly designs: (1) BWR GE14 10 × 10; and (2) SVEA-100, for the full core and criticality analysis. The BWR GE14 assembly was set as a reference, while SVEA-100 was used to estimate the effect of the FA design change on the results of the analysis. BWR fuel assemblies are often non-uniformly enriched. To simply the modelling approach, the current study used an averaged radial fuel enrichment. Work presented in [15] showed that averaging fuel enrichment only has a small

impact on the keff and isotopic composition in BWR spent fuel. As a real-life fuel enrichment patterns are rarely available in the open literature for the modern BWR fuel assembly designs, that would be of high interest to investigate their behaviour if the operator provides detailed data.

The fuel in BWR GE14 assembly has a U-235 content of 4.5 wt.%, and gadolinia rods contain in addition 7 wt.% Gd_2O_3. The fuel assembly consists of 92 fuel rods in total out of which 14 are the part-length rods dividing the FA into two lattices—dominant and vanished, and 15 are burnable poison rods (Figure 5.1). The assembly design parameters are explicitly described in the first part of this study [22] with the key data summarised in Table 5.1.
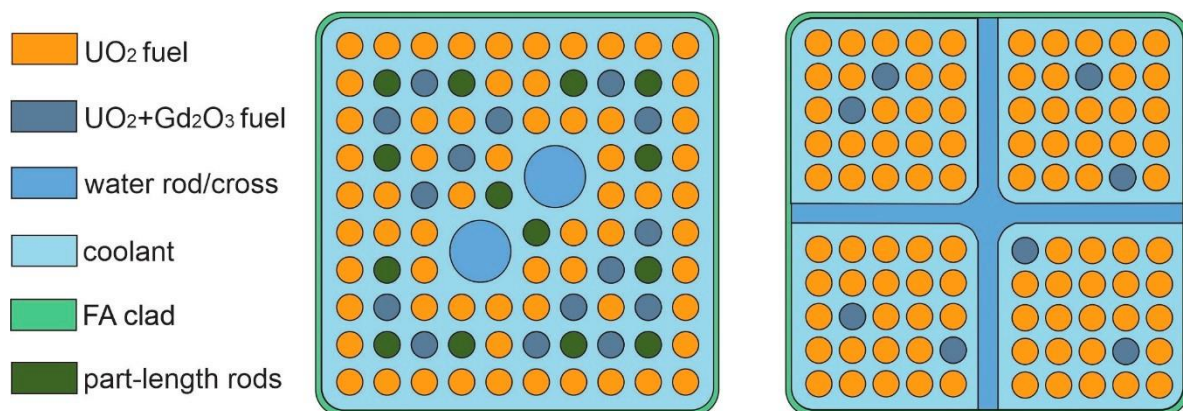
Figure 5.1. BWR GE14 10 × 10 (left) and SVEA-100 (right) fuel assembly designs.

Table 5.1. BWR GE14 10 × 10 and SVEA-100 assembly parameters [27,28].

Parameter	GE14 10 × 10	SVEA-100
Fuel pellet radius, cm	0.438	0.4095
Zr clad radius, cm	0.513	0.481
Fuel rod pitch, cm	1.295	1.24
Fuel rods number	92	100
Assembly pitch, cm	15.24	15.475
Assembly height, cm	381	375

5.3.1.2. SVEA-100

The considered SVEA-100 fuel assembly design is based on the data from the Swedish Forsmark Unit 3 reactor description [28,29]. The fuel is enriched to 3 wt.% U-235 and contains 8 burnable poison rods (Figure 5.1) with 4.4 wt.% Gd_2O_3. The FA consists of 100 fuel rods separated by a water cross which splits FA into four sub-bundles of 5 × 5 size each, as shown in Figure 5.1. The summary of the main SVEA-100 FA parameters is also presented in Table 5.1. The SVEA-100 FA design is significantly less complex than the GE14 design, and pellet radii, as well as assembly height values, are lower than in the GE14 assembly design, leading to an approximately 6.5% lower total fuel volume.

5.3.2. Reactor Core Design

The current study uses the BWR full core model based on Ref. [23] but with a modified core layout, as outlined in [22]. The reactor core comprises 872 fuel assemblies of four fuel cycles, with the core layout shown in Figure 5.2. The number of fresh, first and second cycle assemblies is equal to 224, while only 200 fuel assemblies are used in the third cycle (224 × 3 + 200 = 872). In contrast to an industrial standard model, the full core model considered in this study aims to reproduce the general behaviour of the FA in the core, thus only a reduced number of safety parameters were controlled during the simulation.
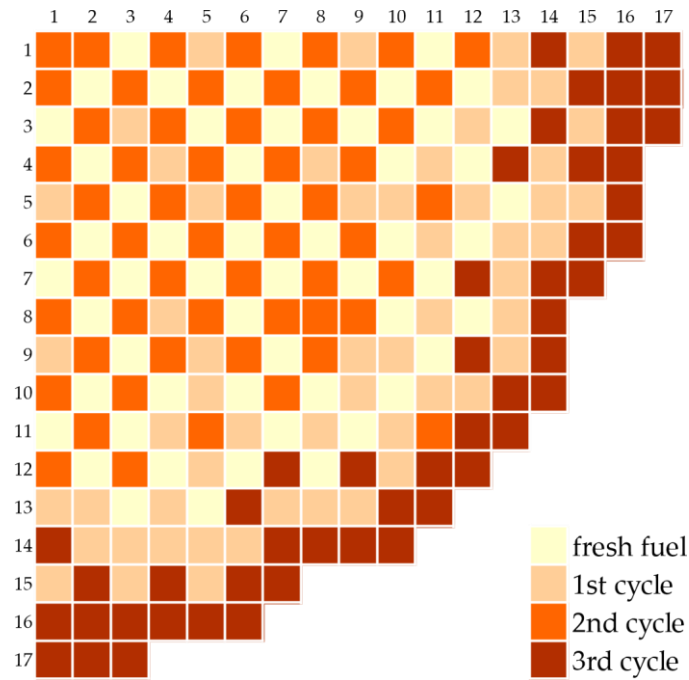
Figure 5.2. BWR full-core layout (1/4).

5.3.3. GBC-68 Storage Cask Design

The capacity of the storage and transport casks for BWR spent fuel varies significantly for different suppliers (44 to 89 FAs per cask) [27], with all designs including neutron absorber panels. The generic storage cask design GBC-68 with 68 FA capacity was proposed for BWR burnup credit analysis in the study [27]. The main parameters of GBC-68 cask are presented in Table 5.2. Figure 5.3 shows the GBC-68 cask model loaded with GE14 FAs in 180-degree symmetry. Each fuel assembly is placed in a separate cell which surrounds the FA with four stainless steel (SS304) walls. The boral panels (B4C/Al) are located between the cells and play an important role as a neutron absorber. The cask wall material is SS304 stainless steel. The cask is flooded with unborated water to imitate accident conditions [30].
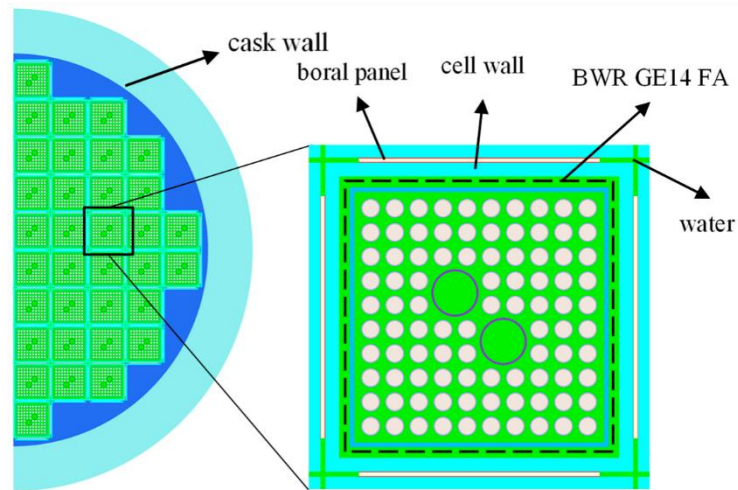
Figure 5.3. SCALE model of GBC-68 storage cask filled with BWR GE14 spent fuel assemblies.

Table 5.2. GBC-68 cask parameters [27].

Parameter	Value, cm
Outer diameter	215
Inner diameter	175
Inside height	410.76
Lid thickness	20
Cell pitch	16.8
Boral panel thickness	0.2565

5.4. Computational Methods

5.4.1. Reactor Core Analysis

Two-group homogenised cross-section sets for the fuel assemblies and reflectors were prepared using Polaris with 56-group ENDF/B-VII.1 master library of the SCALE system. In the case of the GE14 fuel assembly, cross-section sets were produced for dominant and vanished lattices, while in the case of SVEA-100, for a single lattice. The branch conditions were applied to the coolant density and fuel temperature, while the coolant temperature remained constant due to its little change during the normal reactor operation. The nodal data obtained with Polaris was converted to the DYN3D cross-section library format for further nodal reactor analysis. The full-core analysis results, such as coolant density and burnup profiles, were used further for the lattice depletion and criticality calculations using Polaris and KENO modules, respectively (see Section 4.2).

The vital information about reactor operation such as refuelling process is limited in the open literature. Hence, the authors developed their own refuelling model [22]. After each cycle, the fuel assemblies were arranged from low to high burnup using a Python script. They were then moved according to the specific pattern described by one of four hypothetical shuffling procedures (SP)—SP_A, SP_B, SP_C and SP_D [22]. The different strategies are based on:

- SP_A shuffling procedure which moves FAs with the highest burnup from cycle i ($i = 0$, N where N—is the number of cycles) to the positions of the lowest burnt FAs from the cycle ($i + 1$) and so on, is an optimal one.

- SP_B shuffling procedure follows the opposite pattern and moves FAs with the lowest burnup of the cycle i to the positions of the FAs with highest burnup of the cycle ($i + 1$).

- SP_C shuffling procedure, which is also the least optimal strategy, moves the FAs with the lowest burnup from cycle i to the position of the FAs with lowest burnup of the cycle ($i + 1$) and so on or, in other words, the FA saves its burnup position.

- SP_D procedure repeats the pattern of the SP_C, but at the (N − 1) cycle it follows the SP_B pattern by moving least burnt FAs to the positions of highest burnt ones from the cycle N.

The above shuffling procedures but for 4 cycle reactor operation are described in more details in the first part of the research [22]. Five scenarios of the reactor operation were considered based on single or mix of two shuffling procedures: four of them are based on SPs with the same name and SP_E case, is on altering SP_A and SP_B after each cycle. The nodal core model consisted of 27 axial layers in total, 25 of which represented the FA and 2 represented the top and bottom reflectors. The nodal analysis was performed with 5-day burnup steps for four cycles of reactor operation. The neutron flux distribution over the core was evaluated after each burnup step.

5.4.2. Criticality Analysis

The traditional depletion analysis in the lattice (2D) or Monte Carlo (2D-3D) codes cannot reflect real operational parameters of the fuel assembly in the reactor core since they simulate the fuel assembly in radially reflective boundary conditions. In addition, data like water density and fuel temperature are based on an initial estimate since neither thermodynamic nor thermal-hydraulic models are incorporated into the lattice codes. To overcome these limitations, the authors performed depletion analysis of the BWR fuel assembly using axial coolant density distributions and axial burnup profiles obtained with the nodal analysis of the reactor core. The BWR spent fuel composition resulting from these calculations were used in further criticality analysis of the GBC-68 storage cask.

A series of Python scripts were developed to transfer data from the nodal calculations into the KENO Monte Carlo solver used for the cask modelling. The flowchart of the modelling sequence is presented in Figure 5.4. After each simulation of the operational cycle in DYN3D, the coolant density and burnup profiles of the discharged FAs are extracted from the code's output file and saved to the text file by the Dyn3dPars script. When the required number of cycles N has been simulated, the saved data is used by the PolOPinp script to create input files for the depletion and decay calculations in Polaris/ORIGEN sequence. At this point, Polaris is used again to produce an isotopic composition for the BWR spent fuel for further criticality analysis with KENO. The PolOPinp script also performed an automatic composition extraction from the ORIGEN binary concentration file using the OPUS post-processor. To reduce the required amount of calculations, the PolOPinp also averages burnup and coolant density obtained for each of 25 axial layers in DYN3D down to 6 layers

for the KENO cask model–top and bottom natural uranium blankets and the 4 layers within the FA as shown in Figure 5.5. Next, Polaris/ORIGEN performs depletion/decay calculations for each layer in the traditional lattice approach, with layer's corresponding to coolant density and burnup value, as well as with a fixed set of cooling times. The fuel temperature is equal to 900 K as the estimated average for BWR fuel simulations during normal operation [27], and 560 K, for the coolant [31]. Then, the NumDensTrans script converts number densities obtained with Polaris/ORIGEN for each layer from the binary concentration file to KENO V.a input.

This study considered the set of 28 leading nuclides for criticality analysis—major and minor actinides and major fission products (AFP set) as presented here:

- Major actinides set [27]—U234, U235, U238, Pu238, Pu239, Pu240, Pu241, Pu242, Am241.

- Minor actinides and major fission products set [27]—U236, Am243, Np237, Mo95, Tc99, Ru101, Rh103, Ag109, Cs133, Sm147, Sm149, Sm150, Sm151, Sm152, Nd143, Nd145, Eu151, Eu153, Gd155.

The AFP set is formed from nuclides playing the most important role for burnup credit analysis of LWR spent fuel [6].
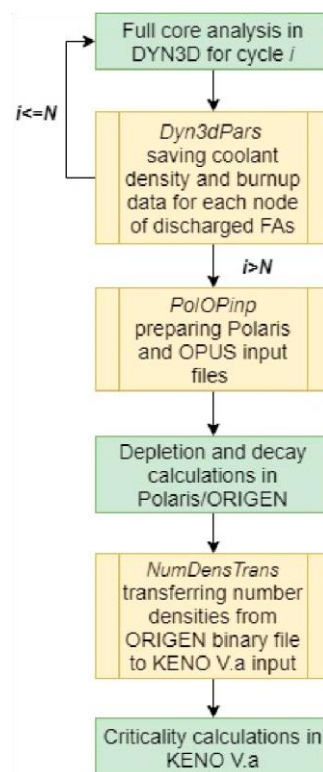
Figure 5.4. Flowchart of the modelling sequence from the full core nodal analysis to the cask criticality evaluation.
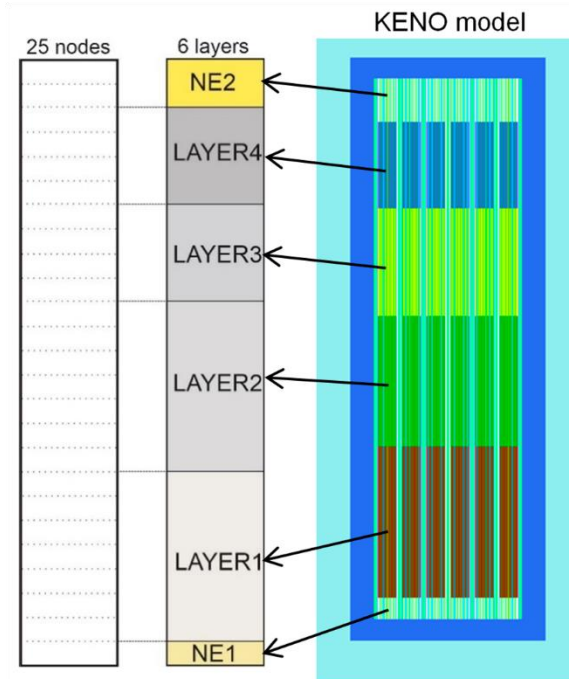
Figure 5.5. GBC-68 cask model in KENO V.a and the transformation of the layer structure form the core simulation to the cask model (NE—natural uranium blanket, LAYER—the FA layer).

5.5. Results and Discussion

5.5.1. Depletion Analysis of BWR GE14 and SVEA100 Fuel Assemblies

To estimate the difference in BWR GE14 and SVEA100 fuel assemblies' behaviour during the irradiation, the depletion analysis has been performed for burnups up to 60 GWd/tU [27] for both assembly types. The study considered the following FA models used in first part of the study [22]:

- 2D lattice model of the fuel assembly without burnable poison (M1).

- 2D lattice model of the fuel assembly with Gd burnable poison (M2). M1 and M2 configurations estimate criticality of the FA in reflective boundary conditions with constant fuel temperature, coolant density and coolant temperature.

- 3D nodal model of realistic fuel assembly with thermal-hydraulics coupling (M3). The FA configuration includes natural uranium blankets and has reflector from top and bottom. The FA is modelled with reflective boundary conditions in a radial direction, and vacuum at the assembly's ends. The coolant density along with fuel and coolant temperatures are non-uniformly distributed and obtained by the nodal code.

The so-called leading bottom layer of the FA mainly defines the final criticality [22], so the lattice models had coolant density as average for that layer of 0.6 g/cm^3. Fuel and coolant temperatures were set as average for BWRs, 900 K and 560 K, respectively [27,31]. The criticality curves for both FA types and all considered models are presented in Figure 5.6.
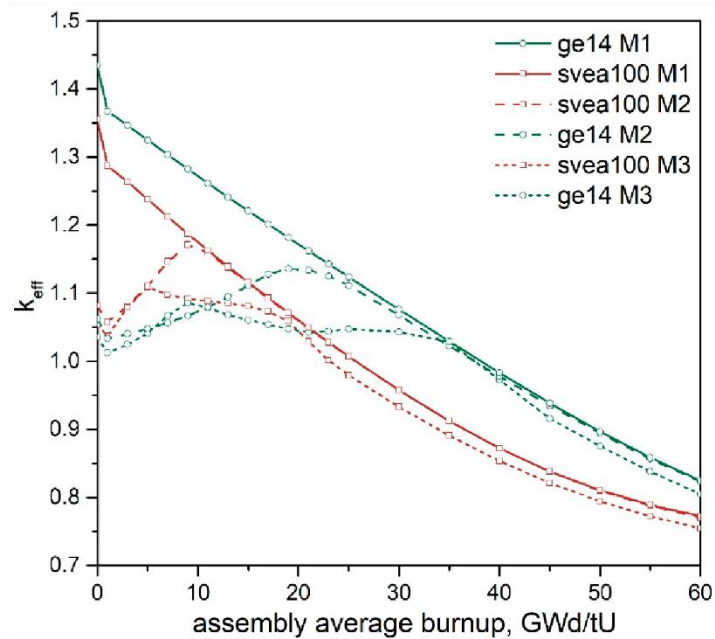
Figure 5.6. keff vs. burnup for three different models BWR GE14 and SVEA100 fuel assemblies.

The SVEA100 fuel assembly has lower average initial enrichment than GE14 fuel assembly. Consequently, the SVEA100 criticality curve obtained with M1 model (UO_2 fuel only) is lower than of GE14. The difference between infinite multiplication factors (k_{inf}) at the beginning of life (BoL) is 6%. At the same time, the criticality at the reactivity peak obtained with the M2 model, which contains gadolinium, is 3% higher and occurs ~10 GWd/tU earlier in the burnup for the SVEA100 fuel assembly due to lower initial gadolinia content compared to the GE14 fuel assembly. For the realistic nodal model M3, the difference in k_{eff} between first reactivity peaks decreased to 2% with SVEA100 peak being higher and occurring 5 GWd/tU earlier in comparison with the GE14 FA. It is seen that for both FA types the peak reactivity appears earlier for the 3D realistic model M3 than for simplified 2D lattice model M2. This is due to the non-uniform coolant density profile considered in the M3 model. In this case, the power is mostly concentrated at the bottom part of the FA [22] resulting in intensive depletion of the burnable poison there and consequently, in the earlier peak reactivity appearance compared to the lattice approach. A similar outcome was also demonstrated in the work summarised in Ref. [15]. Overall, the SVEA100 FA criticality reduces faster than for GE14 due to the lower initial fissile content, so its average discharged burnup should also be lower. The typical discharged burnups for FAs enriched up to 3% is less than 40 GWd/tU according to [27], and around 50 GWd/tU for higher enriched FAs (up to 5%) [32].

5.5.2. GBC-68 Cask Criticality Analysis

5.5.2.1. The Impact of the Refuelling Scenario on Cask Criticality

The first part of the research outlined the effect of the different shuffling procedures on final burnup distribution of the BWR fuel assemblies discharged from a reactor core [22]. This section investigates the shuffling procedure's impact on the cask reactivity. The fullcore calculations were performed for five refuelling scenarios SP_A, SP_B, SP_C, SP_D and SP_E

(see Section 4.1), four cycles of reactor operation and GE14 fuel assembly. The criticality analysis of the GBC-storage cask was carried out for two loads from the obtained burnup distributions:

- 68 fuel assemblies from the centre (L_{68});

- 5% least burnt fuel assemblies ($L_{5\%L}$).

L_{68} and $L_{5\%L}$ cask loads are of interest for the criticality analysis since the first one represents the typical cask load since it contains FAs from the burnup distribution centre. The second is the worst-case load as it has the FAs with the lowest burnup and, thus, most critical. The different cooling times were introduced to estimate the effect of the fuel assemblies' storage time in the cooling pond on the later cask criticality. Five years is the minimum cooling time in the US before spent fuel can be moved to further transport or dry storage [33]. However, shorter times can be permitted in other countries such as Germany with a nine months minimum storage time before loading and an average storage time of approximately three years [34]. Here, five-year cooling time was considered a reference, with one- and ten-year lower and upper boundaries.

Figure 5.7 represents the effective multiplication factor as a function of cooling time for the GBC-68 cask filled with BWR GE14 FA from L_{68} and $L_{5\%L}$ loads from the five considered loading patterns. The average line provides with the averaged for the five refuelling scenarios k_{eff} for the considered cask load. In the case of 68 typically burnt FAs (Figure 5.7a), the k_{eff} deviates at a maximum of 0.7% at the highest cooling time ten years compared to the average for five distributions. This demonstrates that the average fuel burnup of the different refuelling scenarios exhibits limited variation, with slight advantages for the SP_A and a slight disadvantage for the SP_B which coincides with the conclusions from [22], where the maximum difference between average discharged burnups of different loading patterns were 1 GWd/tU. For the 5% least burnt FAs (Figure 5.7b) the difference is significantly higher, up to 3.7%. It means that the choice of shuffling procedure mainly affects the cask's criticality for the worst-case study ($L_{5\%L}$ load) compared to the typical fuel assemblies (L_{68} load). These differences can be explained by the significantly lower than average burnups of the least burnt fuel assemblies in some of the refuelling patterns, for example, SP_C [22].

Another reason for the wider k_{eff} spread for $L_{5\%L}$ load is that the FAs from L_{68} load see closer axial coolant density profiles for different refuelling scenarios (Figure 5.8a). Hence, it does not affect the cask criticality as much as in the case of $L_{5\%L}$ load where the profiles are more spread (Figure 5.8b). Since fuel assemblies see different operational conditions under various refuelling scenarios, their final axial burnup profiles will also vary. The difference between coolant density profiles can also explain why some scenarios with higher burnup values (Table 5.3) have higher k_{eff}. The general trend is that fuel with higher burnup has lower criticality. Ref. [12] highlighted that the criticality at the upper layers of some BWR fuel assembly at their average discharge burnups increases with lowering the coolant density. Here, this effect is seen between, for example, SP_B and SP_D burnup distributions for L_{68} load and SP_B and SP_E burnup distributions for $L_{5\%L}$ load. In the first case, the SP_B coolant density is lower than for SP_D (Figure 5.8a) for L_{68} load, and k_{eff} of SP_B scenario is higher than of SP_D despite having the higher burnup. In the second case, the coolant density on the upper layers is lower for SP_E than for SP_B scenario for $L_{5\%L}$ load, but k_{eff} and burnup are higher. It is also seen that for optimal distribution SP_A, k_{eff} values of the L_{68} load

are the lowest ones out of all distributions, while for L5%L, they are close to average values. For the least optimal, SP_C distribution, the effective multiplication factor of L68 load is close to average and has the highest keff values for L5%L load.

(a)   (b)
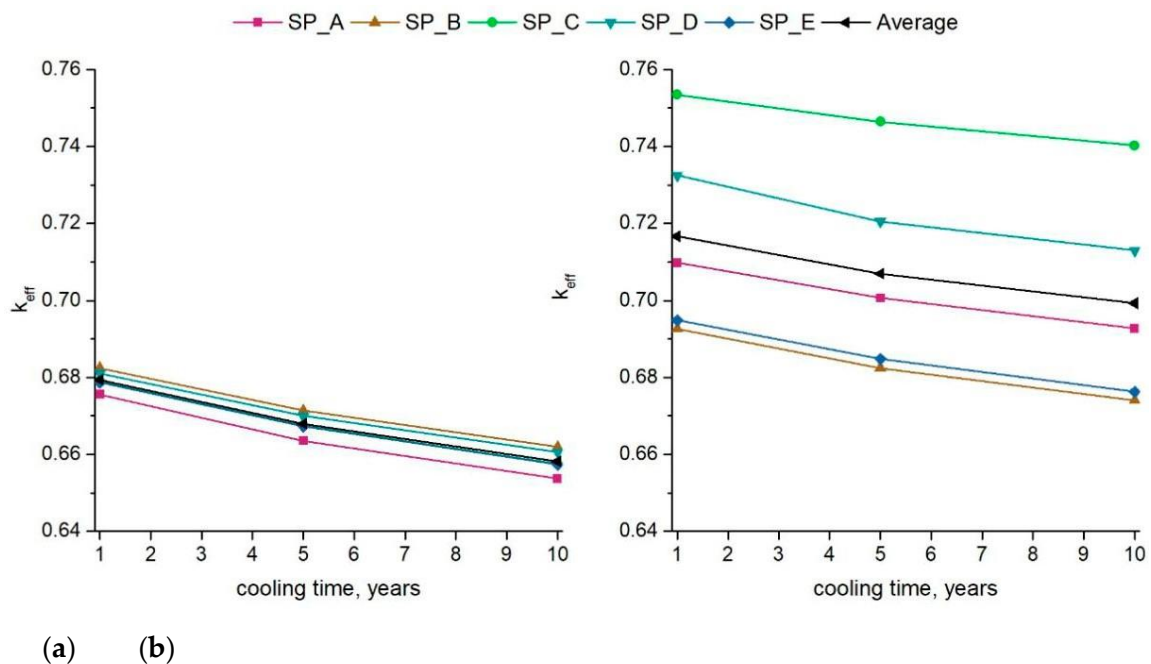
Figure 5.7. keff of the GBC-68 cask filled with FAs from (a) L68 and (b) L5%L loads vs. cooling time for different refuelling scenarios.

(a)   (b)
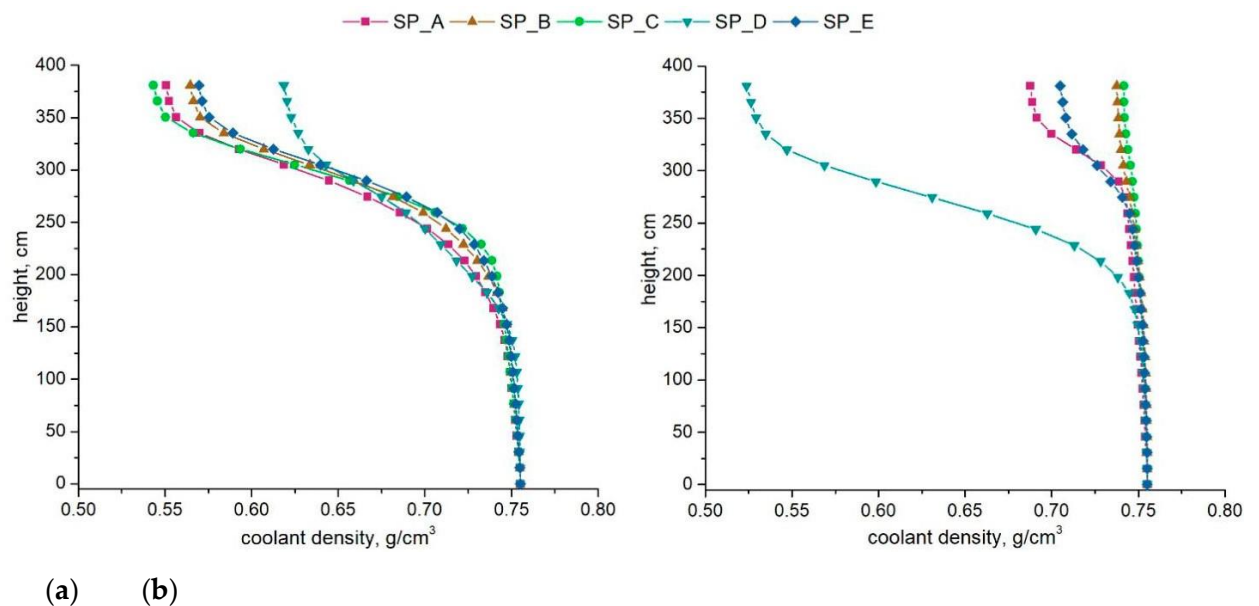
Figure 5.8. The coolant density profiles of the FAs from (a) L68 and (b) L5%L cask loads for different refuelling scenarios.

To summarise, the choice of shuffling procedure mainly affects the criticality of the cask filled with least burnt FAs (worst case) due to the significantly lower than average burnups for some shuffling procedures. Another reason could be a substantial difference between axial coolant density profiles which FAs see during the reactor operation under different reloading scenarios.

Table 5.3. The summary of parameters for five refuelling scenarios.

Distribution Parameter	Refuelling Scenario				
	SP_A	SP_B	SP_C	SP_D	SP_E
L_{68} load burnup, GWd/tU	50.5	49.9	50.3	49.8	50.1
$L_{5\%L}$ load burnup, GWd/tU	46.9	47.0	38.0	45.7	47.3

5.5.2.2. The Impact of Targeted Discharged Burnup on Cask Criticality

In the first part of this study, the burnup distributions for discharged fuel assemblies of several different reshuffling strategies were provided for an identical target burnup of approximately 50 GWd/tU for all cases or as we call it here, the reference target burnup. To evaluate the effect of the target burnup on the final burnup distribution and the cask criticality, the full core analysis was performed for the most (SP_A) and least optimal (SP_C) shuffling procedures and BWR GE14 fuel assembly type but with the reduced cycle length 10.3 GWd/tU instead of 11.75 GWd/tU for the reference case leading to a lower target burnup. In this case, the target burnup was decreased to approximately 44.5 GWd/tU burnup, which corresponds to the maximum assembly average burnup limit of 53 GWd/tU used in Germany for BWRs [35]. This new target burnup is called the modified target burnup.

Figure 5.9 represents four burnup distributions obtained for SP_A and SP_C shuffling procedures with reference and modified target burnups. First, it indicates that the shape of burnup distribution does not change significantly with the target burnup decrease. However, the burnup range, the difference between the minimum and maximum burnups of the distribution, becomes slightly lower. At the same time, the number of FAs in the highest bin increases by 30% for optimal SP_A distribution, and by 18% for the least optimal SP_C in the modified target burnup case. The average, maximum and minimum burnups along with FA number in the highest bin of the SP_A and SP_C distributions with reference and modified target burnups are presented in Table 5.4.

(a)

(b)
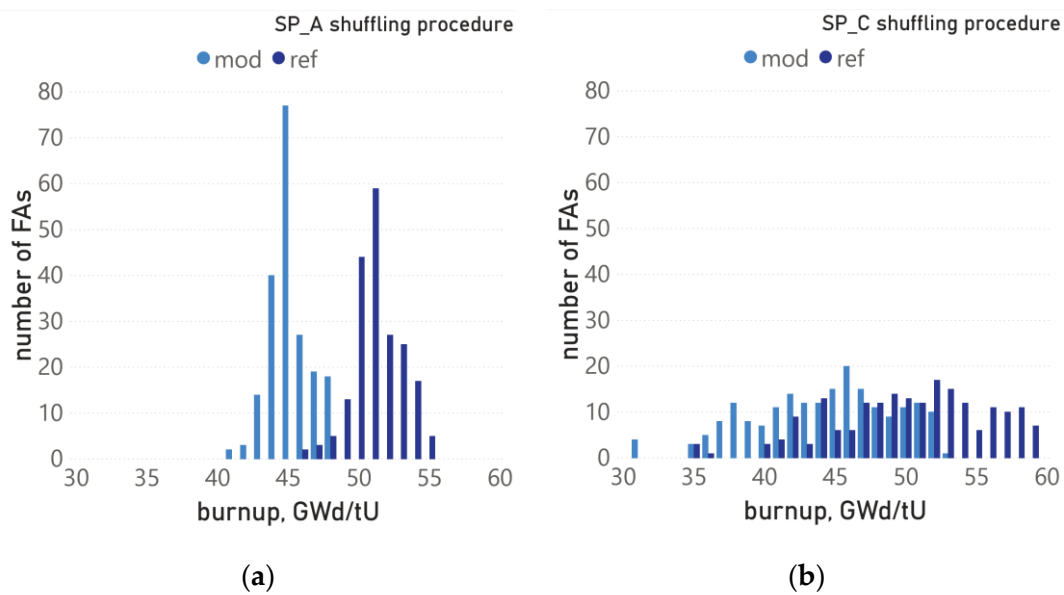
Figure 5.9. Burnup distributions for reference and modified target burnups for **(a)** SP_A and **(b)** SP_C shuffling procedures.

Table 5.4. The summary of parameters of the SP_A and SP_C distributions with reference and modified target burnups.

Distribution Parameter	Distribution			
	SP_A_ref	SP_A_mod	SP_C_ref	SP_C_mod
Average burnup, GWd/tU	50.7	44.6	49.7	43.7
Minimum burnup, GWd/tU	45.7	40.9	34.5	30.1
Maximum burnup, GWd/tU	54.5	47.8	58.7	52.5
FA number in the highest bin	59	77	17	20

Figure 5.10 represents burnup credit from applying realistic FA data (ARD) in comparison with fresh fuel (a) and peak reactivity (b) approaches for L_{68} and $L_{5\%L}$ cask loads, produced using optimal and least optimal shuffling procedures and reference and modified target burnups at one-year cooling time. The ARD is defined as:

$$ARD = \left(\frac{k_j - k_i}{k_j k_i}\right) \cdot 10^5 \tag{1}$$

where k_j is k_{eff} of the GBC-68 cask filled with fresh or at their peak reactivity BWR fuel assemblies, k_i is of the GBC-68 cask filled with BWR fuel assemblies from L_{68} or $L_{5\%L}$ load of specific burnup distribution.

It is seen that in the case with modified target burnup and least optimal shuffling procedure (mod SP_C), the burnup credit from ARD for both fresh fuel and peak reactivity approaches is higher for the $L_{5\%L}$ cask load (labelled as 5% in Figure 5.10) in comparison with L_{68} load (68 in Figure 5.10). However, it was expected that all ARDs would be lower for $L_{5\%L}$ than for L_{68} load as in the case with reference target burnup (ref SP_C) since the fuel burnups of $L_{5\%L}$ load are lower. Further analysis revealed that the presence of significant gadolinia concentrations in the upper parts of the fuel assemblies from $L_{5\%L}$ load causes this issue (see Figure 5.11).

Figure 5.10. BUC in comparison with fresh fuel approach **(a)** and peak reactivity approach **(b)**.

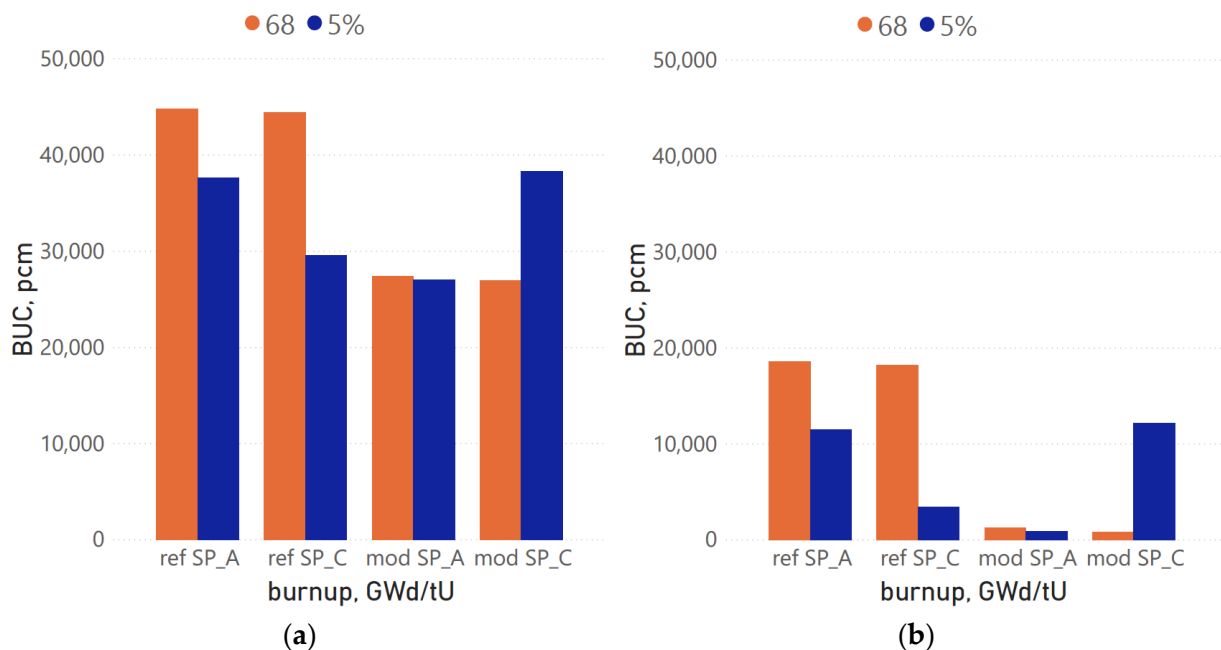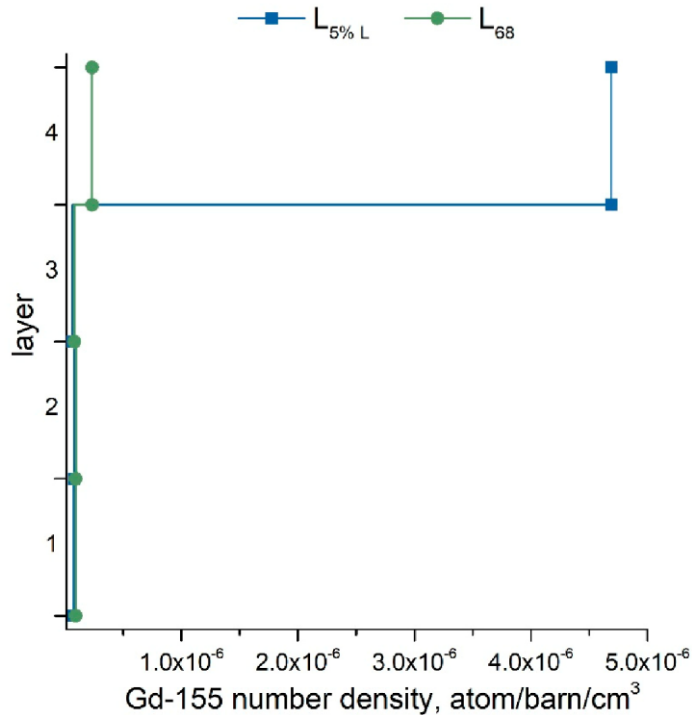**Figure 5.11.** Gd-155 concentration in FA layers for $L_{5\%L}$ and L_{68} loads.

To understand the reason of the residual Gd presence, the axial burnup profiles of the FAs from L_{68} and $L_{5\%L}$ loads (green and yellow lines, respectively, in Figure 5.12) and criticality curve (red line) for the vanished layer of the GE14 fuel assembly were investigated. Figure 5.12 shows that the burnup of the fuel assembly's upper layer (layer 4) from $L_{5\%L}$ load (5% LB yellow dash line) is around 15.8 GWd/tU. It corresponds to the part on criticality curve of the vanished layer (van) where gadolinia is still present, which means that fuel assemblies have not even reached the highest criticality level (peak reactivity). On the other hand, the upper layer burnup of the FAs from L_{68} load is 22 GWd/tU (68 LB green dash line) which corresponds to the part of the criticality curve where Gd is burnt (after the peak reactivity). Thus, for the least optimal burnup distribution SP_C with modified target burnup, the least burnt fuel assemblies are strongly underburned on the upper layer and therefore will be called here underburned fuel assemblies. This effect can occur if fuel assemblies designed for a much higher target burnup are not burnt close enough to it. The considered here GE14 fuel assembly variation is intended for a higher average burnup than the one from the modified target burnup case. Thus, this economically unsustainable approach would have somewhat surprising additional implications on the storage of the fuel assemblies due to the insufficient reduction of the burnable poison caused by the too low burnup.

The criticality inconsistency related to the underburned fuel assemblies disappears when considering the major actinides only set which is used for burnup criticality analysis on actinide-only level. This is due to the removal of gadolinia and fission products from the analysis. In the case of least optimal SP_C distribution obtained for the modified targeted burnup (mod SP_C), the ARD in comparison with fresh fuel approach is 13,400 and 18,700 pcm for $L_{5\%L}$ and L_{68} load, respectively. Hence, the results repeat the expected pattern: lower ARD values for lower discharged burnups. Thus, the different approaches to the burnup credit analysis, such as the choice of the isotopic set can lead to different conclusions.
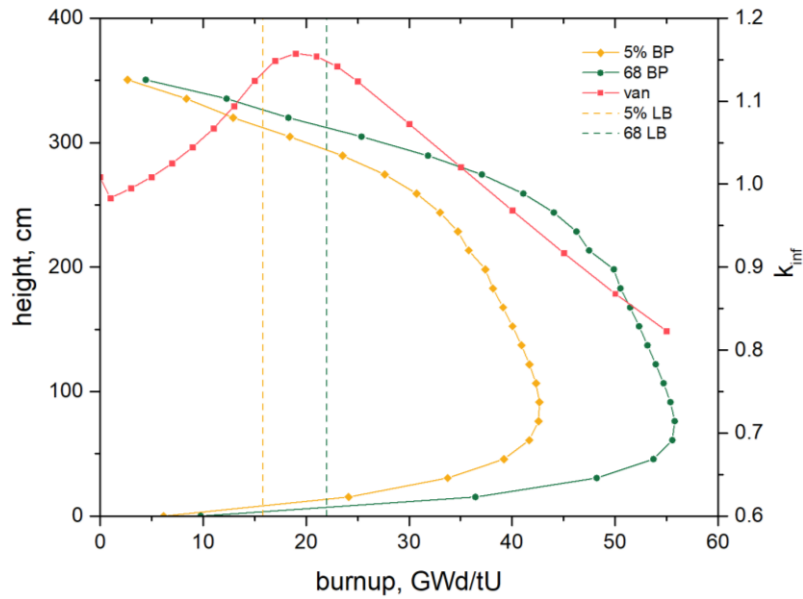
Figure 5.12. Burnup profile (BP) for FAs from $L_{5\%L}$ load and L_{68} loads and k_{inf} as a function of the average burnup of layer 4 of the GE14 FA model (van).

To sum up, as expected, the reduction of target burnup of a fuel assembly without reducing the initial enrichment (under burning the FA) leads to a substantial change in final assembly reactivity (increase in most cases) and consequently increase the reactivity of the storage system. In the classical 2D lattice approach, the criticality of the FA decreases with time for UO_2 fuel, while in case of poisoned fuel, this behaviour is observed after the peak reactivity. This outcome will consequently be propagated to the criticality analysis of the systems with the spent fuel composition estimated from lattice calculations. The criticality analysis of the GBC-68 cask performed here uses isotopic data of the fuel obtained from the nodal calculations. For this case, the described above trend can be reversed as shown in this section for actinides plus fission product set, while it will follow the expected trend for major actinides set.

5.5.2.3. The Impact of the FA Type on the Cask Criticality

This section will explore the effect of the different FAs on burnup credit. For this part of the study, the additional BWR SVEA-100 fuel assembly design was considered. The four-cycle core map used for the full-core simulations is unsuitable for FAs of this type since the fuel is low enriched and normally its average burnup does not go above 40 GWd/tU. However, for the comparison, the current core layout with the already established reshuffling schemes but reduce the cycle length was used. To make sure that both reactor cores, one with GE14 fuel assembly type and another with SVEA-100, are burnt to the same extent, the cycle length was chosen, so the core criticality after the last cycle is similar for both cases. The cycle length for SVEA-100 FA was estimated as 8.5 GWd/tU, which is 33% lower than for the reference GE14 assembly.

Figure 5.13 shows a comparison between the burnup distributions for the reactor core with the different FA types for SP_A and SP_C shuffling procedures. The target burnup in the case with SVEA-100 assembly is 32.5 GWd/tU and 50 GWd/tU for GE14. The burnup range decreases by 30% in the case with SVEA-100 for optimal and least optimal shuffling procedures, while the height of the distribution increases. This narrower burnup

distribution suggests that the loading scheme is more optimal for the SVEA fuel assemblies with the lower target burnup. However, there are two things to be kept in mind. First, the very short cycle time for the SVEA-100 would not be attractive; thus, in reality, the FA would not be operated in four cycles, but more probably in three cycles. Second, the short cycle time created by the four-cycle scheme and the relatively low burnup increase per cycle has also helped to achieve this very favourable result. Thus, the four-cycle scheme designed for the GE14 fuel assembly seems to favour the SVEA-100 FA, which has a much shorter lifetime than a higher enriched GE14 configuration.
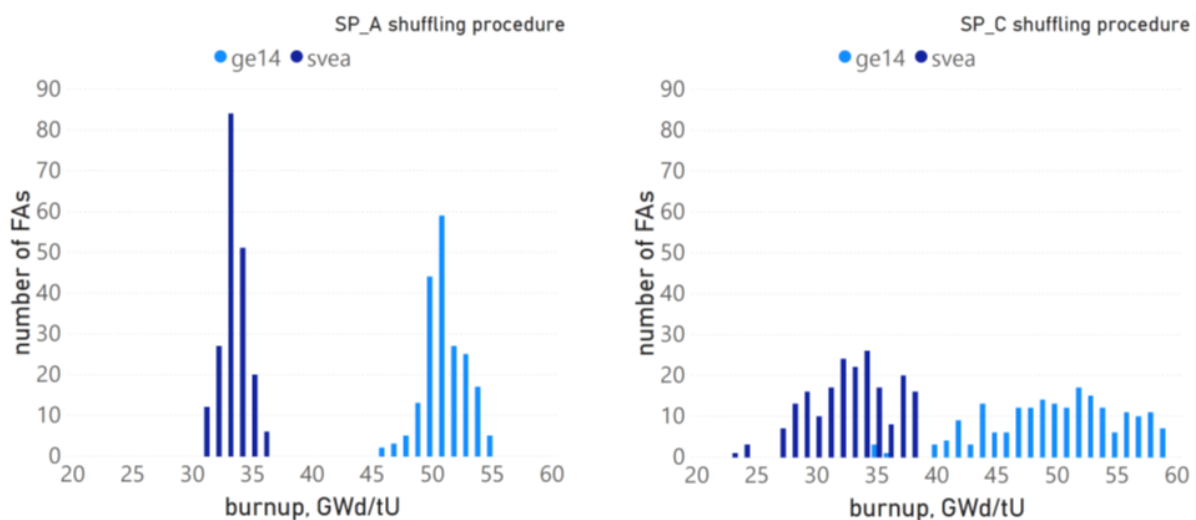
Figure 5.13. Burnup distribution for two FA types SVEA100 and GE14 and SP_A and SP_C shuffling procedures.

Figure 5.14 compares burnup credit from applying realistic FA data (Equation (1)) between the two different assembly types. It is seen that ARD in comparison with fresh fuel approach (Figure 5.14a) for both shuffling procedures SP_A and SP_C is slightly higher for GE14 assembly than for SVEA in case of L_{68} load (4300 pcm on average) and slightly lower (2200 pcm on average), for $L_{5\%L}$. The L_{68} load could be better in the case with GE14 FA since its design is much more sophisticated than the SVEA-100 fuel assembly design and is optimised to achieve higher burnup and improve the economic performance of the fuel: part length rods, higher initial enrichment and heavy Gd load. The SVEA100 assembly is better in the case of $L_{5\%L}$ load due to narrower structure of the burnup distribution, which makes the burnup of the 5% least burnt FAs slightly closer to the average discharge burnup.
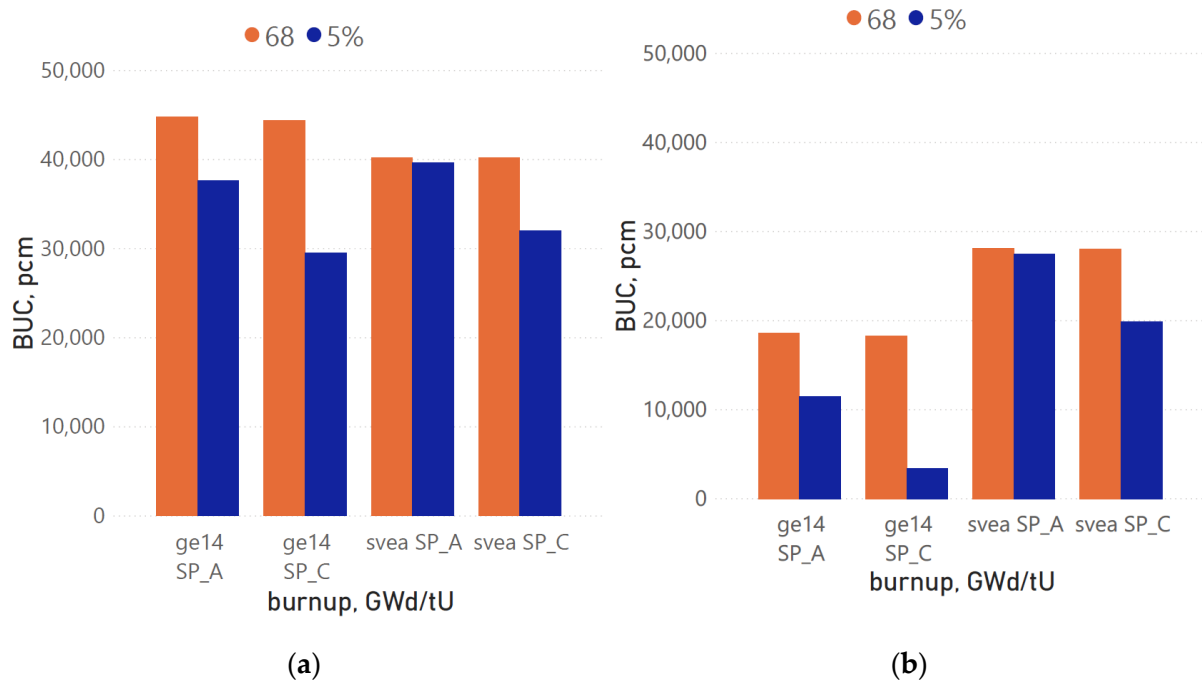
Figure 5.14. BUC in comparison with fresh fuel (a) and peak reactivity (b) approach.

Compared to the peak reactivity approach, the ARD is lower for GE14 assembly than for SVEA-100 (Figure 5.14b). The difference in ARDs between GE14 and SVEA-100 FAs is 9600 pcm on average in the L_{68} load, and 16,200 pcm for $L_{5\%L}$. This is due to the higher peak reactivity value of the SVEA100 criticality curve (Figure 5.6). Thus, the benefit from applying realistic assembly conditions instead of the peak reactivity approach is lower for GE14 assembly, which represents here a modern BWR fuel assembly design, than for the previous generation SVEA100 assembly design. On the other hand, the ARD for fresh fuel approach is approximately at the same level for both FA types with a slight advantage of GE14 assembly.

In conclusion, although the burnup credit from applying realistic assembly data in comparison with the fresh fuel approach is substantial for modern BWR GE14 assembly design, it does not show the same level of benefit compared to the peak reactivity approach. The peak reactivity is achieved much later in the burnup history of the GE14 assembly; thus, there is less time to create differences between the peak reactivity approach and the more detailed full-core analysis. Considering that the reactor core was burnt to the similar extent for both FA types, in this research, the modern GE14 FA design did not show the significant increase in burnup credit values in comparison with older SVEA100 FA design. However, this outcome requires further investigation, and the first point would be developing a three-cycle reloading scheme which seems to be more appropriate for the SVEA-100.

5.5.2.4. Removal of Boral Panels from the GBC-68 Cask

This section explores the possibility of removal of boral panels from the storage cask filled with BWR spent fuel with realistic characteristics. The criticality analysis was performed for the GBC-68 storage cask loaded with 5% least burnt BWR GE14 fuel assemblies from the least optimal SP_C distribution with target burnup 50 GWd/tU and one

year cooling time which represents the worst-case scenario for the reactor core and shuffling procedures investigated here.

The effective multiplication factor of the described above cask loading was determined to be 0.8622 compared to 0.7529 with the same loading but with boral panels present, 0.9684 for the fresh fuel approach and 0.7728 for the peak reactivity. The k_{eff} of the cask without boral panels with spent fuel from $L_{5\%L}$ load is 10,700 pcm lower than the NRC requirements of 0.95 k_{eff} value for accident conditions (storage rack flooded with unborated water) [30], and 27,000 pcm lower when boral panels are included. The fresh fuel approach exceeds the safety limit by 2000 pcm, while the peak reactivity approach results are 24,000 pcm lower.

According to the estimation of the 2005 year, the cost of installation and manufacturing of the absorber panel is approximately USD 7000 [36,37]. The calculations were performed for Metamic™ panels containing Al-B4C mix, similar to boral panels used in this study [37]. The GBC-68 storage cask contains 156 panels resulting in a total cost 156 × USD 7000 = USD 1,092,000 for one cask. Considering that reactor core described here has 200 FAs from the third cycle, around three casks are needed to store the discharged fuel after one cycle of the reactor operation and may result in a cost of 3 × USD 1,092,000 = USD 3,276,000 per cycle. It should be noted that the estimation of the costs is approximate and presented here for illustrative purposes.

To summarise, the application of the model developed here based on the realistic spent fuel properties can potentially reduce SF transport and storage costs. It is also necessary to invest in the burnup credit method development, especially for high-enriched modern BWR assembly configurations. For example, the safety limit under the conservative fresh fuel approach was exceeded for GBC-68 storage cask loaded with GE14 fuel assembly.

5.5.3. The Modelling Approximations Impact on the Cask Criticality

One of the main modelling approximations here was the data averaging of 25 DYN3D nodes to six layers (Figure 5.5) within the fuel assembly. A series of calculations with a 25-layer FA model was performed to evaluate this approximation effect on the GBC-68 storage cask criticality. The criticality calculations were conducted for L_{68} and $L_{5\%L}$ loads of the least optimal burnup distribution SP_C with BWR GE14 fuel assembly with one-year cooling time. The six-layer model underestimated cask k_{eff} by approximately 3800 pcm or 2.6% compared to 25-layer in case of L_{68} load and overestimated it by 4800 pcm or 3.6% in case of $L_{5\%L}$ load. These values give a good approximation of the expected uncertainty from reducing the number of the layer. Thus, the estimated burnup credit value for sixlayer model can be higher for L_{68} load and lower for $L_{5\%L}$. Overall, the current research focuses on creating a general understanding of the benefit from the BUC method using a best estimate approach. Thus, this level of discrepancy was considered as acceptable.

Recent research [15,16] developed and utilised for the burnup credit analysis a detailed 3D model of the BWR GE14 fuel assembly to reflect on various operational difficulties of the BWRs. Although the current research is also focused on developing a realistic BWR FA model, there are substantial differences between the approaches outlined in this investigation and those from studies [15,16]. For example, the authors of the above study performed depletion calculations using only one coolant density profile. However, the given study used the data obtained from the full core analysis and, thus, considered a more realistic FA behaviour in the reactor core. Another difference is that the BUC method in the

research [15,16] was applied to the fuel discharged at the peak reactivity while, in this study, realistic discharged burnups were considered. Another recent study [14] investigated the effect of the variation of the several operating parameters (compound effect) on the burnup credit using the BWR GE14 fuel assembly design. The study included a wide range of assumptions and simplifications regarding the fuel assembly design and operating parameters, such as lack of part-length rods or gadolinia rods.

In general, the current modelling approach provides a much more realistic model of the fuel assembly during the operation compared to the studies in Refs. [14–16] since it uses more realistic axial coolant density distributions and burnup profiles delivered by the thermal-hydraulics module of the coupled core simulation.

5.6. Conclusions

This paper has investigated the potential benefit of applying the burnup credit method for BWR spent fuel using the data obtained from the full-core calculations. The criticality analysis for the GBC-68 storage cask filled with BWR spent fuel was performed for five different refuelling scenarios developed by the authors in the last part of the research, two target burnups and two fuel assembly types: modern GE14 and the previous generation SVEA100. The BUC analysis results were based on a realistic FA model and compared with fresh fuel, and peak reactivity approaches.

The depletion analysis for both GE14 and SVEA100 FAs, using both lattice and nodal modelling approaches, showed that while the SVEA100 assembly has lower initial enrichment and hence mostly lower criticality, its peak reactivity is higher and occurs earlier than for GE14 fuel assembly due to the lower initial gadolinia content. Further analysis showed that the refuelling scenario substantially affects the cask criticality of the loads formed from least burnt fuel assemblies. The target burnup decrease leads to the expected increase in cask criticality and reduces the benefit of the BUC except for underburned FAs, which still contain a significant amount of gadolinia in an upper FA layer leading to a reduction in cask criticality. Comparison of cask criticality filled with different FA types— GE14 and SVEA100—revealed that if FAs are burnt up to their typical target burnup, the benefit from the applying BUC is at the relatively same level in comparison with fresh fuel approach for both L_{68} and $L_{5\%L}$ loads. However, the burnup credit for the realistic model of SVEA100 assembly shows better results compared to the peak reactivity approach. This is due to the reactivity peak appearing earlier on the criticality curve and having a higher criticality value than for GE14 assembly. It was also estimated that the potential saving costs in terms of the cask manufacturing due to the burnup credit method application could potentially reach several million US dollar savings per reactor operational cycle.

In conclusion, despite that development of the burnup credit method for BWRs is a complex problem, our research showed that it is worth investing in it due to potential savings. The burnup credit method is especially beneficial for more complex and higher enriched modern BWR fuel assembly designs.

References

1. International Atomic Energy Agency. Criticality Safety in the Handling of Fissile Material; IAEA Safety Standards Series No. SSG-27; IAEA: Vienna, Austria, 2014.
2. Hanlon, D.; Richards, S.; Ware, T.; Lindley, B.; Porter, J.; Raap, M.B. Use of Burn-up Credit in the Assessment of Criticality Risk; Amec Foster Wheeler: London, UK, 2017.
3. Crossland, I. Nuclear Fuel Cycle Science and Engineering; Elsevier: Amsterdam, The Netherlands, 2012.
4. International Atomic Energy Agency. Advances in Applications of Burnup Credit to Enhance Spent Fuel Transportation, Storage, Reprocessing and Disposition, IAEA-TECDOC-CD-1547. In Proceedings of the Technical Meeting, London, UK, 29 August–2 September 2005.
5. International Atomic Energy Agency. Implementation of Burnup Credit in Spent Fuel Management Systems, IAEA-TECDOC-1013. In Proceedings of the Advisory Group Meeting, Vienna, Austria, 20–24 October 1997.
6. Parks, C.V.; DeHart, M.D.; Wagner, J.C. Review and Prioritisation of Technical Issues Related to Burn-up Credit for LWR Fuel; Oak Ridge National Laboratory: Oak Ridge, TN, USA, 2000; NUREG/CR-6665 (ORNL/TM-1999/303).
7. Division of Spent Fuel Storage and Transportation. Burn-up Credit in the Criticality Safety Analyses of PWR Spent Fuel in Transportation and Storage Casks. In Division of Spent Fuel Storage and Transportation Interim Staff Guidance–8 Revision 3; US Nuclear Regulatory Commission: Rockville, MD, USA, 2012.
8. Detkina, A.; Peakman, A.; Litskevich, D.; Liang, J.-H.; Merk, B. Evaluation of BWR Burnup Calculations Using Deterministic Lattice Codes SCALE-6.2, WIMS-10A and CASMO5. Energies 2020, 13, 2573.
9. International Atomic Energy Agency. Nuclear Power Reactors in the World, 39th ed.; International Atomic Energy Agency: Vienna, Austria, 2019.
10. Fennern, L. Design evolution of BWRs: Dresden to generation III. Prog. Nucl. Energy 2018, 102, 38–57.
11. Marshall, W.J.; Ade, B.J.; Gauld, I.C.; Ilas, G.; Mertyurek, U.; Clarity, J.B.; Radulescu, G.; Betzler, B.R.; Bowman, S.M.; Gonzalez, M. Overview of the Recent BWR Burnup Credit Project at Oak Ridge National Laboratory; Oak Ridge National Lab: Oak Ridge, TN, USA, 2019.
12. Marshall, W.; Ade, B.J.; Bowman, S.M.; Martinez-Gonzalez, J.S. Axial Moderator Density Distributions, Control Blade Usage, and Axial Burnup Distributions for Extended BWR Burnup Credit; US Nuclear Regulatory Commission, Office of Nuclear Regulatory Research: Rockville, MD, USA, 2016.
13. Rearden, B.; Jessee, M. SCALE Code System, ORNL/TM-2005/39, Version 6.2.2; Oak Ridge National Laboratory: Oak Ridge, TN, USA, 2017.

14. Wu, S.C.; Chao, D.S.; Liang, J.H. Compound effects of operating parameters on burnup credit criticality analysis in boiling water reactor spent fuel assemblies. Nucl. Eng. Technol. 2018, 50, 18–24.
15. Radaideh, M.I.; Price, D.; O'grady, D.; Kozlowski, T. Advanced BWR criticality safety part I: Model development, model benchmarking, and depletion with uncertainty analysis. Prog. Nucl. Energy 2019, 113, 230–246.
16. Price, D.; Radaideh, M.I.; O'Grady, D.; Kozlowski, T. Advanced BWR criticality safety part II: Cask criticality, burnup credit, sensitivity, and uncertainty analyses. Prog. Nucl. Energy 2019, 115, 126–139.
17. Gauld, I.C. Strategies for Application of Isotopic Uncertainties in Burnup Credit; Oak Ridge National Laboratory: Oak Ridge, TN, USA, 2003; ORNL/TM-2001/257.
18. Radaideh, M.I.; Price, D.; Kozlowski, T. On using computational versus data-driven methods for uncertainty propagation of isotopic uncertainties. Nucl. Eng. Technol. 2020, 52, 1148–1155.
19. Ilas, G.; Liljenfeldt, H. Decay heat uncertainty for BWR used fuel due to modeling and nuclear data uncertainties. Nucl. Eng. Des. 2017, 319, 176–184.
20. Radaideh, M.I.; Price, D.; Kozlowski, T. Criticality and uncertainty assessment of assembly misloading in BWR transportation cask. Ann. Nucl. Energy 2018, 113, 1–14.
21. Rochman, D.; Dokhane, A.; Vasiliev, A.; Ferroukhi, H.; Hursin, M. Nuclear data uncertainties for core parameters based on Swiss BWR operated cycles. Ann. Nucl. Energy 2020, 148, 107727.
22. Detkina, A.; Litskevitch, D.; Peakman, A.; Merk, B. Burnup Credit Evaluation for BWR Spent Fuel from Full Core Calculations. Appl. Sci. 2020, 10, 7549.
23. Peakman, A.; Grove, C.; Fitzgerald, K.; Gregg, R. Development of an equilibrium loading pattern and whole-core fuel performance assessment in the Advanced Boiling Water Reactor (ABWR) with UO2 and U3Si2 fuels. Prog. Nucl. Energy 2019, 117, 103053.
24. Jessee, M.A.; Wieselquist, W.A.; Mertyurek, U.; Kim, K.S.; Evans, T.M.; Hamilton, S.P.; Gentry, C. Lattice physics calculations using the embedded self-shielding method in Polaris, Part I: Methods and implementation. Ann. Nucl. Energy 2020, 150, 107830.
25. Mertyurek, U.; Jessee, M.A.; Betzler, B.R. Lattice physics calculations using the embedded self-shielding method in polaris, Part II: Benchmark assessment. Ann. Nucl. Energy 2020, 150, 107829.
26. Rohde, U.; Kliem, S.; Grundmann, U.; Baier, S.; Bilodid, Y.; Duerigen, S.; Fridman, E.; Gommlich, A.; Grahn, A.; Holt, L.; et al. The reactor dynamics code DYN3D–models, validation and applications. Prog. Nucl. Energy 2016, 89, 170–190.
27. Mueller, D.E.; Scaglione, J.M.; Wagner, J.C.; Bowman, S.M. Computational Benchmark for Estimated Reactivity Margin from Fission Products and Minor Actinides in BWR Burnup Credit; ORNL Report to the NRC; Oak Ridge National Laboratory: Oak Ridge, TN, USA, 2013.
28. Zwicky, H. Isotopic Data of Sample F3F6 from a Rod Irradiated in the Swedish Boiling Water Reactor Forsmark 3; Zwicky Consulting: Remigen, Switzerland, 2008; ZC-08/001.
29. Karnbranslehantering, S. Measurements of Decay Heat in Spent Nuclear Fuel at the Swedish Interim Storage Facility, Clab, R-05-62; Swedish Nuclear Fuel and Waste Management Co.: Stockholm, Sweden, 2006.
30. NRC. 10 CFR 50.68 Criticality Accident Requirements. Available online: https://www.nrc.gov/reading-rm/doc-collections/cfr/ part050/part050-0068.html (accessed on 15 October 2020).

31. IAEA. Status Report 97—Advanced Boiling Water Reactor (ABWR). Available online: https://aris.iaea.org/PDF/ABWR.pdf (accessed on 30 August 2020).

32. Brown, C.; Hartley, K.; Hulsman, J. Extended Power Uprates and 2-yr Cycles for BWRs—Where Do We Go from Here? Nucl. Technol. 2005, 151, 120–125.

33. Marshall, W.B.; Ade, B.J.; Bowman, S.M.; Gauld, I.C.; Ilas, G.; Mertyurek, U.; Radulescu, G. Technical Basis for Peak Reactivity Burnup Credit for BWR Spent Nuclear Fuel in Storage and Transportation Systems; Oak Ridge National Lab (ORNL): Oak Ridge, TN, USA, 2015.

34. Merk, B.; Broeders, C.H.M. Overview of the amounts of plutonium generated against the background of the fixed electricity amount regulated by law in Germany. Actin. Fission Prod. Partit. Transmutat. 2007, 663–671.

35. OECD. Nuclear Fuel Safety Criteria; Technical Review; OECD Nuclear Energy Agency: Paris, France, 2012.

36. Electric Power Research Institute. Cost Impact of Using ISG-8 Rev. 3 for PWR Spent Fuel Pool Criticality Analysis; Technical Report; Electric Power Research Institute: Palo Alto, CA, USA, 2012.

37. Holtec International. Holtec Report HI-2043149 (Non-Proprietary); ADAMS Accession No. ML060900259; Holtec International: Marlton, NJ, USA, 2005.

6. Options for the long-term management of LWR spent fuel

The current chapter continues a discussion started in Chapter 1 about the problem of spent fuel accumulation from decommissioned, existing and future nuclear power plants up to Generation III+, and possible solutions. As was previously outlined, many countries remain indecisive regarding long-term management strategy for dealing with spent fuel from nuclear power plants, while others have chosen a reprocessing or final disposal option implementing partly closed and open fuel cycles respectively. The existing reprocessing strategy of the spent fuel management is based on the separation of uranium and plutonium from the spent fuel and production of mixed oxide (MOX) or enriched reprocessed uranium (ERU) fuel out of the separated elements [50]. The remaining fission products and minor actinides are placed into a glass matrix for further disposal. The MOX fuel contains a mix of uranium and plutonium dioxides and was originally developed for utilisation in either light water reactors or liquid metal fast breeder reactors [51]. Some countries, mostly in Europe, have successfully utilised MOX fuel in the existing light water reactors [52]. At the beginning of 2020, the Russian sodium-cooled fast breeder reactor BN-800 was loaded with the first batch of 18 MOX fuel assemblies. A year later, the reactor was refuelled with 160 MOX fuel assemblies which replaced UO_2 fuel assemblies [53]. ERU fuel assemblies are produced either by enriching uranium separated from the LWR spent fuel during reprocessing or by combining the separated uranium with high enriched uranium [54]. ERU fuel assemblies are also widely used throughout Europe. For example, the French company Framatome supplied around 500 ERU fuel assemblies out of a total 1000 to the UK nuclear power plant Sizewell B since 2009 [55]. In terms of reprocessing efficiency, AREVA's experience suggests that 7-9 UO_2 spent fuel assemblies are needed to produce 1 ERU and 1 MOX fuel assembly [50].

The direct disposal strategy suggests that spent fuel can be safely stored "as it is", hence, without reprocessing, in a deep geological formation. Such disposal facility is called a deep geological repository (DGR) [5]. There were other suggestions for the ways of final disposal of spent fuel such as placing it under the seabed but were abandoned because of safety and/or political concerns [5]. So far, only two countries – Finland and Sweden, have made significant progress towards the construction of DGRs [56]. In Finland, a construction licence for the repository was issued in 2015 to Finnish nuclear waste management company Posiva Oy [56]. The disposal process is expected to start as early as 2024 [57]. In Sweden, the host municipality approved the construction of the repository proposed by the Swedish Nuclear Fuel and Waste Management Company SKB at the end of 2020. The company is now seeking a final authorisation from the government. In the case of approval, the construction can begin in the middle of the 2020s.

Both described long-term spent fuel management options have advantages as well as disadvantages. Spent fuel reprocessing can reduce the volume, radiotoxicity and decay heat of the nuclear wastes and recover fissile and fertile material from spent fuel for further reuse. However, it does not eliminate the problem of the long-term spent fuel storage completely since the newly fabricated fuel out of reprocessed uranium and plutonium should also be disposed after irradiation. Although, the volumes of the new spent fuel will be lower than in straight disposal without reprocessing. Spent fuel reprocessing also rises proliferation concerns due to plutonium separation, which can be resolved by fabricating MOX fuel out of produced plutonium or using reprocessing technologies that retrieve

uranium and plutonium together [5]. Overall, reprocessing complicates the nuclear fuel cycle in general and increases the number of operations with spent fuel leading to an increased risk of exposure in comparison to the disposal. The final disposal, however, has many uncertainties in terms of ensuring the long-term safety of the repository due to the slow reduction to the safe levels of decay heat and radioactivity of the spent fuel.

Economical evaluation performed in [5] forecasts a trend towards reduction of the spent fuel reprocessing costs and rise of the final disposal costs. The former trend is thought to be happening due to improving the reprocessing technology, and the latter due to final disposal technology being young and incompletely studied. Overall, recent estimations of the costs of open and partly closed nuclear cycles showed that the historically higher price of the partly closed fuel cycle can become soon lower than one for open fuel cycle [5].

With that said, an important question arises: "Is there anything else that can be done to reduce volumes and toxicity of nuclear spent fuel?" The answer could be in the development of one or more of the following technologies:

- Generation IV (Gen IV) nuclear reactors;

- Accelerator driven systems (ADS);

- Fusion-fission hybrid systems; and

- Molten salt reactor operating directly on spent fuel.

Generation IV reactors are the perspective reactor systems that aim to fulfil the goals related to [7]:

✓ *Sustainability* – low carbon footprint, effective nuclear fuel utilisation and minimisation of the production of nuclear waste;

✓ *Economics* – can compete with other energy sources in terms of financial risk and overall costs;

✓ *Safety and reliability* – a very low probability and extent of damage to the reactor core;

✓ *Proliferation resistance and physical protection* – reducing attractiveness associated with nuclear material misuse and increased protection against acts of terrorism.

Six potential reactor systems were chosen for future research and development by the Generation IV International Forum (GIF) which have the potential to meet the above goals. A brief description of the Generation IV (Gen IV) reactor systems is presented in Table 6.1. As was outlined by the sustainability goal, Gen IV systems are expected to optimise utilisation of their nuclear fuel along with significant reduction of the nuclear waste in comparison to previous reactor generations. The goal can be achieved by either adopting a completely closed nuclear fuel cycle or by increasing the coolant outlet temperature which will result in higher thermal efficiency. The completely closed nuclear fuel cycle approach suggests that nuclear fuel can be reused in the reactor multiple times. Thermal efficiency in Gen IV systems is expected to be higher than for modern nuclear power plants, which have an efficiency of about 33 % [58], and can reach more than 50% as in the case with some VHTR systems, for example [59].

Table 6.1. Brief overview of the Generation 4 reactor systems [60,9,61]

Gen IV reactor type	Neutron Spectrum	Fuel cycle	Outlet temperature, °C	Fuel type	Breeder	Burner
Gas-cooled Fast Reactor (GFR)	fast	closed	850	carbide/nitride (s*)	yes	yes
Lead-cooled Fast Reactor (LFR)	fast	closed	480-570	nitride/metal/oxide (s)	yes	yes
Molten Salt Reactor (MSR)	thermal/fast	open/closed	700-800	Th/U-Pu based salt (l*)	yes	yes
Supercritical Water-cooled Reactor (SCWR)	thermal/fast	open/closed	510-625	oxide (s)	yes	no
Sodium-cooled Fast Reactor (SFR)	fast	closed	500-550	oxide/metal/carbide/MOX (s)	yes	yes
Very High Temperature Reactor (VHTR)	thermal	open	850	oxide/carbide/U-Pu/Pu/MOX/Th (s)	no	no

* s – solid fuel;
** l – liquid fuel.

Most of the Gen IV systems have the possibility to reduce the radiotoxicity of spent fuel from existing nuclear power plants, in particular the spent fuel from LWRs. It can be delivered by incorporating materials for transmutation into the reactor after delivering the appropriate partitioning steps. Partitioning is a process of separation elements of interest, such as plutonium and long-lived minor actinides, from spent fuel which is typically performed in the reprocessing facility. Transmutation is the process of converting those elements into short-lived or non-radioactive elements in a reactor. Partitioning can be done by aqueous or non-aqueous methods, while transmutation can be performed either in fast reactors and, hence, in most Gen IV systems, or in accelerator-driven systems which will be described in details later. It is worth pointing out that dealing with minor actinide bearing fuels is difficult both in terms of manufacturing of these fuels and the level in which they can be incorporated into a core. Partitioning and transmutation technology (P&T) can potentially reduce the radiotoxicity of spent fuel by a minimum of 100 times with spent fuel radioactivity possibly reaching safe levels at around 1000 years instead of 10^6 years [5, 62]. Although substantial progress has been made in the recent decades towards the demonstration of the efficiency of P&T technologies and their potential application in Gen IV reactor systems, it is still a few decades away from the application on the industrial scale.

The summary of possible fuel types that can be used in Gen IV reactors is presented in Table 6.1.

As was outlined above, accelerator-driven systems are considered as another option for the transmutation of plutonium and minor actinides separated from the spent fuel. ADSs include a subcritical reactor and a proton accelerator which provides the reactor with an external neutron source. k_{eff} of the core of such reactor is significantly below 1 (0.95-0.98) [63], thus, there will be no self-sustained chain reaction without the external source. ADSs have been identified as an attractive option since they can operate as pure burners for minor actinides, have a possibility to burn a wider range of isotopes and have an enhanced safety behaviour in comparison to fast reactors since there is no need to account for delayed neutrons due to subcriticality of the core. The major drawback is the increased complexity of the whole system, such as high requirements on the reliability of the accelerator. Hence, it is unlikely ADSs will be used for electricity generation, but they could act as a so-called tier two system in the double strata approach [64] with the focus on burning low quality plutonium and minor actinides.

A fusion-fission hybrid system (FFS) is another research area of interest for burning long-lived actinides and fission products from the spent fuel. The overall idea is similar to accelerator driven systems, but neutrons are produced by a fusion source instead of through an accelerator. The FFS consists of a fusion core which is surrounded by a blanket from nuclear fuel [65]. Due to the external source of neutrons (fusion), the fission reactor can remain subcritical. Although, the FFS option is attractive in terms of burning MAs and FPs, the technology is still very immature in comparison to fast reactors and also in comparison with ADSs [66].

Out of the options described above, the sodium-cooled fast reactor operating with a fully closed nuclear fuel cycle is considered as the most developed technology for application on an industrial scale due to the substantial operating experience of SFRs [4]. Also, a huge experience is accumulated in terms of spent fuel reprocessing from the LWRs. However, proliferation problems; the challenge of the transmutation fuel production; the lack of MOX fuel reprocessing technology; and the high costs of Generation IV systems still require further attention and development.

Beyond the options outlined above, the concept of the molten salt reactor working directly on spent fuel has emerged in recent years which became a basis for the iMAGINE project [67, 4]. The approach suggests that the spent fuel can be placed into the MSR core without prior reprocessing which makes the solid fuel fabrication facility and explicit reprocessing unnecessary for such reactor system. It means that if the technology is developed, the most expensive parts of the nuclear cycle can be removed. Figure 6.1 represents the different nuclear fuel cycle options. The nuclear fuel cycle of MSR working on LWR spent fuel (MSR cycle) is compared to the traditional closed fuel cycle and open fuel cycle. It is seen that while MSR cycle removes reprocessing and fuel fabrication chains from the closed cycle it adds an extra chain to the open cycle – solely the MSR itself. As was discussed earlier, the direct disposal approach misses out to use the energy that still remains in spent fuel after discharge from the reactor core (still 95% of the uranium) and leaves the nuclear waste radiotoxic for hundreds of thousand years due to the plutonium and minor actinides contained. The P&T and closed fuel cycle operation can eliminate the drawbacks of the open fuel cycle, but the technology still needs expensive investments into the spent fuel

reprocessing and a facility for transmutation (fast reactor or ADS, or both for a double strata approach). At this point, MSR operating directly on spent fuel can be a much cheaper and safer alternative to solve the problem of the spent fuel accumulation. It should be noted that despite Figure 6.1 showing that the nuclear waste from all cycle types ends up at the final disposal site, the volumes and activity of the final waste will vary for each scenario and even the design requirements of the final disposal can be different.
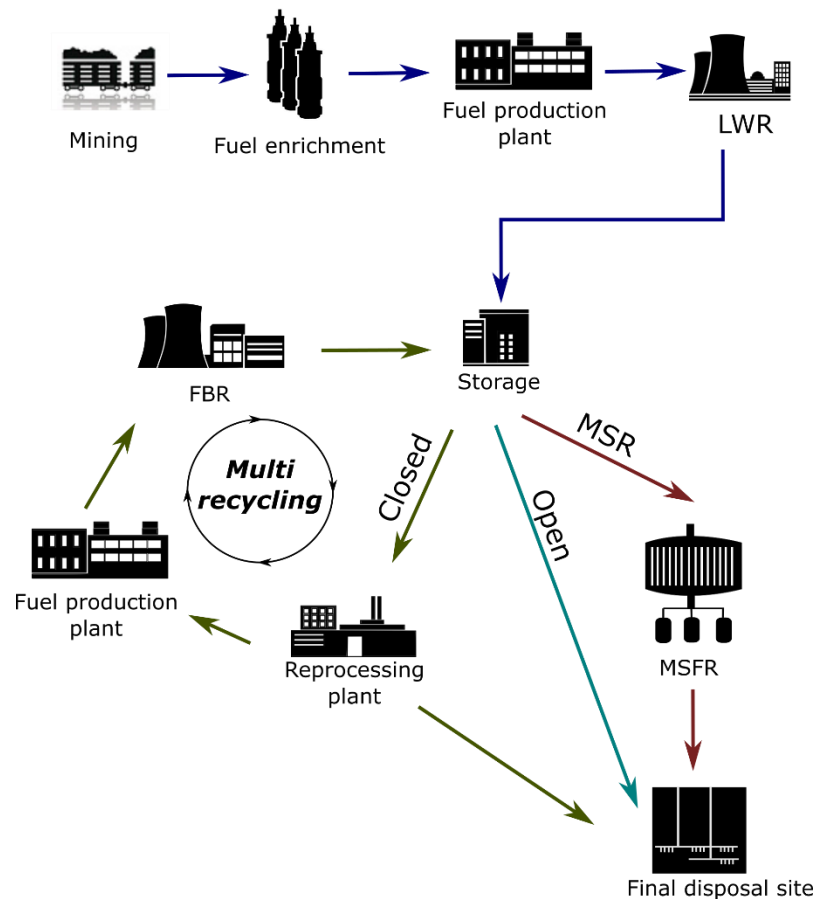

Figure 6.1. A simplified scheme of closed, open and MSR nuclear fuel cycles.

A Molten Salt Reactor is a reactor that uses a liquid fuel in a form of hot salt, for example, chloride or fluoride salts, under low pressure (~70-150 times lower than for LWRs), instead of conventional solid fuel. The salt in the system is also the coolant for the reactor core. As outlined in Table 6.1 MSRs can work as both, burner and breeder, and operate in thermal or fast spectra. In the thermal MSR system, graphite can be used for neutron moderation. The first MSR experiment was conducted in the 1960s by Oak Ridge National Laboratory with results summarised in the series of reports and publications in the early 1970s [68,69]. Despite promising experimental results, the MSR program in the US has been stopped in the mid-1970s. However, the interest in MSR technology is growing again in the nuclear industry and the research community [70].

The main safety advantages of MSRs in comparison to LWRs are the following [70]:

- low pressure in the core;
- no accidents associated with core melting as the fuel is already molten;
- the ability of continuous online refuelling which simplifies reactivity control;

- the ability of continuous removal of fission products from the system which leads to the low radioactivity of the reactor core and, consequently, lower radioactivity release in the case of a severe accident compared to the solid fuel.

MSRs are also considered as compact reactors with higher thermal efficiency than LWRs due to the higher operational temperatures. There is no need to manufacture solid fuel pellets as well as complex fuel assemblies or to shut down the nuclear power plant for refuelling. MSRs operating without separation of fissile material are considered a proliferation resistant. MSRs also have capabilities to burn Pu-239 from disassembled nuclear weapons or civil sources [71,72] avoiding fabrication of complex fuels such as MOX fuel.

There are currently series of unresolved challenges associated with the design and operation of MSRs working directly on spent fuel which should be addressed in order to improve understanding of the feasibility of the technology. The author of the thesis was involved in the series of MSR studies associated with:

1) the demonstration of achieving sufficient breeding in sodium chloride – uranium chloride (NaCl-UCl_n) based molten salt system [73];

2) understanding the molten salt system's behaviour under different reactivity control strategies [74];

3) justification of a need for a zero-power facility for the development of a new reactor type [75].

The first study [73] evaluated the breeding performance over the burnup for a simplified 2D MSR model. The analysed MSR system consisted of a core, stainless steel vessel and sodium reflector as shown in Figure 6.2. The outer part of the reflector was represented by a vacuum gap and a strong absorber simulating vacuum boundary conditions as the utilised computational tool SCALE/Polaris can only simulate in the reflective boundary conditions. The NaCl-UCl_n salt was chosen for investigation since it fulfilled with important criteria of: 1) high solubility of the fertile material; 2) affordability; and 3) operational experience within the UK.
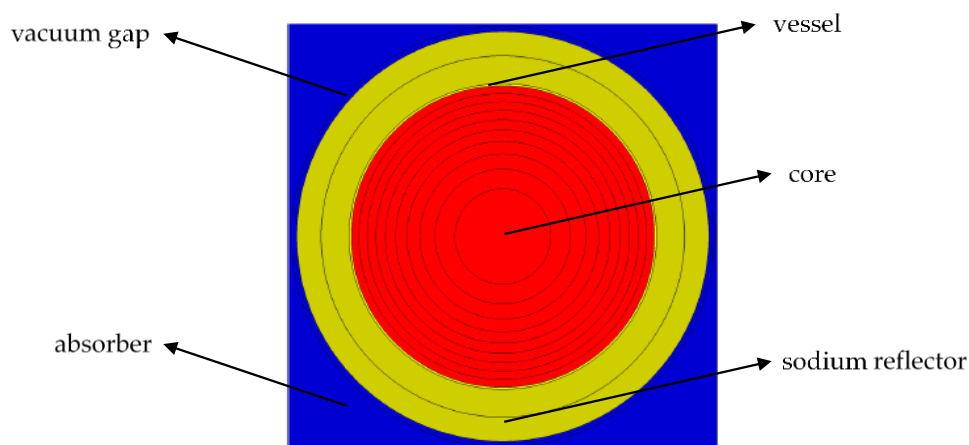

Figure 6.2. 2D model of MSR core.

The initial analysis showed that two component NaCl-UCl_4 and three component NaCl-UCl_3-UCl_4 salt systems satisfied the desirable characteristics of the salt mentioned above.

The fissile component of the examined systems was either in a form of enriched uranium or plutonium mixed with the natural uranium. The size of the core has been varied to identify its impact on breeding performance of the system. In addition, the consequences of using the cheap naturally composed chlorine (76% ^{35}Cl and 24% ^{37}Cl) in NaCl component instead of more expensive highly enriched chlorine which is currently often used for research of the chlorine based MSR systems were estimated. As SCALE/Polaris code has been mainly developed for LWRs, the MSR model described here was verified against of Monte-Carlo code Serpent for one of the outlined cases.

The results of the study indicate that plutonium-based systems have a better breeding performance over burnup than those with enriched uranium. A core with a radius of 170 cm loaded with plutonium-based salt produced a criticality curve that had the lowest reactivity swings, or in other words, had the most flattened shape. The performance similar to the Pu-based system can be achieved by an enriched uranium system if its core size is increased. It was also demonstrated that the usage of the naturally composed chlorine requires an increase of the initial fissile content of the salt (for example, higher ^{235}U enrichment in the considered case) in comparison to the case with enriched chlorine in order to produce similar results. The final decision about the utilisation of the naturally composed chlorine as a way to reduce the costs of the reactor should also consider costs associated with the potential increase of the core size, the fissile material content and the Cl-36 formation in the salt. The comparison of the SCALE/Polaris and Serpent codes revealed the difference in results from 1500 to 2400 pcm depending on the data library (ENDF/B-VII.0 or ENDF/B-VII.1). Overall, the study [73] demonstrated the feasibility of the reactor operation at a low power considering that the fuel (a major part would be spent nuclear fuel) exhibits a low cost as in the case of the MSR working on spent fuel.

The second study [74] was focused on investigating a possible way of the reactivity control in a molten salt reactor which is based on the inherent feedback processes rather than on complex control systems such as control rods in LWRs. The assumption is based on the mechanism which distinguishes the liquid fuel salt from the existing solid fuels – thermal expansion of the salt, which is a coolant and a fuel, under ambient pressure [70]. The expansion of the liquid fuel salt during the heating leads to a strong negative feedback effect in addition to the existing Doppler effect. The study [74] used the same model of the MSR system as in [73] which is shown in Figure 6.2. The analysis has been performed for the three component NaCl-UCl$_3$-UCl$_4$ salt only since it can dissolve more fertile material at the eutectic point than two component NaCl-UCl$_4$ salt as outlined in [73]. The fissile content was in a form of the enriched uranium with variable enrichment of 11-12 %. The SCALE/Polaris code with 252 group ENDF/B-VII.1 data library was utilised for the calculations.

In order to estimate temperature feedback in the salt system, it was necessary to identify the relation between the salt density and temperature. The data on the salt density-temperature dependence was identified for a temperature range of 900-1050 K. The analysis revealed that NaCl-UCl$_n$ system can offer a strong thermal feedback effect of -6.5 pcm/K in the eutectic composition which can compensate for a change in criticality due to breeding for burnups up to 90 GWd/tU. If the considered system is loaded with high heavy metal content, the feedback effect increases up to 13 pcm/K which would be enough to control the criticality for burnups up to 130 GWd/tU. Overall, the research showed that reactivity

control in the outlined MSR configuration is possible through the negative feedback effect which is an inherent mechanism of the fuel salt.

In conclusion, the current chapter outlined possible scenarios for the long-term management of spent fuel from LWRs which can potentially happen after the end of the temporary storage period. The current widely accepted solutions are either the final disposal of spent fuel or reuse of the fissile and fertile material in the nuclear reactor with burning long-lived minor actinides and fission products. The concept of molten salt reactor working directly on a spent fuel is shown to be another feasible solution along with existing well-established approaches for reduction of the volume, radiotoxicity and decay heat of the spent fuel. The MSR working directly on spent fuel can provide the benefits of the P&T technology as well as the massively increased sustainability indexes through leveraging U-238 for energy production. In addition, there is a strong potential to reduce the costs of development and operation by removing the stages of the fuel reprocessing and fabrication of a new fuel out of reprocessed material.

The first step towards the development of a new reactor system would usually be a zero-power experiment which can provide the key experimental data for further development and understanding of the technology. The paper [75] comprehensively outlines the advantages and possible outcomes of building a zero-power facility for novel nuclear research. It states that zero-power facility can be a low-cost project which is less complex than a full-scale reactor, requires less time to build but still provides scalable data for further development of the innovative technology.

The information about the research papers [73], [74] and [75] to which the author of the thesis has contributed is presented in Appendix A, B and C, respectively. The author's contribution to the studies outlined in the List of Publications section.

7. Conclusions

The research explored the potential benefit of applying advanced modelling & simulation for BWR burnup credit analysis. The burnup credit method developed in the research utilised the realistic operational data obtained from the coupled nodal full-core analysis. The quality of the applied computational tools for BWR simulations was estimated by comparing the results of the calculations either to other codes in the case of lattice analysis or to another computational approach in the case of the nodal reactor core analysis. In addition, the perspective solutions for the long-term spent fuel management has been identified and discussed.

Adequate modelling of the reactor core behaviour requires, firstly, robust computational tools and, secondly, extensive initial data. The first point is extensively covered in Chapter 2 and Chapter 3 of the thesis. The results of the lattice physics computations in the TRITON module of SCALE-6.2 for the simplified BWR models (with and without gadolinia burnable poison) showed a good level of agreement with the well-validated industry code CASMO5. At the same time, the UK code WIMS-10A produced results with a high level of discrepancy in comparison to both, CASMO5 and TRITON codes as a function of burnup. Although the TRITON module showed to be suitable for the purpose of the research, it was decided to use the newly developed Polaris module of SCALE for lattice physics computations due to its simpler input, reduced computational time and optimisation for LWR calculations, but with the results being close to TRITON.

The nodal approach which is currently used by industry for reactor physics simulations and represented here by Polaris/DYN3D sequence was compared to the high-fidelity Monte Carlo/subchannel analysis approach represented by Serpent/CTF sequence to define the limitations of both methods in application to modern BWR systems. The comparison was performed on the fuel assembly and reactor core level with and without thermal-hydraulics coupling. The Polaris module, which was used for the cross-section library preparation for the nodal analysis, demonstrated good agreement with the MC code Serpent for the modern BWR fuel assembly configurations which included variable radial and axial enrichment, part-length and burnable poison rods. A deeper investigation demonstrated that the major difference between nodal and high-fidelity approaches is caused by the difference in the estimation of axial power distribution during pure neutronics calculations with burnup for the realistic 3D fuel assembly model. The 3D fuel assembly model of Polaris/DYN3D sequence consisted of multiple layers each having its own cross-section sets. The results of the coupled neutronic/thermal-hydraulic analysis in both approaches showed a good agreement for the 3D fuel assembly model at the beginning of the life (i.e. no depletion). Despite the observed discrepancies in the burnup data preparation for 3D FA models, both approaches showed acceptable agreement for the pure neutronics analysis of the reactor core model without burnup. The coupled neutronic/thermal-hydraulic solution could not converge in the high-fidelity Serpent/CTF approach and, thus, the outcome of the coupled solutions in both sequences could not be compared. Overall, the results of the nodal analysis in Polaris/DYN3D sequence can be considered precise enough for the purpose of the study.

In terms of the initial data availability for BWR reactor core analysis, the reloading schemes are the least covered part in the open literature, especially for modern BWR core designs. To cover the gap of the open literature, four shuffling procedures have been developed to simulate various refuelling scenarios in the considered ABWR reactor core.

Each of the refuelling scenarios produced its own burnup distribution of the discharged fuel assemblies after four cycles of the reactor operation which is equal to the assembly's lifetime. The comparison of the burnup distributions' properties identified the most and least optimal refuelling scenarios in terms of fuel utilisation in the reactor core.

The innovative 3D coupled nodal model of the BWR fuel assembly revealed the difference in FA criticality as a function of burnup, in comparison to the 2D lattice approach. The developed model is thought to be more realistic since it can incorporate the effect of, for example, coolant density or fuel temperature profiles, more realistic power settings which is computationally expensive to implement in a high-fidelity approach, and not possible in 2D lattice approach. For this new, more realistic model, the peak reactivity occurs earlier and with a lower k_{eff} value than for the 2D model. There is also a presence of the second peak in reactivity related to the delayed depletion of the upper FA layers in comparison to the bottom layers. Overall, the k_{eff} values are lower in the realistic model for the burnups beyond peak reactivity.

The final part of the BWR burnup credit study explored the impact of utilising the realistic 3D fuel assembly model on the criticality of the spent fuel storage cask in comparison to the traditional fresh fuel and peak reactivity approaches. The assessment included a variation in refuelling scenarios, types of fuel assemblies and target burnups. The storage cask was loaded with either 5% least burnt FAs ($L_{L5\%}$ load) from the considered burnup distribution or 68 typical FAs (L_{68} load). The study identified that the choice of the refuelling scenario affects significantly the cask criticality for $L_{L5\%}$ load, while the difference is small for L_{68} load. The reduction of the target burnup has generally led to a decrease of the potential criticality gain (in pcm) from burnup credit method application with realistic data in comparison to fresh fuel and peak reactivity approaches, but, surprisingly, not for all cases. The rule did not apply for the underburnt fuel assemblies which still had residual gadolinia in the upper layers and thus lower criticality than for the case with higher target burnup. The underburnt FAs corresponded to the low burnt FAs from the least optimal burnup distribution. Finally, the burnup credit analysis for two different BWR fuel assembly types (GE14 with 4.5% enrichment and SVEA100 with 3% enrichment) did not identify a significant impact of the assembly type on the potential gain in criticality from applying burnup credit method with realistic data in comparison to fresh fuel approach. While in comparison to the peak reactivity approach the impact of assembly type has shown to be substantial. It was estimated that the potential savings from the application of the described burnup credit approach can be around $3.3 million per fuel cycle due to the removal of boral panels.

The optimisation of the interim fuel storage is an essential task for the nuclear industry considering the growing volumes of spent fuel from LWRs. However, an effective and sustainable solution for the problem of spent fuel accumulation requires the development of safe and effective measures for the long-term management of the spent fuel. Hence, in addition to the performed work on the burnup credit method, an overview of potential solutions for the long-term spent fuel management has been outlined. Among considered options, the author of the thesis contributed to the research related to the novel idea of the Molten Salt Reactor system working directly on spent fuel, or, in other words, without prior reprocessing. The MSR working directly on spent fuel is thought to reduce the cost of the closed nuclear fuel cycle and the toxicity of the spent fuel, including transuranic waste while

delivering very large amounts of energy out of the spent fuel. The author's contribution included proving the feasibility of the operation of such a reactor system, exploring possible reactivity control mechanisms that are inherent to the molten salt system's properties and outlining the benefits of a zero-power experiment for developing a new reactor.

8. Future work

The first part of the study analysed the difference between three well-known deterministic lattice codes for burnup calculations using simplified BWR models containing uranium dioxide and gadolinia burnable poison rods. Future work regarding codes comparison can be extended to the full-scale BWR fuel assembly model, including analysing the effect of the control blades presence on the difference between lattice codes.

The next part of the study highlighted a series of problems and limitations of the nodal and high-fidelity computational methods for the BWR full-core analysis with highly heterogenous fuel assemblies, which can be possibly addressed in the future. Further research may include:

- in-depth investigation of the discrepancy between axial power profiles for 3D BWR fuel assembly model obtained in both methods as a result of burnup calculations;

- improving the nodal calculations by applying high-fidelity methods to the fuel assemblies with high errors such as those near the reflector or control rods;

- using the computational tools of the CASL project to model modern BWR systems in order to create reference solutions to help to improve the solution provided by industrial nodal codes.

In terms of burnup credit analysis, the future scope of work may include the development of even more enhanced reactor core models by incorporating control rods movements, for example, which is ideally based on real reactor operation data. The model for the cask criticality assessment can also be improved by including axial fuel temperature distribution into the fuel assembly analysis and increasing the number of considered fuel assembly layers in the cask model. It would also be necessary to perform an uncertainty analysis for the developed burnup credit method to define necessary safety margins to spent fuel cask criticality for the acceptability by the regulator. The potential source of uncertainties could include the loading pattern, the modelling and simulation simplifications, the usage/disregard of control blades, nuclear data, or potential leaking fuel assemblies. Overall, verification of the calculations against experimental data is required in case if the burnup credit approach based on the realistic modelling and simulations will be further developed. This could open an interesting study with an industrial partner to find a realistic level of introduction of advanced modelling & simulation into the back end of the fuel cycle based on real industrial operation data. The potential tool to support such investigations could be, for example, the SNF code developed by Studsvik Scandpower. SNF takes an output directly from LWR industry standard codes CASMO5 (neutron transport and depletion) and SIMULATE5 (reactor simulator) to provide various spent fuel characteristics (isotopic composition, decay heat power, neutron spectra, etc.) [76]. This would allow to directly use available load following data of the plant owner without massive data management as input for the cask studies.

References

1. International Atomic Energy Agency. Estimation of Global Inventories of Radioactive Waste and Other Radioactive Materials. IAEA-TECDOC-1591; IAEA: Vienna, Austria, 2008.
2. International Atomic Energy Agency. Spent Fuel Reprocessing Options. IAEA-TECDOC-1587; IAEA, Vienna, 2008.
3. International Atomic Energy Agency. Nuclear Fuel Cycle Information System, A Directory of Nuclear Fuel Cycle Facilities 2009 Edition. IAEA-TECDOC-1613; IAEA: Vienna, April 2009.
4. Merk, B.; Litskevich, D.; Whittle, K.R.; Bankhead, M.; Taylor, R.J.; Mathers, D. On a Long Term Strategy for the Success of Nuclear Power. Energies 2017, 10, 867.
5. Rodríguez-Penalonga, L.; Moratilla Soria, B.Y. A Review of the Nuclear Fuel Cycle Strategies and the Spent Nuclear Fuel Management Technologies. Energies 2017, 10, 1235.
6. International Atomic Energy Agency. Country Nuclear Fuel Cycle Profiles - Second Edition. Technical Reports Series No. 425; IAEA: Vienna, Austria, 2005.
7. Generation IV International Forum website. Genereation IV goals. Available online: https://www.gen-4.org/gif/jcms/c_9502/generation-iv-goals (accessed on 5 April 2021).
8. Greene, C. Global Spent Fuel Overview. Avaliable online: https://cdn.ymaws.com/inmm.org/resource/resmgr/docs/events/spentfuel2020/proceedings/greene_uxc_political_landsca.pdf (accessed on 7 April 2021).
9. Crossland, I. Nuclear Fuel Cycle Science and Engineering; Elsevier: Amsterdam, The Netherlands, 2012.
10. International Atomic Energy Agency. PRIS Power Reactor Information System. Avaliable online: https://pris.iaea.org/PRIS/WorldStatistics/OperationalReactorsByType.aspx (accessed on 30 March 2021).
11. Alonso, G.; Bilbao, S.; Del Valle, E. Impact of the moderation ratio over the performance of different BWR fuel assemblies. Annals of Nuclear Energy, 85, 2015, pp.670-678.
12. Robers, L.; Prasser, H.M. Effect of part-length rods for different BWR subchannel geometries. Nuclear Engineering and Design, 2020, 370, p.110909.
13. Westinghouse Electric Company LLC. Reference Fuel Design, SVEA-96 Optima3, WCAP-17769-NP, Revision 0; Westinghouse: USA, November 2013.
14. Malcolm, J. Chapter 10 - Mainstream Power Reactor Systems In Nuclear Engineering. Edited by Malcolm Joyce. Butterworth-Heinemann, 2018, pp. 227-261.
15. K-A. Magnusson, K. Lundgren, P. Rudling. Management of BWR Control Rods. Advanced Nuclear Technology International. April, 2011. Available online: https://www.antinternational.com/docs/samples/FM/11/publication.pdf (accessed on 15 November 2021).
16. Bozzola, S. Fundamentals of boiling water reactor (BWR). IAEA: Vienna, 1982, pp. 71-130.
17. International Atomic Energy Agency. Fundamental Safety Principles. IAEA Safety Standards Series No. SF-1; IAEA: Vienna, Austria, 2006.
18. International Atomic Energy Agency. Storage of Spent Nuclear Fuel; IAEA Safety Standards Series No. SSG-15; IAEA: Vienna, Austria, 2012.

19. International Atomic Energy Agency. Criticality Safety in the Handling of Fissile Material. IAEA Safety Standards Series No. SSG-27; IAEA: Vienna, Austria, 2014.

20. International Atomic Energy Agency. Advisory material for the IAEA regulations for the safe transport of radioactive material (2012 Edition). Specific Safety Guide No. SSG-26; IAEA: Vienna, Austria, 2014.

21. Office for Nuclear Regulation. Criticality Safety Assessment of Transport Packages. ONR Transport Technical Assessment Guide, NS-TAST-GD-097 Revision 2. ONR: UK, 2020. Available online: http://www.onr.org.uk/operational/tech_asst_guides/ns-tast-gd-097.pdf (accessed on 15 April 2021).

22. Advances in Applications of Burnup Credit to Enhance Spent Fuel Transportation, Storage, Reprocessing and Disposition. IAEA-TECDOC-CD-1547. In Proceedings of a Technical Meeting Held in London, UK, 29 August–2 September 2005.

23. Implementation of Burnup Credit in Spent Fuel Management Systems, IAEA-TECDOC-1013. In Proceedings of an Advisory Group Meeting Held in Vienna, Austria, 20–24 October 1997.

24. Bowden, R. The application of burnup credit for spent fuel operations in the United Kingdom. Proceedings of an Advisory Group Meeting Held in Vienna, Austria, 20–24 October 1997, pp. 97-107.

25. SCALE Code System. ORNL/TM-2005/39, Version 6.2.2; Oak Ridge National Laboratory: Oak Ridge, TN, USA, 2017.

26. Gauld, I.C. Strategies for Application of Isotopic Uncertainties in Burnup Credit; Oak Ridge National Laboratory: Oak Ridge, TN, USA, 2003; ORNL/TM-2001/257.

27. Marshall, W.J.; Ade, B.J.; Bowman, S.M.; Martinez-Gonzalez, J.S. Axial Moderator Density Distributions, Control Blade Usage, and Axial Burnup Distributions for Extended BWR Burnup Credit; NUREG/CR-7224, ORNL/TM-2015/544; U.S. Nuclear Regulatory Commission, Oak Ridge National Laboratory: Oak Ridge, TN, USA, 2016.

28. WIMS A Modular Scheme for Neutronics Calculations; User Guide for Version 10, ANSWERS/WIMS/REPORT/014; Publisher: Dorchester, UK, 2014.

29. Rhodes, J.; Smith, K.; Lee, D. CASMO5 Development and Applications. In Proceedings of the PHYSOR-2006, ANS Topical Meeting on Reactor Physics, Vancouver, BC, Canada, 10–14 September 2006.

30. Rohde, U.; Kliem, S.; Grundmann, U.; Baier, S.; Bilodid, Y.; Duerigen, S.; Fridman, E.; Gommlich, A.; Grahn, A.; Holt, L.; Kozmenkov, Y.; Mittag, S. The reactor dynamics code DYN3D – models, validation and applications. Progress in Nuclear Energy 2016, 89, pp. 170-190.

31. Knott, D.; Yamamoto, A. Lattice physics computations. In Cacuci D.G. (eds) Handbook of nuclear engineering. Springer: Boston, MA, USA, 2010; pp. 913-1239.

32. Rhodes, J., Xu, Z., Lee, D. and Smith, K., 2009. Benchmarking of CASMO-5 ENDF/B-VII nuclear data against critical experiments. Proc. Advances in Nuclear Fuel Management IV (ANFM 2009), pp.12-15.

33. Haugh, B.P.; Ferrer, R.M. CASMO5 PWR Methods and Validation Report. Studsvik Scandpower Report SSP-14-P01/012-R Rev. 1 (2015)

34. Smith, K.S. Nodal diffusion methods and lattice physics data in LWR analyses: Understanding numerous subtle details. Progress in Nuclear Energy 2017, 101, pp.360-369.

35. Gomez-Torres, A.M.; Sanchez-Espinoza, V.H.; Kliem, S.; Gommlich, A. Implementation of a fast running full core pin power reconstruction method in DYN3D. Nuclear Engineering and Design 2014, 274, pp.44-55.

36. Xulubana, V.; Tippayakul, C.; Ivanov, K.; Levine, S.H.; Mahgerefteh, M. Accuracy evaluation of pin exposure calculations in current LWR core design codes. Annals of Nuclear Energy 2008, 35(3), pp.414-424.

37. Jessee, M.A.; Wieselquist, W.A.; Mertyurek, U.; Kim, K.S.; Evans, T.M.; Hamilton, S.P.; Gentry, C. Lattice physics calculations using the embedded self-shielding method in Polaris, Part I: Methods and implementation. Annals of Nuclear Energy 2020, 150, 107830.

38. Leppänen, J.; Pusa, M.; Viitanen, T.; Valtavirta, V.; Kaltiaisenaho, T. The Serpent Monte Carlo code: Status, development and applications in 2013. Annals of Nuclear Energy 2015, 82, 142–150.

39. Salko, R.K.; Lange, T.; Palmtag, S.; Gehin, J.; Avramova, M. Development of COBRA-TF for Modeling Full-Core, Reactor Operating Cycles. Advances in Nuclear Fuel Management V; ANFM, South Carolina; 2015.

40. Mertyurek, U.; Jessee, M.A.; Betzler, B.R. Lattice physics calculations using the embedded self-shielding method in polaris, Part II: Benchmark assessment. Annals of Nuclear Energy 2020, 150, 107829.

41. Szilard, R.; Kothe, D.; Turinsky, P. The Consortium for Advanced Simulation of Light Water Reactors (No. INL/CON-11-22917); Idaho National Laboratory (INL): 2011.

42. https://info.ornl.gov/sites/publications/Files/Pub75551.pdf

43. Radaideh, M.I.; Price, D.; O'grady, D.; Kozlowski, T. Advanced BWR criticality safety part I: Model development, model benchmarking, and depletion with uncertainty analysis. Prog. Nucl. Energy 2019, 113, 230–246.

44. Ade, B. Impact of Operating Parameters on Extended BWR Burnup Credit. United States Nuclear Regulatory Commission, Office of Nuclear Regulatory Research: USA, 2018.

45. Nylund, O., Fredin, B. and Johansson, A. SVEA - A New BWR Fuel Assembly Concept for Improved Fuel Utilization. ANS meeting in Newport, 20-23 September 1981.

46. Nylund, O., and L. Hjaerne. The SVEA BWR fuel: Eight years of further development. No. IAEA-TECDOC--577. 1990.

47. Hitachi-GE Nuclear Energy. UK ABWR Generic Design Assessment Generic PCSR Chapter 11: Reactor Core; Hitachi-GE Nuclear Energy, Ltd.: Ibaraki-ken, Japan, 2017.

48. Schneider, R., Cantonwine, P. and Lutz, D., 2016. GNF fuel and channel performance: 2016 update. In TOP FUEL 2016 Proceedings.

49. Parks, C.V.; DeHart, M.D.; Wagner, J.C. Review and Prioritisation of Technical Issues Related to Burn-up Credit for LWR Fuel; Oak Ridge National Laboratory: Oak Ridge, TN, USA, 2000; NUREG/CR-6665 (ORNL/TM-1999/303).

50. Moratilla Soria, B.Y.; Uris Mas, M.; Estadieu, M.; Villar Lejarreta, A.; Echevarria-López, D. Recycling versus long-term storage of nuclear fuel: Economic factors. Science and Technology of Nuclear Installations, vol. 2013, Article ID 417048, 7 pages, 2013.

51. Peiman, W.; Pioro, I.L.; Gabriel, K.; Hosseiny, M. Thermal aspects of conventional and alternative fuels. In Handbook of Generation IV Nuclear Reactors (pp. 583-635). Woodhead Publishing, 2016.

52. Supko, E. Nuclear fuel fabrication. In Uranium for Nuclear Power (pp. 353-382). Woodhead Publishing, 2016.

53. Press release on Rosatom's website from 24 Febrary 2021. Avaliable online: https://rosatom.ru/en/press-centre/news/bn-800-fast-reactor-undergoes-the-first-full-refueling-with-mox-fuel/ (accessed on 19 April 2021).

54. Combs, J. Nuclear fuel from secondary supplies of uranium and plutonium. In Uranium for Nuclear Power (pp. 215-238). Woodhead Publishing, 2016.

55. Koban I. Enriched reprocessed uranium, operational feedback. Framatome, avaliable online: https://www.framatome.com/solutions-portfolio/docs/default-source/default-document-library/product-sheets/a0511-z-ge-g-en-poster-eru-v7.pdf?Status=Master&sfvrsn=294d57c3_2 (accessed on 19 April 2021).

56. Litmanen, T.; Kari, M.; Kojo, M.; Solomon, B.D. Is there a Nordic model of final disposal of spent nuclear fuel? Governance insights from Finland and Sweden. Energy research & social science 2017, 25, pp.19-30.

57. Mikhailova N. Developing the first ever facility for the safe disposal of spent fuel. In Management of Spent Fuel from Nuclear Power Reactors, Learning from the Past, Enabling the Future. IAEA Bulletin, Vienna, Austria, June 2019, pp. 14-15.

58. Taiwo, T.A.; Hill, R.N. Summary of Generation-IV transmutation impacts (No. ANL-AFCI-150). Argonne National Laboratory (ANL), Argonne, IL, 2005.

59. Kim T.K. GEN-IV Reactors. In: Tsoulfanidis N. (eds) Nuclear Energy. Springer, New York, NY, 2013.

60. Generation IV International Forum website. Genereation IV systems. Available online: https://www.gen-4.org/gif/jcms/c_9353/systems (accessed on 5 April 2021).

61. Pioro, I.L. Introduction: Generation IV International Forum. In Handbook of generation IV nuclear reactors. Woodhead Publishing, 2016, pp. 37-54.

62. Merk, B.; Litskevich, D.; Bankhead, M.; Taylor, R. J. An innovative way of thinking nuclear waste management – Neutron physics of a reactor directly operating on SNF. PLOS ONE, 12(7).

63. Bowman, C.D. Accelerator-driven systems for nuclear waste transmutation. Annual Review of Nuclear and Particle Science, 48(1), 1998, pp.505-556.

64. Takano, H.; Nishihara, K.; Tsujimoto, K.; Sasa, T.; Oigawa, H.; Takizuka, T. Transmutation of long-lived radioactive waste based on double-strata concept. Progress in Nuclear Energy, 37(1-4), 2000, pp.371-376.

65. Freidberg, J.; Finck, P.; Bolton, C.; Hill, R.; Machiels, A.; Morley, N.; Sadowski, W.; Sheffield, J.; Weitzner, H.; Dagazian, R.; Goldner, F. Research needs for fusion-fission hybrid systems. In Report of the research needs workshop (ReNeW), Gaithersburg, Maryland, USA, September 2009.

66. Freidberg, J.P.; Kadak, A.C. Fusion–fission hybrids revisited. Nature Physics, 2009, 5(6), pp.370-372.

67. Merk, B.; Litskevich, D.; Peakman, A.; Bankhead, M. IMAGINE—A disruptive change to nuclear or how can we make more out of the existing spent nuclear fuel and what has to be done to make it possible in the UK?. ATW Int. J. Nucl. Power 2019, 64, 353–359.

68. Taube, M.; Ligou, J. Molten Chlorides Fast Breeder Reactor–Problems and Possibilities. (No. EIR-215). Eidgenoessisches Inst. fuer Reaktorforschung, June 1972.

69. Smith, J.; Simmons, W.E. An Assessment of a 2500 MWe Molten Chloride Salt Fast Reactor. AEEW – R 956. Technical Assessments and Studies Division, Atomic Energy Establishment, Winfrith, Dorchester, Dorset, the UK, August 1974.

70. Dolan, T.J. ed. Molten salt reactors and thorium energy. Woodhead Publishing, 2017.

71. Merk, B.; Litskevich, D. On the Burning of Plutonium Originating from Light Water Reactor Use in a Fast Molten Salt Reactor—A Neutron Physical Study. *Energies* 2015, *8*, 12557-12572.

72. Merk, B.; Litskevich, D. A disruptive approach to eliminating weapongrade plutonium - Pu burning in a molten salt fast reactor. PLOS ONE 2018, 13(8).

73. Merk, B.; Detkina, A.; Atkinson, S.; Litskevich, D.; Cartland-Glover, G. Evaluation of the Breeding Performance of a NaCl-UCl-Based Reactor System. *Energies* 2019, *12*, 3853.

74. Merk, B.; Detkina, A.; Litskevich, D.; Atkinson, S.; Cartland-Glover, G. The Interplay between Breeding and Thermal Feedback in a Molten Chlorine Fast Reactor. *Energies* 2020, *13*, 1609.

75. Merk, B.; Litskevich, D.; Detkina, A.; Cartland-Glover, G.; Atkinson, S.; Bankhead, M. A Zero-power Facility as a Multi-fold Opportunity to Support Quick Progress in Innovative Reactor Developments. ATW Int. J. Nucl. Power 2021, Vol. 66, Issue 3.

76. Simeonov, T. and Wemple, C., 2021. Advances in Studsvik's System for Spent Fuel Analyses. In EPJ Web of Conferences (Vol. 247, p. 02021). EDP Sciences.

Appendix A

Evaluation of the Breeding Performance of a NaCl-UCl-Based Reactor System

by Bruno Merk [1,2,*] ✉, Anna Detkina [1] ⓘ, Seddon Atkinson [1], Dzianis Litskevich [1] and Gregory Cartland-Glover [3] ⓘ

[1] School of Engineering, University of Liverpool, Liverpool L69 3GH, UK

[2] National Nuclear Laboratory, Chadwick House, Warrington WA3 6AE, UK

[3] Scientific Computing Department, Science and Technology Facilities Council, Daresbury Laboratory, SciTech Daresbury, Cheshire WA4 4AD, UK

[*] Author to whom correspondence should be addressed.

View Full-Text	Download PDF	Browse Figures	Citation Export

Abstract

The energy trilemma forms the key driver for the future of energy research. In nuclear technologies, molten salt reactors are an upcoming option which offers new approaches. However, the key would be closed fuel cycle operation which requires sufficient breeding for a self-sustained long term operation ideally based on spent fuel. To achieve these attractive goals two challenges have been identified: achieving of sufficient breeding and development of a demand driven salt clean up system. The aim is to follow up on previous work to create an initial approach to achieving sufficient breeding. Firstly, identification of a salt system with a high solubility for fertile material and sufficiently low melting point. Secondly, evaluation of the sensitivity of the breeding performance on the sort of fissile material, the fissile material loading, and the core dimension all based on a realistic salt system which provides the solubility for sufficient fertile material to achieve the required breeding in a homogeneous reactor without breeding blanket. Both points are essential to create an innovative solution to harvest the fruits of a closed fuel cycle without the penalty of the prohibitively huge investments. It is demonstrated that the identified and investigated NaCl-UCl based systems are feasible to deliver the requested in-core breeding within the given solubility limits of fertile material in the salt system using either uranium as start-up fissile component or plutonium. This result is enriched by the analysis of the achievable full power days per inserted mass of plutonium. These new insights support reactor optimization and lead to a first conclusion that systems with lower power density could be very attractive in the case of low fuel cost, like it would be given when operating on spent nuclear fuel. View Full-Text

https://www.mdpi.com/1996-1073/12/20/3853

Appendix B

The Interplay between Breeding and Thermal Feedback in a Molten Chlorine Fast Reactor

by Bruno Merk [1,*] ✉, Anna Detkina [1] ✉ ⓘ, Dzianis Litskevich [1] ✉, Seddon Atkinson [1] ✉ and Gregory Cartland-Glover [2] ✉ ⓘ

[1] School of Engineering, University of Liverpool, Liverpool L69 3GH, UK

[2] Scientific Computing Department, Science and Technology Facilities Council, Daresbury Laboratory, SciTech Daresbury, Cheshire WA4 4AD, UK

[*] Author to whom correspondence should be addressed.

View Full-Text	Download PDF	Browse Figures	Review Reports	Citation Export

Abstract

The energy trilemma and UN SDG 7 form the key drivers for the future of all kinds of energy research. In nuclear technology, molten salt reactors are an interesting option, since they can offer a game-changing approach to deliver an attractive, highly sustainable option for a zero-carbon society by providing sufficient breeding for a self-sustained long-term operation based on spent nuclear fuel from existing reactors while being able to be controlled ideally by inherent processes. To achieve these goals, several basic challenges have already been identified and worked on; demonstration of sufficient breeding and development of a demand driven salt clean up system. This study follows up on the opportunity for reactor control based on inherent feedback mechanisms. It is demonstrated that the investigated sodium chloride-uranium chloride-based systems can feasibly deliver a thermal feedback effect, which is strong enough, to compensate for the critically change due to breeding and fission product accumulation for two different compositions. The achieved results provide a very positive outlook on the system inherent ability for reactor self-control and even for the feasibility of a load following operation based on inherent feedback effects instead of massive and costly manual/automated control system operation. View Full-Text

Keywords: nuclear energy; nuclear reactors; molten salt reactors; closed fuel cycle; feedback effects; reactor control; homogenous reactor; spent nuclear fuel; sustainability; low carbon technologies

https://www.mdpi.com/1996-1073/13/7/1609

Appendix C

A Zero-power Facility as a Multi-fold Opportunity to Support Quick Progress in Innovative Reactor Development

Bruno Merk, Dzianis Litskevich, Anna Detkina, Greg Cartland-Glover, Seddon Atknison and Mark Bankhead

Introduction and history Nuclear has a very unique role to play in a sustainable energy future, since it is the only currently available technology which can assure 24/7 availability and controllability while delivering massive amounts of low carbon energy on demand for a net-zero future. However, in the recent decades there has not been any significant progress in the development of viable innovative nuclear technologies in comparison with the golden age of the nuclear development (1950's-1970's). Most new designs are iterative improvements of the nuclear technologies developed at that time (e. g. EPR in France, BN in Russia), or are more radical designs with little substantiation with an exception made for BREST-OD-300 [1], currently under development/construction [2]. Regardless of the different nuclear technologies studied and developed, the majority of the NPPs built around the world are still light water reactors. Unfortunately, light water reactor technologies have their limits due to their operational characteristics and cannot address major challenges which nuclear industry faces at the moment. Core points are: reducing nuclear waste, the availability of resources to manage assets over 100's years and the complexity systems leading to elevated cost. To be accepted by both, business and public, nuclear must deliver and be cost competitive compared to other flexible, on-demand producing, power plants with similar financial risks applied. Thus, nuclear needs innovations to be more sustainable, but even more importantly, we need to regrow the trust that nuclear can deliver these innovations. Finally, we need innovative approaches to reduce the risks associated with nuclear power plant construction becoming complex mega projects.